Characteristic Raman Bands of Amino Acids and Halophiles as Biomarkers in Planetary Exploration

Thesis

Characteristic Raman Bands of Amino Acids and Halophiles as Biomarkers in Planetary Exploration

Samantha Melanie Rolfe
MPhys (Hons), University of Leicester, 2010

September 2016

The Open University

School of Physical Sciences

A THESIS SUBMITTED TO THE OPEN UNIVERSITY IN THE

SUBJECT OF PLANETARY SCIENCES FOR THE

DEGREE OF DOCTOR OF PHILOSOPHY

Acknowledgements

To my parents, Mark and Melanie, and my brother, Alex, who have always supported and encouraged me to follow my dreams and overcome all and any obstacles to achieve them.

To my grandparents, Anthony and Margery Wilson, Aubrey and Val Rolfe and Marjorie and Russell Whitmore, this work is dedicated to you.

To Chris, my rock, without you I absolutely would not have been able to get through this process. I would have had no clean clothes or fresh vegetables in my diet. You know how much you mean to me, you are my best friend and your support means more to me than you can know.

To Manish, Karen, Iain and Tim, my supervisors, thank you for your guidance and instruction, especially on a multi-disciplinary project, where you taught me analytical techniques and skills, and entirely new to me, microbiology. I could not have done this without you.

Regardless of your walk of life - to those who may not realise their mental health is suffering, every now and then take a moment to look up the symptoms of depression and if you fit any of them, I encourage you to get help. Do not suffer alone.

Thank you to my examiners, Susana Jorge-Villar and Monica Grady, who made my viva examination an enjoyable experience after a nerve-wracking build-up.

Unending thanks goes to Mabs Gilmour for help with many hours of GCMS analysis that did not make it into this thesis, but from whom I learned a lot, plus instruction on chemical preparation of samples, and, most importantly, general but necessary support – I could not have got through this without you.

Thank you to Simona Nicoara for help with GCMS analysis, Marc Davies for help with basalt powder preparation, Michelle Higgins for basalt thin section preparation and chips of basalt, Stephen Summers for extensive tutoring on microbiology work and confocal microscopy, Sasha Verchovsky for custom glass work, Diane Johnson for conducting FIB-SEM imaging, Heather Davis for preparing and conducting TEM images, and Igor Kraev for information about the TEM sample preparation process, Gordon Imlach for FEG-SEM imaging (unfortunately, this work did not go to plan), and Karen Guyler and Beverley Bishop for their support and help.

To my colleagues and support base: Jon Mason, Euan Monaghan, Dan Dawson, Adam Stevens, Feargus Abernethy, Felicity Williams, Kathryn McDermott, Michael Goodyear, Jess Barnes, Rebecca Wolsey, Elliot Curtis-Harper, Pete Landsberg, Ben Dryer, Phillipa Smith and the other CEI residents, JD Bodenan, Mohit Melwani Daswani, Natalie Starkey, Louisa Preston, Tom Barrett, Roy Adkin, Zoë Ellery, Alex Barrett, Helen Davidge, Beth Steer, Ian Franchi, Sally Jordan, Terry McGenity, Lewis Dartnell – thank you for your friendship and help and collaboration and I wish the you all the best for the future.

To everyone in the Science Department at Beaumont School, but especially Karen, Caroline and Rathi, you are all so fabulous and dedicated, I have nothing but the greatest respect for you all and I miss working with you every day.

To my neglected friends, you know who you are, those I have known many years and those who I have recently got to know. You have stood by me and put up with diminished communications but were always there for me when I did get in contact, after many weeks or months of radio silence. I love you and I am so grateful for you being in my life.

N.B. As mentioned in Section 1.2.3, the term biomarker, biosignature and bioindicator are interchangeable. However, since beginning this PhD project, biomarker and biosignature now have more well-defined uses. At the time of publication, the term ‘biosignature’ refers to evidence for life, extant or extinct; whereas ‘biomarker’ is more readily used in medicine as indicators of disease and by geologists and geochemists when analysing molecular fossils in crude oils and petroleum. Due to historical definitions biomarker is used throughout this thesis, however, it is recommended that biosignature is used in future astrobiology-related writing.

Abstract

Evaporitic environments that could provide habitats for life exist on present day Mars, in addition to Recurring Slope Lineae (RSL), which have been observed suggesting a briny liquid in the subsurface with a seasonal occurrence at the surface. Life detection is the focus for future missions, including use of the Raman Laser Spectrometer (RLS) instrument on board the ESA *ExoMars* rover for this purpose. Martian simulation chambers were used to expose a subset of the α-amino acids (AA) and halophilic ('salt-loving') microbes to the surface and near surface environment. Post-exposure, the detectability of biological molecules with Raman spectroscopy (where the Raman spectrum is the biomarker) was examined, with the intention to inform future missions.

Results from this work suggest that a statistical method (independent of band intensity) should be used to rigorously define a set of characteristic Raman bands to unambiguously identify AA, a technique applicable to all biomolecules. Following exposure, both AA and halite entombed archaeal halophiles survived a combination of simulated martian conditions, *e.g.* freeze-thaw cycling resulted in a maximum of 20 % biomarker signal loss for AA. Halophilic microbes survived UV exposure up to 3.5 sols, though with a complete biomarker signal loss. However, cell counts and hence, survival in near surface, freeze-thaw conditions (indicative of RSL conditions) remained similar to the control sample. Furthermore, the Raman biomarker signal remained intact and detectable, regardless of a reduced intensity.

Importantly, for AA doped onto crushed basalt the Raman band biomarkers were lost, which has major implications for the *ExoMars* rover which will crush rock samples before examination with the RLS instrument. Future missions should be designed to examine samples with the Raman spectroscopy instrument prior to any crushing to avoid destroying the biomarker signal that could be used to imply the presence of life.

Publications

As a result of this work the following *manuscript* was accepted for publication, upon which Chapter 3 is based:

Rolfe, S. M.; Patel, M. R.; Gilmour, I.; Olsson, K. and Ringrose, T. J. (2016) Defining Multiple Characteristic Raman Bands of α-Amino Acids as Biomarkers for Planetary Missions Using a Statistical Method. *Origins of Life and Evolution of Biospheres*, 46, 323-346.

The following are *conference presentations* given as a result of work conducted throughout this study:

Rolfe, S. M.; Patel, M. R.; Gilmour, I.; Olsson, K. and Ringrose, T. J. (2013). Detecting biomarkers on Mars using Raman spectroscopy. In: *Molecules and Life in Extremes: UK Astrobiology Conference 2013 - (ASB5)*, 17-19 April 2013, Edinburgh, UK.

Rolfe, S. M.; Patel, M.; Gilmour, I.; Olsson, K.; Ringrose, T. J. and Cockell, C. (2012). Raman spectroscopy of biologically relevant amino acids under martian conditions. In: *Astrobiology Science Conference 2012 Exploring Life: Past, Present, Near and Far*, 16-20 April 2012, Atlanta, GA, USA.

Rolfe, S. M.; Patel, M. R.; Olsson, K.; Cockell, C. S. and Ringrose, T. J. (2011). Raman spectroscopy of amino acids and other biomarkers on Mars. In: *11th European Workshop on Astrobiology (Annual workshop of EANA)*, 11 - 14 July 2011, Cologne, Germany (poster).

Rolfe, S. M.; Patel, M. R.; Ringrose, T. J. and Leese, M. R. (2011). Planetary simulation and hypervelocity impact at the Open University. In: *Exploring Mars Habitability*, 13-15 June 2011, Lisbon, Portugal (poster).

Contents

List of Figures

List of Tables

List of Abbreviations

amb ambient

C carbon

C=C double bonded atoms, *e.g.* carbon

C−C single bonded atoms, *e.g.* carbon

D_{37} dose with a 37 % survival

DNA deoxyribonucleic acid

ESA European Space Agency

FTIR Fourier transform infrared

GCMS Gas Chromatography Mass Spectrometer

H hydrogen

H. sal NRC-1 *Halobacterium salinarum* NRC-1

Halite NaCl salt

HCl hydrochloric acid

IR infrared

ISS International Space Station

J m^{-2} Joules per metre squared

kJ m^{-2} kilo Joules per metre squared

LEO Low Earth Orbit

LWD long working distance

mbar millibar

MER Mars Exploration Rover

MGS NASA *Mars Global Surveyor*

mGy milligrays (1 Gy = 1 J/kg)

mRNA messenger RNA

MSC Mars Simulation Chamber

MSL NASA Mars Science Laboratory (inc. *Curiosity* rover)

N nitrogen

N3.1 *Haloferax* N3.1

N4.1b *Haloarcula* N4.1b

NaCl sodium chloride

NASA National Aeronautics and Space Administration

O oxygen

OD optical density

OD_{600} OD measurements taken with wavelength 600 nm

P phosphorous

ppb parts per billion

ppm parts per million

ppt parts per trillion

RLS Raman Laser Spectrometer (*ExoMars* rover instrument)

RNA ribonucleic acid

rRNA ribosomal RNA

RSL recurring slope lineae

RTD real time display

RWD relative wavenumber difference

S sulphur

SAM Sample Analysis at Mars (*Curiosity* rover instrument)

SEM scanning electron microscopy

SNC Shergotty-Nakhla-Chassigny

sol a martian solar day (24 hr 39 m 35.24409 s)

TEM transmission electron microscopy

TES Thermal Emission Spectrometer (MGS instrument)

TGO ESA *ExoMars* Trace Gas Orbiter

tRNA transfer RNA

UV ultraviolet

$W\ m^{-2}$ Watts per metre squared

wt% weight percent

μ specific growth rate

“Two possibilities exist: Either we are alone in the Universe or we are not. Both are equally terrifying.”

– Arthur C. Clarke

1. Introduction

1.1. Introduction

The human race has been asking itself for many generations: are we alone in the Universe? The discipline of Astrobiology, originally Exobiology, has recently become well defined and is thriving as an independent, multidisciplinary field of research. Astrobiology addresses several areas pertaining to life in the Universe: (1) the study of the origin of life; (2) the search for, and study of, habitable environments in our Solar System and habitable planets outside of our Solar System; (3) the study of how life adapts to challenges on Earth and in space (*e.g.* Morrison, 2001; Des Marais *et al.*, 2008; NASA, 2015).

Biomarkers have been defined as molecules that cannot be synthesised in large quantities by abiogenic means (Eglinton *et al.*, 1964). In the search for life elsewhere in the Solar System, the definition for biomarkers extends to whole cells, components of the cell, molecules altered by biological processes and geochemical markers such as macro- and micro-fossils. A collaboration reported by Parnell *et al.* (2007) suggests which biomarkers are of high priority for robotic missions to planetary bodies. Amino acids and carotenoids are among those suggested as a priority. Furthermore, Aerts *et al.* (2014) have reviewed in detail "what to look for" in terms of biomarkers and "where to look", *i.e.* Mars and used extreme terrestrial environments as examples of laboratories for *in situ* measurements of biota and biomolecules as analogues for "how to look for it" during exploration of the martian environment.

The planet Mars has been a huge source of hope and disappointment in the search for life in the Solar System (Klein, 1974). Surface features described by Giovanni Schiaparelli in Italian as 'canali' in the late 1800s, in English 'canals' or 'channels', was misunderstood to mean artificial structures. Percival Lowell, who drew detailed observational drawings of Mars, strongly believed that these canals were built by an intelligent civilization. In the early 20th century improvements in optics allowed observers to conclude there were no canals and in 1965, the spacecraft *Mariner 4* returned images of a desolate, impact laden surface unmistakably showing no evidence of an intelligent civilization. Nonetheless, liquid water, required for terrestrial-like life, has been present on Mars in the past with evidence of valley networks visible from orbit (*e.g.* Hynek *et al.* (2010)) and water molecules being found at the surface by rover missions. For example, the *Curiosity* rover has discovered evidence for water molecules bound in an amorphous component within martian regolith samples (Leshin *et al.*, 2013).

Though there is no evidence of macro-organisms on Mars, it is possible that microbial life may have arisen, possibly leaving biomarkers awaiting discovery. Searching for possible microbial life, the National Aeronautics and Space Administration (NASA) sent the *Viking* mission in the 1970s with a life detection experiment to the surface of Mars, but yielded inconclusive results (Biemann *et al.*, 1977; Jorge Villar and Edwards, 2006). Despite these results, which created more questions than answers, the search for life on Mars has continued. Optimism, extended by knowledge of extremophiles on Earth and the understanding gained from *Viking* about the difficulty in designing life detection experiments has led to further research and exploration. Today, the NASA *Mars Science Laboratory* (MSL) *Curiosity* rover is searching Gale Crater for evidence that Mars was once habitable. In 2020, a joint European Space Agency (ESA) – Roscosmos mission will launch the *ExoMars* rover, designed to search directly for evidence of life, where one of

the life detection instruments is a Raman spectrometer. In 2020, NASA plans to also launch a rover mission with the aim to search for evidence of past life and cache samples for a sample return mission in the future.

Raman spectroscopy is used for many applications including forensic science (*e.g.* Ryder, 2002; Day *et al.*, 2004), in pharmaceutical research (*e.g.* Mehrens *et al.*, 2005) and fraudulent art detection (*e.g.* Saverwyns, 2010). Since the *Viking* experiments in the 1970s, emphasis has been placed on exploiting pre-existing or designing new instruments and techniques for life detection. The technique of Raman spectroscopy has been suggested to be an invaluable tool to astrobiology as it can used to study both minerals and organic molecules (*e.g.* Jorge Villar and Edwards, 2006). Furthermore, samples need minimal preparation and are not destroyed in the process (when due care and attention is applied to factors such as the laser power and/or exposure time), which makes it an ideal technique for investigating the surface and the near surface of planetary bodies with the potential to harbour life.

The focus of this thesis is to use Raman spectroscopy as a biomarker detection method on future missions to Mars. One type of biomarker is molecules that are known to be used by life, such as amino acids, carotenoids, or are the signature of a whole cell (where the Raman spectra of molecules are unique 'fingerprints'). Simulation chambers can model extraterrestrial environmental conditions, to which microorganisms and molecules would be exposed on Mars. Such model organisms for studying possible life on Mars are halophilic microorganisms (either obligate or tolerant to high salinity environments, where obligate microbes are restricted to and would not survive outside of a high salinity environment). Evidence for brine activity at the surface of Mars in the form of Recurring Slope Lineae (RSL) provides a potential habitat for halophilic microbial life, so increasing

understanding of their survivability and detection by techniques such as Raman spectroscopy would be useful for informing future life detection missions.

Knowing the Raman bands that can be used for identifying biological molecules for halophiles is crucial for a positive identification in samples taken by future planetary missions and hence, the following research questions need answering.

RQ1. Using statistical techniques, can a set of characteristic Raman bands be rigorously defined for use as identifiers of amino acids?

RQ2. Does exposure to the martian near surface and surface conditions affect the Raman spectra of amino acids?

RQ3. Can halophilic microbial life entombed within halite crystals survive when exposed to coupled martian conditions and their Raman signatures remain detectable?

1.2. Life in the Solar System

1.2.1. Terrestrial life

Terrestrial life requires the chemical elements carbon, hydrogen, nitrogen, oxygen, phosphorous and sulphur (also known as the CHNOPS elements), an energy source, and liquid water at some point in its lifecycle. Life is divided in three major domains: the multicellular Eukaryote, and the single celled Bacteria and Archaea (Woese *et al*., 1990) shown in Figure 1-1. Archaea are thought to be the oldest examples of life on Earth, and are often found living in extreme conditions.

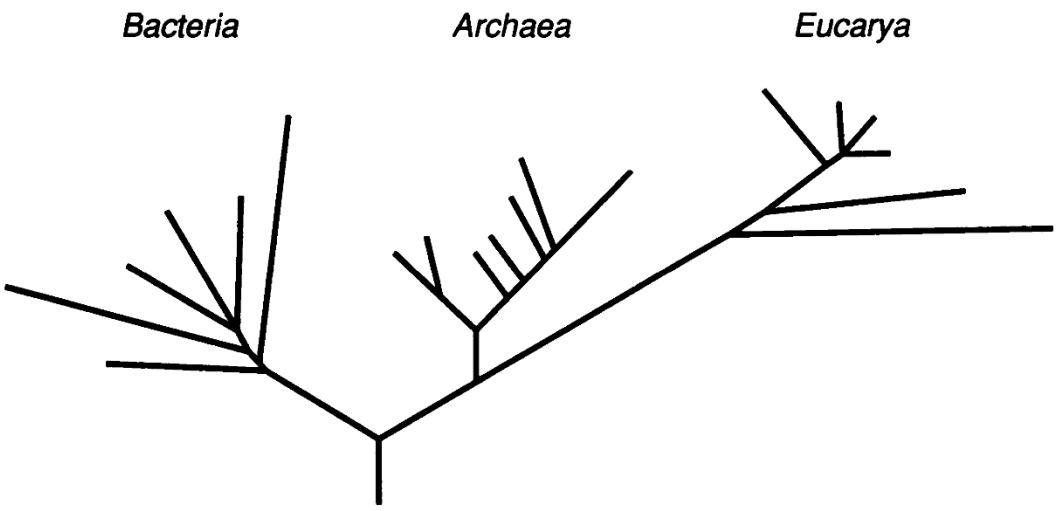

Figure 1-1: A cartoon of the simplified rooted Universal phylogenetic tree as proposed by Woese *et al.*, to show the three domains of life, with a universal common ancestor. Adapted from Woese *et al.* 1990.

1.2.2. Extremophiles

Extremophiles are found in all three domains of life; they grow and replicate in (one or more) conditions of extreme chemical concentration, temperature, pressure, acidity or alkalinity. For example, outside the normal temperature range and pressure of 20 to 40 °C and 1000 mbar, but where there are also satisfactory availability of liquid water and other nutrients needed to sustain life. Examples of extremophiles include thermophiles, *i.e.* capable of living in temperatures of 45 – 122 °C (*e.g.* Blöchl *et al.*, 1997); psychrophiles, *i.e.* able to survive at temperatures of –15 °C or lower for extended periods (*e.g.* Bowman *et al.*, 1997); and acidophiles, *i.e.* known to live at a pH of 3 or below (*e.g.* Golyshina *et al.*, 2000). Halophiles are 'salt lovers' and survive, grow and reproduce in high saline environments (*e.g.* Gruber *et al.*, 2004). The current upper salinity limit known is 5 M NaCl (Rothschild and Mancinelli, 2001).

1.2.2.1. Halophiles

Halophiles are found in each of the three domains of life (Oren, 2006). *Halobacteriaceae* are the only family for halophiles within the Archaea domain. The haloarchaea were originally denoted within the Bacteria domain, because the domain of Archaea was not officially recognised until the late 1970s (*e.g.* Woese *et al.*, 1978). The haloarchaea have characteristics that differentiate them from halophilic bacteria, for example, like all archaea, haloarchaea have ether-linked isoprenoid lipid membranes, whereas bacteria have ester-linked lipid membranes (*e.g.* Ross *et al.*, 1981). Those that belong to the most recently confirmed domain, Archaea, are among the oldest living organisms on Earth (Woese and Fox, 1977; Woese *et al.*, 1978), with the potential of similar life arising on Mars during its early history.

Using 16S (and 18S) ribosomal ribonucleic acid (rRNA), Woese and Fox (1977) began to distinguish the newly defined domain Archaea from life forms in the other two domains; methanogens (archaea that metabolise carbon dioxide to methane by reduction), clearly showed a distinction in the sequence comparison leading to the conclusion they were of the archaeal domain, rather than the bacterial domain and have existed from around 3 to 4 billion yr ago. Woese *et al.* (1978) stated the differences found between archaeal and bacterial rRNA and transfer RNA (tRNA) sequences are as dissimilar as those found between equivalent bacterial and eukaryotic sequences. Magrum *et al.* (1978) found using 16S rRNA sequences that the halophile *Halobacterium halobium* was related to methanogens rather than belonging to the domain of Bacteria, confirming the existence of ancient halophilic life forms.

Halophilic archaea are found in environments such as salt lakes and have been discovered in ancient salt deposits. Grant *et al.* (1998) have suggested that some species could have longevity in their survival and it is thought that isolates have been cultured from ancient halite deposits as old as 260 million years. However, there were no distinguishable 16S rRNA sequence patterns from these isolates to present day evaporite deposit isolates that correlated with the geological age of the sample site; though the technique resolution may not be sufficient to examine such a short geological timespan (*ibid*). Furthermore, brine movement through the rock salt may have replenished fluid inclusions with organic matter and acted as a transport mechanism for the cells (*ibid*). Nonetheless, these deposits and other terrestrial environments could be analogues for the martian environment (*e.g.* Wierzchos *et al.*, 2006; Preston and Dartnell, 2014) as there is known evidence for chloride-bearing salts on Mars, including martian meteorites (Bridges and Grady, 1999), inferred saline flows seen on slopes on craters marked by RSL (McEwen *et al.*, 2011; 2013) and *in situ* evidence from the *Curiosity* rover (Martin-Torres *et al.*, 2015) (see

Section 1.3.2). The evidence for longevity of halophiles on Earth could apply to Mars and therefore the study of these organisms is useful for understanding the potential for similar life forms that may be extant or extinct on Mars.

1.2.3. Biomarkers

In situ, the existence of extant or extinct life can be inferred by the detection of individual components of cells, including amino acids, carotenoids, deoxyribonucleic acid (DNA) and lipids. These components, which are unable to be synthesised in large quantities by abiogenic means, are called biological markers or biomarkers (Eglinton *et al.*, 1964). Other terms are also used interchangeably, such as biosignature (Schulze-Makuch *et al.*, 2002) and bioindicator (Des Marais *et al.*, 2002); however, the term biomarker will be used throughout this thesis (see N.B. after Acknowledgements, before Abstract, p. ii).

1.2.3.1. Preparatory biomarker studies

Being able to detect biomarkers within or outside of the Solar System is the main focus of many mission proposals. Outside of the Solar System the 'red edge' signal proposed to signify vegetation on distant planets was highlighted as a likely way of detecting a biosphere (Sagan *et al*., 1993); however, considering the vast number of microorganisms in the biosphere of the Earth and the extensive geological time of their existence compared to vegetation, it is possible that a signal from microorganisms will be detected first. Hegde *et al.* (2015) have compiled a database of 137 pigment-containing microbes, including the halophilic archaea *Halorubrum chaoviator*, in preparation for future telescopic missions with the potential to detect life. Aerts *et al.* (2014) review the techniques being used on current and upcoming missions to search for biomarkers, as well as where on Mars to

consider as potential sites that biomarkers may exist. Without stating a preference, Aerts *et al.* (2014) described the potential of several biomarkers as target molecules on Mars: amino acids, lipids and DNA. Amino acids have chiral properties, but only one chirality is used by terrestrial life, so if an excess of a chiral molecule used in terrestrial life was detected on Mars it could suggest the presence of similar life (see Section 1.2.3.2). All known living organisms use lipid membranes for the cell wall (Archaea use isoprenoids, Bacteria and Eukarya use fatty acids); lipids and their fossil equivalents are known to survive for long geological periods of time (*ibid*), hence could be very reliable biomarkers. DNA may survive on Mars for much longer periods than on Earth because of lower temperatures and a generally less erosive environment, with respect to weather, than seen on Earth; furthermore, nucleobases have been detected on meteorites suggesting the building blocks of terrestrial life could feature in the evolution of life on other planetary bodies (*ibid*). In addition to this, with an outlook to discovering life on other planetary bodies, various studies on biomarkers such as nucleotides, isoprenoids, steroids, amino acids (*e.g.* Simoneit *et al.*, 1998; Westall *et al.*, 2000; Ehrenfreund *et al.*, 2001a; ten Kate *et al.*, 2006; Bertrand *et al.*, 2012; Johnson *et al.*, 2012), porphyrin (*e.g.* Suo *et al.*, 2007; Cook *et al.*, 2014) and polycyclic aromatic hydrocarbons (PAHs) (*e.g.* McKay *et al.*, 1996; Alajtal *et al.*, 2010; Izawa *et al.*, 2014), have been conducted. In preparation for the ESA *ExoMars* mission, Parnell *et al.* (2007) have suggested a list prioritising potential biomarkers in order of their significance that would suggest evidence for life. The non-exhaustive list of molecules and their priorities (A, B, C; decreasing importance) include; Priority A: amino acids, adenosine triphosphate (ATP), nucleobases, DNA, porphyrin (*e.g.* chlorophyll), isoprenoids, pristane, phytane and hopane; Priority B: generic carotenoid (photoprotective pigment) and squalene; and Priority C: whole cells such as methanogens and cyanobacteria. These, among numerous studies conducted on amino acids and microbes as biomarkers (for detailed reviews see Sections 1.4.1, 1.4.2, 1.5.3 and

1.5.3.2, and further discussion in Chapters 3, 4 and 5), provides strong justification for the continued study of biomarkers in the context of planetary exploration.

1.2.3.2. Amino acids

Amino acids are essential for life on Earth. They are the 'building blocks' of proteins, form enzymes and participate in various chemical reactions. Specifically, there are twenty amino acids that are used by life, known as the natural or proteinogenic amino acids. Plants and microbes can synthesise all the natural amino acids (Hardy, 1985). These amino acids are all α-amino acids, where the functional groups are bonded to the alpha carbon atom, shown in Figure 1-2.

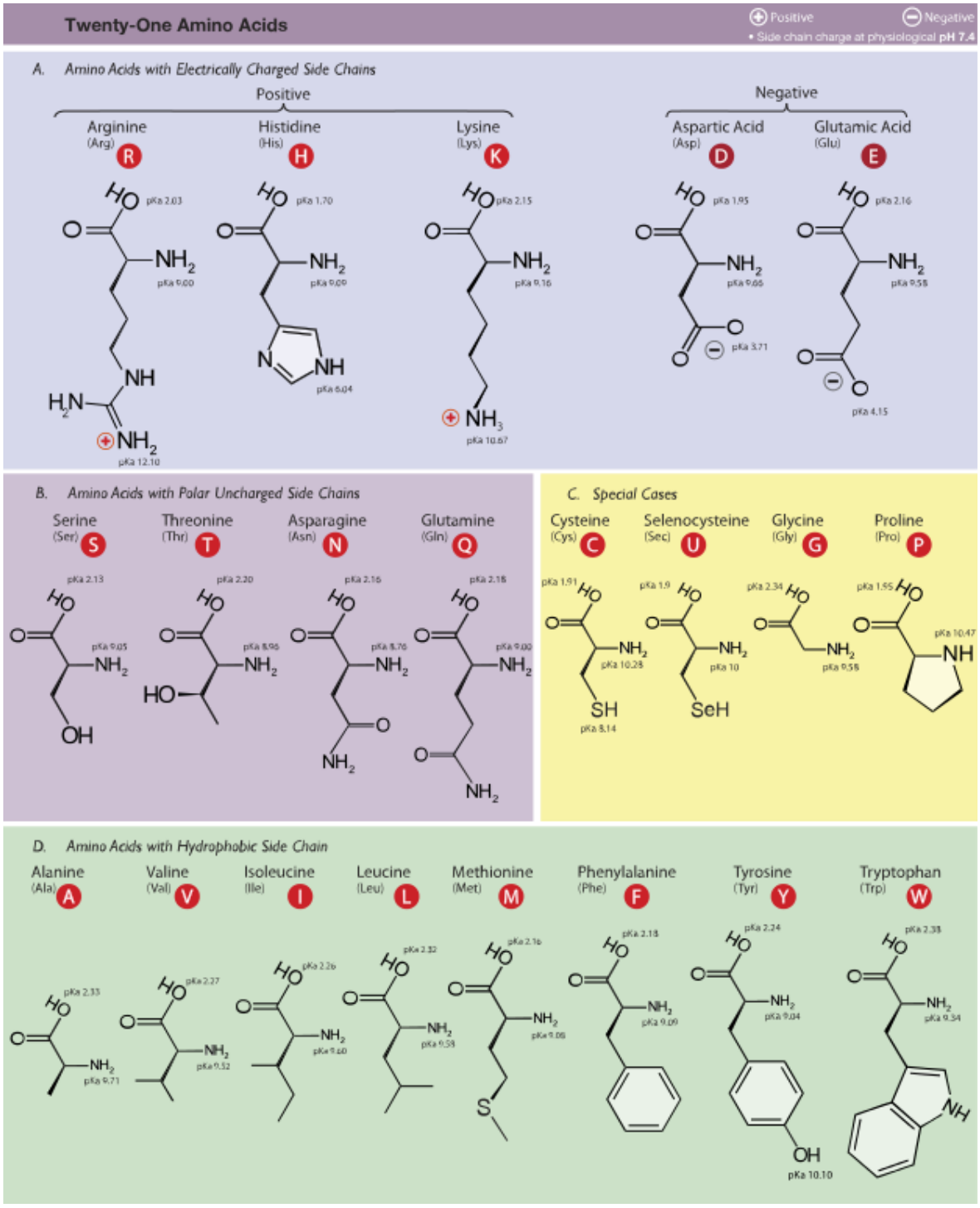

Figure 1-2: The molecular structure of the proteinogenic amino acids used by terrestrial life (created by Dancojocari https://commons.wikimedia.org/w/index.php?curid=9176441).

The neutral molecular structure of amino acids is NH_2–CHR–COOH but they are more often of zwitterion form NH_3^+–CHR–CO_2^-, especially in solid form (Taylor, 1971). R is representative of the side chain that defines each amino acid. The simplest is a single hydrogen (H) atom in glycine, building to the more complex ring structures seen in aromatic α-amino acids such as tryptophan or phenylalanine.

Amino acids are enantiomers, hence can be 'right-handed' (D- form) or 'left-handed' (L- form) chiral molecules (Tobin, 1971), illustrated in Figure 1-3. Terrestrial biology displays 'enantioselectivity', where only L-amino acids are used. Interactions between a left-handed and a right-handed molecule are not always the same, but interactions between two left-handed or two right-handed molecules are always the same; this selectivity is part of their functionality (Lunine, 2005). However, one exception to the rule is glycine, the only biologically selected amino acid that is achiral. In this study, unless otherwise stated, when discussing amino acids, it is the L-enantiomer to which reference is made.

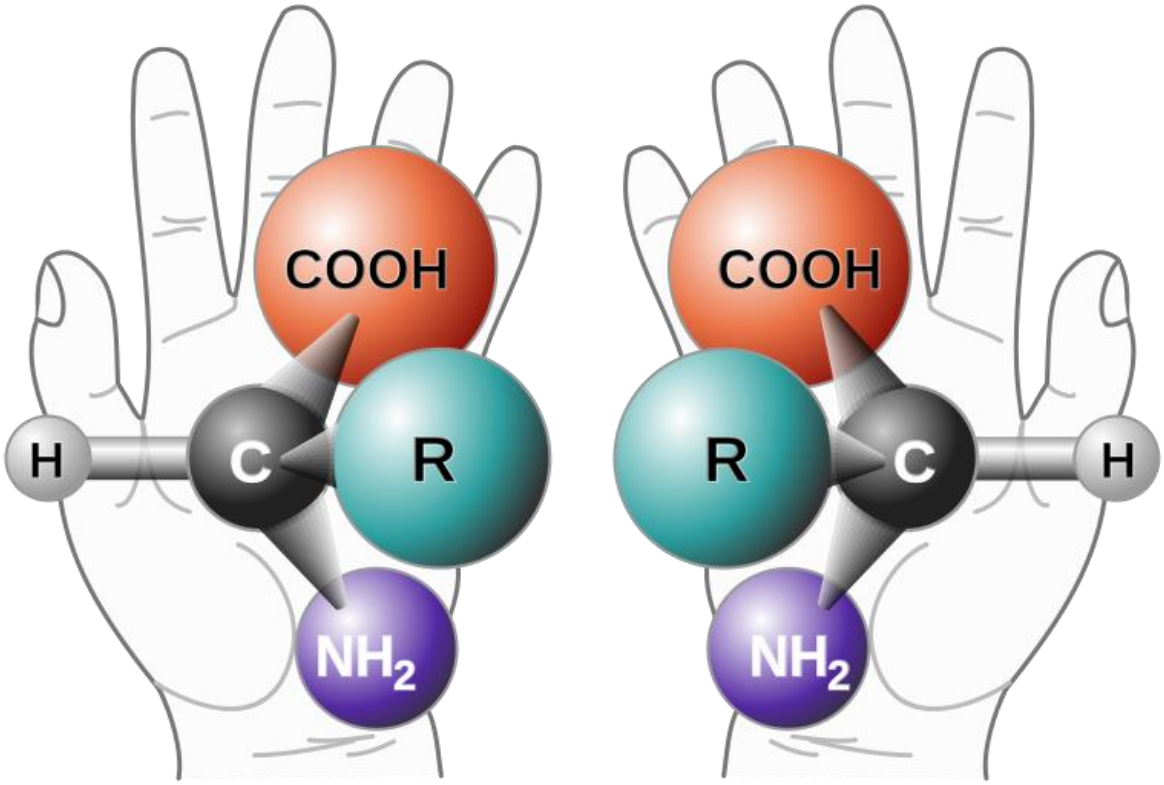

Figure 1-3: A cartoon to represent the chirality of amino acids. The L-form is used by terrestrial life, it is a mirror image of the D-form and they cannot be superimposed. (By Unknownderivative work: -- περήλιο ℗ - Chirality with hands.jpg, Public Domain, https://commons.wikimedia.org/w/index.php?curid=17071045.)

1.2.3.3. Origin of amino acids

The precise origin of amino acids and other biological molecules on Earth is not known. A laboratory simulation of the early Earth using a closed system with an atmosphere similar to that thought to exist on early Earth was exposed to electrical discharges (simulating lightning); this experiment resulted in the production of amino acids: glycine, α-alanine, β-alanine and possibly aspartic acid (chirality not specified), with an estimated total approximate yield of milligrams (Miller, 1953). Despite amino acids being empirically formed, a more favoured idea is that amino acids form on interstellar ice grains from

simpler compounds found in the interstellar medium, for example H_2O, CO_2, CO, CH_3OH and NH_3, and were delivered to Earth by meteoritic in-fall (Bernstein *et al.*, 2002; Munoz Caro *et al.*, 2002). A study by Martins *et al.* (2013) simulated shock conditions on ice mixtures analogous to comet material and found proteinogenic (and non-proteinogenic) amino acids formed; this included glycine and equal amounts of L- and D-alanine, providing a potential pathway for the formation of life through cometary impacts. However, studies in this area must be cautious as the chemical building blocks of life appear to be ubiquitous (Shock, 2002).

1.2.3.4. Carotenoids

Carotenoid pigments are widespread in biology. They are thought to act as DNA repair agents for cells that have been damaged by radiation, including ultraviolet (UV) radiation, and protect against ionising radiation (low wavelength). There is a diversity of UV screening molecules prevalent in biology, for example, in later evolution stages aromatic molecules (*e.g.* melanins in animals and flavonoids in plants) were selected in preference for carotenoids. However, in haloarchaea, the carotenoid bacterioruberin is common; it has a primary conjugated isoprenoid chain length of 13 C=C units, the molecular structure is shown in Figure 1-4. Shahmohammadi *et al.* (1998) showed a wild-type culture of *H. salinarum* could withstand a UV dose approximately five times greater than a colourless mutant culture before being reduced to a 37 % viability (D_{37}), concluding that the bacterioruberin was highly efficient in its protective function against UV. UV radiation is known to be damaging to biological molecules; protection against UV radiation would be crucial in extraterrestrial conditions, including on Mars, where UV is prevalent because of the thin CO_2 atmosphere (*e.g.* Cockell *et al.*, 2000, see Section 1.3.1.2).

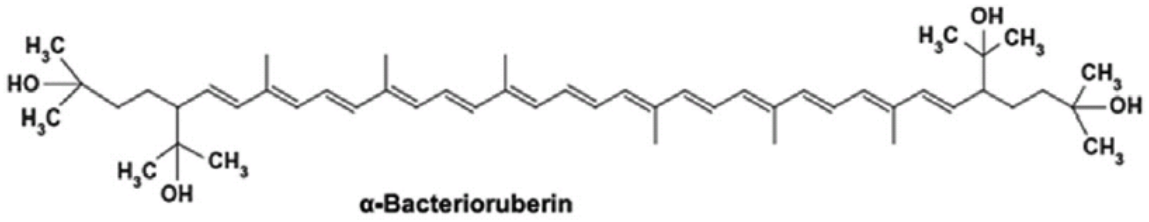

Figure 1-4: The molecular structure of bacterioruberin, the major carotenoid found in the microbial species *H. salinarum*. Adapted from Jehlička *et al.* (2013).

1.2.4. Potential locations for life elsewhere

Giordano Bruno (c. 1548 – 1600) was one of the first to suggest that the stars were suns like our own with the potential to host planets and life like our own. Life on other planetary bodies in our Solar System is something that humans have considered for many centuries. More recently, planetary bodies, previously considered unwelcoming to life, are showing new potential as habitats for extant life resulting from new data from interplanetary missions (*e.g.* Marion *et al.*, 2003; Raulin, 2008; Courtin, 2009). Environments within our Solar System can be defined by three categories: uninhabitable, uninhabited habitats and inhabited habitats as demonstrated schematically in Figure 1-5 (Cockell *et al.*, 2012). Mars has environments that can be defined by the habitability triad (*ibid*). The survival potential of biomarkers that could exist in these environments is the focus of this thesis.

1.3. Mars

There is great debate about whether Mars ever had a warm, wet climate in the past and hence was conducive to the start of biological processes and an epoch of life. Geological, geochemical, and geomorphological observations have provided definitive evidence of large, ancient fluvial systems, which may have been conducive to life (Arvidson *et al.*, 2014; Grotzinger *et al.*, 2014; McLennan *et al.*, 2014). Recent and current missions have focused on habitability and since potentially habitable environments are known to exist on Mars (*e.g.* Cockell *et al.*, 2012), the ultimate holy grail of planetary missions to Mars (or elsewhere) is discovering firm evidence that life exists elsewhere in our Universe.

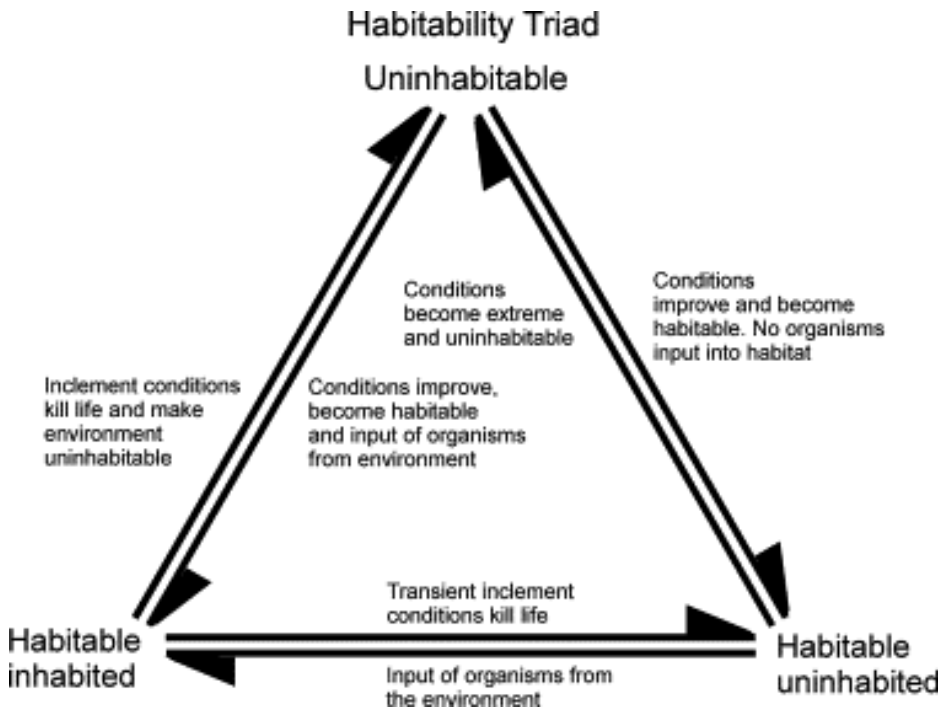

Figure 1-5: The Universe defined in terms of a triad of habitability. From Cockell *et al.* (2012).

1.3.1. Present martian environmental conditions

1.3.1.1. Surface composition

The first analysis of the martian surface *in situ* was conducted by the *Viking* landers. From observations made during the *Viking* mission, it was confirmed that the majority of the surface appeared to be igneous in nature, but with some evidence of sedimentary deposits (Binder *et al.*, 1977; Mutch *et al.*, 1977). Following on from this, the Mars Exploration Rover (MER) *Spirit* rover landed in the Gusev crater and the composition of the regolith was found to generally be similar to that of the *Viking* and *Pathfinder* results (Gellert *et al.*, 2004). However, at the landing site of the MER *Opportunity* rover, evidence was also found of hematite, an oxide mineral that can only form in the presence of water, and some of the concentrations of elemental compositions were found to vary slightly (Rieder *et al.*, 2004).

The surface is thought to be oxidising because of superoxides or peroxides that are formed because of the the exposure of the regolith to UV radiation (Yen *et al.*, 2000). The perchlorate salts discovered on the surface of Mars by the NASA *Phoenix* lander further strengthens the argument that liquid water existed on Mars. The salts would allow for the depression of the freezing point of water, and although perchlorate does not readily oxidise organics under martian surface conditions, in high temperature environments (*e.g.* lander/rover instrument ovens) the perchlorate would induce the combustion of organics (Hecht *et al.*, 2009).

Remote sensing from orbit by the Thermal Emission Spectrometer (TES) on the NASA *Mars Global Surveyor* (MGS) detected minerals with spectra that had the best fit to feldspar (namely plagioclase), clinopyroxene, olivine and sheet silicates (Christensen et al., 2000). The Sample Analysis at Mars (SAM) instrument suite on the *Curiosity* rover

analysed a martian regolith aeolian deposit detecting water, sulphur dioxide, carbon dioxide, oxygen, hydrogen chloride, hydrogen sulphide, ammonia, nitric oxide and hydrogen cyanide, suggesting possible hydrated amorphous material and perchlorate salts, clay minerals, carbonates, perchlorates and nitrogen-bearing materials (Archer *et al.*, 2014). Stern *et al.* (2015) have described the results of further analyses of an aeolian deposit and two drill samples from mudstone deposits, finding the presence of nitrogen (N) (a CHNOPS element, necessary for terrestrial life). Molecules of nitric oxide (NO), hydrogen cyanide (HCN) and trifluoro-*N*-methyl-acetamide (TFMA) were observed; the highest abundance molecule was NO, with several hundred nanomols at each test site (*ibid*). This result has implications for astrobiology, as N is necessary for key biomolecules, including amino acids.

1.3.1.2. Atmosphere, pressure, temperature and ultraviolet radiation

The atmosphere of Mars comprises mostly of carbon dioxide (CO_2), with small amounts of Argon (Ar), nitrogen (N_2), oxygen (O_2) and carbon monoxide (CO). In 2012, the *Curiosity* rover measured the volume mixing ratios of these gases over the first 105 sols of its operation on the martian surface (Mahaffy *et al.*, 2013) (where a sol is the martian equivalent of a day and is equal to approximately 24 hr 39 min 35 s). This is in close agreement with the results from other lander and rover missions to Mars; the *Viking* landers also measured fractions of other gases (Owen *et al.*, 1977), summarised in Table 1-1.

Atmospheric component	Proportion	Reference
Carbon dioxide	96.00 ± 0.7 %	
Argon	1.93 ± 0.03 %	
Nitrogen	1.89 ± 0.03 %	Mahaffy *et al.* (2013)
Oxygen	0.145 (±0.009) %	
Carbon Monoxide	< 0.1 %	
Water Vapour	0.03 %	
Neon	2.5 ppm	
Krypton	0.3 ppm	Owen *et al.* (1977)
Xenon	0.08 ppm	
Ozone	0.03 ppm	
Methane	≤ 7 ppb (transient)	Webster *et al.* (2014)

Table 1-1: Summary of gaseous components of the martian atmosphere.

Furthermore, localised methane has been remotely detected in the atmosphere (Formisano *et al.*, 2004; Mumma *et al.*, 2009) and *in situ* by the *Curiosity* rover (Webster *et al.*, 2014), though the source is not known. The source could be geological or biological (Krasnopolsky *et al.*, 2004). An ESA mission, the *ExoMars Trace Gas Orbiter* (TGO), launched in 2016, will map the global distribution of methane and other trace gases in the martian atmosphere (Zurek *et al.*, 2011). TGO aims to create an inventory of the trace gases, followed by seasonal and geographical mapping of the trace species. Furthermore, it is expected to characterise the atmospheric temperature and aerosol, water vapour and ozone components in order for circulatory models of the atmosphere circulation to be further constrained (ESA, 2014).

In 1976, *Viking* 1 and 2 recorded pressure measurements of between 6.8 and 10.1 mbar at the surface for over 700 sols, shown in Figure 1-6 (Hess *et al.*, 1980). In 2007, *in situ* pressure measurements were recorded by the *Phoenix* mission, which lasted 151 sols. It recorded a maximum pressure of 8.60 mbar, which dropped to a minimum daily average pressure of 7.24 mbar on sol 140 at a solar latitude (L_s) of 143° (Taylor *et al.*, 2010). The initial results from the REMS-P (Rover Environmental Monitoring Station, Pressure) instrument on *Curiosity* has measured a pressure range of approximately 6.9 to 8.7 mbar and has shown sol-to-sol variation, including thermal tide signatures as measured by previous *in situ* missions (Schofield *et al.*, 1997; Taylor *et al.*, 2010; Harri *et al.*, 2014). As a consequence of the extreme edifice height of Olympus Mons of 21.3 km (as measured by Mars Orbiter Laser Altimeter (MOLA) on board MGS (Smith *et al.*, 2001)) and the depth of the Hellas impact basin of 8.2 km (*ibid*), the global surface pressure range on Mars is approximately 0.5 to 12.4 mbar (Haberle *et al.*, 2001).

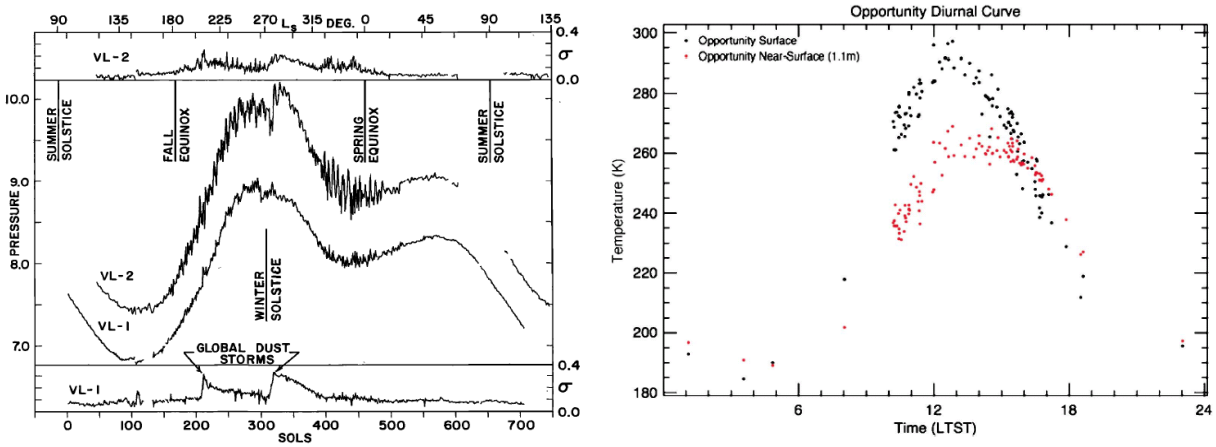

Figure 1-6: The pressure variations over 700 sols as recorded by the *Viking* landers (left), from Hess *et al.* (1980). VL-1 denotes the *Viking* 1 lander measurements and VL-2 denotes the *Viking* 2 lander measurements. The diurnal temperature variation as recorded by the *Opportunity* rover (right), from Spanovich *et al.* (2006), where LTST is the local true solar time.

A consequence of having a thin atmosphere is that there is a greater temperature range compared to Earth. The MER *Spirit* (at approximately 15° S, 185° W) and MER *Opportunity* (at approximately 2° S, 6° W) measured a temperature range of 175 - 295 K (Spanovich *et al.*, 2006), an example of the diurnal temperature cycle is shown in Figure 1-6. While some mid-sol temperatures can be similar to that of Earth, the coldest are below the lowest recorded temperature on Earth: 183.8 K, recorded in Antarctica in 1983 (Wharton, 2002). The average surface temperature on Mars is approximately 240 K (Barlow, 2008).

As a result of the composition and low density of the atmosphere, harmful UV radiation of the wavelength range 200 to 400 nm from the solar spectrum is able to reach the surface of Mars (Cockell *et al.*, 2000; Patel *et al.*, 2002; Patel *et al.*, 2004). This UV radiation range is damaging to cells, rendering them unviable in about 30 min (Cockell *et al.*, 2000). UV wavelengths < 200 nm do not reach the surface because of CO_2 absorption (*ibid*). A typical maximum flux at about midday on Mars in the equatorial region is expected to be approximately 45 W m^{-2} (Patel *et al.*, 2002). *Curiosity* has a UV sensor on board as part of the REMS instrument measuring a UV range of 200 to 380 nm and within the first 100 sols on the surface measured midday irradiances of approximately 20 W m^{-2} (Gómez-Elvira *et al.*, 2014). Although the surface of Mars is not conducive to microbial life, the near surface could offer refuge from UV radiation for microbial communities on Mars. Modelled penetration of solar radiation in regolith is only a few mm and, at worst, at the poles this extends to up to 30 cm in snow (Cockell and Raven, 2004).

Environmental component	Value	Reference
Pressure	6.8 – 10.1 mbar (*Viking* 1 and 2)	Hess *et al.* (1980)
	7.24 – 8.60 mbar (*Phoenix*)	Taylor *et al.* (2010)
	6.9 – 8.7 mbar (*Curiosity*)	Harri *et al.* (2014)
	0.5 – 12.4 mbar (hypothesised global range)	Haberle *et al.* (2001)
Temperature	175 – 295 K (MER rovers)	Spanovich *et al.* (2006)
Ultraviolet radiation	λ range: 200 – 400 nm	Cockell *et al.* (2000)
	Maximum midday, equatorial flux (modelled): 45 W m^{-2}	Patel *et al.* (2002)
	Curiosity REMS: 20 W m^{-2}	Gómez-Elvira *et al.* (2014)

Table 1-2: Summary of environmental conditions on present day Mars.

1.3.2. Water and evaporites on Mars

"Follow the water" and "seek signs of life" were two umbrella-term strategies used for determining the scientific goals for missions to Mars. The search for water on Mars has been successful: numerous evidence exists for past liquid water at the surface as recorded from orbit (*e.g.* Hynek *et al.*, 2010; Carter *et al.*, 2015, and references therein). An abundance of flowing liquid water on Mars is thought to have ceased around the late Noachian or early Hesperian (martian geological chronology described in Table 1-3), supported by older craters showing more erosion than younger craters (Craddock and Howard, 2002) and valley networks present in Noachian aged features, but fewer are present on younger features (Gulick and Baker, 1990). Chemical evidence that water

existed on Mars has been extensively collected by the Observatoire pour la Mineralogie, l'Eau, les Glaces et l'Activité (OMEGA) instrument on board the ESA mission, *Mars Express*. Phyllosilicate minerals, by analogy to formation processes on Earth, have to form in the presence of liquid water; detection of these hydrated minerals on Mars in Noachian-aged regions further supports the idea that Mars had liquid water flowing at the surface in its early history, denoted the phyllosian period by Bibring *et al.* (2006), with later periods up to and including present day Mars being generally devoid of liquid water at the surface. However, there is direct evidence for present-day water found at the poles in the polar caps as a water ice/CO_2 ice mixture (Bibring *et al.*, 2004), clouds (Wang and Ingersoll, 2002) and near surface morning fog (Möhlmann *et al.*, 2009). Evidence from rover missions include, for example, hematite found by the *Opportunity* rover at Meridiani Planum (Squyres *et al.*, 2006) and the *Curiosity* rover discovered conglomerates (grain size: 2 to 40 mm) in Gale Crater that could have only formed in the presence of a flowing liquid, most likely water (Williams *et al.*, 2013) (see Figure 1-7). There is evidence that liquid is currently present at the surface of Mars, most likely as brine. RSL have been observed on the inclines of crater walls, where dark streaks appear to grow with the warm seasons and diminish as the cold seasons approach (see Figure 1-8) (McEwen *et al.*, 2011). As examples of a non-exhaustive list of possible habitats that exist on Mars, brines and evaporites could be the residence of microbial life similar to halophilic organisms found on Earth. The interpretation of data pertaining to the detection of deposits of chlorides, sulphates and perchlorates on the present-day surface of Mars is suggestive of evidence for a water-rich evaporitic past (McKay, 1997; Gendrin *et al.*, 2005; Hecht *et al.*, 2009).

Timescale	Feature
<1 Ma	Many dune fields
⩽ few Ma	Exhumation of selected low-lat. Areas from beneath weak sedimentary layers
⩽ few Ma	Some gullies
~4–5 Ma	Last high obliquity cycle
~20 Ma	Last 2 high obliquity cycles
<20 Ma	Exhumation in Terra Meridiani hematite area
<5–50 My	Glaciation?
<10–50 Ma	Youngest lava flows, Elysium–Cerberus, Amazonis, Olympus Mons
Few Ma to 200 Ma	Unusually young major outflow channel (Marte/Athabasca Vallis)
170 Ma	Basaltic lava flows, unknown locations
100–1000 Ma	Background lava flows in Elysium, Amazonis, Cerberus, Olympus Mons
300–500 Ma	Basaltic lava flows, unknown locations
200–600 Ma	Late/mid Amazonian boundary
⩽670 Ma	Transient water exposure in nakhlite Lafayette, unknown location
~1000–2000 Ma?	Mid/early Amazonian boundary
1300 Ma	Igneous rock-forming episodes, unknown location
2000–3200 Ma	*Amazonis/Hesperian boundary*
1300–4500 Ma	No martian meteorites ⇒ uplands not coherent
3000–3500 Ma	Many outflow channels
~3200–3600 Ma?	Late/early Hesperian boundary
3000–3500 Ma	Oldest <2 km-scale craters
~3500–3700 Ma	*Hesperian/Noachian boundary*
3700–4500 Ma	Resurfacing rates 10X–100X higher than in Amazonian
3700–4500 Ma	Oldest >20 km craters
~3600–3900?	Late/mid Noachian boundary
~3800–4100?	Mid/early Noachian boundary
~3970 Ma	Carbonates in ALH 84001
~4510 Ma	Formation of martian crust and ALH 84001

Table 1-3: Summary of the martian geological chronology, adapted from Hartmann (2005).

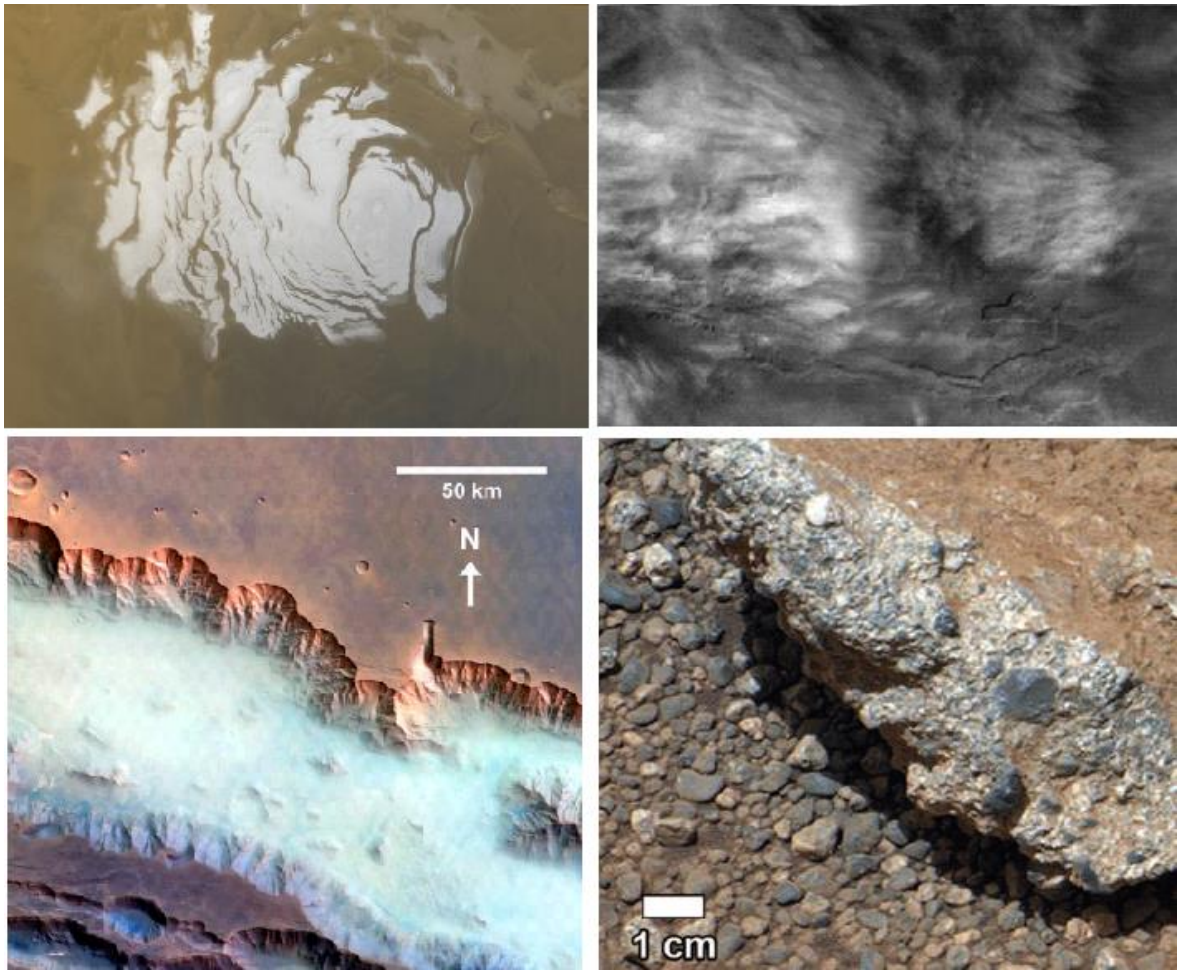

Figure 1-7: Images of evidence found for water on Mars. Clockwise from top left: water ice/CO_2 ice mixture at the southern pole, image credit: NASA/MGS; fibrous clouds north of Valles Marineris, adapted from Wang, Huiqun and Ingersoll (2002); image from the 100 mm Mastcam on the *Curiosity* rover, adapted from Williams *et al.* (2013); and fog in Valles Marineris from orbit by ESA *Mars Express*, adapted from Möhlmann *et al.* (2009).

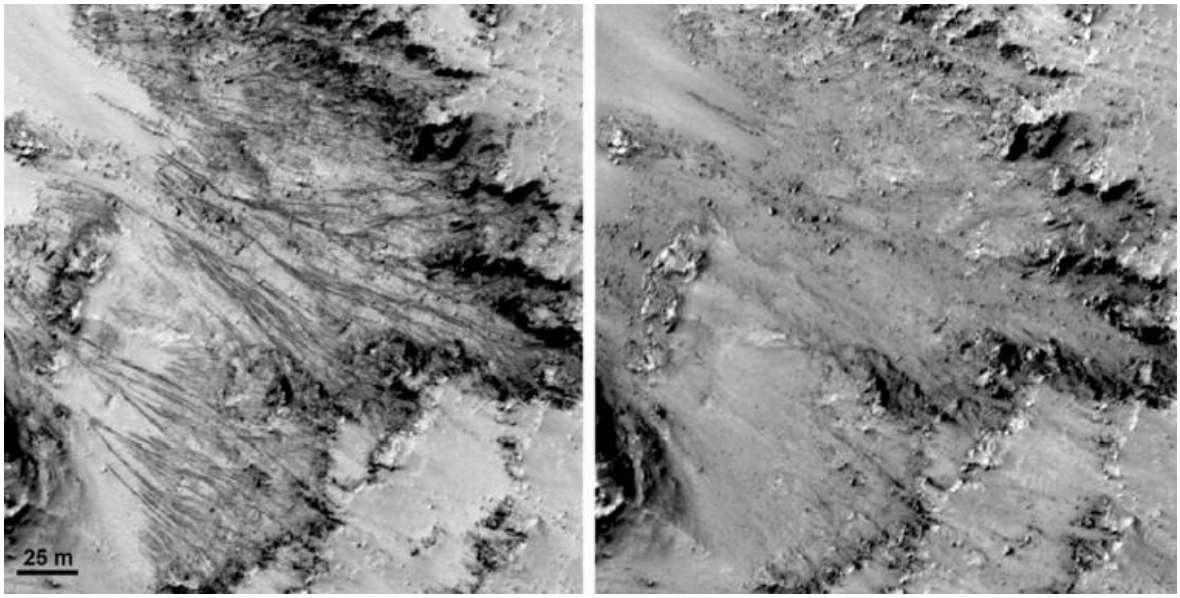

Figure 1-8: Evidence of liquid water in the form of a brine at the surface of Mars. The features are denoted Recurring Slope Lineae (RSL) as they appear to be seasonal. Streaks that grow during the spring/summer are at their darkest in late summer (left) and diminish during the winter, leaving almost no evidence by the beginning of the next spring (right).

1.3.2.1. Halite and other evaporites on Mars

The current environmental conditions at the surface of Mars are not conducive to the stability of pure liquid water. The temperature range at the surface as measured by the *Spirit* and *Opportunity* rovers is 175 to 295 K (Spanovich *et al.*, 2006) and the surface pressure range from *in situ* measurements is known to be between 6.8 and 10.1 mbar (Hess *et al.*, 1980; Taylor *et al.*, 2010). The pressure at the triple point of water is 6.11 mbar (see Figure 1-9); although the pressure on the Mars surface is above this pressure in some places, for water to remain stable as liquid water the temperature must be between 273 and 283 K (Haberle *et al.*, 2001), but the diurnal temperature range is often outside of this (*e.g.* Kieffer *et al.*, 1976; Spanovich *et al.*, 2006). As described above in Section 1.3.2 stable liquid water is thought to have existed on the surface in the early history of Mars (*e.g.* Bibring *et al.*, 2006; Hynek *et al.*, 2010).

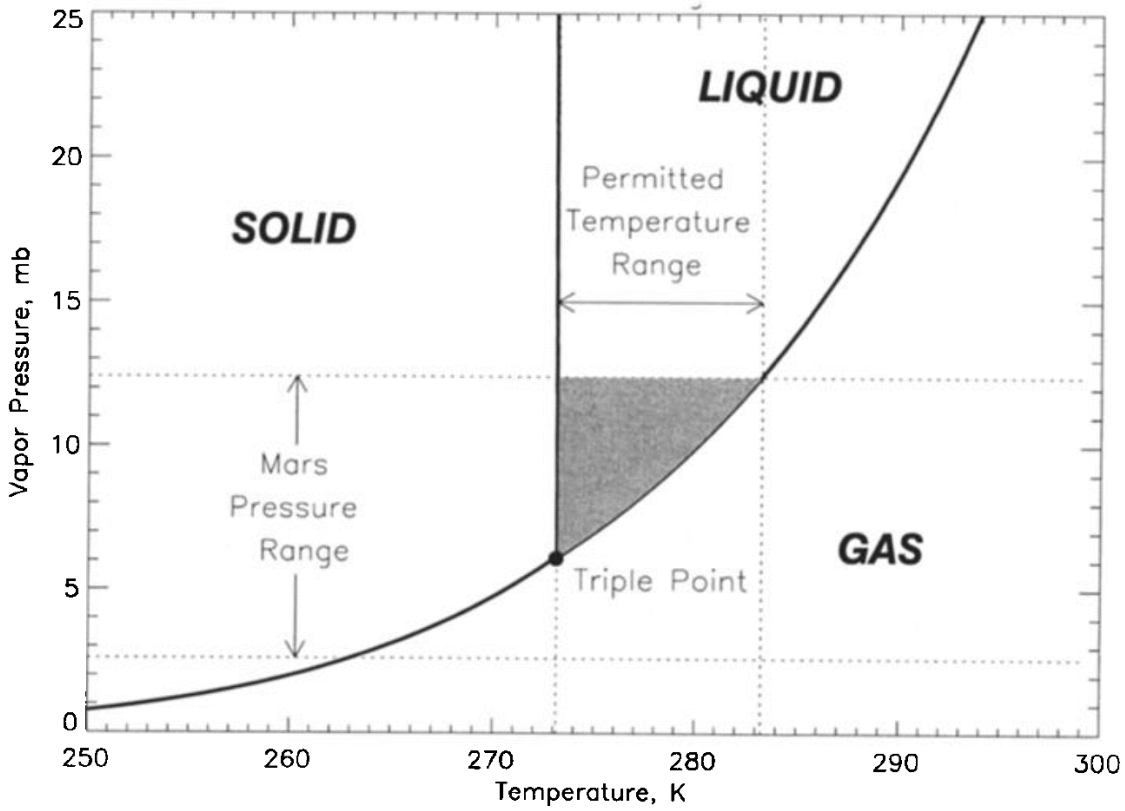

Figure 1-9: Pressure-temperature space phase diagram for water. The greyed out area represents the pressure and temperature ranges on Mars in which it is possible for liquid water to form. From Haberle *et al.* (2001).

As the stability, and hence availability, of liquid water on the surface greatly decreased evaporite environments are thought to have formed on Mars.

Direct evidence for brines at the near surface at Gale Crater has been reported by Martin-Torres *et al.* (2015) using the Dynamic Albedo of Neutrons (DAN) and SAM instruments on board the *Curiosity* rover. Data recorded throughout the length of the mission have shown that there is a transient diurnal presence of brines; the process of deliquescence is creating these brines, the evidence suggests an active regolith-atmosphere interface exchange with water in the top 15 cm of regolith (*ibid*). Furthermore, the rover is

situated near the equator, so for brines to be commonplace suggests the rest of the planet may have an abundance of available brine at the near surface (*ibid*).

Evaporites, indicative of an ancient aqueous environment, have been found on Mars, including those found by the *Opportunity* rover in Meridiani Planum; there were high proportions of sulphate salts, namely jarosite (the abundance of sulphur was a factor of approximately five greater than at Gusev crater, as discovered by the *Spirit* rover) (Squyres *et al.*, 2004). Hematite spherules were also found, which further suggests an ancient aqueous environment at this site. Squyres *et al.* (2004) state that there is adequate sodium (Na) available for halite, though double salts containing Na^+ such as bloedite, vanthoffite or glauberite may also have been found in the outcrop. Furthermore, it was proposed that the geological record pertaining to water activity at Meridiani Planum indicates that conditions were suitable for biological activity for a period of time during martian history (*ibid*). Further evidence was found during the first two years of the *Opportunity* rover mission, possible halite was located in the form of cubic crystal polymorphs in the target rock "Lemon Rind", just north of Erebus crater (Squyres *et al.*, 2006). The presence of evaporites on Mars provides a potential habitat for microbial life.

Denoted the SNC meteorites because of their terrestrial fall sites, Shergahti (India), El-Nakhla (Egypt) and Chassigny (France); the SNC meteorites are volcanic in origin and have different compositions: Shergottites are basaltic, lherzolitic, olivine-orthopyroxene and olivine-phyric; the nakhlites are olivine-rich and the chassignites are dunites (Barlow, 2008). Oxygen isotope analysis of the meteorites showed the SNCs were distinct from lunar, terrestrial and other meteorites, hence are suggested to be from Mars (Clayton and Mayeda, 1996). Evidence of halite on Mars was found in the meteorite Nakhla, an SNC meteorite (see Figure 1-10) (Bridges and Grady, 1999). Crystals of halite found within the Nakhla meteorite were up to 400 μm in diameter, which corresponds to possibly one or

more crystals; the halite is not thought to be terrestrial contamination as the meteorite was recovered quickly, appeared unweathered (no time for weathering to occur), the samples were never in a terrestrial salt-rich environment and the halite has no apparent connection to the fusion crust (*ibid*). Furthermore, the siderite surrounding the halite had high $\delta^{13}C$ values, which is consistent with a martian origin (*ibid*). Where $\delta^{13}C$ is a measure of how the ratio of ^{13}C to ^{12}C varies with different geological, physical and biological processes, so can be used to discriminate between groups of samples or geochemical reservoirs; the variation is a per mil (‰, parts per thousand) deviation from a terrestrial standard (belemnite carbon standard).

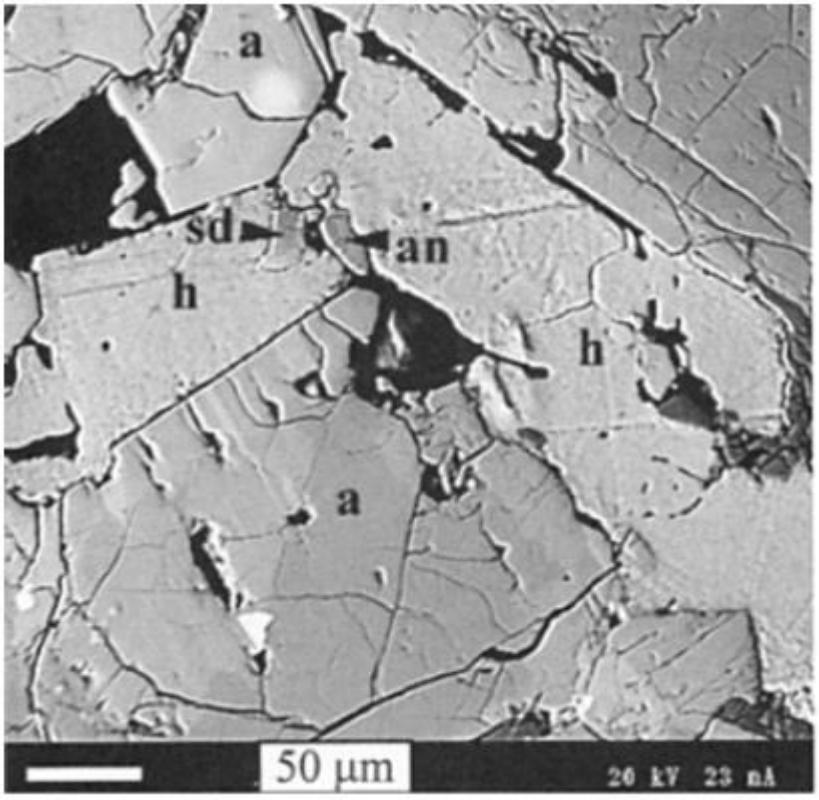

Figure 1-10: Backscattered electron images of Nakhla sections. Siderite and anhydrite grains created a boundary between two halite grains. Adapted from Bridges and Grady (1999); h = halite, sd = siderite, an = anhydrite and a = augite.

In the natural crystallisation of halite, ‘hopper’ growth is the standard morphology, concentric squares, with steps from the smallest dimension square at the centre up to the largest dimension square at the outermost surface. Figure 1-11 shows halite crystals, hopper growth and the fluid inclusions that the crystals contain. Pasteris *et al.* (2006) conducted a study to determine whether synthesised organic macromolecules, similar in size to proteins, lipoproteins and viruses, would be incorporated into the structure of the halite as it forms. It was found that the macromolecules were not incorporated into the halite structure, but were entombed in fluid inclusions or onto the hopper-enhanced surface and along discontinuities within the crystal (*ibid*). This is also true of microbial cells when experimentally entombed in halite (*e.g.* Fendrihan *et al.*, 2009b; Stan-Lotter *et al.*, 2010; Fendrihan *et al.*, 2012), shown in Figure 1-12. Hence, fluid inclusions provide a potential habitat/shelter for microbes within halite crystals. The fluid would be likely to contain some nutrients that could be used by the microbes towards growth and reproduction or may just sustain survival until more favourable conditions arise.

Though if the evaporite exists in an area of freeze-thaw conditions, the evaporation-melting cycle may provide a renewed reservoir of nutrients (*e.g.* Schimel and Clein, 1996; Sjursen *et al.*, 2005; Wipf *et al.*, 2015).

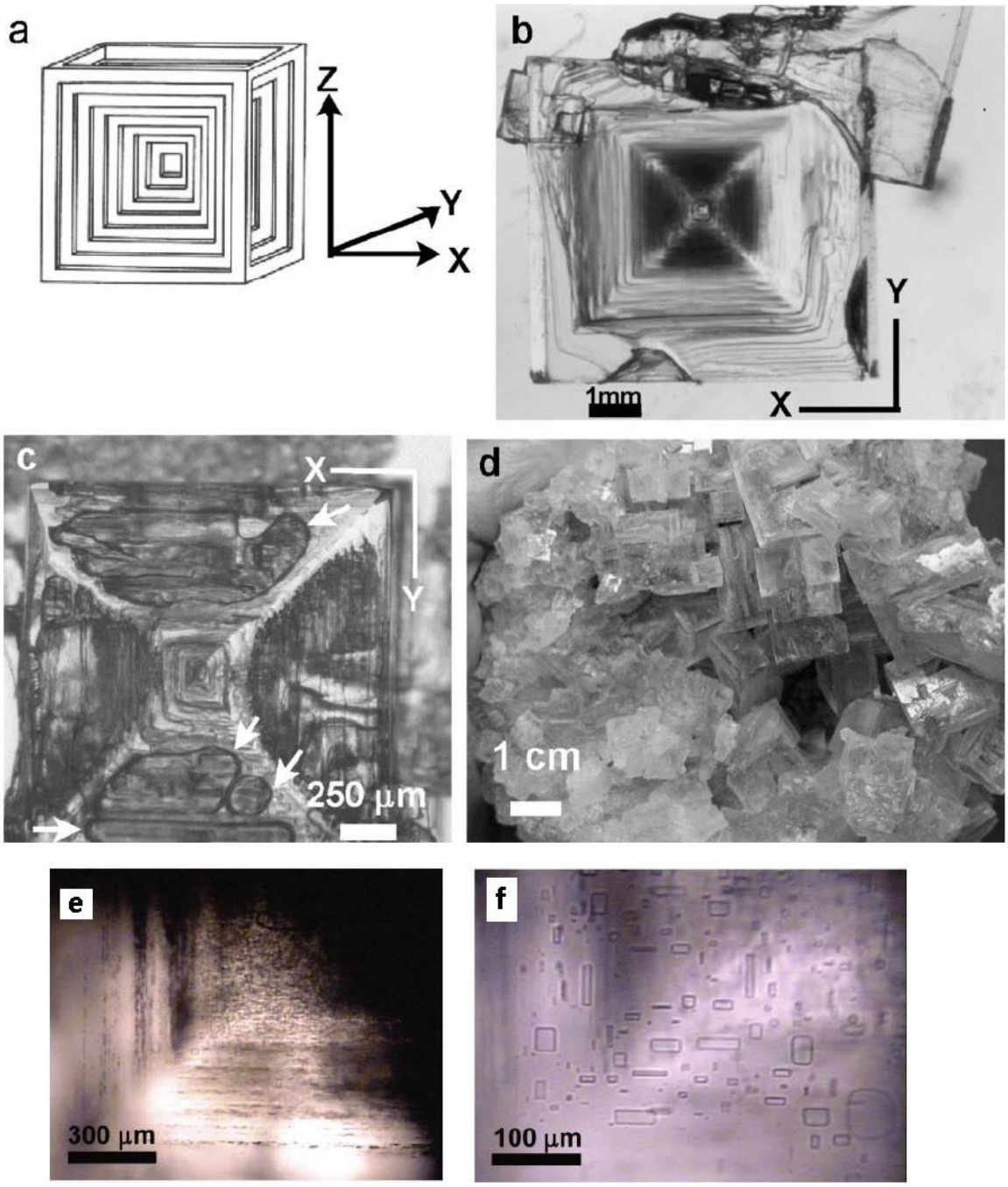

Figure 1-11: (a) A cartoon of hopper formation in halite crystals from http://www.minerals.net/mineral_glossary/hopper.aspx and the definition of the coordinate system used in this study; (b) and (c) laboratory-grown halite crystal, where the arrows in (c) indicate fluid-filled areas; (d) natural halite from Searles Lake, California, USA; (e) and (f) microscopic images of halite crystals showing the minute fluid inclusions that are arranged parallel to the direction of crystal growth. Adapted from Pasteris *et al.* (2006).

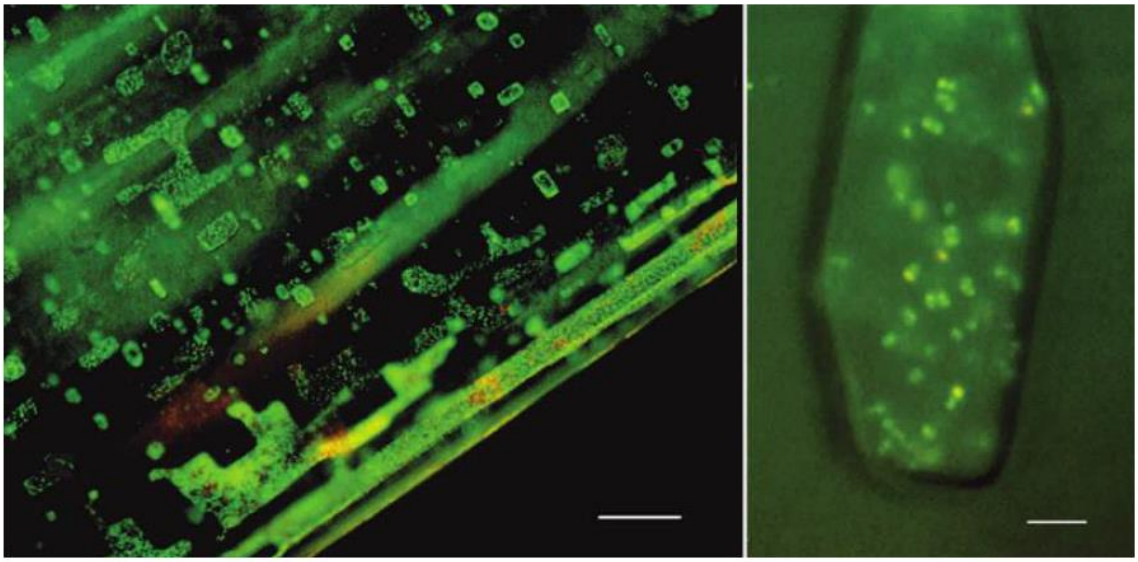

Figure 1-12: Microscopy images of fluorescence stained microbes within fluid inclusions in halite crystals. Individual cells can be seen in the right hand image. The bars represent 25 µm (left) and 5 µm (right). From Fendrihan *et al.* (2009a).

Additionally, halite is known to attenuate UV radiation, thus providing some protection to microbes and nutrients from harmful UV radiation experienced at the surface of Mars; Fendrihan *et al.* (2009a) found a 50 to 70 % reduction in transmittance in the UV range 200 to 400 nm. The UV radiation is absorbed by colour centres in the crystal lattice, where a colour centre is described by an ordinary lattice vacancy; in halite, this does not affect visible absorption, but absorbs in the UV instead (Kittel, 2005).

1.3.3. Organic molecules on Mars

Given the high abundance of organic molecules on the Earth, it is not unreasonable to expect Mars also to have organic molecule reserves. One of the main science goals for the *Curiosity* rover is to find and catalogue organic molecules at the surface and in the near surface (Grotzinger *et al.*, 2012). The previously unsuccessful (inconclusive) *in situ* search for organic molecules in the regolith on Mars (see Section 1.3.4) has culminated with an

announcement that the *Curiosity* rover found localised and temporal measurements of a maximum 7 ppb of methane in the atmosphere surrounding the rover, where the background is ten times less than these readings (Webster *et al.*, 2014).

It is estimated that there is also an influx of organic material to Mars from comets, meteorites and dust particles of approximately 10^6 kg yr^{-1} (Flynn, 1996). Possible contributors include: extraterrestrial organic molecules, such as amino acids, hydrogen cyanide (HCN), formaldehyde (H_2CO), polycyclic aromatic hydrocarbons (PAHs) and purines (also pre-cursors for life), have been detected in the interstellar medium (see, Ehrenfreund and Charnley, 2000, for a review and references therein), comets (see, Crovisier, 2005, for a review), meteorites (*e.g.* Lawless *et al.*, 1971; Pizzarello and Cronin, 1998; Gilmour, 2003).

Furthermore, it is possible that there is *in situ* production of martian organic molecules via past and present mechanisms, similar to those experienced on early Earth: coronal discharge, lightning and UV radiation (Chyba and Sagan, 1992). Between the two *Viking* landers, four samples of the martian surface were taken, detecting 0.1 – 1.0 wt% water, 0.05 – 0.6 ppm CO_2, organics benzene and toluene, chloromethane and dichloromethane (Biemann *et al.*, 1976; 1977). Regardless of the detection of organic molecules and the same molecules not being detected in the blank runs to the same magnitude, it was concluded that they were terrestrial contaminants and that no organics of martian origin had been found (*ibid*). On board the *Phoenix* lander an instrument called the Thermal and Evolved Gas Analyzer (TEGA) was used to search for organics at the landing site, but none were found (Sutter *et al.*, 2009).

Methane is the simplest alkane and it was thought to have been remotely detected on Mars using various methods; detection from orbit by the Planetary Fourier Spectrometer (PFS)

on board *Mars Express*, globally varying amounts between 0 – 30 ppbv, with a global average of 10 ± 5 ppbv (Formisano *et al.*, 2004), whereas terrestrial ground-based telescopes detected a mixing ratio of 10 ± 3 ppbv (Krasnopolsky *et al.*, 2004). The global variations suggest that there are sources and sinks of the methane; the global variation was confirmed by Mumma *et al.* (2009), who assumed a seasonal cycle, opposed to periodic release, inferred a rate of production of > 0.63 kg s^{-1}, with oxidation by contact with the regolith and photodestruction suggested as possible sinks. Methane can be produced by biotic and abiotic means; Zahnle *et al.* (2011) examined the arguments against the reported methane presence on Mars: the spectral data from *Mars Express* are at the limits of the resolution of the instrument, with the methane signal confined only to a single resolution element, hence it was not entirely convincing; ground-based observations could be contaminated by telluric methane interference, martian isotopic CO_2 lines or what Zahnle *et al.* judged to be an instrumental artefact. Despite these arguments the remote observations were supported by the recent measurements of methane of a maximum of 7 ppb by the *Curiosity* rover (Webster *et al.*, 2014).

1.3.4. Previous and current life detection missions

The first mission with the intention to detect life at the surface of Mars was the *Viking* landers in the late 1970s. Using three experiments: a gas exchange, pyrolytic release and a labelled release with labelled ^{14}C organics, the *Viking* landers were expected to be able to detect molecules pertaining to life on Mars. The results were inconclusive as the sensitivity of the Gas Chromatography Mass Spectrometer (GCMS) meant that the carbon fixed in the experiments (if any) would have been below detection limits (Horowitz *et al.*, 1977). It was not possible to discriminate between possible biological and non-biological processes that could have produced the results that were seen (Klein, 1977). However, more recently

since the discovery of perchlorate salts by the *Phoenix* lander (Hecht *et al.*, 2009), reanalysis of the *Viking* results have suggested that organics may have been detected, though with some controversy surrounding this argument (Navarro-González *et al.*, 2010; Biemann and Bada, 2011; Navarro-González and McKay, 2011). Navarro-González *et al.* (2010) mixed and heated a martian analogue from the Atacama Desert that contained 32 ± 6 ppm of organic carbon with magnesium perchlorate, resulting in almost all of the organics being decomposed to water and carbon dioxide and with some chlorination products, specifically chloromethane and dichloromethane – the products seen in the *Viking* results – leading Navarro-González *et al*. to conclude that organics were present in the *Viking* samples. However, Biemann and Bada (2011) were not satisfied that the terrestrial analogue experiment compared to the *Viking* landing sites or that it was a good model for the *Viking* results, so countered these claims with points such as: Navarro-González *et al*. had assumed that perchlorate was present at the two *Viking* landing sites and the experimental set-up used did not correspond to the one used on the landers, hence could not represent the *Viking* results. Navarro-González and McKay (2011) replied stating that Biemann and Bada did not demonstrate any experimental or theoretical justifications for their objections. Therefore, Navarro-González and McKay concluded that their results were robust enough to state that both perchlorates and organics are present in the martian regolith at mid latitudes and that their results are important for the design of future instruments and methods to search for organics on Mars. Though the assumption that there is perchlorate at the *Viking* landing sites could be unfounded, it will be important on future missions to consider the effect of perchlorates on organics if samples are to be heated.

Beagle 2 was an unsuccessful British-led mission, which launched as part of the ESA *Mars Express* mission in 2003 (Sims *et al.*, 1999). The Gas Analysis Package (GAP) was the

main instrument with the scientific objective of searching for life signatures. Samples were to be heated in ovens and the CO_2 released would have been delivered to a mass spectrometer to measure the ^{12}C to ^{13}C ratio (*e.g.* Wright *et al.*, 2003; Pullan *et al.*, 2004), which can be used to distinguish biological processes. Furthermore, the various temperatures at which CO_2 is released are unique to the carbon material, allowing identification of the molecules within the regolith (*ibid*). It also carried various instruments designed to characterise the astrobiologically relevant surface environment, including a UV sensor (Patel *et al.*, 2002).

Though not directly searching for life, the *Curiosity* rover is searching for evidence that Mars has environments that are presently, or were in the past, habitable. The biological science objectives include: detecting complex organic molecules, searching for and creating an inventory of the CHNOPS elements and attempt to identify features that could be suggestive of biological processes (Grotzinger *et al.*, 2012).

Launched in 2016, on arrival at Mars the TGO orbiter will characterise the trace gases in the martian atmosphere to a precision not yet achieved (Zurek *et al.*, 2011). Following this, ESA-Roscosmos plans to launch *ExoMars* in 2020, a rover designed to search directly for signs of life. Future missions to Mars will have a Raman spectrometer as part of the science package, including the *ExoMars* rover with the Raman Laser Spectrometer (RLS) instrument, to achieve life detection science goals. The NASA *Mars 2020* rover mission has a proposed deep UV (DUV, 248.6 nm) Raman spectrometer as part of the instrument package SHERLOC (Scanning Habitable Environments with Raman and Luminescence for Organics and Chemicals) (Beegle *et al.*, 2014).

1.4. Experimental studies of biomarkers and microbes under martian and extraterrestrial conditions

The following section details previous work that has been undertaken to understand how amino acids, which can be used as a biomarker, and microbes survive exposure to simulated martian conditions. Raman spectroscopy is the main analytical technique used in this study and will be described in detail in Section 1.5. This section reviews the current status of investigations into amino acids and microbes under simulated martian conditions, providing a brief background.

1.4.1. Previous investigations of amino acids

Racemisation is the process where an excess of one enantiomer of a molecule partly converts to the other enantiomer so there are equal amounts of L- and D-enantiomers of the molecule. L-amino acids are used in terrestrial biology (see Section 1.2.3.2), so after eliminating the possibility of terrestrial contamination (by comparison to blank runs), discovering an excess of L-amino acids on Mars could suggest that life arose on either Mars or Earth and was transferred between the two by means of ejected material from large impacts (Melosh, 1988); although an L-amino acid-based biology could arise independently on both planetary bodies. However, the discovery of an excess of D-amino acids would suggest that life had independently arisen on Mars. These chiral excesses are considered a biomarker (McKay, 2004). However, if racemisation occurs, this evidence would be lost. Bada and McDonald (1995) used kinetic data to estimate the amount of time needed to racemate an enantiomer of amino acids under martian conditions. Of the terrestrial α-amino acids, aspartic acid was used as the lower limit for time scales because of its fast racemisation rate. Under dry, cold conditions (no liquid water, temperatures of

< 250 K) the racemisation half-life of aspartic acid was found to be more than a billion years, indicating that a homochiral signature could still be detected long after an extinction event. However, if warmer conditions existed, allowing liquid water to be in contact with the molecules, the racemisation was found to accelerate, with the half-life reduced to between 8×10^2 yr (300 K) and 4×10^6 yr (250 K); hence if warm, wet conditions persisted on Mars for several millions of years after an extinction event, any excess of homochiral amino acids from martian life would be completely racemised (*ibid*). These racemisation calculations are based on terrestrial surface chemistry and rely on the amino acids being in the near surface at a depth below the effects of UV, ionising radiation and an oxidising environment that affect the top few metres of regolith. Furthermore, this has implications for geological features such as craters that may have been filled or partly filled with liquid water, or had water running into them at some time, so any enantiomer excess biomarker there may have been destroyed. The *Curiosity* rover is currently exploring Gale Crater, which is known to have a fluvial fan feature (*i.e.* the water that created this feature may have had an effect on the racemisation rate of any amino acids that may be present) and sedimentary rocks creating a feature at the centre of the crater known as Mount Sharp. *Curiosity* is searching for organic molecules and has the ability to detect volatile chiral molecules using a chiral GCMS column (Freissinet *et al.*, 2013); future planetary missions may also have instrumentation to detect chiral amino acids.

Environmental conditions on present day Mars (described in Section 1.3.1 above) are damaging to organic molecules and their biomarker signatures. UV radiation on Mars is damaging to organic molecules (*e.g.* Cockell *et al.*, 2000), hence experiments to test, for example, the survivability of these molecules have been performed. Ten Kate *et al*. (2005) investigated the exposure of thin films of glycine and D-alanine to Mars-like UV radiation (though not any other Mars-like environmental conditions) to calculate the rate of

photodestruction. A microwave-excited hydrogen flow lamp and deuterium discharge lamp provided the UV source in the wavelength range 120 to 180 nm and 190 to 400 nm, respectively. The amino acids were exposed to the UV radiation at room temperature within a vacuum chamber (average pressure of 4×10^{-6} mbar) and monitored using an infrared (IR) spectrometer during the irradiation. The half-lives of glycine and D-alanine when exposed to the deuterium lamp were approximately 1.8×10^{6} and 2.9×10^{5} s (0.057 and 0.009 yr), respectively. By extrapolation from these results, ten Kate *et al* found that a concentration of 1 ppb of amino acids in the martian regolith would degrade to a concentration of 1 ppt in 5×10^{6} yr for D-alanine and 4×10^{7} yr for glycine; this suggests that amino acids, which may have existed on early Mars, could still be present on the surface at sub ppt levels (*ibid*). Further to this, in a comparative study, with the inclusion of other martian environmental conditions, glycine was exposed to (a) Mars-like atmospheric composition (CO_2) and pressure (~ 7 mbar) conditions at room temperature and (b) to 210 K under a vacuum (~ 10^{-7} mbar); both sets of experiments were exposed to UV radiation (deuterium discharge lamp, 190 to 325 nm) (ten Kate *et al.*, 2006). Destruction rates of the glycine thin films were not affected by the presence of a 7 mbar CO_2 atmosphere, but the cooled samples had their destruction rate slowed by a factor of 7, with an extrapolated half-life of approximately 10^{8} yr on the martian surface (1 ppb mixing ratio), suggesting that low temperatures may stabilise amino acid molecules, which could be important when considering the origin of life (*ibid*). The uncertainty on the result for the half-life of glycine in a low temperature environment on Mars given by ten Kate *et al* (2006) was almost one magnitude larger than the result itself ($0.9 \pm 7.5 \times 10^{6}$ s), which does not display great confidence in the original result. Although the low temperature experiment shows a slowed destruction rate of the amino acids, this experiment was only repeated twice; further repeats may have demonstrated different results and reduced the large uncertainty. Furthermore, in the results reported by ten Kate *et al*, the amino acids

were not exposed to the full complement of martian environmental conditions; for example, temperature and martian atmospheric pressure were never tested together. For a terrestrial comparison, amino acids have been detected to 100,000 ppb in samples from a desert using GCMS (Martins *et al.*, 2011).

The experiments described above placed samples of amino acids on silicon discs (ten Kate *et al.*, 2005; 2006). For more in depth understanding of potential conditions on Mars for organic molecules, other work has introduced analogue martian regoliths into simulated martian conditions. Garry *et al.* (2006) used high-performance liquid chromatography (HPLC) to analyse the native amino acid content of established martian analogue regoliths JSC Mars-1 (Allen *et al.*, 1998) (described in more detail in Section 2.3.4.1) and Salten Skov (Nørnberg *et al.*, 2004). Of the naturally occurring amino acids in these regoliths, the α-amino acids found included; L-aspartic acid, L-glutamic acid, L-serine, glycine, L-alanine, L-valine and L-leucine. When the analogue regoliths were exposed to a vacuum (~ 10^{-5} mbar) and Mars-like UV radiation (190 to 360 nm) amino acids were generated, possibly by the degradation products from extant biota that resided in the regolith, *i.e.* the amino acids measured are indicative of the degradation of cell walls (Garry *et al.*, 2006).

Johnson *et al.* (2011) conducted a study into the survival of various microorganisms and amino acids; they inoculated 100 μg g^{-1} of amino acids into an analogue regolith called the Indiana-Mars analogue regolith (I-MAR) and found that the half-life of L-alanine, L-valine, L-aspartic acid, L-glutamic acid and glycine exposed to simulated martian conditions was 132 ± 87 days and 477 ± 295 days with and without exposure to UV, respectively (where the martian conditions here were: the diurnal cycle at a low-latitude, low-elevation region of present day Mars was mimicked, temperature: −40.4 to 24 °C; pressure: 10 to 22 mbar; UV flux: 19.3 W m^{-2}, xenon arc lamp wavelength range 200 to 400 nm; and a 48.6 % CO_2, 50.0 % Ar plus trace gases atmosphere. For comparison, the current martian environmental

factors are summarised in Section 1.3.1.2). The amino acids were sampled from the exposed surface and at 1 cm increments below the surface (maximum depth, 3 cm). The half-life of the amino acids does increase with regolith depth; however, the uncertainty of these results is quite large with respect to the calculated half-life values because of the loss of the amino acids over time and depth using this method.

Furthermore, the survival of amino acids has been investigated in Low Earth Orbit (LEO, approximately 300 km altitude). The PROCESS experiment was flown on board the International Space Station (ISS) and used filtered solar radiation (quartz window, 190 to 400 nm) to simulate the UV radiation at the surface of Mars (Noblet *et al.*, 2012). The samples were also subjected to the other environmental factors of spaceflight, such as a temperature range of −21 to 61 °C and cosmic radiation. Glycine and serine (chirality not specified), and some carboxylic acids, were sealed in sample cylinders under a 1.5 bar argon atmosphere and attached to the exterior of the Columbus module for 1.5 yr. The samples were analysed pre- and post-exposure using Fourier transform infrared (FTIR) spectrometry. Laboratory experiments extrapolated to the conditions on board the ISS for the Mars-like filtered samples suggest that the half-life on Mars of glycine and serine would be 51.3 ± 1.3 hr and 73.9 ± 10.8 hr, respectively; the post-exposure FTIR spectra of the organic molecules showed no spectral features measured in the pre-exposure spectra, where the diminished spectral features was indicative of complete photodestruction of the molecules (*ibid*). These results contradict the other studies detailed above as the half-lives are much shorter, only hours to destroy the biomarker signature compared to fractions of years or longer. However, the range of half-lives reported is great, spanning hours to millions of years depending on the conditions to which the amino acids are exposed.

In summary, initial experiments suggested that the lifetime of amino acids on the surface of Mars could extend to the equivalent of geological time periods when decoupled from

some martian conditions such as UV radiation and/or regolith (*e.g.* ten Kate *et al.*, 2005). However, further experimentation has shown that the presence of filtered solar radiation reduces the half-life to hours or, at best, days (extrapolation) (*e.g.* ten Kate *et al.*, 2006; Johnson *et al.*, 2011). The PROCESS experiment on board the ISS did not account for heating and cooling that would have occurred in LEO, so when coupled with Mars-like temperatures, the half-life may increase as seen in earlier experiments.

1.4.2. Previous investigations of microbes

Microbes entombed in an environment such as fluid inclusions within halite crystals is analogous to possible habitats/refuges on current day Mars. Halite (NaCl) has a cubic crystal system (*i.e.* the unit cell forms a cube), hence when halite is formed naturally or in the laboratory it generally grows in cuboid shapes. Naturally occurring halite tends to be clear or white in appearance, but can have impurities in the crystal structure that cause it to have a colour including blue, red, and yellow.

Pasteris *et al.* (2006) found the crystal structure of halite did not easily allow for the incorporation of nanoparticles that were representative (of size) of biological macromolecules/nanostructures including proteins and viruses. The nanoparticles had functional groups including carboxylic acids, amides and amines, which are present in amino acids, peptides and proteins (*ibid*). A solution doped with the nanoparticles was allowed to dry at different rates, producing different sized halite crystals; independent of the crystal size, the nanoparticles were not incorporated into the cubic crystalline structure, but accumulated in fluid inclusions, along discontinuities and the surface of the crystals instead (*ibid*). This result is true with larger biological structures such as archaeal and

bacterial cells, which also become entombed in fluid inclusions opposed to within the crystalline structure, as described below.

Adamski *et al.* (2006) genetically modified a non-halotolerant bacterial species, *Pseudomonas aeruginosa*, and inoculated the culture into an NaCl saturated solution that was allowed to precipitate as halite crystals. The genetic modification caused the cells to produce green fluorescent protein, which allowed the authors to observe that cells were still viable after 13 months of entrapment; this has implications for non-halophilic bacteria and archaea being preserved in ancient terrestrial halite deposits (*ibid*); if viable cells can survive in laboratory grown crystals, it is possible that similar life that may have arisen on Mars could also survive long term within evaporitic deposits. Conversely, this laboratory test was only 13 months long, further experimentation on longevity is required. Furthermore, culturing from the long term entombed bacteria was inconclusive, as only cells that did not produce the green fluorescent protein generated colonies, which could suggest contamination or that the cells had lost the ability to produce the protein through mutation (*ibid*). Outside of the laboratory, it is thought that halophilic microbes could survive millions of years of entombment, though this is not confirmed (Grant *et al.*, 1998).

Moeller *et al.* (2010) exposed an archaeal strain, *Natronomonas pharaonis*, to simulated UV conditions that were expected on the early Earth (where UV $\lambda > 220$ nm could penetrate the terrestrial atmosphere) to assess its photobiological response. The F_{10} value (the fluence required to reduce the original colony to a 90 % loss of viability) for the cells exposed to early Earth simulated UV wavelengths was 91.2 ± 8.7 J m^{-2}, equivalent to 1.75 % of the F_{10} value for present day terrestrial UV wavelengths. *N. pharaonis* was not as tolerant to a monochromatic UVC wavelength (254 nm, F_{10} 52.3 ± 8.0 J m^{-2}) as the halophile *H. salinarum*, which has an F_{10} of approximately 110 to 160 J m^{-2} (McCready and Marcello, 2003; Crowley *et al.*, 2006), but in comparison to other microbes it is

moderately resistant to UV. For example, *Deinococcus radiodurans* (F_{10} 660 ± 50 J m^{-2}) was highly resistant (Bauermeister *et al.*, 2009) and *Shewanella oneidensis* (F_{10} < 7 J m^{-2}) had a low resistance to monochromatic UVC radiation (Qiu *et al.*, 2004). Radiation experiments of this nature can be analogous to conditions on present day Mars, where the UV conditions at the surface are very biologically damaging. *H. salinarum* was exposed to UVC by Martin *et al.* (2000) where a dose of 154.3 J m^{-2} resulted in a 1.1 % survival. This dose is approximately 30 % of the average daily dose expected at the Mars surface, indicating that non-shielded halophilic microbes would not survive at the surface of Mars for longer than a portion of a sol. The microbial studies described here are relevant to this work, but are part of a non-exhaustive list of studies of microbes in extreme environments (for a review see, Lage *et al.* (2012)). These studies are analogous to Mars and relevant to astrobiology, and hence, future planetary missions. The next section on Raman spectroscopy provides a focus of past studies that provide further background to the work conducted in this study.

1.5. Raman spectroscopy

1.5.1. Introduction

Discovered in the late 1920s, this active method of spectroscopy has only recently become a widespread tool since efficient lasers were invented. The Raman effect is the inelastic scattered component of light, observed when the frequency of the incident radiation is shifted because of the vibrational bonds in molecules. Laser excitation wavelengths in the near-UV to near-IR are used to exploit this effect.

Advantages to Raman spectroscopy include: it can be used to detect both minerals and biological molecules, samples requiring little to no preparation before analysis and water

has a broad band feature above 3000 cm^{-1}, so does not interfere in the organic molecule 'fingerprint' region (500 to 1700 cm^{-1}) allowing aqueous solutions to be examined (Auer and Skinner, 2008). Furthermore, it is important to note that Raman spectroscopy is referred to as non-destructive (here and in cited sources), which is generally true when care is taken to consider the laser power applied to the sample, especially during analysis of organic compounds; *i.e.* the power of the laser can damage or alter the sample, but the laser power at which damage occurs is related to each sample type. A disadvantage is that Raman spectroscopy is unable to differentiate between the chirality of molecules (Gu and Grant, 2006), so in the case of an unknown, potentially biological sample, it would be necessary to detect the chirality using another method, such as Raman Optical Activity (ROA) or GCMS.

1.5.2. Raman theory

Electromagnetic radiation travelling in the *z*-direction consists of two components, the electric component in the *x*-direction and the magnetic component in the *y*-direction. The *x*-*y*-*z* planes are all perpendicular to one other, defined in Figure 1-13.

Only the electric component will be discussed as the Raman effect does not affect the magnetic component of electromagnetic radiation. The electric field strength *E* is described by

$$E = E_0 \cos 2\pi\nu_0 t \qquad (1\text{-}1)$$

where at a given time, *t*, the amplitude and the incident frequency are E_0 and ν_0, respectively.

The frequency, *v*, is the number of wavelengths per second given by

$$\nu = \frac{\lambda}{c} \qquad (1\text{-}2)$$

where *c* is the speed of light in a vacuum (approximately 3×10^8 m s^{-1}).

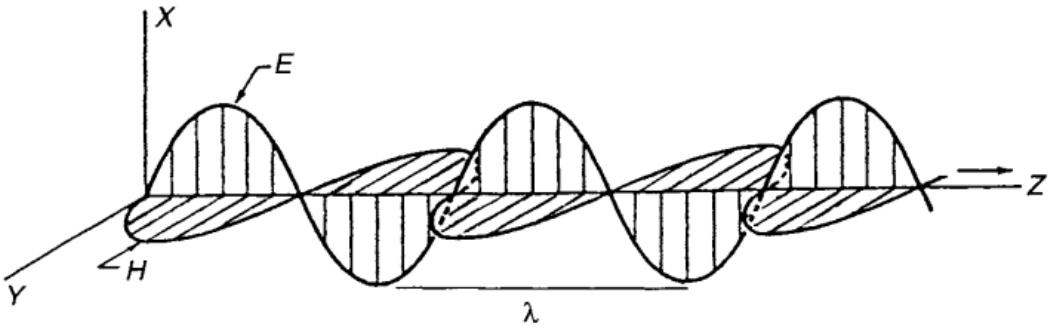

Figure 1-13: Coordinate system for electromagnetic waves, where *E* is the electric component and *H* is the magnetic component. From Ferraro *et al.* (2003).

Raman and Krishnan (1928) first noted the Raman effect in the late 1920s. Modern day Raman spectrometers use monochromatic laser beams to exploit the inelastic scattering effect. However, before the invention of a working laser, Raman and Krishnan used a telescope to focus the light from the Sun to get a powerful illumination of their samples. They observed, by eye, the modified scattered radiation using complementary light filters after the incident beam had passed through the sample (*ibid*). The scattered light from the Raman effect is of the order 10^{-3} less intense than that of Rayleigh scattering, which in itself is 10^{-3} less intense than the original incident excitation radiation (Long, 1977). The Raman effect involves no absorption of radiation and the scattering process takes less than 10^{-12} s to occur (Tobin, 1971). The nature of the effect is shown in Figure 1-14, generally the Rayleigh band is removed from instrument measurements as it would overwhelm the Raman signal and the Stokes bands are usually analysed as the anti-Stokes bands are weaker.

Rayleigh scattering is an elastic effect where the incident frequency (v_0) is absorbed and then re-emitted at the same frequency. Raman scattering is an inelastic scattering process where the scattered photon can have frequencies of $v_0 \pm v_m$, where v_m is the vibrational frequency of the molecule. The bands seen at $v_0 - v_m$ are named the Stokes lines and the bands at $v_0 + v_m$ are the anti-Stokes lines. More often the Stokes lines are studied opposed to the anti-Stokes line as intensity of these bands decreases rapidly over increasing wavenumbers because of the exponential decrease in the population of the higher energy states (under normal conditions).

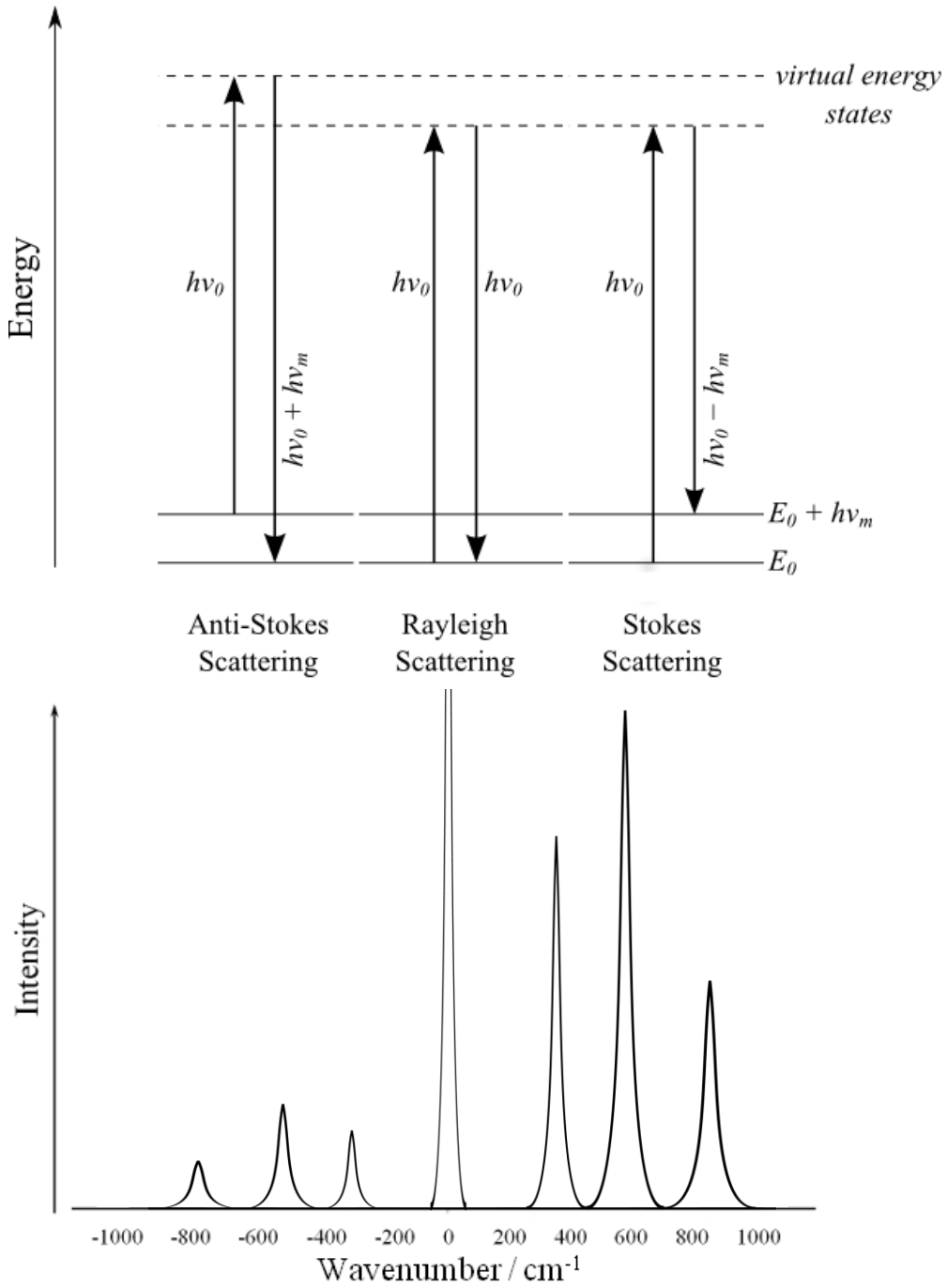

Figure 1-14: The energy bands showing the electronic behaviour when an excitation wavelength is incident on a molecule (top). A cartoon showing Rayleigh scattering is an elastic scattering effect, whereas the Raman effect, comprising of Stokes and anti-Stokes scattering, is an inelastic effect (bottom).

The Raman effect can be measured from around 10 cm^{-1} to 4000 cm^{-1} (Koenig, 1972). Within this, the region of 500 to 1700 cm^{-1} is known as the 'fingerprint' region for organic molecules, where each molecule has its own unique set of bands allowing it to be identified (Auer and Skinner, 2008). It is often difficult to assign the individual peaks to vibrational modes in the fingerprint region (Jenkins *et al.*, 2005), though studies do attempt this either empirically (*e.g.* Dhamelincourt and Ramirez, 1993) or using *ab initio* methods (*e.g.* Kumar *et al.*, 2005).

1.5.3. Previous studies of amino acids using Raman spectroscopy

1.5.3.1. Reference spectra and terrestrial studies

Past studies have presented Raman spectra for the protein amino acids for reference (in the context of human biology and drug applications) (*e.g.* Jenkins *et al.*, 2005; De Gelder *et al.*, 2007; Zhu *et al.*, 2011). Using a 532 nm solid state laser, Jenkins *et al.* (2005) discussed the 20 α-amino acids, and some related biopolymers. They presented Raman spectra for some of the 20 amino acids (the L- and DL- isomers) and reported some of the bonds that are associated with the band positions recorded (band assignments). In a detailed report of reference Raman spectra using a 785 nm laser, De Gelder *et al.* (2007) presented information for several biological molecules including amino acids, DNA and ribonucleic acid (RNA) bases, fatty acids and fats, saccharides, primary metabolites and others such as β-carotene; they provided the spectra for each molecule, lists of band positions and band intensity. Zhu *et al.* (2011) also used a 785 nm laser and reported on 18 of the 20 α-amino acids in solid and liquid states, providing Raman spectra to be used as reference spectra for the interpretation of proteins and biological materials; they provided the band positions, the associated band intensities and some discussion on the band

assignments. These reference studies have largely described only the strongest Raman bands as identifiers for specific molecules. For glycine and alanine, intense bands were found in the region 850 to 900 cm^{-1} (De Gelder *et al.*, 2007), assigned to the symmetric CNC stretch mode. More specifically for glycine, the strong bands at 894 and 1327 cm^{-1} were considered identifiers; the identifying band for alanine is reported as the strong band at 852 cm^{-1}; and for aspartic acid, the band at 939 cm^{-1} is described as the most intense, with another strong intensity band at 1338 cm^{-1} (Zhu *et al.*, 2011).

Many studies have been conducted on the Raman bands of individual amino acids, using computational *ab initio* or empirical methods to assign bonds to spectral bands. Kumar *et al.* (2005) used Raman and IR spectroscopy to investigate the bands of glycine and compared the empirical methods to *ab initio* results. The band assignments were denoted using previous studies of molecules with similar functional groups to assign bonds to bands for glycine; in the difficult process of assigning vibrational modes to bands, some bands were found to match previous studies and others were at different positions or have different assignments. Furthermore, the intensity designation process was not described and only strong to medium bands are discussed. Rosado *et al.* (1997) assessed the vibrational spectra of α- and β-alanine (neutral and zwitterionic forms) using FTIR, Raman and matrix-isolation infrared spectrometry (MI-IR) and compared to *ab initio* computations for band positions. It was found that most of the experimental and calculated results were in agreement, but for some of the modes (*e.g.* CH stretch) the predicted band positions were lower than the experimentally observed position, possibly resulting from Fermi resonance interactions (*ibid*). Furthermore, where there was more than one band per assignment, the most intense band was highlighted. Knowing the most intense band was useful for identifying molecules in a matrix of materials (*ibid*); however, the bands were not assigned to an intensity scale. Kumar *et al.* (2006) found similar results from their

comparison of an *ab initio* study to the IR, electronic and Raman spectra of alanine. Though they reported fewer bands, the observational and computed band positions and band assignments were comparable to the assignments and positions in the earlier study by Rosado *et al.* (1997). For example, both studies reported an observed Raman band at 1469 cm^{-1}, with calculated bands at 1458 and 1572 cm^{-1} and associated assignments of an asymmetric bend of the CH_3 group and a deformation of the CH_3 group, Rosado *et al.* (1997) and Kumar *et al.* (2006) respectively. Dhamelincourt and Ramírez (1991; 1993) reported the IR and Raman spectra of glutamine and glutamic acid using a polarised Raman spectrometer, with band assignments made on the basis of other amino acids or similar molecules with similar functional groups. The parallel-parallel (polariser and analyser were in the same direction as the crystal) and perpendicular-parallel (polariser was perpendicular with respect to the y-axis of the crystal) polarisations of the Raman spectrometer revealed different intensities of bands, which aided band assignment (Dhamelincourt and Ramirez, 1993). A computational *ab initio* study and comparative Raman, IR and neutron spectra were recorded by Pawlukojć *et al.* (2005). It was found that the *ab initio* calculations did not match the observed torsion angles in the molecules as a result of a three dimensional network of hydrogen bonds and hence, the geometry of a crystal of cysteine does not represent a 'free' molecule of cysteine. Navarrete *et al.* (1994) report the Raman and IR bands of aspartic acid and used the semi empirical Modified Neglect of Diatomic Overlap method (MNDO) to help with band assignments. Using a 514.5 nm laser, Lima *et al.* (2005) and Almeida *et al.* (2006) obtained Raman spectra of valine and isoleucine crystals, respectively. As well as stating band positions and assignments (at 300 K), both studies report differences in the Raman spectra over a temperature range of 17 to 300 K, where, for example, splitting of Raman bands at lower temperatures occurs.

In summary, these studies are useful aids for determining whether various amino acids are present in a matrix of material, given the extensive detail of the band position and assignments that are included. However, these studies are conducted across a variety of Raman spectrometer instruments and laser wavelengths, and some lack some useful information such as the temperature at which the studies were conducted, the relative intensities of the bands and whether bands are useful as identifiers in an unknown sample.

1.5.3.2. Raman spectroscopy in the context of astrobiology and martian simulation conditions

Raman spectroscopy can be used to detect both minerals and biological molecules; in a field study of martian analogue specimens, Pullan *et al.* (2008) used a Raman spectrometer in conjunction with other typical rover instruments (such as a stereo camera) to identify sub-mm to cm sized morphological biomarkers. Summarised data from the Raman spectrometer includes which biomarkers and minerals were found by identifying their Raman bands (band positions were not given); biomarkers detected include chlorophyll, carotenes and organic carbon (*ibid*). The authors concluded that the collaborative effort of several instruments plus a multidisciplinary analytical approach is an effective method for conducting astrobiological investigations of extraterrestrial environments.

Using a portable Raman instrument, Culka *et al.* (2010) studied 12 of the α-amino acids and β-alanine using a 785 nm laser. The authors exposed solid forms of the amino acids to "outdoor conditions" individually and collected Raman spectra by covering the area of interest and the portable device in a black cloth. Recorded band positions and intensities were reported from two different portable devices, with both sets of measurements in good agreement. It was demonstrated that two 'off-the-shelf' portable Raman instruments were

able to unambiguously identify biomarkers relevant to astrobiology. Further to this work, Culka *et al.* (2011) examined a biomarker/matrix using portable Raman devices in alpine conditions (including heavy snowfall) to attempt to identify the individual components from their Raman signatures. Gypsum and epsomite were used as the matrix material doped with the amino acids: glycine, alanine, proline, leucine, valine and glutamic acid, as well as other biomarkers: nucleobases thymine and adenine, metlitic acids and metabolic urea. At concentrations of 1 wt% the nucleobases were detectable; alanine and glycine were not successfully detected at this concentration, but their bands were seen at higher concentrations, *e.g.* 10 and 50 wt%. This demonstrated that on future planetary missions, if amino acids exist on Mars, depending on the concentration of molecule, they could be distinguished from a matrix of materials, such as regolith.

The use of martian environmental simulation is important for understanding what to expect when searching for biomarkers on future planetary missions. For example, Dartnell *et al.* (2007) determined that approximately 160 mGy yr^{-1} of cosmic ionising radiation is expected at the surface of Mars, reduced to approximately 30 mGy yr^{-1} at a depth of 1 to 1.5 m (for comparison, at the surface of Earth, due to natural sources, it would be expected that a dose of approximately 2.4 mGy yr^{-1} would be experienced (UNSCEAR, 2008)). Following this, Dartnell *et al.* (2012) used environmental simulation to expose carotenoids to ionising radiation and analysed them with Raman spectroscopy finding that the Raman spectral signatures were diminished after exposure; prominent bands were greatly reduced after 15 kGy and entirely destroyed after 150 kGy of irradiation. These doses of radiation were equivalent to approximately tens to hundreds of millions of years between the surface and 1.5 m; with sufficient shielding at deeper depths carotenoid biomarkers could survive to the present day, however, biomarkers that may have existed on the surface will be undetectable (*ibid*). Böttger *et al.* (2012) used powdered samples, to mimic future *ExoMars*

rover samples that will be powdered before Raman analysis, Raman bands of β-carotene from cyanobacteria were found to be the most dominant over mineral bands when mixed in laboratory prepared martian analogue regoliths.

Another environmental factor that would affect biology at the surface of Mars is UV radiation, as discussed in Section 1.3.1.2. Microbes and biomarkers could be partially shielded from this environmental hazard by halite crystals, which are known to attenuate UV radiation (*e.g.* Fendrihan *et al.*, 2009a), hence could potentially be used as a refuge by possible life on Mars. Vítek *et al.* (2010) collected samples from the Atacama Desert (the driest non-polar desert on Earth) and used them to test whether Raman spectroscopy could identify natural terrestrial colonisation of halite crusts; they identified bands relating to carotenoids and chlorophyll, which are associated with cyanobacteria present in the rock samples, hence evaporitic, chloride bearing rocks on Mars may be a suitable habitat for past or present life. Osterrothová and Jehlička (2011) conducted laboratory based halite experiments in which they dried solutions of NaCl and amino acids (glycine, L-alanine, β-alanine, L-serine and γ-aminobutyric acid) to create halite crystals with the amino acids trapped in the fluid inclusions. The bands of the amino acids were easily observed (shown in Figure 1-15) and there was an apparent correlation between the intensity of the bands and concentration of the biomarkers within the inclusions (*ibid*); however, a suggestion for the relationship pertaining to this correlation was not expressed by the authors.

Fendrihan *et al.* (2009b) entombed halophilic microorganisms in halite crystals and detected them using Raman spectroscopy. Raman bands at 1002, 1152 and 1507 cm^{-1} associated with a C_{50} haloarchaeal carotenoid were detected, allowing the positive identification of the halophiles within the halite crystals (*ibid*).

Raman bands (cm^{-1}) of biomolecules observed in fluid inclusions at different concentration levels.

Compound	Concentration in solution	Raman bands (in cm^{-1})
Glycine	0.5 M	3016w, 2972m, 1446m, 1413s, 1329s, 1033m, 899s, 669w, 590w, 508m
	0.1 M	3016vw, 2972w, 1446m, 1416s, 1329s, 1033w, 899s, 508w
	0.05 M	2972vw, 1446w, 1415w, 1329w, 899w
L-Alanine	0.5 M	2990m, 2948s, 2893m, 1461s, 1414s, 1378m, 1354s, 1301m, 1113m,1001m, 920m, 848s, 774w, 530w, 410w
	0.1 M	2990vw, 2948w, 2893vw, 1462m,1415m, 1354m, 1113w, 1001w, 848m
	0.05 M	2948vw, 1462w,1415w, 1354w, 1001w, 847w
β-Alanine	0.5 M	2983m, 2929m, 1464m, 1419sh, 1410s, 1388w, 1333s, 1301w, 1261w, 1048m, 965w, 931m, 872m, 846w
	0.1 M	2983w, 2929w, 1464m, 1419sh, 1410s, 1388vw, 1333s, 1299w, 1261w, 1048w, 966w, 929m, 872w
	0.05 M	1464vw, 1417vw, 1333vw
L-Serine	0.5 M	2962s, 2901w, 1468m, 1411m, 1350m, 1312sh, 1287w, 1242w, 1057w, 865m, 852m, 811w
	0.1 M	2962w, 2901vw, 1468w, 1411w, 1350w
	0.05 M	
γ-Aminobutyric acid	0.5 M	2940m, 1452sh, 1412m, 1330m, 1310m, 1059m, 898w, 864w
	0.1 M	
	0.05 M	

m, medium; s, strong; w, weak; vw, very weak; sh, shoulder.

Figure 1-15: Table from Osterrothová and Jehlička (2011) displaying the Raman bands of the amino acids at different concentrations within fluid inclusions. The method used to determine the intensity designations is not described by the authors.

Further to this work, Fendrihan *et al.* (2009a) exposed halite entombed halophiles to simulated martian UV radiation. The LIVE/DEAD kit, a fluorescent stain used to determine the viability of cells (Leuko *et al.*, 2004), was used to assess the survival rate of the halophiles.

The D_{37} (the dose required to reduce the colonies to 37% survival) for non-entombed cells of the strain *H. salinarum* NRC-1 was 0.7 kJ m^{-2}, whereas entombed cells had an D_{37} of at least 148 kJ m^{-2}; *Halococcus dombrowskii* had a much higher resistance to Mars-like UV radiation surviving doses as high as 10^4 kJ m^{-2} (Fendrihan *et al.*, 2009a). However, the survival rates were extrapolated as exposure to the UV lamp was limited to one hour, so it was possible that survival rates would not have been as high as predicted. Furthermore, other martian environmental conditions were not considered; as seen with amino acids, it may be true that martian conditions could improve the survival rate or the opposite effect may occur.

These previous studies of the exposure to martian conditions of biomarkers and microbes are important for the use of Raman spectroscopy on future planetary missions. The methods for culturing, extracting and entombing halophiles conducted in these studies were used to inform the work undertaken in this study, to be described in Chapters 2 and 5. In addition, where these studies provide a basis for understanding halophiles in individual extraterrestrial conditions, this study focuses on the effects of coupled simulated martian conditions on halophiles.

1.5.4. Raman spectroscopy on ExoMars and future planetary missions

The detection of biomarkers is a priority for the ESA *ExoMars* rover mission, to be launched in 2020. A Raman spectrometer equipped with a 532 nm laser will be among the suite of instruments on board to aid the detection of biomarkers; it has a 50 μm diameter spot, a wavenumber range of 100 to 4000 cm^{-1} and acquisition times between 0.1 and 60 s (Edwards *et al.*, 2012a; 2012b; Hutchinson *et al.*, 2014). Raman spectroscopy has several potential advantages over other methods of life detection: every molecule has an identifiable Raman 'fingerprint'; samples require little or no preparation prior to analysis; samples are not destroyed by the analysis; and water does not interfere with the fingerprint region for organic molecules, which is between 500 and 1700 cm^{-1} (Auer and Skinner, 2008). Newsom *et al.* (2001) used a terrestrial test rover called *Marsokhod* to demonstrate that Raman spectroscopy could be used to identify carotenoids in samples independently identified by the rover team as biologically interesting. The rover was part of a fully simulated analogue Mars landing mission and was controlled remotely by a science team that had not visited the field site previously (Stoker *et al.*, 2001). Images collected by the

rover on its journey were visually assessed and sites of interest were analysed *in situ* by visible/near-infrared spectroscopy for microbiological biomarkers, *e.g.* greenish colouring near rock surface fractures and spectroscopic bands relating to chlorophyll; at the time of the study miniaturised portable Raman spectrometers had not yet been developed, hence Raman analysis was conducted in a laboratory. "Endolithic" samples collected from the field site had bands relating to CH stretches associated with carotenoids were measured (Newsom et al., 2001).

Jorge Villar *et al.* (2005) conducted an extensive study of extremophilic organisms using a range of Raman excitation wavelengths to determine optimal analytical parameters. An excitation wavelength of 1064 nm required long exposure times to collect useful spectra, especially for compounds of low concentration (undefined) and wavelengths such as 514 and 488 nm were not able to obtain good results for geomarkers (geological markers remaining resulting from microbial influence on the rock sample, such as depletion or generation of certain minerals); Jorge Villar *et al.* (2005) concluded that an excitation wavelength of 785 nm provided a compromise for the study of both biological and geological samples in extraterrestrial environments. The conclusion that the 785 nm wavelength laser provided a compromise appears well founded; however, not all laser wavelengths were used on all the samples and the concentrations studied are not defined, making it unclear the importance that should be placed on this part of the results. Furthermore, when studying halophilic cyanobacteria using a 514 nm wavelength laser, it was possible to identify the presence of two different species. Though good results were obtained from the 785 nm wavelength when searching for biomarkers such as carotene bands, the 514 nm wavelength seemed to have provided a greater depth of information by being able to distinguish between species. Other samples that were analysed often showed

strong biomarker spectra with the 514 nm wavelength, therefore, microbial biomarkers were more accessible with the mid-optical range of wavelengths.

Detection limits of Raman spectroscopy for the analysis of biomarkers have been discussed by Vandenabeele *et al.* (2012), who have considered the limit of detection and identification of a molecule in spectra from future missions, but this can also be applied to laboratory recorded spectra that are used in comparison to unknown sample spectra. They remarked that there are no standard International Union of Pure and Applied Chemistry (IUPAC) definitions for the intensity annotations for Raman spectroscopy and proposed a definition (detailed discussion of intensity annotations in Section 3.1). The authors alluded to discussing how Raman band intensity relates to the concentration of a molecule in a sample, but do not discuss the relationship between intensity and concentration; they demonstrated that there appeared to be a relationship where the intensity of the Raman spectra of β-carotene reduced with smaller quantities of the molecule (see Figure 1-16). However, the intensities of the bands are not given and there was no discussion to whether they believed there was a relationship between intensity and concentration or what the relationship might be. Furthermore, they suggested that it would be necessary to define the minimal number of bands for each individual molecule needed to make a positive identification of that molecule when in an unknown mixed material. On future missions unknown samples could contain several types of molecules, the Raman bands of which may overlap or be overwhelmed by other bands. Therefore, the identification of a molecule cannot be determined based on a single Raman band; ideally all bands in the reference spectrum would be observed in the spectrum of the unknown sample. However, ambient light, fluorescence or other molecules may cause some bands to not be observed; hence it is important to define the minimal number of bands needed to confirm the presence of a biomarker molecule (*ibid*). Nonetheless, the authors do not suggest a method for defining

the minimum number of bands; Chapter 3 explores a statistical method for defining the characteristic bands of a biomarker which could be used for identification of biomarkers on future missions.

Future missions (selected or proposed) that have proposed Raman spectroscopy as part of the instrument suite include the Compact Integrated Raman Spectrometer (CIRS) on the NASA *Mars 2020* mission (Wang *et al.*, 2013) and on a lander mission to Europa (Pappalardo *et al.*, 2013). The Mars 2020 Science Definition Team have provided a detailed report on the mission concept for the *Mars 2020* rover with the likely inclusion of a Raman spectrometer; the main functions as described by this report of a Raman spectrometer would be fine-scale mineralogy and reduced and organic carbon detection, with some contribution to fine-scale imaging and context mineralogy (Mustard *et al.*, 2013). The CIRS instrument will be based on the design of the Mars micro-beam Raman spectrometer (MMRS) (Wei *et al.*, 2014).

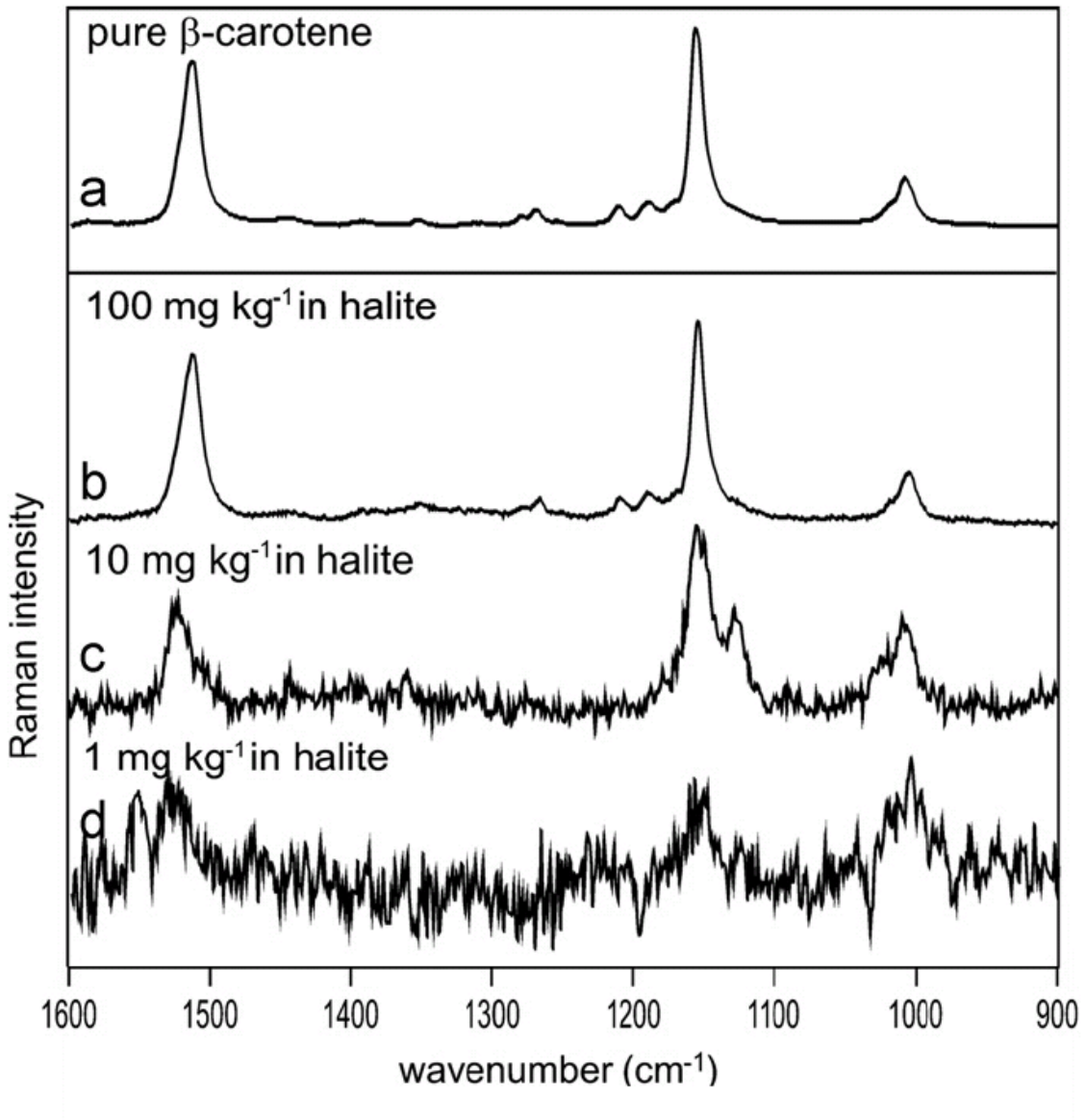

Figure 1-16: The Raman bands of β-carotene mixed with halite. Each spectrum represents a different, known quantity of β-carotene molecule. Adapted from Vandenabeele *et al.* (2012).

1.6. Research questions and thesis overview

This thesis investigates the following questions (stated in Section 1.1, repeated here for ease of reference) and hypotheses.

RQ1. Using statistical techniques, can a set of characteristic Raman bands be rigorously defined for use as identifiers of amino acids?

Hypothesis RQ1.1: Previous studies have been able to identify the strongest bands of amino acids; therefore it should be possible to identify several other bands (very strong to medium intensity) that are useful in the process of the identification of amino acids.

RQ2. Does exposure to the martian near surface and surface conditions affect the Raman spectra of amino acids?

Hypothesis RQ2.1: Near surface conditions (samples on 1: glass or 2: analogue martian regolith substrate exposed to martian atmospheric composition, pressure and temperature; no ultraviolet or ionising radiation) will not affect the amino acids significantly, whereas surface conditions (samples on 1: glass or 2: analogue martian regolith substrate exposed to ultraviolet radiation environment, atmospheric composition, pressure and temperature; no ionising radiation) will affect amino acids significantly.

RQ3. Can halophilic microbial life entombed within halite crystals survive when exposed to coupled martian conditions and their Raman signatures remain detectable?

Hypothesis RQ3.1: The Raman signatures of terrestrial halophilic microbes will be detectable after exposure to surface conditions or freeze-thaw cycles when entombed in halite crystals.

Hypothesis RQ3.2: The position of fluid inclusions within the halite crystal can influence the survival of the entombed microbes; the further from the surface the more likely the survival.

The structure of this thesis is as follows: this chapter provided a review of the current knowledge of the astrobiological state of the planet Mars, the theory of Raman spectroscopy and previous work conducted using Raman spectroscopy as an astrobiological tool. Chapter 2 provides the methods and techniques used throughout this project.

Chapter 3 examines the Raman bands of amino acids in ambient conditions and develops a statistical method to define a set of characteristic bands, which could be used to identify these molecules on future planetary missions.

Chapter 4 studies the changes to Raman spectra of amino acids that may occur because of exposure to Mars-like conditions and how this could affect future missions attempting to search for signatures of molecules such as amino acids.

Chapter 5 investigates the survivability of halophiles, in simulated martian conditions. It also examines whether their Raman spectra is altered, and if so, whether it remains detectable, or not.

Chapter 6 discusses the main findings from the work presented in the above chapters in terms of the contribution to knowledge about using Raman spectroscopy during future planetary missions to Mars. This chapter also provides ideas for developing follow on work from this project for future research.

2. Methods and Materials

2.1 Introduction

Though the main analytical technique used in this project was Raman spectroscopy, there were several other techniques and apparatus that were used during experiments to complete the main aims of the work, including exposure of amino acids and halophilic microorganisms to simulated martian conditions. This chapter details the methods and materials used to carry out the following:

- **Characterisation of characteristic amino acid Raman bands.** This was conducted using Raman spectroscopy (Section 2.2), but also required the preparation of the amino acid samples (Section 2.4).

- **Exposure of amino acids to martian conditions.** The amino acid samples were prepared and analysed with Raman spectroscopy pre- and post-exposure, where the exposure was conducted using martian environment simulation (Section 2.3). Further complementary techniques, such as a Scanning Electron Microscope (SEM), were applied to support the Raman spectroscopy results (Section 2.6).

- **Exposure of halite embedded halophilic microbes to martian conditions.** Similar to the exposure of amino acids, samples were prepared, analysed with Raman spectroscopy pre- and post-exposure and the exposure was conducted using martian environment simulation. Other microbiological techniques including measuring culture density, embedding the microbes in halite crystals were necessary for constructing the microbiological experiments (Section 2.5).

2.2 Raman spectroscopy

2.2.1 *Apparatus*

Samples were examined using a *HORIBA Jobin Yvon LabRAM HR* bench top apparatus, equipped with a 473 nm (blue) laser and a 514 nm (green) laser, shown in Figure 2-1. It had two gratings, 600 and 1800 grooves per mm (the range of data collection approximately 1800 wavenumbers using the 600 grooves per mm grating, the 1800 grooves per mm provided a much smaller range, approximately 600 wavenumbers). It had five objective lenses: ×10, ×20, ×50, ×50 LWD and ×100 LWD, where LWD is a lens with a Long Working Distance. A non-LWD lens had a working distance of approximately a millimetre or less; on an uneven sample (that is unable to be covered by a coverslip) there is a chance that the lens could crash into the sample, so a LWD lens allowed for a few millimetres between the lens and the sample when collecting data. The diameter of the spot size, *d*, of the laser through these objective lenses can be described by:

$$d = \frac{1.22\,\lambda}{NA}, \tag{2-1}$$

where λ is the wavelength of the excitation laser and *NA* is the numerical aperture.

From Equation 2-1, the *d* for the lenses are described in Table 2-1. The scattered light from the sample was detected using a CCD detector cooled to −70 °C and equipped with two gratings, 600 and 1800 grooves per mm. The operating software that controlled the system was originally *LabSpec5*, which was upgraded to *LabSpec6* during the course of this study.

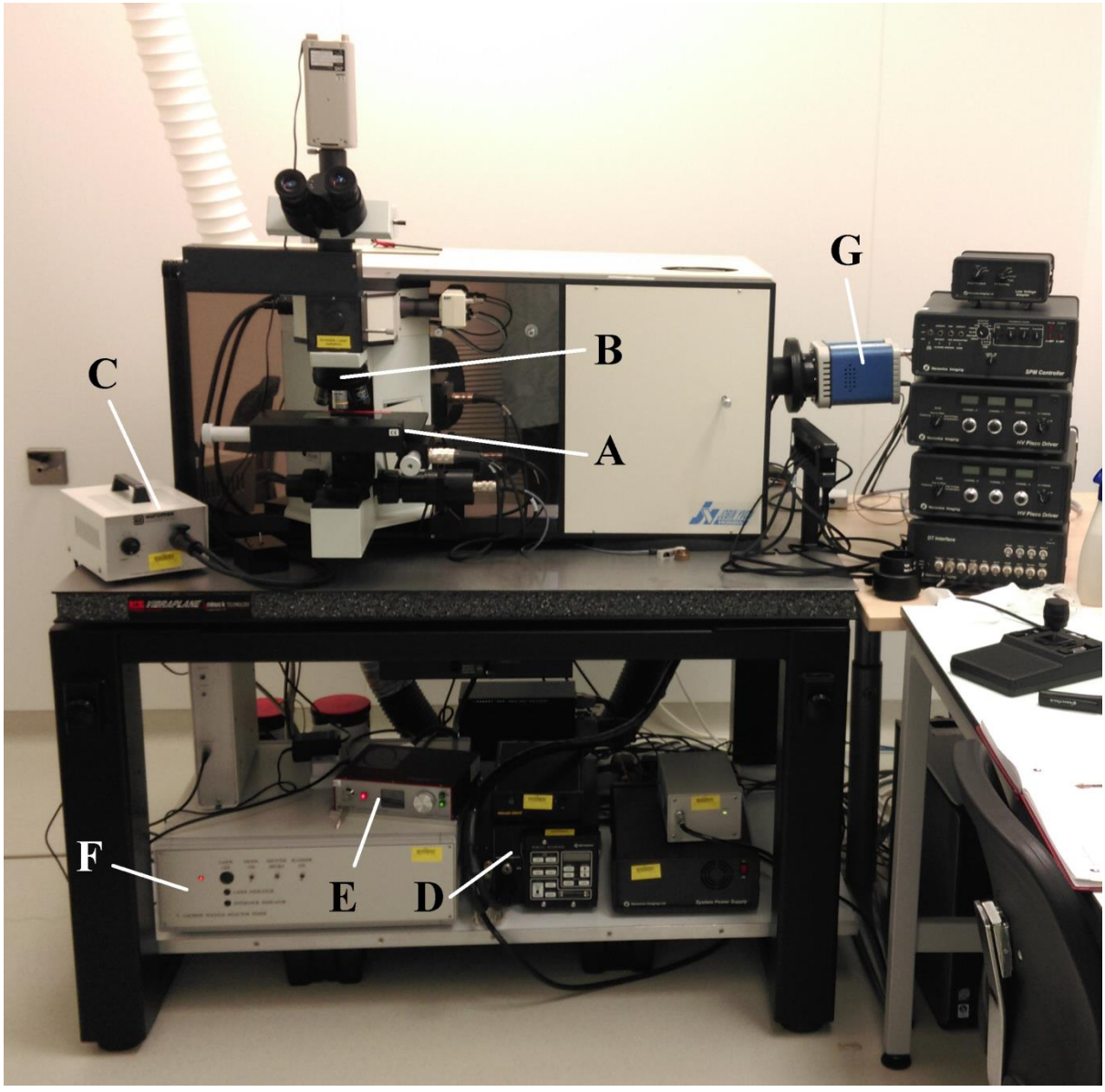

Figure 2-1: The Horiba Jobin Yvon 'LabRam HR'. A, the sample stage; B, the objective lenses; C, the white light source; D, the 514 nm laser source; E, the 473 nm laser source; F, the main power source; G, the CCD detector.

Aperture	*NA*	*d* / μm *514 nm*	*d* / μm *473 nm*
×10	0.25	2.5	2.3
×20	0.40	1.6	1.4
×50	0.75	0.8	0.8
×50 LWD	0.50	1.3	1.2
×100 LWD	0.075	0.8	0.8

Table 2-1: The numerical aperture (*NA*) of the lenses on the HORIBA Jobin Yvon Raman spectrometer and hence, the diameter (*d*) of the spot size incident on the sample.

2.2.2 *Calibration*

Before samples were examined, the Raman system was calibrated to ensure the same initial state. To achieve this, two techniques were used, depending on the version of the software that was installed. *LabSpec5* required manual adjustment of some the system settings, whereas *LabSpec6* integrated this into an *AutoCalibration* routine. As a known standard, a chip of pure silicon was used in the calibration of the system; the Raman band of silicon has an accepted value of 520.7 cm^{-1}.

The *LabSpec5* calibration routine was as follows: the source laser was selected, the grating (600 grooves per mm), slit (150 μm) and hole (300 μm) values were set, and the spectrometer was zeroed then centred on 1000 cm^{-1}. The spectrometer was calibrated to a value of 0.0 cm^{-1} using a white light source (depicted at 'C' in Figure 2-1) by adjusting a software value called the *zero*. The software value called the *koeff* was adjusted to calibrate the band position of the silicon standard to the accepted value of 520.7 cm^{-1}.

The *LabSpec6* calibration routine was as follows: the spectrometer was zeroed then centred on 1000 cm^{-1} and the grating, slit and hole values were set. A signal from the silicon standard was registered and the automatic *AutoCalibration* software routine was run. This

routine automatically configures the *zero* and the *koeff*, which are bound by set parameters. If the result of the calibration lay outside of these parameters the *AutoCalibration* routine would fail. If the routine passed, the zero position would be in the range −0.03 to 0.03 cm^{-1}, but the silicon band could have a position in the approximate range 520.50 to 521.0 cm^{-1}. For the work conducted in this study, this range was not acceptable, so unless the returned silicon band result was within the range 520.65 to 520.75 cm^{-1} the *AutoCalibration* routine was re-run. As a built-in precaution, the *AutoCalibration* routine had to be re-run after 12 hours had passed or if the source laser or grating was changed. The calibration range of one wavenumber was chosen because of the nature of the work to characterise Raman bands with accuracy.

Raman system user guides were written as part of this work to ensure that the same procedure was followed for each set of data collected and to help guide future users of the Raman spectrometer.

2.2.3 *Data collection technique*

Once calibration was complete, samples were placed on the sample stage for examination. Samples on a microscope slide were lined up against a straight edge on the sample stage to keep the orientation in the *x-y* plane consistent. For samples on a Petri dish, the orientation was defined with a mark on the edge of the dish. An origin point was defined on the sample so point or mapping coordinates could be returned to and repeat measurements could be recorded. The origin was often situated at a small dot marked with a *Sharpie* permanent marker pen on the underneath of the slide or Petri dish at the edge of the sample (for example, see Figure 2-2); in some cases if there was a prominent feature then no pen mark was needed. Using a live image from the camera, the pen mark or prominent feature

was located with the ×10 objective lens and an image of the field of view was captured to mark the origin. Returning to an origin field of view on samples on a microscope slide was relatively simple as the *x*-*y* plane of the slide was fixed, however, for samples in a Petri dish the origin was more difficult to realign. The mark on the edge of the dish was realigned to the approximate original orientation, followed by comparing the live image with the original image of the origin point to ensure the orientation in the *x*-*y* plane was correct. Samples were preferably examined on a microscope slide where possible as alignment and realignment was more accurate than Petri dishes (the method that was used for each experiment will be stated when relevant).

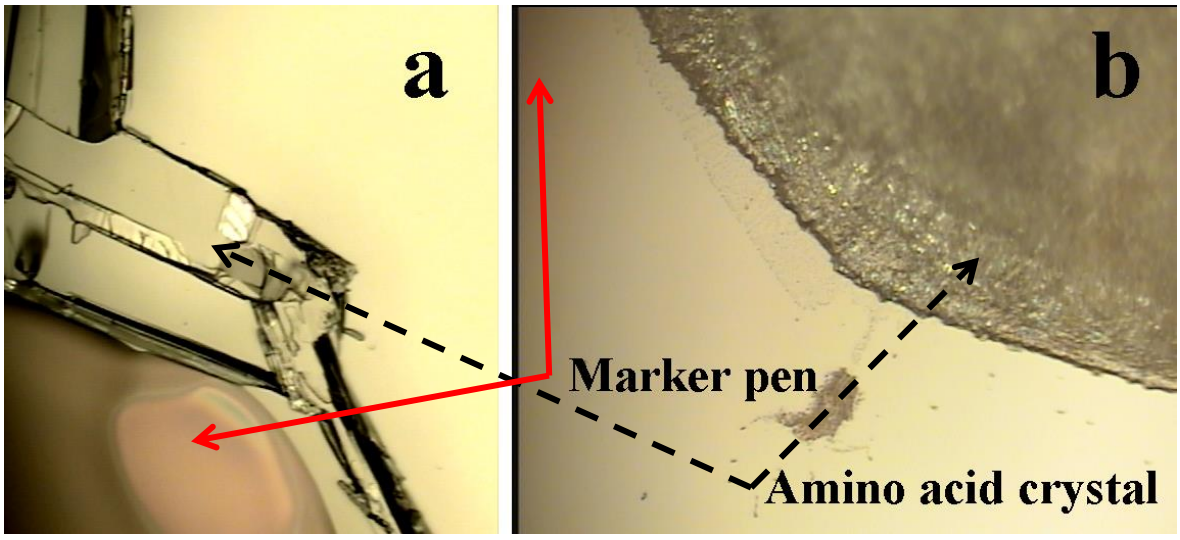

Figure 2-2: Images, (a) and (b), of origin points for amino acid samples. The red solid line shows the darker areas of the image that are a result of marks made by a *Sharpie* pen to locate an origin point on the sample.

Once an origin point was defined, the stage position, given by *x*, *y*, *z* coordinates, was zeroed in the software and a data site field of view was located using the joystick to control the stage movements. The stage position coordinates were recorded for future reference if repeat measurements of the same data site were required. Data sites were chosen on the basis that the lighting across the sample was even and the area was flat to avoid the lens crashing into the sample. An image of the field of view was captured and the map area was defined. The ×50 or ×50 LWD objective lens was selected and an image of the field of view was captured. The imaging camera was switched off and the laser switched on. A real time display (RTD) function, which displayed a live spectrum refreshed at a user defined interval (0.5 s), was then used to check the focus at the sample. Once the focus was optimised, the point capture or mapping function was initiated.

Point capture allowed for one or more points to be defined within the field of view before measuring the Raman spectrum at that point(s). This technique was used for recording preliminary spectra to ensure there was a good signal before recording a spectral map of the area using the mapping function. For the mapping function, the size of the map could be defined by dragging an area out over the field of view or by typing map coordinates into user input fields *x*, *y* or *z*. Once the map area was decided, the number of points to be recorded and their spacing could be defined. For example, a map area might be 100 × 100 μm with 16 points evenly spaced in a four by four grid; exact map details for each experiment are to be described in the chapters that follow. Spectral mapping provided context at many individual points as well as an average over the mapped area of the sample.

2.2.4 *Raman system settings and user inputs*

Preliminary point capture tests were used to test and decide the values of the parameters that required user input. The filter could be set to 0.1, 1, 10, 25, 50 or 100 % and hence determined the percentage of the laser light that was incident on the sample. The hole parameter was generally set to 300 μm by default, expanded occasionally to 1000 μm; if the diameter of the hole was wider, the spot size of the laser incident on the sample was larger, allowing the signal from a larger number of molecules to be measured.

Trial and error was used to obtain the optimum filter setting and exposure time for acquiring spectra. Ideally, the highest filter setting and the lowest exposure time was desired as this would increase the intensity of the spectra and reduce the total time taken to record data. However, the filter setting related to the laser power at the sample; high power at the sample could cause damage to the sample. A test spot on a sample, in an area that was not a desired data site, was subjected to the laser with differing filter settings for varied exposure times to determine that the laser power was not causing damage to sample. It was found that longer exposure times with fewer repetitions produced a better signal to noise ratio than a shorter exposure time with many repetitions, see Figure 2-3. Exposure times and number of repetitions for each sample will be stated in the chapters that follow. The resulting (non-destructive) power of each laser used was 4.56 ± 0.27 mW and 4.49 ± 0.27 mW for the 514 and 473 nm excitation lasers, respectively.

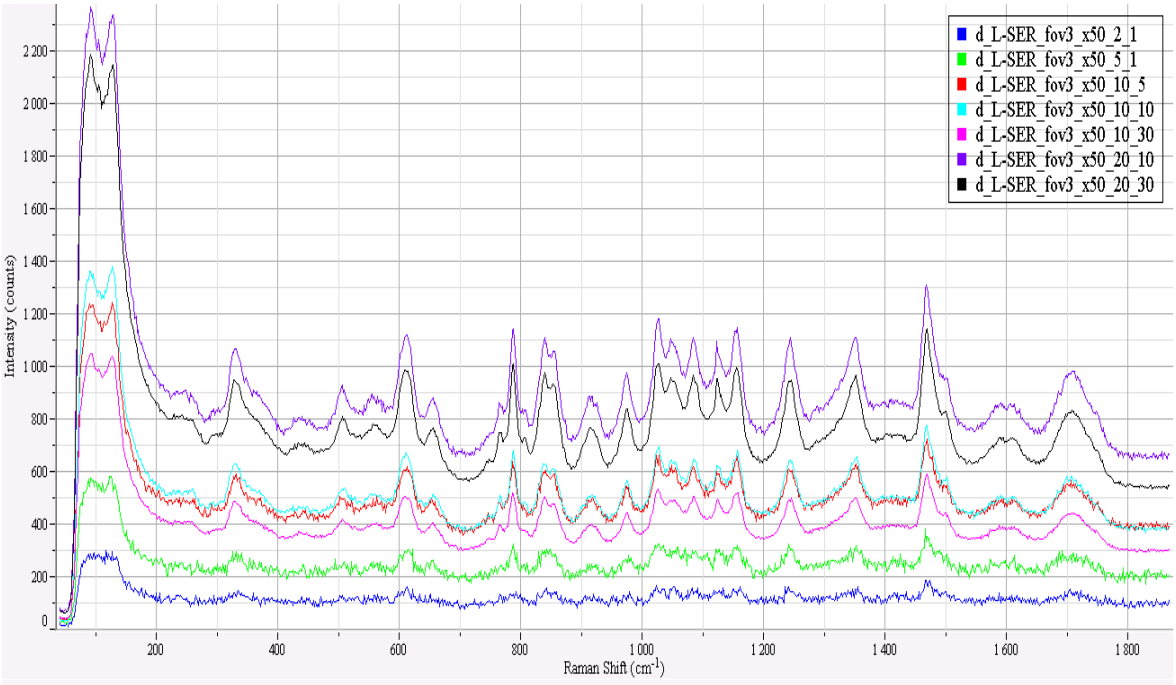

Figure 2-3: Examples of different exposure times and different number of repetitions. The key gives the number of seconds of the exposure followed by the number of repetitions in the final two figures of the file name. For example, the red spectrum had a 10 sec exposure times, repeated 5 times. A longer exposure increases the intensity and the number of repetitions results in a smoother spectrum as it is averaged out.

AutoFocus was an available software function that found the focal position that returned the strongest signal at that data point. It could be used over the whole wavenumber range or user input could set it to a specific wavenumber range to focus on a particular band or band group. *AutoFocus* could be initiated at the start of the data recording process or at each individual point. As the surfaces of the samples used in this study were often uneven, *AutoFocus* was used unless stated otherwise, as it provided repeatable signal intensity and shape at individual data points. Figure 2-4 shows the results of a preliminary experiment to test the repeatability of the signal when using *AutoFocus*. The signal at a data site was recorded five times, but the stage was returned to the origin site in between each measurement. It was found that when *AutoFocus* was on, the band intensity varied by less than 2.2 %, compared to up to 18.7 % when *AutoFocus* was not used.

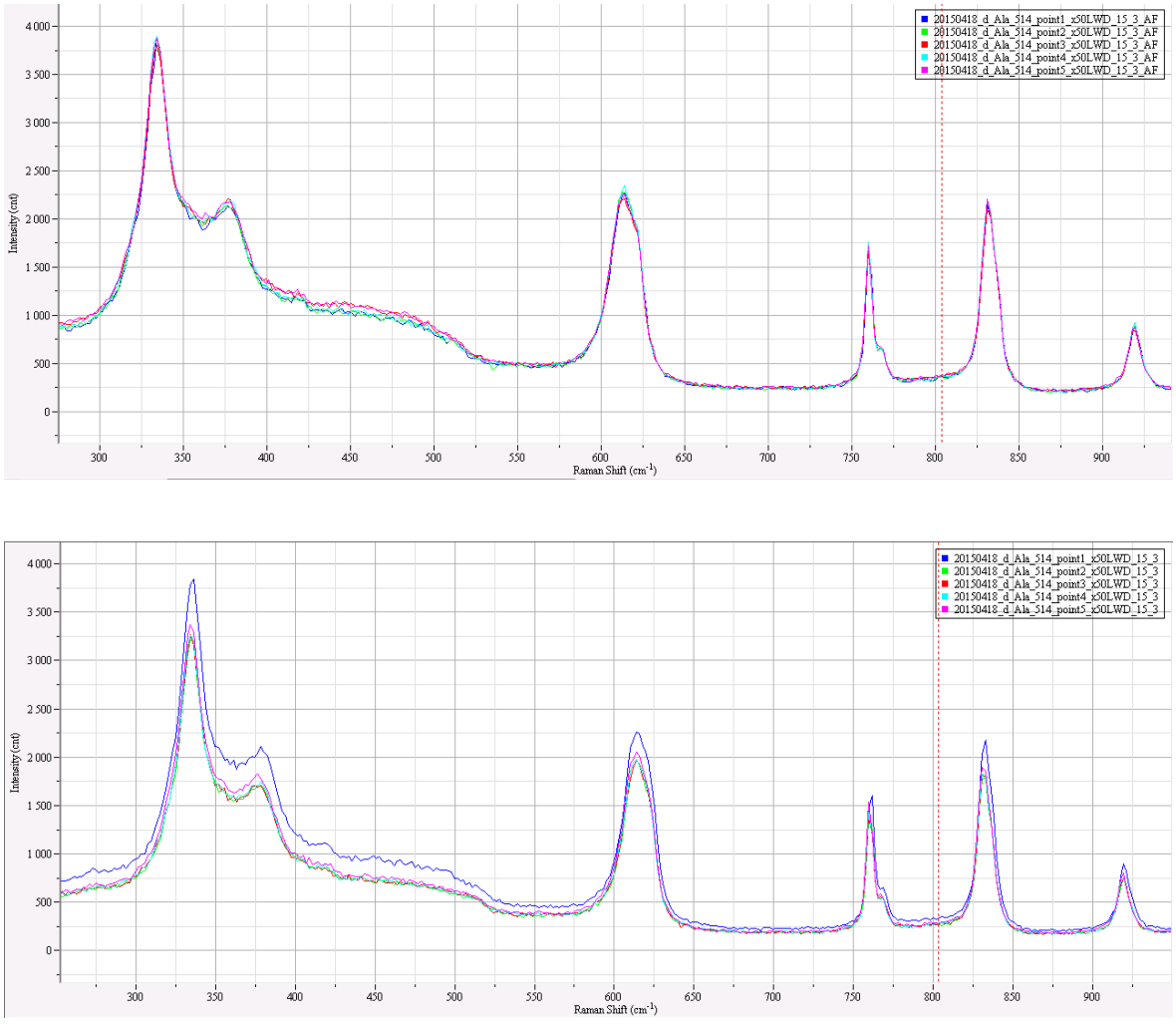

Figure 2-4: Five spectra (200 to 1000 cm^{-1}) of alanine, taken with (top) and without (bottom) autofocus. The shape and intensity of the bands using *AutoFocus* are almost visually indistinguishable in comparison with the data taken without using *AutoFocus*, the shape and intensity of the bands is variable.

2.3 Martian environment simulation

Mars simulation chambers (MSCs) have become an important part of understanding the processes that occur on the martian surface and near surface. The first simulations that used conditions similar to that on Mars were by Zhukova and Kondratyev (1965). The authors maintained a pressure of 0.1 atm, used an automated temperature regime and an illumination source that was similar to the solar spectrum within a sealed chamber. Though these conditions are not those at the present martian surface, it was shown that not all the microbes that were exposed survived these conditions. Since then many experiments in improved simulated conditions have been conducted (see, Olsson-Francis and Cockell, 2010, for a review), some in anoxic tubes but mostly in simulation chambers.

Most simulation chambers are now made using stainless steel and use automation to control the conditions. A 'rough Mars' (95 % carbon dioxide, 5 % nitrogen) or Mars gas mix (95.3 % carbon dioxide, 2.7 % nitrogen, 1.7 % argon, 0.2 % oxygen and 0.03 % water vapour) are commercially available, which can be used to simulate the martian atmosphere. Furthermore, the illumination of simulation chambers commonly use xenon lamps to represent the Mars-nominal spectrum expected at the surface (*e.g.* Schuerger *et al.*, 2003).

2.3.1 Mars simulation chambers

MSCs were used to conduct exposure experiments of amino acids (biomarkers) and halophiles to simulated martian conditions; these chambers could recreate temperature, atmospheric composition, pressure and some of the radiation environment conditions similar to those found on Mars based on *in situ* and remote observations (described in Section 1.3.1).

The MSCs were connected to a custom vacuum system, which was evacuated using an *Edwards 18 E2M18* dual stage rotary pump. The vacuum system could be automated to keep the pressure within a specified range. In practice this was applied as a back-up while the gas flow and evacuation rate were manually balanced at a pressure of approximately 8 mbar (selected as an approximate average of the pressure measurements taken *in situ*). Individual components could be isolated from the rest of the system if, for example, a pressure experiment was being conducted and the desired pressure had been introduced in the chamber. A needle valve was used to introduce gas into the system. This allowed small adjustments to the gas flow rate to be made, with control of the pressure to an accuracy of 0.01 mbar.

2.3.1.1 Bernard-class chamber

Figure 2-5 (right) shows a chamber, *Bernard*, with an inner diameter of 97 mm by 175 mm. Pressure ranges between 2×10^{-3} to 1000 mbar can be achieved, introduced using various gases; it is possible to cool the chamber to a temperature of 253 K and UV illumination can be added if required. There was an interchangeable stainless steel or UV quartz fused silica viewport lid that could be used for allowing UV radiation into the chamber (see Section 2.3.3). The quartz viewport had a greater than 90 % transmission at 250 to 400 nm; this was reduced to approximately 75 % at 190 nm. The *Bernard* chamber was used to conduct ‘full’ Mars simulations, *i.e.* coupling the environmental conditions of atmospheric composition, pressure, temperature and solar-like UV radiation.

Figure 2-5: Examples of martian simulation facilities at the Open University. Left: MSC *Edmund*, for large scale experiments, not specifically used in this project. Right: a small scale MSC, *Bernard*.

2.3.1.2 Melchett-class chamber

There were three *Melchett* class chambers that had no viewports, so were available for simulations that did not require illumination (see Figure 2-6). The inner dimensions were a diameter of 95 mm by 270 mm. The pressure range and atmosphere simulations available were the same as the *Bernard*-class chamber. *Melchett* chambers had a one way entry valve; hence a desired gas mix at a desired pressure could be introduced to the chamber and then isolated from the vacuum system for long duration experiments. *Melchett*-1 had a pressure sensor attached at the gas inlet valve, allowing the pressure to be monitored throughout the experiment, whereas the other chambers had to remain attached to the main vacuum control rig for the pressure to be monitored. The *Melchett* chambers were used to conduct atmospheric composition and/or pressure simulations.

2.3.1.3 Percy-class chamber

Percy had the same dimensions as the *Melchett*-class chambers, but with a central inlet with flexible piping, allowing it to be attached to the vacuum system and be partially portable (see Figure 2-6). It had a stainless steel lid that was interchangeable with a quartz viewport, if observations of the samples were required. The portability of *Percy* was conducive to conducting freeze-thaw experiments in the temperature cycling oven (described in Section 2.3.2). Samples were introduced into *Percy* before the chamber was manoeuvred into the temperature cycling oven. A valve intersected the connection to the vacuum system at the entrance to the flexible piping, so *Percy* could be isolated from the system if required.

Figure 2-6: *Percy* (left) in the temperature cycling oven (described in 2.3.2). Though some ice formation was inevitable, if the oven was not baked out for long enough, large amounts of condensation could form blocks of ice during the cycle as pictured above. Two of the *Melchett* (right) chambers, one with the pressure sensor attached.

2.3.2 Temperature cycling oven

Samples were placed in *Percy* within a *Clima Temperatur Systeme* (CTS) *T-40/25* oven, which was capable of a temperature range of −40 to 180 °C. As a result of the lower limit of the temperature range achievable by the oven, freeze-thaw cycles simulations were approximations of conditions found during a portion of the martian southern summer (Spanovich *et al.*, 2006) (see Figure 1-6, right). The temperature cycling oven was used to simulate the freeze-thaw cycles that occur on Mars and hence whether freeze-thaw cycles altered the samples. Freeze-thaw cycles could affect the fluid inclusions in brines, with a direct impact on the survival of any halophiles that are resident within them. The amino acids in this study are in crystalline form, so freeze-thaw could affect the structure of the crystal and/or the molecular structure of the amino acids, which may be detectable by Raman spectroscopy.

The oven was programmed to repeat the following phases 90 times, simulating potential freeze-thaw cycles occurring over 90 sols: (1) 10 °C hold for 12 min; (2) 10 °C to −40 °C ramp for 78 min; (3) −40 °C hold for 12 min; (4) −40 °C to 10 °C ramp for 42 min; (5) go to (1). The full cycle took nine days to complete, a portion of which is shown in Figure 2-7. As a result of the ambient temperature of the lab the minimum the oven could reach was approximately −38 °C. Furthermore, during phase (1), temperatures would range between 10 °C and a maximum of 14 °C. The shape of the cycle was set to mimic, to a best approximation, the known shape of the diurnal temperature cycle measured *in situ* on Mars by the *Spirit* and *Opportunity* rovers during its first 65 sols on the surface (Spanovich *et al.*, 2006), on the assumption that a similar average temperature cycle occurs at the surface.

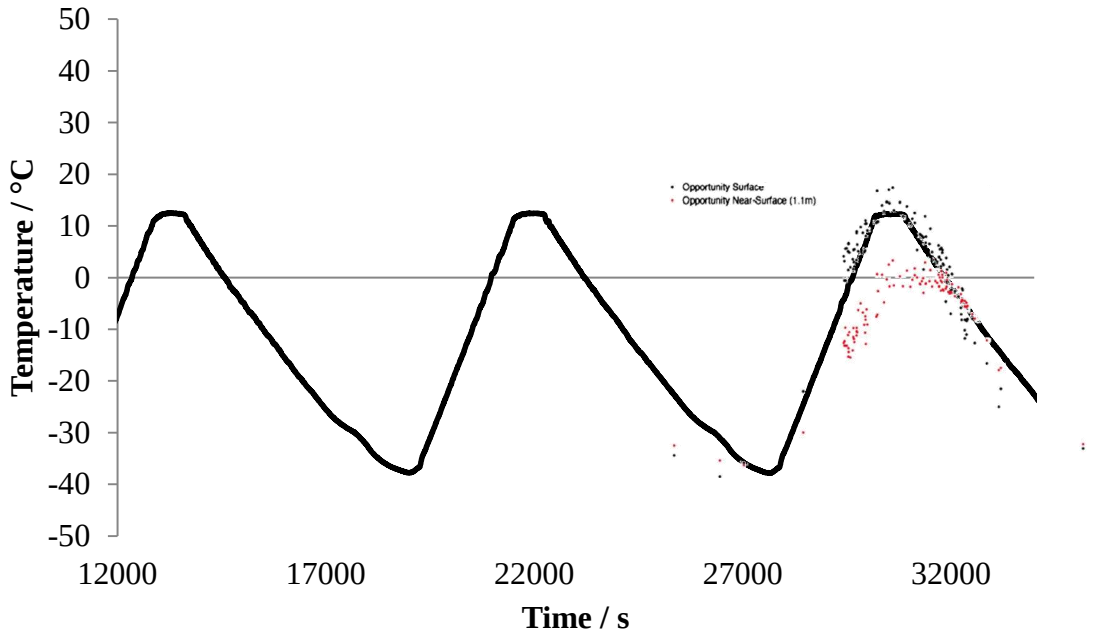

Figure 2-7: A portion of a modelled temperature cycle showing two full cycles of the freeze-thaw conditions (approximately 5.5 hrs of real time). Diurnal temperature data from the *Opportunity* rover is overlaid on the final cycle for comparison, adapted from Figure 1-6.

2.3.3 Simulation of ultraviolet environment

Two types of UV lamps were used to simulate the martian UV radiation environment, a deuterium lamp and a xenon lamp. The deuterium lamp was a *LOT-Oriel* (model *LSB213*) *30 W* source. This provided a UV continuum from 160 to 370 nm. The xenon lamp was a *LOT-Oriel 150 W* source, providing a UV continuum mostly between 240 and 400 nm, with some output between 200 and 240 nm. Although the deuterium lamp had a greater UV output range, the irradiance was not as great as the xenon lamp. Measurements of the irradiance were taken using an *AvaSpec-1024* spectrometer in conjunction with *avantes AvaSoft* (v 7.5.3 Full) software. The irradiance spectra of the lamps are shown in Figure 2-8.

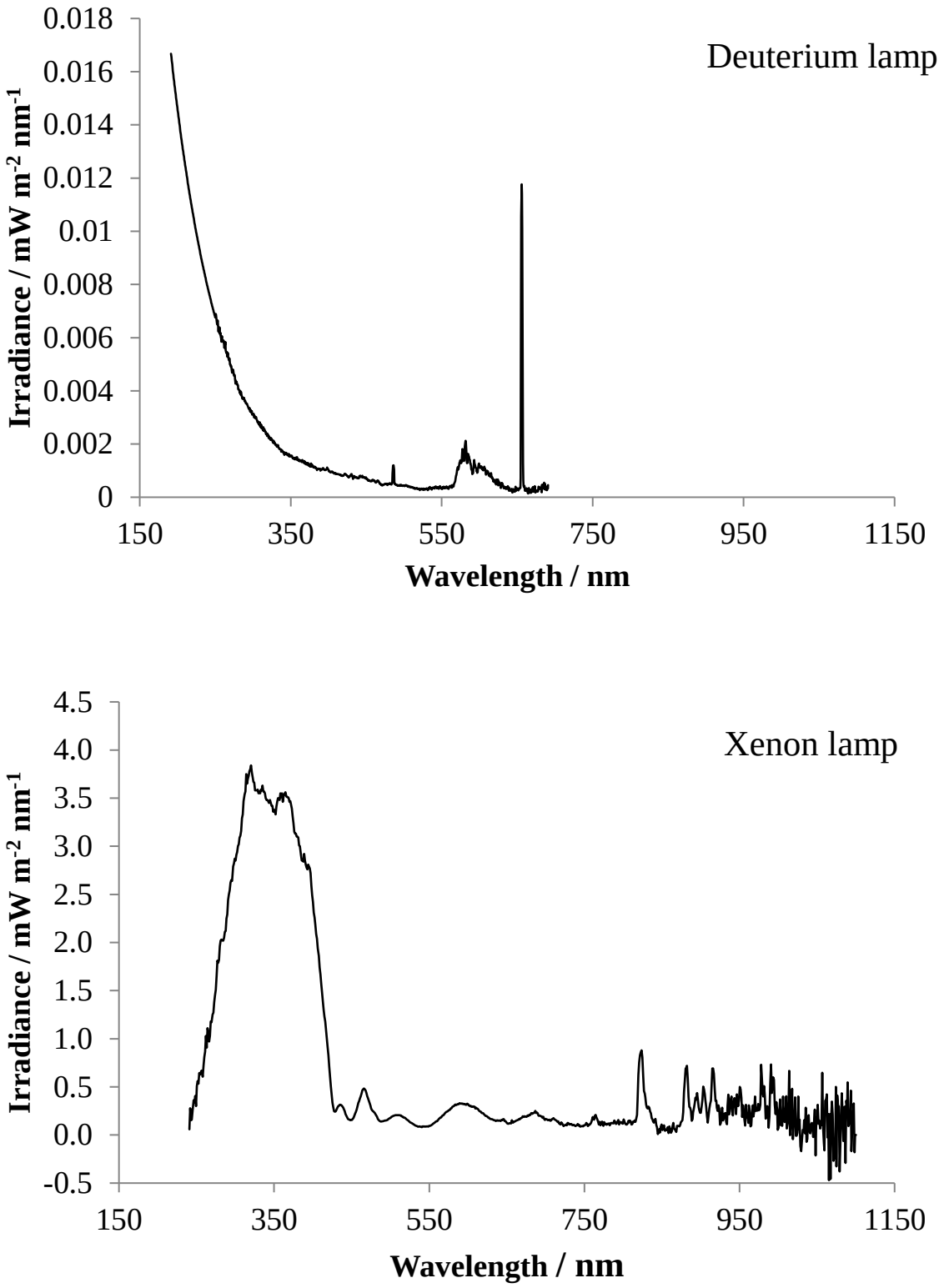

Figure 2-8: The irradiance spectra of the deuterium and xenon lamps. Note that the deuterium lamp has an irradiance two orders of magnitude lower than the xenon lamp.

Using a precision caliper stage (Figure 2-9), the irradiance of the output footprint could be mapped. Experiments using the deuterium lamp were exposed at a working distance (WD) from the aperture of 5 cm, whereas the xenon lamp was used at a WD of 4.5 cm, the output footprints are shown in Figure 2-10 and Figure 2-11 , respectively. The footprints of the deuterium and xenon lamps were 50 mm and 40 mm in diameter respectively. The output of the deuterium lamp was measured along an arbitrary *x*-axis, where *y* was zero and the xenon lamp spectra were measured over a grid of 4 × 8 mm at the lowest resolution and 4 × 4 mm at the highest resolution. In Figure 2-10, the measurements showed a rapid reduction in the irradiance either side of the central point of the footprint, suggesting there was a focal point at the centre. Figure 2-11 showed a similar focal point, but non-central in the top left hand corner of the footprint. The UV footprint of the xenon lamp was mapped after the experiments were conducted, this led to some data having to be excluded because the samples did not receive the correct UV exposure, see Sections 4.2.4 and 5.2.2.3.

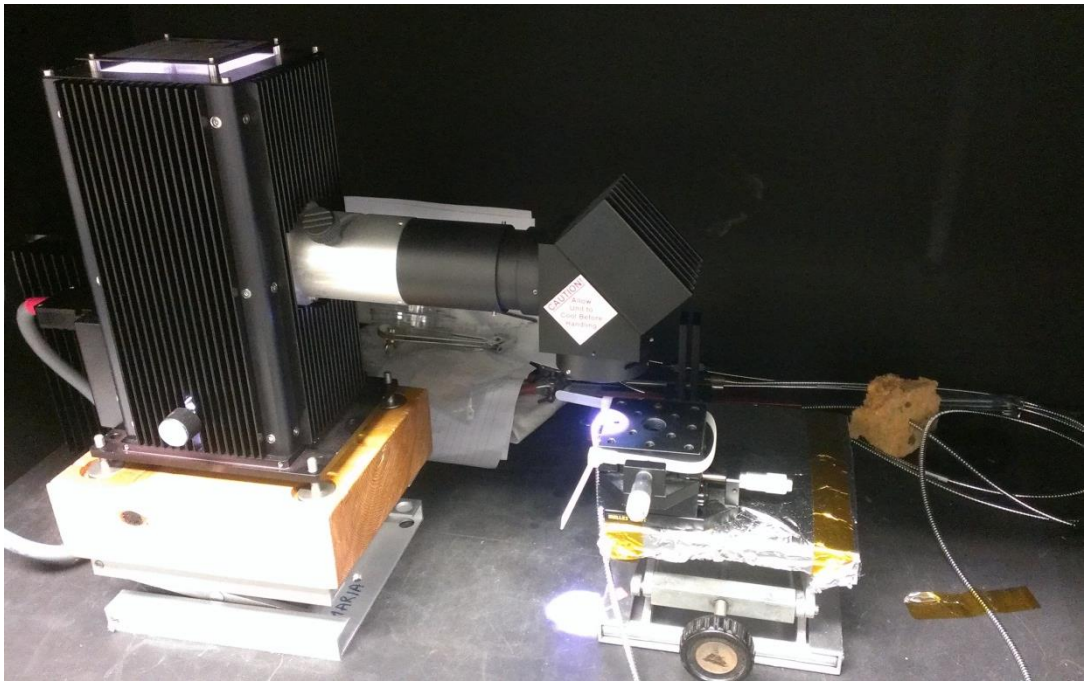

Figure 2-9: Apparatus set-up for measuring the spectrum of the xenon (pictured) and deuterium ultraviolet sources. Light entered the spectrometer via an optic cable with a diffuser attached.

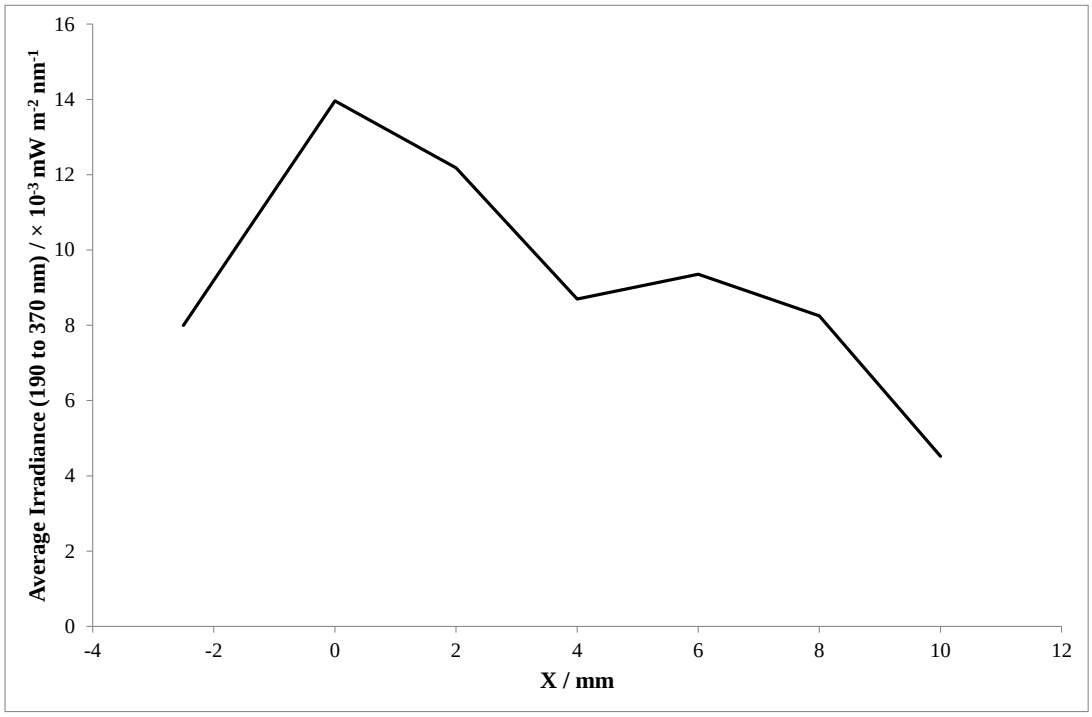

Figure 2-10: The average UV irradiance of the deuterium lamp across the centre of the footprint.

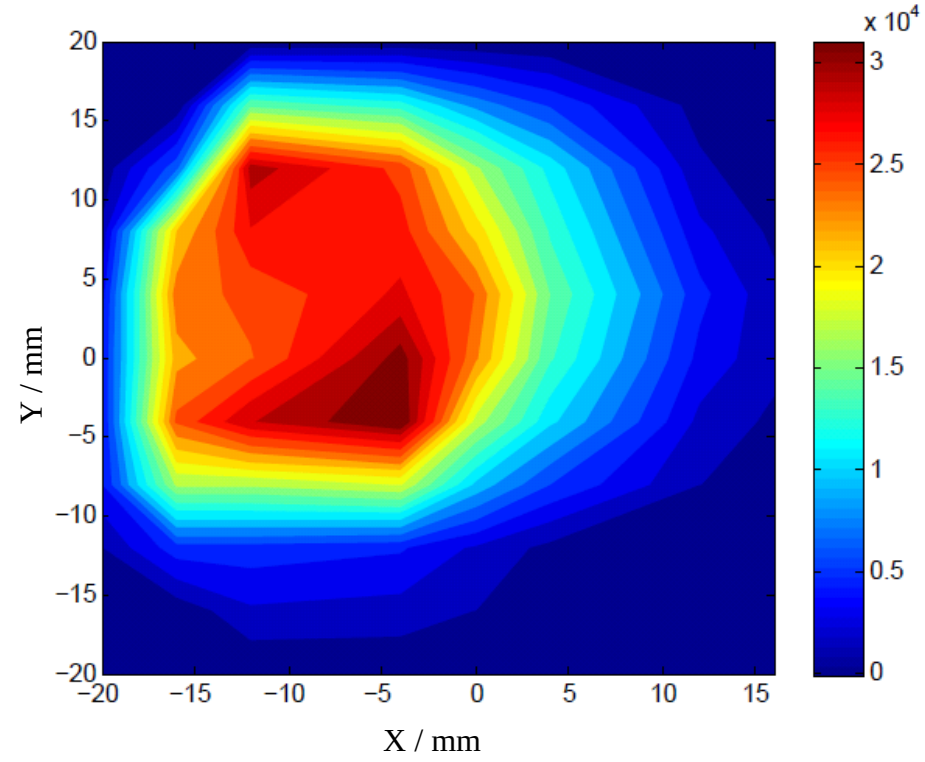

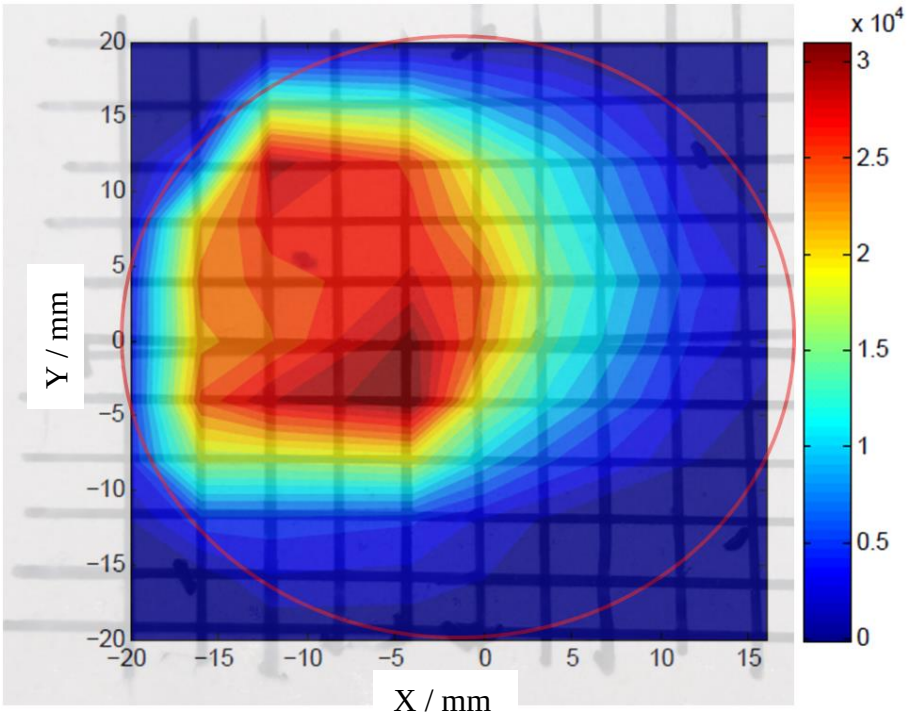

Figure 2-11: The irradiance footprint of the xenon lamp at a height of 4.5 cm; scale bar: J s^{-1} m^{-2} (top). The lower figure shows the actual grid used to take measurements superimposed over the resulting irradiance footprint, where the drawn grid is spaced 4 by 4 mm. Markings to denote and line up where the visible footprint can be seen, made clearer by the addition of a red circle.

The irradiance output of the lamps was used to determine the length of the exposure that would be equivalent to a martian average daily dose of UV radiation. Model UV flux calculations were performed at the equator and at a latitude of 20 °N, using the adapted radiative transfer model from Patel *et al.* (2003) and Otter (2009). The dust optical properties from Wolff *et al.* (2009) use the method of fitting T-matrix phase functions to the measured phase function of martian dust particles. Wolff single scattering properties were in good agreement with other retrievals (Goguen *et al.*, 2003; Mateshvili *et al.*, 2007; Wolff *et al.*, 2010), compared to Ockert-Bell *et al.* (1997), and suggested a higher absorption of light at wavelengths of less than 300 nm. For this reason, the exposure times that were used for UV experiments were those calculated using the Wolff fluxes.

Using a nominal atmospheric dust loading year scenario from the TES on the MGS orbiter, the UV dose rate was calculated for different times of the year and then averaged to give an average daily dose (Table 2-2; Jon P. Mason, private communication).

	Model at surface (Patel *et al.*, 2002)	*Deuterium lamp* (WD at 5 cm)	*Xenon lamp* (WD at 4.5 cm)
Maximum integrated dose rate / Js^{-1} m^{-2} (160 – 400 nm)	0.6819	0.6682	415.3366
Lamp exposure duration (equator equivalent)	-	13.98 hr	21.03 min
Exposure time (20 °N equivalent)	-	12.77 hr	19.22 min

Table 2-2: Equivalent dose rates for the average daily dose and exposure times of the two UV sources compared to the model UV dose rate expected at Mars. WD is the working distance.

To determine the stability of the UV output of the lamps, irradiance measurements were recorded from the moment the lamps were switched on and continued for several hours, with the resulting plots showing that both lamps took approximately 1.5 hrs to warm up to maximum output (Figure 2-12). Experiments using the deuterium lamp had a combined length of 17 or more hours (the exposure time, the time for the lamp to warm up and the pre- and post-exposure Raman spectroscopy); these long exposures with the deuterium lamp would have been affected as the output never stabilised, producing an irregular UV dose. The xenon lamp was favoured for most experiments compromising some UVC range for a more stable output and reduced exposure time. Once the xenon lamp is warmed up, the longest single exposure was 21 minutes over this time period the UV dose can be assumed to be stable. Any multiple exposures using the xenon lamp were conducted within 4 hours of lamp switch on, during which the lamp output is regular with little fluctuation. Figure 2-13 shows an example of the UV lamps being used in an exposure experiment.

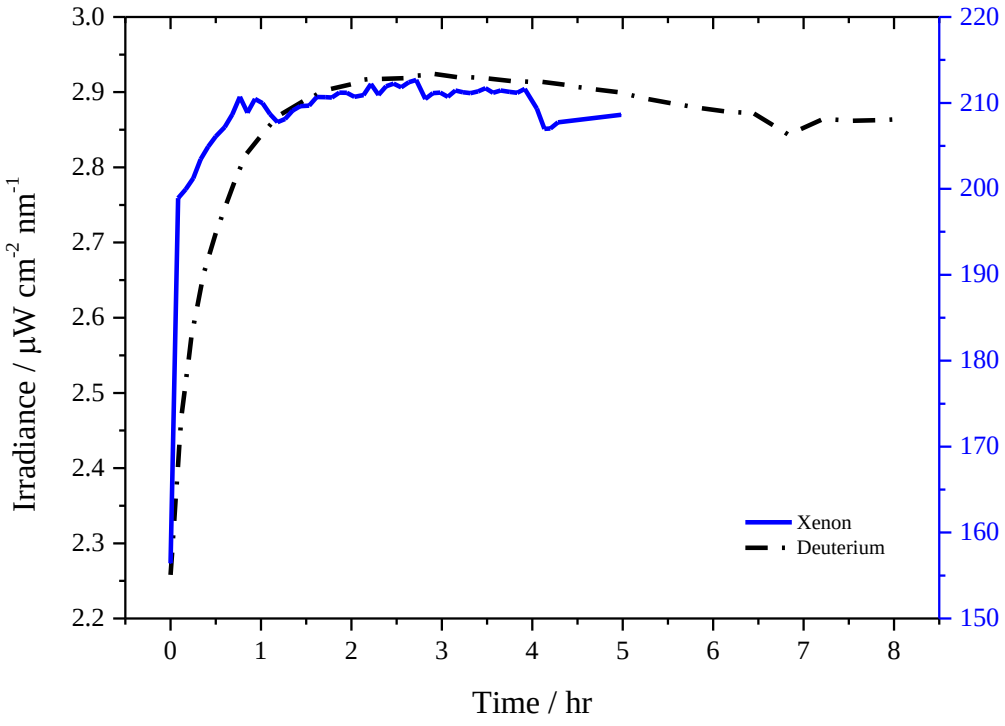

Figure 2-12: The irradiance of the deuterium (dashed line) and xenon (solid line) lamps over approximately 8 and 5 hr respectively. The irradiance of the deuterium lamp has been scaled by 100 times. Having warmed up after approximately 1.5 hr, the irradiance of the deuterium lamp appears to degrade after 4.5 hr by approximately 0.1 µW cm^{-2} nm^{-1}.

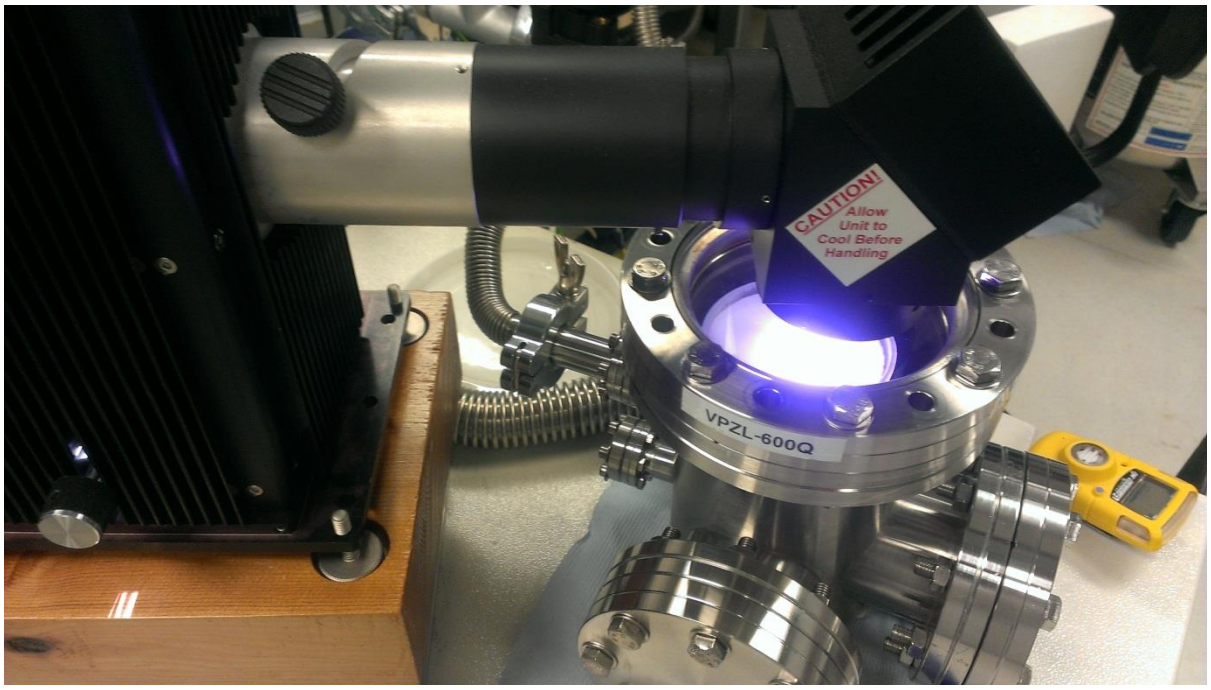

Figure 2-13: An example of the xenon lamp being used in an exposure experiment with the *Bernard* MSC.

2.3.4 Analogue martian environments

To investigate the physical and chemical interactions between the surface, the atmosphere and various elements or molecules, analogue regoliths have been created for use in laboratory simulations; one in common usage is JSC Mars-1 (Allen *et al.*, 1998), described below. In addition, an unaltered basalt from Skye, UK was also used as an analogue for experiments (more detail in Section 4.2.5.1).

2.3.4.1 JSC Mars-1

JSC Mars-1 was sourced by hand by Allen *et al.* (1998) at 1850 m elevation from the Pu'u Nene volcanic cone of the Mauna Kea volcano in Hawai'i, once removed from the source site it was sieved to obtain the < 1 mm sized fraction, dried at 80 °C or less and re-sieved (*ibid*). One disadvantage of JSC Mars-1 is that it contains a significant amount of volatiles, most likely dominated by H_2O with some SO_2 (*ibid*), unlike current day Mars, which is relatively dry (Biemann *et al.*, 1977); these volatiles could affect astrobiological experiments (Seiferlin *et al.*, 2008) as they could interact with any molecules or microbes introduced to the simulant, but they can be reduced by baking the regolith prior to use. The visible and near-infrared reflectance spectra of JSC Mars-1 are similar to the remotely observed spectra on Mars (*e.g.* the Olympus-Amazonis Martian bright region (Mustard and Bell, 1994)), whereas it is less similar to the chemical composition of Mars (Allen *et al.*, 1998). Hargraves *et al.* (1999) suggested that JSC Mars-1 may not be suitable as an analogue in some cases, including use in aeolian magnetic studies. At the time, Allen and Morris (1999) agreed on the basis that there was not enough data from Mars to justify all aspects of JSC Mars-1 as an analogue, that it may not be fully suited to all martian simulation experiments; however it is useful to support research, development education and public outreach activities. As JSC Mars-1 is spectrally similar to Mars in the visible

wavelength range (Figure 2-14), it was chosen as an analogue for this project as visible wavelength spectroscopic techniques will be applied, but appreciative that it is potentially not ideal in other aspects of martian simulation.

2.3.4.2 Use of JSC Mars-1

Samples of grains of JSC Mars-1 approximately 1 mm in size or a pre-powdered sample were selected for use in exposure experiments. To reduce the pre-existing volatiles within samples to a minimum, as noted by Seiferlin *et al.* (2008), samples were baked in a *Pyrex* beaker in an oven for a duration of at least 10 hr, normally overnight, at 350 °C to reduce the volatile content. Samples remained in the beaker they were baked in and covered with *Parafilm* to seal them to reduce contact with moisture in the atmosphere. If any volatiles remained in the sample, it is possible that they could react with the amino acids causing erroneous results; hence every precaution was taken to reduce the volatiles.

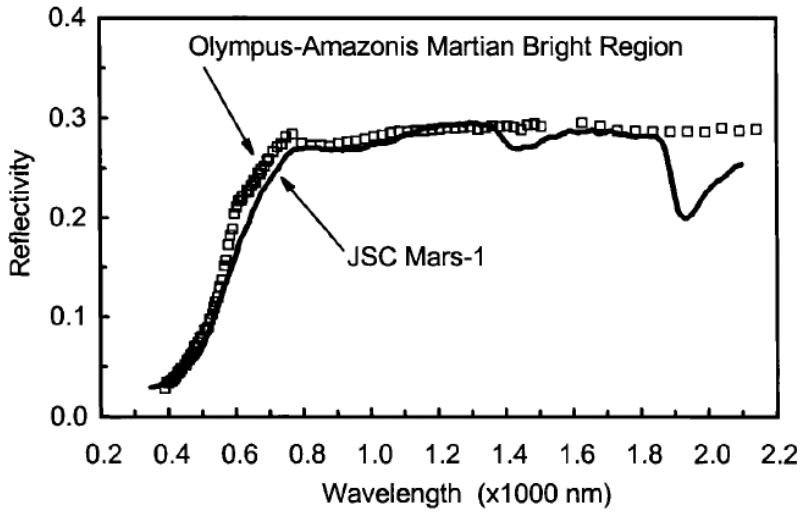

Figure 2-14: The visible and near-IR reflectivity spectrum of JSC Mars-1 compared to the spectrum of the Olympus-Amazonis Martian bright region, from Allen *et al.* (1998).

2.4 Preparation of amino acids

Standards of the amino acids were prepared as a 1 % solution of 0.1 M HCl from solid form (sourced from Sigma Aldrich, UK, 99 + % purity). Glass vials to store the standards were cleaned with 18.2 MΩ H_2O, methanol and dichloromethane (DCM); the vials were rinsed with each solvent three times in turn, or when possible, were sonicated for 10 min in each solvent in turn and dried in a fume cupboard. Approximately 10 mg of solid amino acid was weighed out and placed in a vial, and approximately 1 g of 0.1 M HCl was added to make a 1 % solution. Some amino acids, L-cysteine and L-tyrosine did not easily dissolve in 0.1 M HCl, so a few drops of 1 M HCl were added to these solutions to fully dissolve the solid. To create samples of the amino acids for characterisation or exposure experiments, drops of these standards were placed on Petri dishes or microscope slides (also cleaned and/or sonicated in 18.2 MΩ H_2O, methanol and DCM) and dried on a 65 °C hot plate to evaporate off the HCl solvent, leaving a thin film of amino acid ready for testing.

2.5 Microbiology materials and techniques

As described in Section 1.3.2.1, Mars has evaporite environments that could host halophilic life, extant or extinct. The following microorganisms were chosen as model (*Halobacterium salinarum* NRC-1) and test (*Haloferax* N3.1 and *Haloarcula* N4.1b) microbes for exposure experiments in MSCs to understand how the Raman signature of the carotenoids were affected and whether they could survive simulated martian conditions while entombed in halite crystals. An example of the microbes in media suspensions are shown in Figure 2-15.

2.5.1 *Microbial cultures*

2.5.1.1 *Halobacterium salinarum* NRC-1

Halobacterium salinarum NRC-1 (hereafter referred to as *H.sal* NRC-1) is a thalassic aerobic chemoorganotroph and though it is a member of the domain archaea, it was discovered before the third domain of life was designated (Woese *et al.*, 1978), hence a reference to 'bacterium' in its name. Its total genome sequence is known (Ng *et al.*, 2000) making it useful as a model halophilic organism.

2.5.1.2 *Haloferax* N3.1 and *Haloarcula* N4.1b

The following two species were isolated from crystalliser pond Salterns at Salines es Trenc in Mallorca. *Haloferax* N3.1 is a strain of archaea defined as the genus *Haloferax* through sequence analysis, but is currently an unnamed strain, denoted N3.1. It has a coccoid morphology. A well-studied *Haloferax* species is *Haloferax volcanii*, a moderate halophile (optimal NaCl 1.7 – 2.5 M) and, because of its relatively stable genome and other traits, it is described as a model organism for study of halophiles (Hartman *et al.*, 2010). As *Haloferax* N3.1 has not been fully characterised, it is assumed that it is similar to other *Haloferax* species, such as *Haloferax volcanii*. *Haloarcula* N4.1b is a strain of archaea defined as the genus *Haloarcula* through sequence analysis, but is currently an unnamed strain, denoted N4.1b. It has a coccoid morphology. As *Haloarcula* N4.1b has not been fully characterised it is assumed that it is similar to other *Haloarcula* species. The *Haloferax* N3.1 and *Haloarcula* N4.1b will hereafter be referred to as N3.1 and N4.1b, respectively.

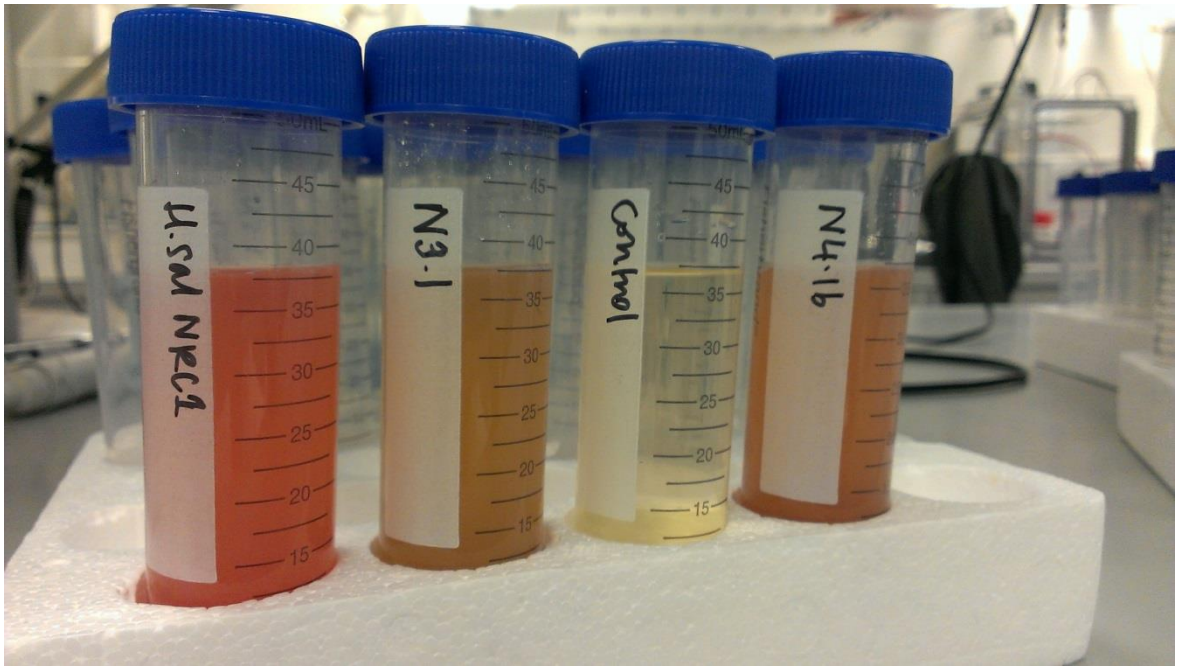

Figure 2-15: Media suspensions of the microbial species used in experiments.

2.5.2 Growth medium and cultivation

The microorganisms were grown in a 20% w/v NaCl medium, as previously described by Payne *et al.* (1960), and modified by Gramain (2009). The contents of the medium were sourced from Sigma Aldrich, UK or Fisher Scientific, UK. The medium contained per litre: 200 g of NaCl; 20 g of $MgSO_4$ $7H_2O$; 2 g of KCl; 3 g of Tri NaCitrate; 10 g of Difco™ Yeast Extract; 7.5 g of Cassein hydrolysate; 36 mg of $FeCl_2$ $4H_2O$ and 0.36 mg of $MnCl_2$ $4H_2O$. The NaCl and $MgSO_4$ $7H_2O$ were added to 700 ml of double distilled (dd) H_2O (solution A); while the nutrients and $FeCl_2$ $4H_2O$ and $MnCl_2$ $4H_2O$ were added to 300 ml of ddH_2O (solution B). The pH of solution B was adjusted to 7.6 using 10 M NaOH. Solution A and B were sterilised separately in an autoclave, then solution B was added to solution A once cooled.

For agar plates, 15 g of agar (Fisher Scientific, UK) was added to solution B post-pH adjustment. After being autoclaved separately, solution B was added to solution A in a water bath at approximately 60 °C to avoid solidification of the agar. Approximately 13 ml of the mixed solution was poured into sterile Petri dishes (90 mm diameter), which gave an agar substrate approximately 5 mm in thickness.

The growth medium was inoculated to 1 or 2 %; generally a 2 % inoculant was used in primary experiments and preliminary tests were conducted using 1 % inoculations. Once inoculated, the culture was incubated at 37 °C in the dark. Growth was monitored by measuring the optical density (OD) of the culture at 600 nm, see Section 2.5.4. If the microbes had been inoculated from a glycerol stock that had been stored at −80 °C, the incubation period was increased by two or three days to enable recovery from deep freeze storage.

2.5.3 Embedding of microorganisms in laboratory grown halite crystals

To obtain the microbes for embedding in halite, the following procedure was followed: the growth medium was centrifuged (4000 × *g*, 4 °C, 20 min) and the resulting pellet was subsequently washed in 4 M Tris-NaCl buffer. The centrifuge cycle and wash were repeated three times before resuspending in the same buffer solution. For 100 ml of the solution, 23.376 g of NaCl and 1.21 g of Tris was added to 90 ml of ddH_2O. A few drops of dilute HCl were added as necessary to obtain a pH of 7.4 before the solution was autoclaved.

Halite crystals were formed by allowing 20 µl of the solution, controls or with the microbes suspended, to dry overnight on microscope cover slips in a sterile laminar flow hood (the flow was switched off once the samples were prepared to avoid the crystals drying too fast, but the hatch was closed). Once dry, the cover slips were stored in sterile plastic Petri dishes under dark conditions at room temperature. An example of the halite crystals once they have formed is shown in Figure 2-16.

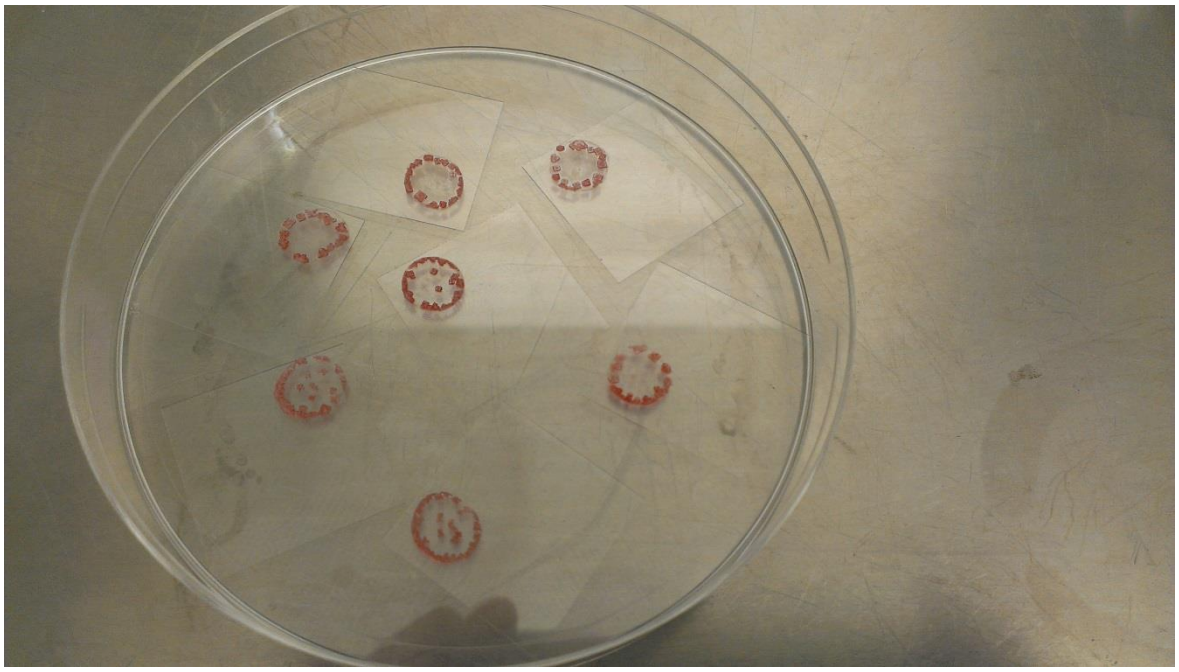

Figure 2-16: The halite crystals containing *H. sal* NRC-1 microbes.

2.5.4 Monitoring microbial growth

Microbial growth was monitored by measurements of the optical density (OD) of the growth media. Measurements were obtained using a *Camspec M107* spectrophotometer at a wavelength of 600 nm (OD_{600}) (Figure 2-17). A sterile aliquot of the growth media was used to record a blank measurement which samples were measured against. OD measurements were taken either in disposable plastic cuvettes or glass test tubes. Cuvettes were used in the earlier experiments to measure the OD. Using cuvettes proved to be impractical (including not cost effective) and a method was devised to use glass test tubes in later experiments (Figure 2-18). The method used in each experiment to measure the OD will be specified in Chapter 5 where necessary.

2.5.4.1 Disposable cuvettes

Disposable plastic cuvettes from Fisher Scientific (1 ml volume) were used in some earlier experiments. To reduce waste, one cuvette was used for each test, within which there were five samples for statistical testing. 1 ml of sample was removed from gold screw lid media bottles using sterile pipette tips. The bottles were handled using the standard technique with a Bunsen burner on a blue flame to create an aseptic environment. The bottles were passed through the flame and, as soon as the lids were removed, the sample was removed and the lid was replaced once the bottle opening was passed through the flame again. The sample was placed in the cuvette, the pipette tip was discarded and the OD was measured. The sample was then replaced into the bottle, which was sterilised using a Bunsen burner as previously described.

Figure 2-17: The *Camspec M107* spectrophotometer.

However, this method was time consuming, allowed for cross-contamination and had high consumable use (pipette tips and plastic cuvettes), so the method below using test tubes was devised for later experiments.

2.5.4.2 Test tubes

Cultures were grown in sterilised test tubes, with cotton wool and foil stoppers, which allowed for direct OD measurements of the culture. This alternative method was devised to greatly reduce the risk of contamination. Furthermore, this method reduced the time taken to record measurements with the disposable cuvettes. The spectrophotometer had interchangeable holders for cuvettes or test tubes.

Figure 2-18: Measuring optical density – gold screw lid media bottles and test tubes with cotton wool and foil stoppers.

2.5.4.2.1 Biological control samples

Control cultures were used to obtain a baseline specific growth rate (described in Section 2.5.6) for each of the isolates. OD measurements of a 1 % inoculant into 5 ml of growth media in test tubes were taken once every 1.5 hours where possible. Before the OD was measured the growth media was briefly vortexed to homogenise the culture within the media. Regular measurements were taken over six days to incorporate the log phase of growth, with a single measurement per day taken for the final three days to ensure stationary phase had been reached.

2.5.4.2.2 Halite entombed samples

Samples of the isolates that were entombed in halite (described in Section 2.5.3) were used in simulated martian environment exposure experiments (described in Section 2.5.5), which were conducted in triplicate. Once complete, the coverslips that the triplicate of halite crystals had dried onto were carefully broken and each piece holding an individual halite crystal was dropped into a pre-prepared test tube containing 5 ml of growth medium. The halite crystals were then allowed to dissolve and OD measurements were recorded daily (freeze-thaw experiments) or every 1.5 hr where possible (Mars-like surface environment exposures). Samples exposed to freeze-thaw cycles were monitored for 26 days and samples exposed to Mars-like surface environment exposures were monitored for 50 days.

2.5.5 Exposure to martian conditions

Halite entombed halophiles were exposed to Mars-like pressure, atmospheric composition, temperature and ultraviolet radiation environments, as described in Section 1.3.1.2. To achieve this, samples were placed inside one of two vacuum chambers, described in Section 2.3; *Percy*, had an interchangeable metal lid or glass viewport and was used for Mars-like freeze-thaw condition experiments in a temperature cycling oven, and *Bernard*, which had a quartz viewport and was used for Mars-like surface environment experiments.

The pressure was regulated in the chamber with the use of a computer-controlled system. The vacuum system was attached to a rotary pump, which was able to evacuate the chambers to ~ 2×10^{-3} mbar. Before samples were placed in the chambers and experiments were started, the chambers were initially evacuated to this minimum pressure and, where possible, were left pumped down at least overnight to ensure the evacuation of molecules,

such as water vapour or isopropyl alcohol (IPA) (used for cleaning the chamber). The atmosphere simulant was a rough Mars-like gas consisting of 95 % CO_2, 5 % N_2. The gas line had a forward pressure of approximately 2 bar and the flow into the system was regulated with a needle valve. The samples were cooled using a bed of CO_2 ice, which has a sublimation temperature of −78.5 °C, similar to martian surface temperatures and the Mars-like surface UV environment was simulated using a UV emitting deuterium or xenon lamp, as described in Section 2.3.3. An example of samples being exposed to these conditions is shown in Figure 2-19. There were varied UV exposure times that corresponded to varying UV irradiances. The exposure times using the xenon UV lamp were 48, 72, 120, 602 and 1261 s corresponding to 20, 30, 50, 250 and 524 kJ m^{-2}, respectively.

These exposure lengths were derived from theoretical martian daily UV fluxes (Patel *et al.*, 2002), as described in Sections 1.3.1.2 and 2.3.3, where 1261 s (21.03 min) of exposure resulted in an equator equivalent daily dose expected to be experienced on Mars.

Figure 2-19: Microbe embedded halite crystals about to be removed from *Bernard* after exposure to 'full' martian conditions. A set of samples being exposed to near surface conditions are covered in tin foil to remove UV exposure.

2.5.6 Biological experiments

Survivability studies were conducted to determine whether the microbial species can survive in Mars-like conditions. Here, it was hypothesised that exposed cells would not remain viable. When exposed to a Mars-like UV environment, Fendrihan *et al.* (2009a) found the dose with a 37 % survival (D_{37}) for *H.sal* NRC-1 in liquid media was 1.5 kJ m^{-2}, and 0.7 kJ m^{-2} when spread on agar plates. However, if entombed in a mineral such as halite, microorganisms can survive higher dosages; for example, the archaea *Halococcus dombrowskii* when entombed in halite survived a dose of 10^4 kJ m^{-2} (*ibid*).

To measure growth after exposure, the OD was plotted against time, which produced a microbial growth curve. Typically, growth curves can be divided into four different phases of growth. (1) The lag phase where microbes are adapting after having been introduced into the media and are not yet dividing; (2) the logarithmic (log) or exponential phase of growth represents the period of time characterised by cell doubling; 3) the stationary phase where there is a depletion of the nutrients and/or a growth inhibiting product; and 4) the death or decline phase, where nutrients have run out and the microbes die.

The log phase is used to calculate the specific growth rate, μ, of the microbial species defined by Equation 2-2:

$$\mu = \frac{\ln 2}{t_d} \tag{2-2}$$

where t_d is the doubling time. Using the growth curves, μ can also be defined as:

$$\mu = \frac{OD_2 - OD_1}{t_2 - t_1} = \frac{\Delta OD}{\Delta t} \tag{2-3}$$

where OD_1 is the initial optical density at an initial time, t_1; OD_2 is the optical density at a given time, t_2; and Δt is equivalent to t_d.

2.5.6.1 Growth rate and cell density in liquid media

Cell numbers were recorded either by direct cell counting or using OD measurements as a proxy. For direct cell counts, cells were counted using a cell counting grid, a Thorna, Preciss, Europe counting grid slide (shown in Figure 2-20). 20 µl of Acridine Orange stain was added to 100 µl of the culture medium to make the cells more visible. Five squares on the grid (0.0025 mm^2; where the space between the cover slip and the grid was 0.1 mm, resulting in a viewed volume of 0.00025 mm^3) were chosen randomly and the number of cells were recorded using a handheld manual tally counter. Cell density and OD have a linear relationship up to OD measurements of approximately 0.5 to 0.6. The theoretical relationship remains linear, but in practice with increasing cell numbers the scattered light by one cell can be scattered multiple times by other cells so the relationship deviates from linearity and OD measurements become less accurate. Multiple ODs of an aliquot of liquid culture were measured and cell counts were subsequently recorded. The relationship of cell density to the turbidity of the growth medium is shown in Figure 2-21.

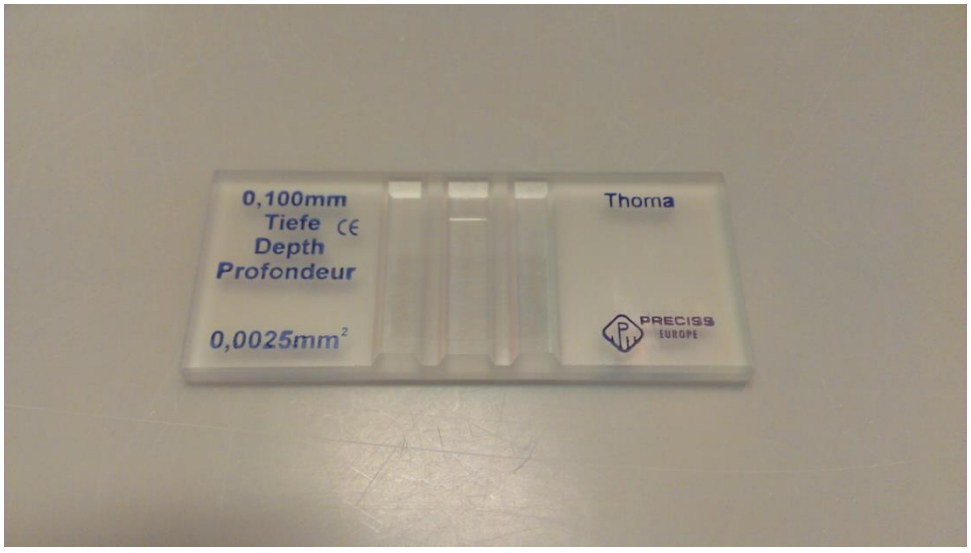

Figure 2-20: The counting grid slide used to count cells.

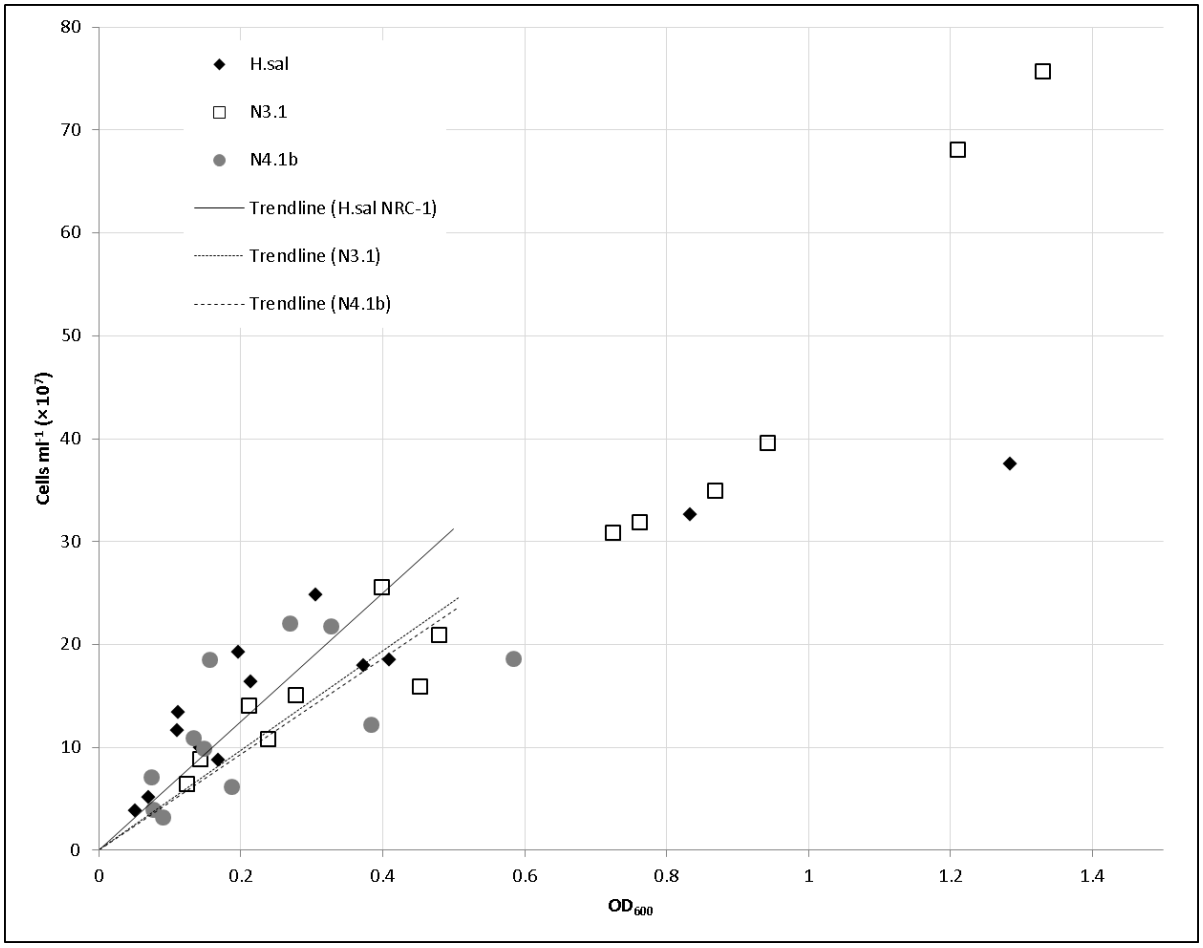

Figure 2-21: Cell concentration as a function of optical density (OD_{600}) for each microbial species. The trend lines represent the linear relationship between cell density and OD up to 0.5, after which the relationship deviates from linear.

2.5.7 Raman spectroscopy of halophilic microbes

Raman spectroscopy was performed on negative control halite crystals and crystals embedded with the halophile species. The apparatus used and the data collection methods are described in Section 2.2. Before exposure to simulated martian conditions, a crystal formed from each of the cell suspensions was imaged and mapped by the Raman spectrometer. The field of view through the × 10 objective lens is approximately 600 × 320 μm. The *x-y* map of the crystal was chosen to be 500 × 300 μm so the mapping area could be imaged using the ×10 objective lens.

More often crystals were approximately four times the size of the mapping area, though some did fit in the field of view. Areas with standard hopper formation with obvious fluid inclusions (appearing as pink shaded areas when microbes were embedded) were chosen for mapping where possible (see Chapter 5, Figure 5-20 for an example).

2.5.7.1 Mapping of the crystal z-axis

The Raman spectrometer could focus to approximately 300 to 400 μm depth in a transparent material, *i.e.* halite crystals, allowing the fluid inclusions containing the microbes within the crystal to be investigated pre- and post-exposure to martian conditions. Using the mapping function as described in Section 2.2.3, with a line along the surface in the *x*-axis of length 500 μm (coordinates −250 to 250 μm in the software), an area that appeared pink (denoting the halophiles) in the microscope images was chosen and the *x*-axis line placed along this area. The *z*-axis coordinates were determined by using the RTD function to check that a reliable signal could be obtained at a given depth, as each crystal was a different thickness. Once the *z*-axis depth was determined, the *x*-*z* map was acquired using the ×50 LWD aperture. The data were processed using a custom *MATLAB* routine that removed the noise under the baseline, recorded the position of any bands and their intensities.

2.5.8 The LIVE/DEAD® BacLight™ Bacterial Viability Kit

The LIVE/DEAD® BacLight™ Bacterial Viability Kit (hereafter referred to as LIVE/DEAD kit) developed for the enumeration of bacteria (*e.g.* Boulos et al., 1999) has been proven for use with archaea over a range of pH and high ionic strengths (Leuko et al., 2004). The LIVE/DEAD kit uses two dyes, propidium iodide (PI) and SYTO® 9 (SYTO 9), to stain microbes red or green, respectively. The SYTO 9 stains all the microbes, whether live or dead. The PI only penetrates cells that have compromised membranes and therefore these cells fluoresce red; the PI molecule is highly charged, so normally would not penetrate the cell. However, it will penetrate damaged membranes and can displace weaker dyes, such as SYTO 9 (*ibid*). The fluorescence provided by the stains allows the percentage of the culture that was viable before and after exposure experiments to be determined for comparison, and hence establish whether the culture had survived. Each microbial species was stained with the LIVE/DEAD kit by adding 0.54 µl of stain to 180 µl of the Tris buffer solution containing cells (Molecular Probes Inc., 2004). 20 µl aliquots of the solution were allowed to dry on microscope cover slips while stored in a dark box.

2.5.9 Confocal microscopy

Fluid inclusions form throughout the halite crystals. During UV exposure experiments it was possible that the UV was attenuated by the halite (described in Section 1.3.2.1); or part of the culture in the same or another fluid inclusion may absorb some of the radiation and shield cells directly beneath, hence, survival of the microbes may depend on their location within the halite crystal. Confocal microscopy allows multiple *x*-*y* cross-sections of the halite crystals along the *z*-axis (coordinate system defined in Figure 1-11) to be examined while imaging cells bound in fluid inclusions that have been stained with fluorescent dyes.

Using the LIVE/DEAD kit (described in Section 2.5.8), two methods of staining were conducted. This involved staining the cells (1) before or (2) after the cells were embedded in halite. For (1) each microbial species was stained with the LIVE/DEAD kit as described in Section 2.5.8 and were allowed to dry on microscope cover slips while stored in a dark box. For (2) crystals that had no pre-stained cells embedded were exposed to UV radiation. The dye mixture was added to the surface of the crystal post-exposure and examined with the confocal microscope. The confocal microscopy was conducted with the assistance of Stephen Summers (OU).

2.6 TEM and SEM

Transmission Electron Microscope (TEM) imaging was used to examine the morphological differences between the microbial cells before and after exposure to UV radiation. The microscope was a TEM JEM1400 (Jeol, Japan), the accelerating voltage used was 80 kV, the camera was an AMT XR60 mid-mount with 11 megapixels and the camera control software was *AMT Capture Engine*. TEM images of the microbial species were obtained with the assistance of Heather Davies (OU). Once growth phase was established, cells were centrifuged (Section 2.5.3) and the pellets were resuspended in the growth medium and aseptically spread onto agar plates. Once there was visible growth on the plates, the colonies were exposed to UV radiation.

A control colony and a UV exposed colony from each microbe species were placed in 2.5 % glutaraldehyde in 0.1 M sodium cacodylate, pH 7.4, containing 0.1 % ruthenium red (cacod/RR). The samples were post-fixed in 2 % osmium tetroxide in cacod/RR by aspiration at each step. The samples were dehydrated through an ascending series of acetone permeated with Epon resin at 60 °C with six changes. Finally, samples were embedded in Epon and polymerised at 60 °C for 48 hrs.

The thickness of the ultrathin sections was 70 nm, which were cut using a diamond knife and then collected on copper slot grids with a formvar/pioloform film and counter-stained with 3.5 % aqueous uranyl acetate and Reynolds lead citrate. The TEM images provided a cross-section of the cells allowing any changes in the cell wall, cell membrane or cytoplasm (containing the plasmid) to be observed.

To understand the extent of the decline in the number of viable cells resulting from exposure to Mars-like conditions the cells were examined for changes in their morphology and were counted. To count the cells in the images, they were marked in *MS Paint* with a green or red line to denote viable or non-viable cells, respectively. The numbers of viable and non-viable cells were counted using a handheld manual tally counter.

A Scanning Electron Microscope (SEM) was used to determine the composition of the basalt used as an analogue regolith in exposure experiments. The SEM apparatus used was a *FEI Quanta 200 3D* and the data were obtained with the assistance of Diane Johnson (OU). The detector was an Oxford Instruments X-Max 80 mm^2 Energy Dispersive Spectroscopy (EDS) detector, with data collection and processing conducted using *Oxford Instruments INCA* software. The beam current was 0.6nA, the accelerating voltage was 20kV and the pressure was approximately 2 to 5×10^{-5} mbar.

2.7 Summary

As a multidisciplinary science, astrobiology uses a wide range of analytical techniques and methods. Work in this project reflected this; though the focus was on Raman spectroscopy, which can provide unique molecular ‘fingerprints’ for organic molecules and minerals and hence measure changes in molecules, other techniques are useful in supporting the results of the Raman analyses.

“Science isn't about why, it's about why not.”

– Cave Johnson, CEO Aperture Science

3. Amino Acid Raman Band Characterisation

3.1. Introduction

Amino acids, among several molecules, have been identified as potential candidates for detection in the search for life elsewhere in the Solar System (*e.g.* Parnell *et al.*, 2007; Aerts *et al.*, 2014). Extraterrestrial amino acids have already been detected in meteorites, for example, the Murchison meteorite (*e.g.* Kvenvolden *et al.*, 1970) and the Orgueil and Ivuna meteorites (Ehrenfreund *et al.*, 2001b). Murchison was found to harbour amino acids that are unique to carbonaceous chondrites, with only eight of the 75 detected amino acids present in terrestrial biology (*e.g.* Kvenvolden *et al.*, 1970; 1971; Cronin *et al.*, 1995). As these studies show, the detection of amino acids is not an unambiguous indicator of life, as there are many amino acids not used by life and a full catalogue of the amino acids that are used by terrestrial biology have not been discovered elsewhere in the Solar System to date. Nonetheless, amino acids are regarded as a high priority for detection on future planetary missions because of their ubiquity in terrestrial life as the building blocks of biologically important biomacromolecules, such as proteins (Parnell *et al.*, 2007). Although other biomarkers could be considered as unambiguous indicators of life, such as porphyrin, which is only produced in large quantities by biological processes (Suo *et al.*, 2007) and β-carotene (Vítek *et al.*, 2009), detecting a localised concentration of all 20 amino acids exclusively used by terrestrial biology in an extraterrestrial environment such as Mars could suggest that life similar to that found on Earth may have arisen there in the past.

On future planetary missions, if amino acids are detected they will need to be distinguished from a matrix of materials, such as regolith. The detection of biomarkers, molecules that cannot be synthesised in large quantities by abiogenic means (Eglinton *et al.*, 1964), is a priority for the ESA *ExoMars* mission in 2020. A Raman spectrometer equipped with a 532 nm laser (Edwards *et al.*, 2012a) will be among the suite of instruments on board to aid the detection process (Edwards *et al.*, 2012b). This excitation wavelength was chosen for the range of molecular targets that could be acquired, while reducing background fluorescence and being able to equip the rover with a commercially available laser that would meet the mission mass and power requirements (Edwards *et al.*, 2012a). Raman spectroscopy has several potential advantages over other methods of life detection: it provides a spectroscopic fingerprint of molecules, samples require little or no preparation prior to analysis, samples are not destroyed by the analysis, and water does not interfere with the fingerprint region for organic molecules, which is between 500 to 1700 cm^{-1} (Auer and Skinner, 2008). There have been several studies that have attempted to assess the efficacy of Raman spectroscopy as a biomarker detection tool in extraterrestrial environments. For example, the Marsokhod test rover demonstrated that Raman spectroscopy could be used to identify carotenoids in samples identified by the rover team as biologically interesting (Newsom *et al.*, 2001). An extensive study of extremophilic organisms using a range of Raman excitation wavelengths sought to determine optimal analytical parameters (Jorge Villar *et al.*, 2005). An IR laser with an excitation wavelength of 1064 nm required prolonged exposure times to collected useful spectra, especially for compounds of low concentration and lower wavelengths such as 514 and 488 nm lasers were not able to obtain good results for geomarkers; they concluded that an excitation wavelength of 785 nm provided a compromise for the study of both biological and geological samples in extraterrestrial environments (*ibid*). Portable Raman instruments,

using an excitation wavelength of 785 nm, were successfully used to determine the Raman spectra of solid amino acids that had been exposed to outdoor conditions: full sunshine and an ambient temperature of 20 °C (Culka *et al.*, 2010). Similarly, Culka *et al.* (2011) and Culka *et al.* (2012) examined several biomarker/matrix mixes using portable Raman devices and were able to identify the individual biomarkers, including glycine and alanine, from their Raman signatures within the gypsum matrix.

Qualitative analyses of the protein amino acids and other molecules have been carried out with Raman spectroscopy (*e.g.* Jenkins *et al.*, 2005; De Gelder *et al.*, 2007; Zhu *et al.*, 2011). These studies present the spectra for reference and have largely described the strongest Raman bands that might best serve as identifiers for specific molecules. For glycine and alanine, intense bands were found in the region 850 to 900 cm^{-1} (De Gelder *et al.*, 2007), assigned to the symmetric CNC stretch mode. For glycine, the strong bands at 894 and 1327 cm^{-1} were considered markers; the marker for alanine was reported as the strong band at 852 cm^{-1}; and for aspartic acid, the band at 939 cm^{-1} was described as the most intense, with another strong intensity band at 1338 cm^{-1}, by Zhu *et al.* (2011). Furthermore, Rosado *et al.* (1997) and Kumar *et al.* (2006) described the bond assignments for the bands of alanine; bond assignments for aspartic acid, cysteine and glycine are reported by Navarrete *et al.* (1994), Pawlukojć *et al.* (2005) and Kumar *et al.* (2005), respectively. Bond assignments for glutamine are defined by Dollish *et al.* (1974) and Dhamelincourt and Ramirez (1993).

However, identification of amino acids based on these studies is complicated by several factors. (1) Identification of characteristic spectral bands for individual amino acids have been based on the position of the strongest band and have not considered weaker bands that may prove useful in identifying amino acids in complex matrix materials. Although studies such as Culka *et al.* (2011; 2012) follow good practice and use multiple bands as

reported elsewhere (*e.g.* Kumar *et al.* (2005) for the Raman bands of L-alanine) to identify molecules within a matrix of materials, it has been noted previously by Vandenabeele *et al.* (2012) that it may be necessary to define the minimal number of bands needed to make a positive identification of a molecule when in a mixed material (though the authors do not suggest what the minimum number should be[1]). (2) Studies that have published relative wavenumber positions of amino acid bands have often examined the samples with single but differing excitation wavelengths and Raman systems, which has led to discrepancies in intensity of bands and shifts of up to 33 cm^{-1} when comparing results between studies (*e.g.* Kumar *et al.*, 2006; Zhu *et al.*, 2011). Furthermore, a range of excitation wavelengths will be used on future planetary missions (*e.g.* 532 nm on *ExoMars*; 248.6 nm on *Mars 2020*, which is highly sensitive to condensed carbon, aromatic organics and minerals relevant to aqueous chemistry (Beegle *et al.*, 2014)), so it is important to study the same astrobiologically relevant molecules with various excitation wavelengths.

The intensity classification of the Raman bands in this investigation followed the classification criteria as defined by Vandenabeele *et al.* (2012), to provide consistency in the field of Raman spectroscopy. There are currently no IUPAC definitions for Raman band intensities, so the following annotations have been applied in this study (*ibid*): very strong (vs), strong (s), medium-strong (m-s), medium (m), medium-weak (m-w), weak (w) and very weak (vw), where the annotation is directly linked to the percentage intensity relative to the strongest band, see Table 3-1.

[1] Ideally all Raman bands would be observed, but this is atypical because of other factors such as fluorescence; or a fraction or a percentage of the total number of bands could be defined, but this would be a non-general case as every molecule has a different number of bands (*ibid*).

The definitions in Table 3-1 were applied in this study by determining the maximum intensity band and equating this to 1 and designating it as the strongest band (and would have a very strong annotation). The intensities of the other bands were divided by the strongest band intensity to give a number between 0 and 1. These results were multiplied by 100 to provide the percentage intensity of the strongest band, and hence, it was then possible to apply the intensity annotations.

Following these points, in this study a quantitative statistical approach was constructed to define the characteristic bands for L-alanine, L-aspartic acid, L-cysteine, L-glutamine and glycine. Multiple characteristic bands are presented as reference for each of the Raman bands of these astrobiologically relevant molecules. Furthermore, band intensities are provided and reference spectra of the amino acids are displayed for future studies of these amino acids.

Annotation	**Abbreviation**	**Relative intensity (to most intense band) / %**
Very strong	vs	90 – 100
Strong	s	75 – 90
Medium to strong	m-s	65 – 75
Medium	m	35 – 65
Medium to weak	m-w	25 – 35
Weak	w	10 – 15
Very weak	vw	0 – 10

Table 3-1: Raman band intensity annotations suggested for universal use and applied in this study, adapted from Vandenabeele *et al.* (2012).

3.2. Methods

3.2.1. Experimental method

Samples of L-alanine, L-aspartic acid, L-cysteine, L-glutamine (hereafter referred to as alanine, aspartic acid, cysteine, and glutamine) and glycine (99+ % purity; Sigma Aldrich, UK) were prepared as 1 % solutions in 0.1 M HCl as described in Section 2.4. Three samples of each of the amino acid solutions were pipetted onto individual glass Petri dishes, so they could be tested in triplicate and dried at 65 °C overnight. This resulted in the formation of a thin film of solid amino acid approximately between 4 to 10 mm in diameter. The samples were examined using a *HORIBA Jobin Yvon LabRAM HR* bench top Raman spectrometer, as described in Section 2.2. The power of each laser was 4.56 ± 0.27 mW and 4.49 ± 0.27 mW for the 514 and 473 nm excitation lasers, respectively. The instrument accuracy of the wavenumber position of the bands is ± 0.98 cm^{-1}, defined by the resolution of the grating, where measurements of the intensity occur on average every 1.96 cm^{-1}.

3.2.2. Calibration and data collection

Prior to data collection the Raman spectrometer was calibrated using the method described for the software version *LabSpec5* in Section 2.2.2. The calibration ensured that the instrument was in a near identical initial state for each sample. For each amino acid, three maps (of dimensions 100 µm × 100 µm), consisting of 16 spectra in a 4 × 4 grid with equal spacing, were produced for the 514 nm and 473 nm laser excitation wavelengths. Each map position was imaged and co-ordinates from a designated origin point were noted (for further details of the data collection and mapping technique, see Section 2.2.3). This

allowed the three maps to be measured in both wavelengths for direct comparison. The triplicate maps will be referred to as map 1, map 2 and map 3. The integration time was 5 × 15 s exposures, a total integration time of 75 s, for each spectrum. To avoid the Rayleigh scattering band overwhelming the less intense Raman signature, the Raman shift with a range of 10 to 2000 cm^{-1} was examined, which incorporates the fingerprint region for organic molecules, 500 to 1700 cm^{-1} (Auer and Skinner, 2008). Each spectrum was processed using the software *LabSpec5* to correct for effects resulting from the background signal, which comprises fluorescence effects, noise and offset from the CCD detector and other optical components of the spectrometer and stray ambient light. An auto-detect baseline function was used with further manual adjustments to ensure the baseline was correctly positioned before the data was reduced. The inbuilt *LabSpec5* band fitting function was used to determine the band positions, which fitted the reduced data with much greater accuracy than if the data had not been baseline corrected (Figure 3-1).

The first step of the process in determining whether the bands in each spectrum were characteristic of the amino acid was to check the frequency of occurrence of each band in the 48 spectra; the upper quartile of the sample bands were categorised as potential characteristic bands of that amino acid. These bands were subjected to further statistical analysis, described in Section 3.2.3, to identify characteristic bands for each amino acid. With every sample there were bands that did not fall into the upper quartile, though these bands may well be associated with the particular amino acid, they may not have been sufficiently intense to be identified by the band fitting algorithm over the 16 points in the map. Occasionally there was a band that was only in the upper quartile range in two of the three maps.

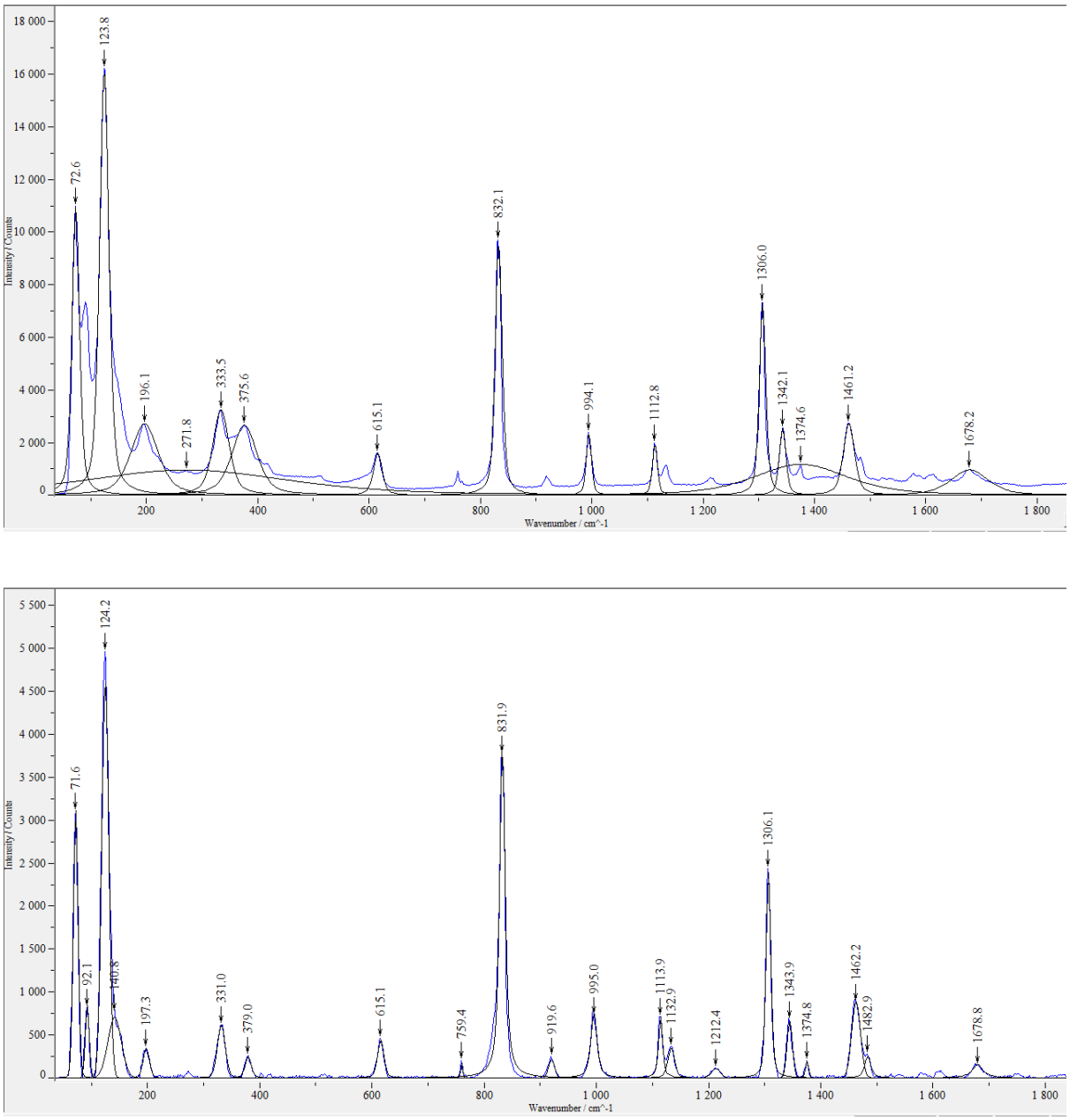

Figure 3-1: An example of a non-baseline corrected and a baseline corrected spectrum. Though some of the more intense bands appear to be fitted well, the less intense bands were poorly fitted or not fitted at all. The blue solid line is the data and the black line is the fitted spectrum, with the band positions displayed above those that are fitted.

3.2.3. The definition of a characteristic band and statistical methods

Statistical approaches have previously been effectively used to characterise Raman spectra of polymorphs of pharmaceutical compounds and therefore distinguish them based on the wavenumber position of the bands (Mehrens *et al.*, 2005). The aim of applying statistical tests to the Raman bands of the amino acids in this study was to define a set of characteristic bands that can be reliably used to identify the molecules in samples, such as the martian regolith, on future planetary missions. Firstly, the spectra from the triplicate maps of each amino acid were tested against one another using the Analysis of Variance (ANOVA) and Tukey-Kramer statistical tests (described below) to check the consistency of the band so a set of characteristic bands could be selected.

Bands were defined as characteristic bands of the amino acid molecule if they satisfied the following criteria:

1) the band appeared in all three maps;
2) the band had an ANOVA test p value of ≥ 0.05.

A band could still be classified as characteristic if it did not pass the ANOVA test if either of the following criteria were met:

3) the intensity of the band is classified as very strong; and/or
4) the means of the triplicate maps were within the instrument accuracy of ± 0.98 cm^{-1}.

Criterion (4) was included as the ANOVA test was, in some cases, too sensitive and was ruling out bands that were sufficiently stable within the instrument accuracy.

Tentative bands that could be used to aid identification of the molecule were also considered. For example, a band may have been close to passing the ANOVA p value test

but the band position in one of the maps had a greater difference in relative wavenumber than the other two band positions, causing the p value to be < 0.05. Therefore the wavenumber position of these bands is not as consistent as the characteristic bands. Tentative bands should not be considered as characteristic bands, but were defined by satisfying at least one of the following criteria:

T1) pass one or more of the post-hoc Tukey-Kramer tests;

T2) the means of two out of the three maps are within the instrument accuracy;

T3) have an intensity rating of medium-weak or above (band intensity classification is described in Table 3-1);

T4) have a standard deviation of 1.00 cm^{-1} or less.

Furthermore, ambiguous bands, defined here as those that were recorded as singlets in some map points and doublets or shoulders in others, were not considered when selecting bands as characteristic of the amino acid for use as identifiers.

Secondly, *t*-tests were applied to the spectra of the amino acids in both excitation wavelengths, to test the consistency of the band position. For this, the term relative wavenumber difference (RWD) is used to define the consistency and hence the presence of the bands in spectra, either within or between wavelengths. The RWD of the amino acid bands were compared in each triplicate map to aid in the identification of characteristic bands.

The null hypothesis assumed that the mean of the band positions were the same and therefore, no RWD had occurred. The ANOVA test was performed to examine the difference between the means of the bands between the three maps. Used in combination with the ANOVA test, the Tukey-Kramer test compared all possible pairs of means, even if there was an uneven sample number. Both one- and two-tailed *t*-tests were used to

compare the band positions between the two wavelengths as it was unknown in which direction (to higher or lower wavenumbers) the RWD would occur. The results from these tests were used to determine the consistency of the band position and therefore their usefulness as characteristic bands. For ANOVA, Tukey-Kramer and the *t*-tests there was an output of a *p* value, which denoted the probability between 0 and 1 that the measurements observed could have occurred by chance. A significance level (α) of 0.05 is used. The ANOVA test also provides a value, *F*, which is equal to 1 if there has been no effect as a result of treatment. *F* becomes increasingly larger the more inconsistent it becomes with the null hypothesis.

3.3. Results

The Raman spectra for alanine, aspartic acid, cysteine, glutamine and glycine are presented in Figure 3-2 and are intended to be standard for these amino acids. In the figure, the characteristic bands, as described in the following sections, are marked with an asterisk. These spectra are an average of a 16 point map using the 473 nm laser, where each point is an average of five 15 second spectra acquisitions as described in Section 3.2.2. The baseline of the resulting spectra were corrected for background noise and other factors (described in Section 3.2.2) to provide a baseline for band intensity and allowed for more accurate band fitting by the fitting algorithm in *LabSpec5*.

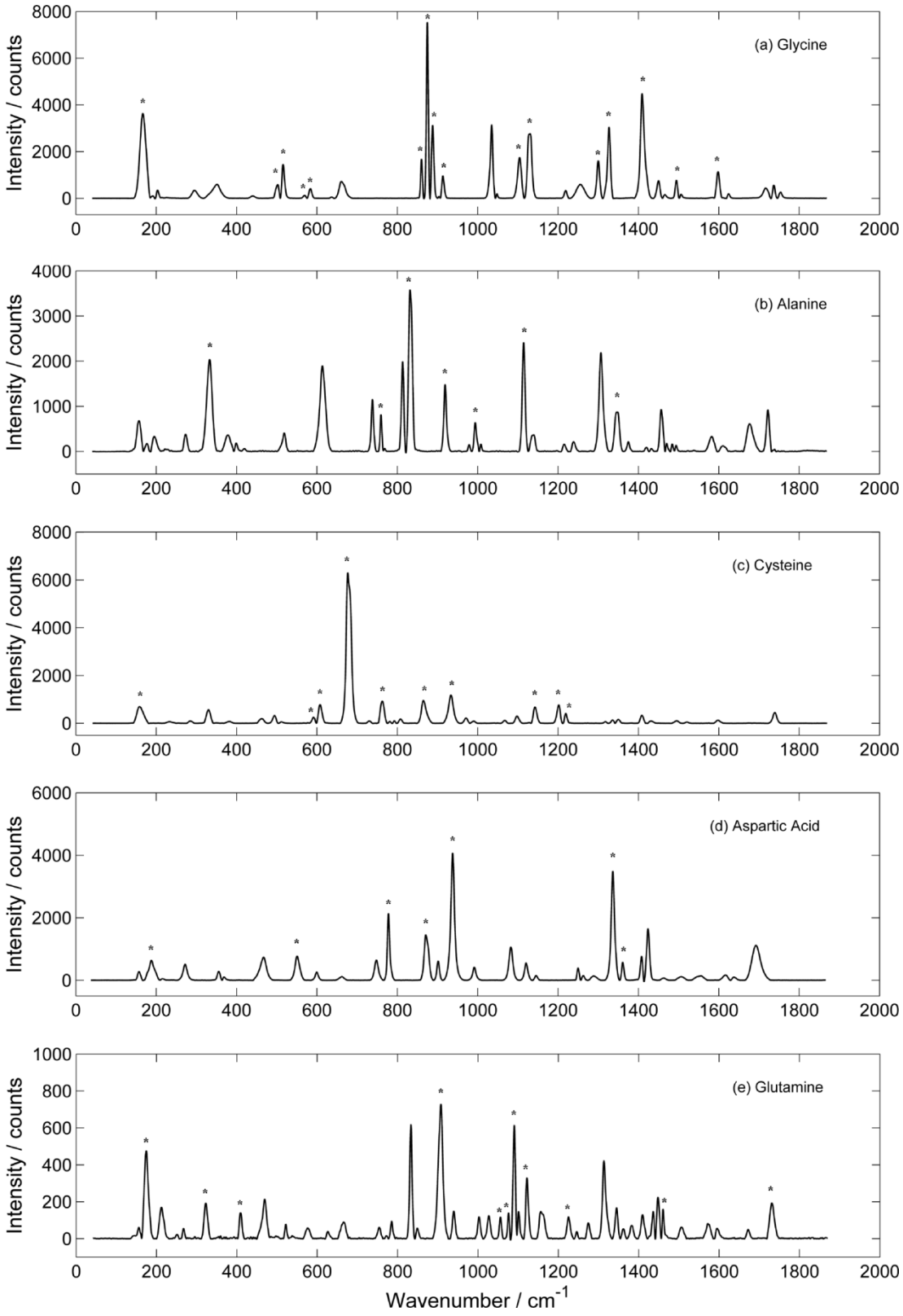

Figure 3-2: The Raman spectra of the amino acids, averaged over the 16 points taken in map 1 using the 473 nm laser. The characteristic bands of each amino acid are marked with an asterisk.

The spectral shapes of alanine, aspartic acid, glycine shown in Figure 3-2 are in agreement with previously published data (Zhu *et al.*, 2011), as well as that of glutamine (Dhamelincourt and Ramirez, 1993). The cysteine spectra presented in Figure 3-2 is consistent with that determined by Pawlukojć *et al.* (2005), except most of the bands recorded in this study are not as intense (relative to the strongest band) as the previously published bands.

Detailed statistical results are presented for aspartic acid in Table 3-2, with the results for alanine, cysteine, glutamine and glycine derived from the same methodology, summarised in Table 3-3. For ease of description, bands are referred to by a wavenumber position in the text, tables (column: Band name) and figures by taking the average of all the bands across the 16 spectra and rounding to the nearest whole wavenumber; where there were differences in the mean band position between the 514 and 473 nm wavelengths the bands are referred to using the 473 nm nearest whole wavenumber.

Aspartic Acid

Band name	*514 nm*						*473 nm*						*514 nm cf 473 nm*			
	Band / cm^{-1}	*F*	*p* value	# of maps	Standard Deviation	Intensity	Band / cm^{-1}	*F*	*p* value	# of maps	Standard Deviation	Intensity	*t*	*df*	*p (one-tailed)*	*p (two-tailed)*
84[#]	84.20	4.54	0.016	3**	0.13	vs										
158							158.4	7.42	0.002	3*	0.76	w				
272[○]	270.8	47.10	<0.001	2	0.27	w	271.5	9.50	<0.001	3*	0.50	w	6.22	77	<0.001	<0.001
356							356.3	1.36	0.253	2	0.24	w				
466	465.2	8.25	0.008	2	0.48	w	465.8	1.27	0.291	3	0.19	w	3.07	71	0.001	0.003
551[○]	550.2	1.25	0.298	3	0.10	w	551.1	9.37	<0.001	3*	0.26	w	10.89	89	<0.001	<0.001
600							599.9	21.65	<0.001	3*	0.64	vw				
663							662.8	18.13	<0.001	3*	1.49	vw				
778[#]	777.0	15.13	<0.001	3*	0.18	m	778.0	2.98	0.061	3	0.12	m	17.72	94	<0.001	<0.001
872[#]	871.5	7.24	0.002	3*	0.28	m	872.3	1.09	0.345	3	0.10	m	9.31	93	<0.001	<0.001
901	900.4	26.15	<0.001	2	0.25	w	901.3	6.11	0.020	2	0.12	w	20.16	61	<0.001	<0.001
938[#○]	936.7	15.25	<0.001	3	0.20	vs	937.6	4.52	0.017	3**	0.18	vs	13.89	90	<0.001	<0.001
992	990.4	16.04	<0.001	2	0.18	w	991.6	2.38	0.105	3	0.11	w	18.95	74	<0.001	<0.001
1082[■]	1081.1	7.15	0.002	3*	0.52	m-w	1082.2	21.23	<0.001	3*	0.71	m-w	5.49	94	<0.001	<0.001
1120	1120.0	13.93	<0.001	3*	0.79	w	1120.4	4.63	0.015	3*	0.19	w	3.11	88	0.001	0.002
1260	1259.3	2.30	0.142	2	1.35	w	1260.4	12.17	<0.001	3*	0.88	w	1.35	70	0.090	0.180
1336[#○]	1335.3	13.54	<0.001	3*	0.23	s	1336.2	8.99	<0.001	3*	0.25	s	12.69	94	<0.001	<0.001
1360[#△]	1359.8	7.29	0.002	3*	0.22	w	1360.8	22.54	<0.001	3*	0.57	w	8.67	92	<0.001	<0.001
1408	1407.1	0.95	0.393	3	0.13	m	1408.0	20.74	<0.001	3*	0.72	m	6.27	93	<0.001	<0.001
1423	1421.7	10.34	<0.001	3*	0.84	m	1423.1	1.59	0.216	3	0.24	m	6.27	90	<0.001	<0.001
1692	1691.0	5.85	0.022	2	0.41	m-w	1692.1	9.17	<0.001	3*	0.96	m-w	3.53	75	<0.001	<0.001

[#] Characteristic band assignment within error in the 514 nm spectra

[○] Characteristic band assignment within error in the 473 nm spectra

[■] Tentative assignment in 514 nm spectra

[△] Tentative assignment in 473 nm spectra

* $p > 0.05$ on one out of three post-hoc Tukey-Kramer tests

** $p > 0.05$ on two out of three post-hoc Tukey-Kramer tests

*** $p > 0.05$ on three out of three post-hoc Tukey-Kramer tests

Table 3-2: Statistical tests for bands associated with aspartic acid. Those highlighted in grey are the bands that are characteristic or tentative bands of aspartic acid. The rest are rejected as bands for characterising aspartic acid, but could be used as secondary identifying bands. The *F* value, *p* value and the number of maps the band appears in is shown for the two excitation wavelengths, 514 nm and 473 nm. One- and two-tailed *t*-tests were also performed showing the degrees of freedom (*df*), *t* and *p* values for 514 nm *cf* 473 nm. The bands are significantly different from one another between the two wavelengths, except for the 1260 cm^{-1} band.

Alanine

Band name	*514 nm*						*473 nm*						*514 nm cf 473 nm*			
	Raman Band / cm^{-1}	*F*	*p* value	# of maps	Standard Deviation	Intensity	Raman Band / cm^{-1}	*F*	*p* value	# of maps	Standard Deviation	Intensity	*t*	*df*	*p (one-tailed)*	*p (two-tailed)*
71	71.4	0.47	> 0.5	3	0.07	vs										
91	91.1	2.80	0.072	3	0.45	m										
124#	124.3	7.97	0.001	3*	0.20	vs										
333■	332.1	132.48	< 0.001	3*	1.01	m-w	332.9	1.11	0.341	3	0.30	m	4.01	8	< 0.001	< 0.001
760△	759.4	3.31	0.046	3***	0.25	w	759.8	0.00016	> 0.5	2	0.00035	m-w	3.16	7	0.001	0.002
832	831.5	5.79	0.006	3*	0.62	vs	832.1	8.30	< 0.001	3*	0.53	vs	-4.49	8	< 0.001	< 0.001
919#	918.9	162.75	< 0.001	3^0	0.46	w							-3.52	7	< 0.001	< 0.001
995#△	995.0	5.99	0.005	3**	0.42	w	994.9	2.88	0.102	2	0.33	w	-3.60	7	< 0.001	< 0.001
1114#	1113.7	8.33	< 0.001	3**	0.22	m	1114.2	1.55	0.224	3	0.22	m	-4.02	8	< 0.001	< 0.001
1346							1345.7	3.13	0.055	3	0.91	w	1.57	8	0.06	0.12

Cysteine

Band name	*514 nm*						*473 nm*						*514 nm cf 473 nm*			
	Raman Band / cm^{-1}	*F*	*p* value	# of maps	Standard Deviation	Intensity	Raman Band / cm^{-1}	*F*	*p* value	# of maps	Standard Deviation	Intensity	*t*	*df*	*p (one-tailed)*	*p (two-tailed)*
68	68.5	1.06	0.358	3	0.47	vw										
131	131.1	0.20	> 0.5	3	0.06	w										
159							158.8	2.63	0.083	3	0.52	vw				
593							593.1	2.55	0.092	3	0.70	w				
608○	608.5	1.65	0.205	3	0.25	w	608.1	3.29	0.048	3**	0.39	w	0.53	8	0.300	> 0.5
679	680.3	2.65	0.084	3	0.55	vs	678.5	5.52	0.007	3**	0.89	vs	4.12	5	< 0.001	< 0.001
762#	762.4	12.61	< 0.001	3*	0.47	w							0.34	4	0.368	> 0.5
866	866.2	1.84	0.173	3	0.51	w	866.2	1.42	0.253	3	0.34	w	-0.14	8	0.443	> 0.5
933	932.3	2.64	0.084	3	0.56	w	933.1	0.45	> 0.5	3	0.14	w	-3.08	8	0.001	0.003
1142							1142.4	0.45	> 0.5	3	0.21	w	-4.92	8	< 0.001	< 0.001
1202△	1203.0	1.74	0.190	3	0.61	w	1202.2	5.45	0.008	3**	0.71	w	2.37	8	0.010	0.020
1220	1220.4	2.37	0.107	3	0.53	vw	1220.2	6.41	0.004	3*	1.02	vw	0.45	8	0.327	> 0.5

Table 3-3: The bands designated as characteristic or tentative bands for identifying alanine, cysteine, glutamine and glycine. Secondary identifying bands or rejected bands are not given.

Table 3-3 continued

Glutamine															
	514 nm						*473 nm*						*514 nm cf 473 nm*			
Band name	Raman Band / cm^{-1}	*F*	*p* value	# of maps	Standard Deviation	Intensity	Raman Band / cm^{-1}	*F*	*p* value	# of maps	Standard Deviation	Intensity	*t*	*df*	*p(one-tailed)*	*p (two-tailed)*
96#	95.9	13.94	< 0.001	3*	0.72	m-s										
112#	111.6	5.58	0.007	3*	0.50	vs										
122#	121.7	18.22	< 0.001	3*	0.60	vs										
174#	176.1	3.61	0.037	3**	0.59	m-w	173.5	3.60	0.036	3***	0.88	s				
323△							323.2	5.48	0.008	3**	0.75	m-w	1.72	90	0.044	0.089
409■○	410.2	120.25	< 0.001	3*	0.59	m-w	409.1	4.23	0.021	3**	0.17	m-w	12.84	92	< 0.001	< 0.001
908△							907.5	28.61	< 0.001	3*	0.66	s	4.02	94	< 0.001	< 0.001
1055#○	1056.5	129.08	< 0.001	3*	0.49	m-w	1055.6	19.98	< 0.001	3*	0.37	w	8.97	86	< 0.001	< 0.001
1076#○	1076.7	52.41	< 0.001	3*	0.49	w	1075.7	13.85	< 0.001	3*	0.25	w	12.05	90	< 0.001	< 0.001
1090#	1091.2	29.07	< 0.001	3*	0.53	vs	1090.1	2.19	0.124	3	0.17	vs	10.00	94	< 0.001	< 0.001
1122#○	1122.6	18.25	< 0.001	3*	0.38	m-w	1121.7	16.18	< 0.001	3*	0.35	m-w	9.05	94	< 0.001	< 0.001
1225							1225.5	1.87	0.168	3	0.21	w	2.05	82	0.022	0.044
1462■	1461.3	71.48	< 0.001	3*	0.55	m-w							6.01	53	< 0.001	< 0.001
1732	1732.2	0.15	> 0.5	3	0.07	w							6.72	91	< 0.001	< 0.001

Table 3-3 continued

Glycine

	514 nm						*473 nm*						*514 nm cf 473 nm*			
Band name	Raman Band / cm^{-1}	*F*	*p* value	# of maps	Standard Deviation	Intensity	Raman Band / cm^{-1}	*F*	*p* value	# of maps	Standard Deviation	Intensity	*t*	*df*	*p (one-tailed)*	*p (two-tailed)*
73[#]	72.9	16.89	< 0.001	2	0.21	m-s										
137[#]	137.3	17.67	< 0.001	2	0.43	m-w										
167[#]	168.4	19.49	< 0.001	2	0.59	m	167.1	1.73	0.198	2	0.20	m	8.34	62	< 0.001	< 0.001
501	502.0	3.93	0.057	2	0.66	w	501.5	6.62	0.015	2	0.69	vw	1.54	62	0.065	0.129
516[#]	516.2	39.88	< 0.001	2	0.93	w	516.1	4.11	0.052	2	0.20	w	0.42	61	0.339	> 0.5
569[#]	569.0	13.63	< 0.001	2	0.46	vw	568.9	3.57	0.069	2	0.27	vw	0.16	59	0.436	> 0.5
584[#○]	584.2	13.83	< 0.001	2	0.35	vw	584.3	54.09	< 0.001	2	0.84	vw	-0.86	61	0.196	0.392
860	859.7	3.74	0.065	2	0.10	w	860.2	0.04	> 0.5	2	0.01	m-w	5.20	53	< 0.001	< 0.001
875	874.5	0.61	0.442	2	0.03	vs	874.6	2.45	0.128	2	0.10	vs	5.41	62	< 0.001	< 0.001
888[#○]	887.4	69.95	< 0.001	2	0.42	m	888.0	8.22	0.008	2	0.22	m	5.44	62	< 0.001	< 0.001
914							913.8	0.00032	> 0.5	2	0.0021	w	-5.32	46	< 0.001	< 0.001
1104[○]							1104.2	4.35	0.046	2	0.24	w	-1.50	46	0.071	0.141
1130[#○]	1129.2	24.62	< 0.001	2	0.96	m-w	1129.9	29.30	< 0.001	2	0.63	m	-3.24	62	< 0.001	0.002
1300[#]	1299.7	7.47	0.010	2	0.11	w	1299.9	0.64	0.430	2	0.06	m-w	-3.17	62	0.001	0.002
1327[#]	1326.8	43.48	< 0.001	2	0.35	m	1327.0	0.23	> 0.5	2	0.03	m	-1.95	62	0.028	0.056
1411							1410.4	1.60	0.216	2	0.32	m	-0.22	62	0.413	> 0.5
1450[#]	1449.8	38.85	< 0.001	2	1.16	vw	1449.7	0.21	> 0.5	2	0.08	vw	0.62	62	0.268	> 0.5
1495							1494.7	0.45	> 0.5	2	0.16	w	-2.31	46	0.013	0.026
1598	1598.2	1.02	0.320	2	0.23	w	1598.1	0.65	0.425	2	0.18	w	0.56	60	0.289	> 0.5

[#] Characteristic assignment within error in the 514 nm spectra
[○] Characteristic assignment within error in the 473 nm spectra
[■] Tentative assignment as a characteristic Band in 514 nm spectra
[△] Tentative assignment as a characteristic Band in 473 nm spectra

* $p > 0.05$ on one out of three post-hoc Tukey-Kramer tests
** $p > 0.05$ on two out of three post-hoc Tukey-Kramer tests
*** $p > 0.05$ on three out of three post-hoc Tukey-Kramer tests
[0] Did not pass any Tukey-Kramer tests

3.3.1. The characteristic bands of aspartic acid

To show the statistical process of eliminating non-characteristic bands from an amino acid species, a complete list of bands recorded in the spectra of aspartic acid, with full details of the statistical output from the tests on the bands, are given in Table 3-2. The bands highlighted in grey met the definition of a characteristic or tentative band as defined in Section 3.2.3. The bands defined as characteristic for the 473 nm excitation wavelength are at 272, 466, 551, 778, 872, 938, 992, 1336 and 1423 cm^{-1}. There is a tentative band at 1360 cm^{-1}. The characteristic bands for the 514 nm excitation wavelength are at 84, 551, 778, 872, 938, 1336, 1360 and 1408 cm^{-1} and there is one tentative band at 1082 cm^{-1}. The bands at 84 and 272 cm^{-1} are outside the fingerprint region for organic molecules. The characteristic bands that passed the ANOVA test had a *p* value range of 0.061 to 0.345. The other bands displayed in Table 3-2, at 158, 356, 600, 663, 901, 1120, 1260, and 1692 cm^{-1}, are rejected at both excitation wavelengths for use as identifying bands for aspartic acid as they do not meet the criteria set out in Section 3.2.3. Three of these bands, at 356, 901 and 1260 cm^{-1}, were rejected because the bands only appeared in two of the three maps.

Table 3-3 summarises the results of the statistical tests for alanine, cysteine, glutamine and glycine, listing only the characteristic and tentative bands. The rejected bands are not displayed.

3.3.2. The characteristic bands of alanine

The characteristic bands in the 473 nm excitation wavelength for alanine are 333, 832, 1114 and 1346 cm^{-1}, the tentative bands are 760, and 995 cm^{-1}. The characteristic bands for the 514 nm laser are 71, 91, 124 (however, these are outside of the fingerprint region for organic molecules), 760, 832, 919, 995 and 1114 cm^{-1}. A tentative band for the 514 nm excitation wavelength is at 333 cm^{-1}. In both excitation wavelengths the strongest band, 832 cm^{-1}, did not pass the ANOVA test, but the means of the bands in two of the three maps are within the instrument accuracy and it does subsequently pass the Tukey-Kramer tests. However, the intensity classification of very strong allows for classification as a characteristic band. The *p* value ranges for the characteristic bands in the 473 and 514 nm spectra were 0.055 to > 0.5 and 0.072 to > 0.5, respectively. Rejected bands for alanine were at 378, 614, 1134, 1213, 1307, 1463, 1375, 1463, 1484, 1667 and 1976 cm^{-1}.

3.3.3. The characteristic bands of cysteine

In the 473 nm excitation wavelength there are six characteristic bands that can be used as identifiers for cysteine; their positions are 159, 593, 608, 679, 866, 933, 1142 and 1220 cm^{-1}. These bands have all been classified as weak or very weak, except the strongest band at 679 cm^{-1}. The band at 1202 cm^{-1} is classified as tentative. There were no tentative assignments among the nine characteristic bands defined for cysteine using the 514 nm excitation laser as all but one of the bands passed the ANOVA test; the band at 762 cm^{-1} did not pass the ANOVA test, but the means of the maps were within the instrument accuracy. Also the strongest band at 679 cm^{-1} in the 514 nm spectra; the other characteristic bands are 68, 131, 608, 762, 866, 933, 1202 and 1220 cm^{-1}, these have weak

or very weak intensities. Only three of 15 bands recorded were rejected as characteristic bands, at 1336, 1349 and 1407 cm^{-1} (statistical data are not shown), on the basis that they were only in the upper quartile range for two of the three maps.

3.3.4. The characteristic bands of glutamine

In the spectra recorded with the 473 nm laser, the characteristic bands that can be used to identify glutamine are 174, 409, 1055, 1076, 1090, 1122 and 1225 cm^{-1}. A tentative assignment was given to the band at 908 cm^{-1}, which has a strong intensity classification. The characteristic bands in the 514 nm spectra are at 96, 112, 122, 174, 1055, 1076, 1090, 1122 and 1732 cm^{-1}. Other bands that can be used as tentative identifiers are at 409 and 1462 cm^{-1}, which have medium-weak intensity classifications. The 96, 112, 122, 174 and 1732 cm^{-1} bands are outside of the fingerprint region for organic molecules of the spectrum. Rejected bands for glutamine are at wavenumber positions: 72, 522, 577, 665, 753, 833, 848, 940, 1003, 1157, 1314, 1361, 1436, 1450 and 1462 cm^{-1} (statistical data are not shown).

3.3.5. The characteristic bands of glycine

The data for glycine were based on duplicate rather than triplicate samples because the third sample was inaccessible to the microscope lenses as it dried adjacent to the wall of the Petri dish. Hence, modified criteria for classifying characteristic bands were used as follows: bands were rejected if the standard deviation was greater or equal to 1.00 or if they failed the ANOVA test; otherwise they were accepted as characteristic bands for glycine. The bands that failed the ANOVA test were accepted as characteristic bands if the

means of the maps were within the instrument accuracy of ± 0.98 cm^{-1}. Glycine has the greatest number of characteristic bands of all the amino acid species examined in this study. When examined with the 473 nm excitation wavelength, bands with the wavenumbers 167, 501, 516, 569, 584, 860, 875, 888, 1104, 1130, 1300, 1327, 1411, 1450, 1495 and 1598 cm^{-1} are characteristic bands. With the 514 nm laser, the characteristic bands are 73, 137, 167, 501, 516, 569, 584, 860, 875, 888, 1130, 1300, 1327, 1450 and 1598 cm^{-1}. The strongest intensity band is at 875 cm^{-1}. Rejected bands that did not meet the criteria for a characteristic band for glycine were at wavenumber positions 192, 351, 663 and 1034 cm^{-1} (statistical data not shown).

3.3.6. Statistical comparison of band position because of excitation wavelength

One- and two-tailed *t*-tests were performed to compare the instrument consistency in band positions in the spectra taken with the two excitation wavelengths. For alanine, although all but one characteristic band failed the *t*-tests, the mean wavenumber positions for all the bands in each wavelength are within the instrument accuracy of ± 0.98 cm^{-1} of each other. The band at 1346 cm^{-1} showed no statistically significant RWD (*t*-test $p = 0.06$, one-tailed; $p = 0.12$, two-tailed); the other bands all had a RWD that were statistically significant (*t*-test $p < 0.05$).

All but one band failed the *t*-test for aspartic acid. The weak band at 1260 cm^{-1} passed both the one- and two-tailed test with *p* values of 0.09 and 0.18, respectively. Nonetheless, the mean positions of the bands at 272, 466, 551, 778, 872, 901, 938, 1082, 1120, 1336, 1360

and 1408 cm^{-1} are all within the instrument accuracy. Those that are not within the instrument accuracy are at 992, 1260, 1423 and 1692 cm^{-1}.

For cysteine, four bands (608, 762, 866 and 1220 cm^{-1}) showed no statistical significance in the RWD, while four bands (679, 933, 1142 and 1202 cm^{-1}) had RWD of statistical significance. All the bands except the bands at 679 and 1142 cm^{-1} were within the instrument accuracy.

For glutamine, the 323 and 1225 cm^{-1} bands showed no statistically significant RWD (*t*-test $p = 0.089$, two-tailed; $p = 0.022$, two-tailed, $p = 0.044$, two-tailed, respectively) between the two excitation wavelengths. The mean wavenumber positions in each excitation wavelength for the bands 409, 1090 and 1732 cm^{-1} are not within the instrument accuracy.

In the *t*-tests, half of the glycine bands had a RWD that was statistically significant ($p < 0.05$); nonetheless all but the band at 167 cm^{-1} are within the instrument accuracy.

3.4. Discussion

Defining multiple characteristic bands for use in identifying amino acids in unknown samples using statistical methods is an aspect of Raman spectral identification that has not been previously addressed. Vandenabeele *et al.* (2012) alluded to the idea that a minimum number of bands should be defined that would allow for a definite, positive identification of a molecule in an unknown sample (ideally all laboratory observed bands would be observed in a sample, but this would be atypical). However, a minimum number defined by a set fraction or percentage of the total number of bands would be a non-general case (*ibid*). Another possibility could be to insist that all medium-strong or greater intensity

bands attributed to a molecule must be observed to make a positive identification. Here, a set of bands that are statistically characteristic of the molecule have been defined, which are independent of the total number of bands or their intensity.

These laboratory defined sets of multiple characteristic bands are proposed as complementary to current methods of molecule identification in an unknown sample, such as those expected from future planetary missions.

Here, the majority of bands were observed in both sets of spectra, though only some met the definition of a characteristic band in one of the excitation wavelengths. Furthermore, the intra-map intensity of the spectra has been considered and it was noted that the intensity was variable even when recorded at the same excitation wavelength.

When considering the bands that were most frequently measured (those in the upper quartile range, described in Section 3.2.2), there were bands that were present in some spectra, but not others or they were weaker in intensity (therefore, not fitted by the software). This could be because the bond associated with the band has an innately weak Raman scattering effect or the scattered light was not received by the instrument because of the angle of the crystal surface. Furthermore, though measures were taken to ensure that the samples remained pure, this upper quartile categorisation allows for bands that may not be associated with the amino acids because of contamination to be ruled out, leaving only those that are statistically significant.

Given that the excitation wavelength and the concentration of the sample were fixed, the Raman system was calibrated to the same configuration, and the measuring time was constant in this study, it was assumed that background fluorescence contributed to the noise (described in Section 3.2.2). The noise in the spectra was minimised during processing using baseline correction, so it is possible that the intensity of the bands was

affected by the spectral processing. However, polarisation and sample orientation effects are also known to affect the intensity of the bands. Detailed and mathematical explanations for changes in intensity can be found, for example, in Long (1977) and Ferraro *et al.* 2003. These details are beyond the scope of this study, but an example of differences in band intensity resulting from crystal orientation in amino acids was reported by Dhamelincourt and Ramírez (1991). They found in a study of L-glutamic acid that some bands are more intense in specific polarisation directions to the extent that some bands appear to not be present. As crystal orientation or microcrystalline effects were not explicitly considered, it is possible that these could have also affected the intensity of the bands recorded in this study.

3.4.1. The effect of sample orientation on band intensity

When designating bands as characteristic for particular amino acids, significant use of the band position was made; however the band intensity was also considered for some tentative assignments (band intensity designations are described in Table 3-1). To investigate the potential contribution of orientation or microcrystalline effects on intensity, a brief study of sample orientation was conducted. The hypothesis was amino acids that crystallise in smaller crystals closer to the size of the laser spot diameter would have a greater variation in intensity compared to those that crystallise in larger crystals when the orientation of the sample is rotated. A sample of alanine (large crystals) and glycine (small crystals) was measured in five positions in a field of view (Figure 3-3). The 514 nm laser was used in this test.

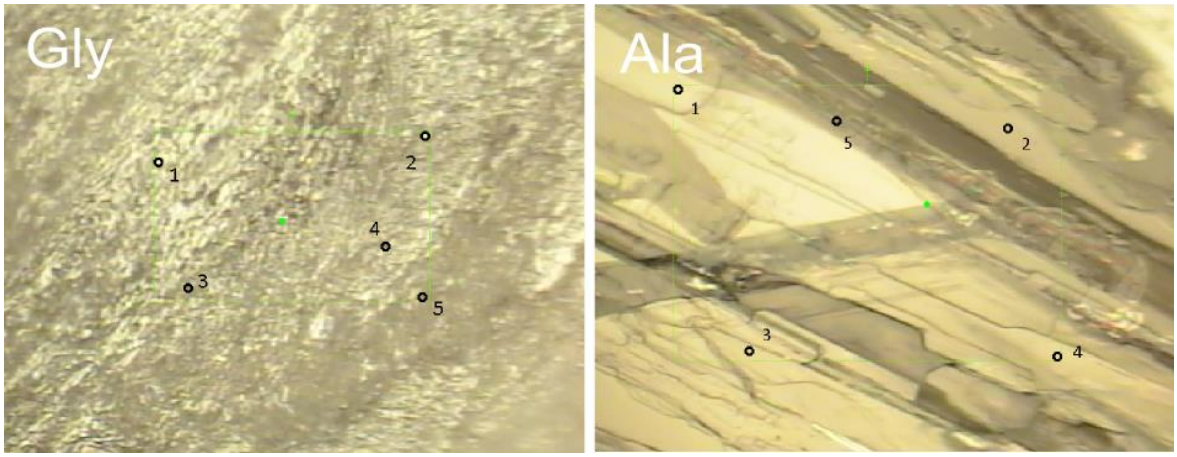

Figure 3-3: Images of the areas of crystalline glycine and alanine used to conduct a study to determine the effect of orientation on band intensity. This field of view was rotated through 360° and spectra were acquired at each numbered point at each angle (0, 90, 180 and 270°).

The sample was rotated through 360°, with measurements at the five points taken at 0°, 90°, 180° and 270°. Smaller crystals allow a higher possibility of measuring differing crystal surface effects or the Raman signature over different unit cell orientations, so a wider orientation of bonds would be subject to Raman scattering leading to a higher variety of band intensities. The intensities of the characteristic bands at 90°, 180° and 270° (B_1, B_2 and B_3, respectively. General case, B_n) were compared to the intensity of the respective characteristic bands at 0° (A) using the relationship:

$$\text{Ɍ} = (A/B_n). \qquad (3\text{-}1)$$

For alanine, the data for point 3 were poor because of the crystal thinness, no bands were recorded, and only a spectrum representative of the glass substrate was seen. Nonetheless, points 1, 2, 4 and 5 produced useful data. As shown in **Error! Reference source not found.**, the intensities of the bands at points 1, 2 and 5 had intensities grouped around a

value of 1 (indicating the intensity measured was similar to that at 0°) with an ℟ value range of 0.51 to 1.15 at all the angles.

The 180° rotation for point 4 had an ℟ value of 1.05, only 5 % difference in the intensity from the 0° measurement, similar to points 1, 2 and 5. Point 4 appeared anomalous where measurements of the intensity perpendicular to the normal at the 90° and 270° rotations were approximately 330 and 320 % different, respectively, than the intensities of the bands at 0°. This suggested that either a surface effect varying from crystal to crystal or different molecular orientation had been observed at right angles to the 0° and 180° rotations.

For glycine, the ℟ value range for the intensities of the bands at points 1, 2, 3 and 4 is 0.44 to 1.66, which was larger than that seen for alanine. This suggested that the hypothesis that amino acids that crystallise with smaller crystals closer to the size of the laser spot diameter would have a greater range of intensities if rotated than those with larger crystals was correct.

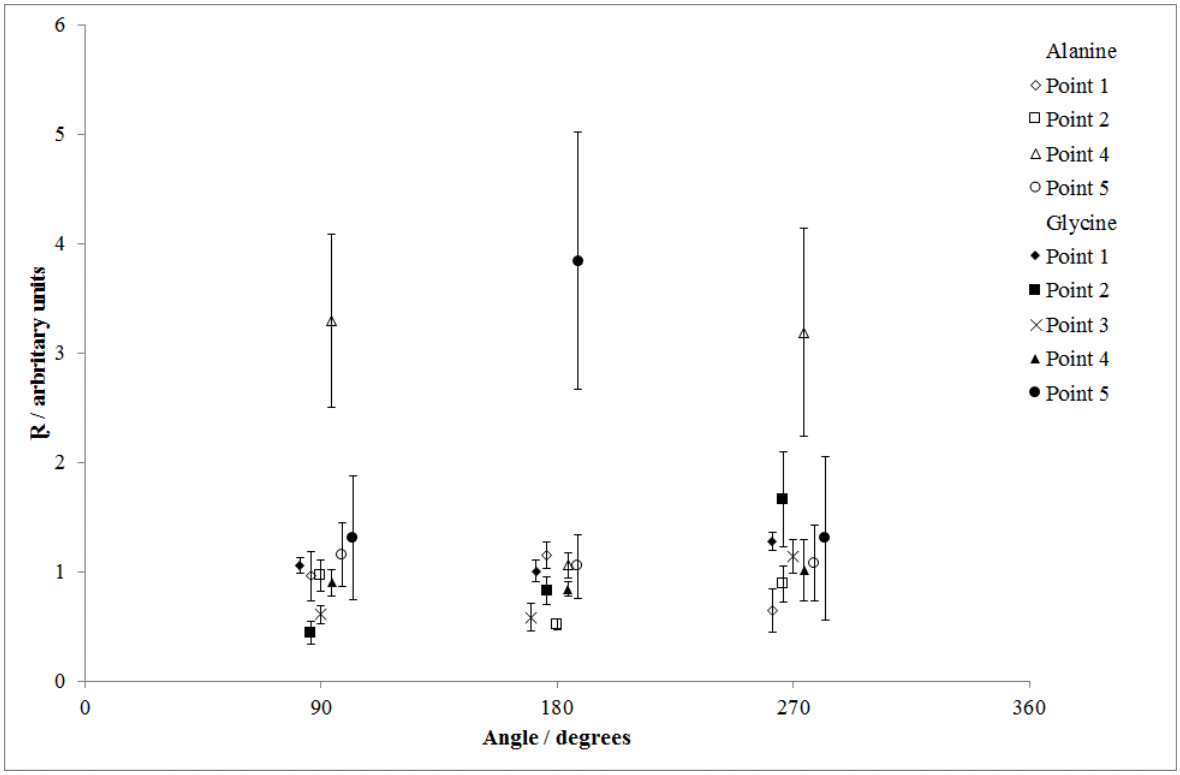

Figure 3-4: Comparison of Ɍ values at different orientations to one standard deviation. The data are artificially offset within each angle group on the *x*-axis for ease of viewing.

The glycine crystal also has an anomalous point; the 180° position at point 5 had an intensity 385% greater than the 0° intensity measurement. This was larger than the alanine anomalous point (point 4), indicating that either there was a greater surface effect at this point or there were different molecule orientations being observed and further suggesting that the hypothesis was correct.

Ergo, though intensities have only been considered here to help define tentative bands and hence do not affect the results of the characteristic band designations; the brief study of sample orientation that was conducted has shown that individual band intensities can vary by up to five times at the same point on a sample depending on the orientation.

3.4.2. The statistical treatment of the characteristic and tentative bands

3.4.2.1. Aspartic acid

For the 473 nm excitation wavelength the characteristic bands, 272, 551, 938, and 1336 cm^{-1}; and for the 514 nm excitation wavelength the characteristic bands 84, 778, 872, 938, 1336 and 1360 cm^{-1} did not originally pass the ANOVA test, but are categorised as characteristic bands because of the mean wavenumber position of the maps being within the instrument accuracy. The statistical testing was rigorous and occasionally ruled out bands that were within in the instrument accuracy, but by expanding the pass criteria for characteristic bands to include these bands a more comprehensive set of characteristic bands was defined. The bands at 938 and 1336 cm^{-1} were assigned as characteristic within the instrument accuracy (*i.e.* did not pass the ANOVA test), but have intensity classifications of very strong and strong, respectively. These characteristic bands will be the most useful for identifying aspartic acid. The other characteristic bands have intensity classifications of medium or lower; it is possible that lower intensity bands may be lost in the spectrum noise. Nevertheless, if measured, these bands will be important to confirm the presence of aspartic acid in a test sample.

The following bond assignments are given to the bands: skeleton in plane bend (272 cm^{-1}), torsion of the NH_3^+ group (466 cm^{-1}), in plane COOH bend (551 cm^{-1}), out of plane OCO^- bending (778 cm^{-1}), CH_2 rocking mode (872 cm^{-1}), out of plane OH bend (938 cm^{-1}), CC stretching mode (992 cm^{-1}), in plane CH bending (1336, 1360 cm^{-1}), CO stretch and in plane OH bend (1408 cm^{-1}) and symmetric CO_2^- stretching (1423 cm^{-1}) (Navarrete *et al.*, 1994). The bands that were rejected were at 158, 356, 901, 990, 1082, 1120, 1260, 1408 and 1692 cm^{-1}; these bands were rejected on the basis of only passing one Tukey-Kramer

test (though often with a *p* value of > 0.5) or only appearing in two of the three maps and were often classified with a weak intensity. Therefore, the bands would likely be lost when observed in a bulk host material, but may be used as secondary identifiers.

3.4.2.2. Alanine

The band at 832 cm^{-1} has the strongest intensity classification. However, it does not pass the ANOVA test and is classified as characteristic because of its intensity. A possible explanation for this is the resolution of the grating allows for a band at approximately 813 cm^{-1} to be resolved in some of the maps, but not enough to be considered for statistical testing. This band may be the cause of the failure of the ANOVA test by the 832 cm^{-1} band; when the lower band is not resolved the 832 cm^{-1} band may incorporate some of the signal causing the wavenumber position to be unstable.

The bond assignment for the characteristic bands were: 333 cm^{-1} is attributed to the CCN bending mode (Rosado *et al.*, 1997). The 1114 and 1346 cm^{-1} are associated with the rocking of the CH_3 group (*ibid*) and a C−H and NH bend (Kumar *et al.*, 2006), respectively. The assignment for 832 cm^{-1} is either the C−COO stretching mode (Rosado *et al.*, 1997) or CN and C−C stretching modes (Kumar *et al.*, 2006). The tentative bands have bonds associated with the COO wagging mode or CN stretching (Rosado *et al.*, 1997), or HNC and CCH bend modes (760 cm^{-1}) (Kumar *et al.*, 2006); and a CNH bend mode (995 cm^{-1}) (*ibid*).

The rejected bands for the 473 and 514 nm spectra were at 614, 1134, 1307, 1463, and 1976 cm^{-1}; and 378, 614, 919, 1134, 1213, 1307, 1375, 1463, 1484 and 1677 cm^{-1}, respectively (statistical data are not shown). These bands did not meet the criteria of a characteristic or tentative band; for example, the band at 614 cm^{-1} had a *p* value of > 0.5,

but only appeared in the upper quartile range in two of the three maps and hence was rejected. Furthermore, these bands have an intensity classification of medium-weak or lower (except the band at 1307 cm^{-1}, which is a medium strength band), so would potentially be indistinguishable from background noise within a matrix of material.

3.4.2.3. Cysteine

Cysteine, in comparison to the other amino acids in this study, has the most statistically consistent band positions, with only characteristic bands being assigned in the 514 nm spectra and seven of nine bands being assigned as characteristic with two tentative assignments in the 473 nm spectra. However, all the bands except the strongest band at 679 cm^{-1} have intensity classifications of weak or very weak. This could mean cysteine could be difficult to identify convincingly in a test sample with only one strong characteristic band, where the other characteristic bands are likely to be lost in the spectrum noise. Furthermore, the 679 cm^{-1} band in the 473 nm spectra is classified as tentative, suggesting it should not be used as an identifying band. It was not classified as characteristic as it did not pass the ANOVA test and only one of the three maps was within the instrument accuracy. In this case, it is suggested that cysteine would be more confidently identified when using a 514 nm laser, but as only one band has a greater intensity classification than weak it may not be possible to positively confirm its presence in a test sample.

The bond assignments for the characteristic bands are: the 68 and 159 cm^{-1} bands are assigned to a CC or CO_2 torsion (calculated) and SH torsion, respectively (Pawlukojć *et al.*, 2005). The 593 cm^{-1} band is computed as the CC stretch, but is unobserved empirically by Pawlukojć *et al.* (2005); the most intense band at 679 cm^{-1} is assigned to the CS stretch;

the 866 and 933 cm^{-1} bands are assigned to the CC stretch and SH bending mode, respectively; 1142 cm^{-1} is possibly associated with the CH bend; and the 1203 cm^{-1} band is allocated to the CH_2 twist (*ibid*).

3.4.2.4. Glutamine

The 514 nm characteristic band positioned just outside the upper limit of the fingerprint region for organic molecules (500 to 1700 cm^{-1}) at 1732 cm^{-1} has a tentative bond assignment of the C=O stretch (Dhamelincourt and Ramirez, 1993). The bands that lie outside the lower limit of the fingerprint region at 96, 112, 122 and 174 cm^{-1} have bonds that are associated with $CH_3{-}CH_2$ and $CH_2{-}CH_2$ torsion and CCC deformation modes (Dollish *et al.*, 1974). The bonds within the fingerprint region at 1055, 1076, 1090 and 1122 cm^{-1} are attributed to the CC stretch (1055 cm^{-1}), CN stretch (1076 and 1090 cm^{-1}) and the NH_3^+ bend and rock modes (1122 cm^{-1}) (Dhamelincourt and Ramirez, 1993). The tentative band at 1462 cm^{-1} has a band assignment of the CH_2 bend and scissor modes (*ibid*). The band at 1090 cm^{-1} has the strongest intensity within the fingerprint region and hence will be the easiest band to identify in the spectra of a test sample. Although it was not statistically accepted as a characteristic band, it was within the instrument accuracy so was added to the set of characteristic bands for glutamine. The characteristic bands in the 473 nm spectra at 409, and 1225 $cm^{-1}$are associated with the skeletal bend, and the CH_2 bend and twist, respectively (*ibid*). Tentative bands at 323 and 908 cm^{-1} are attributed to the skeletal bend, and a mix of CH_2 bending and rocking mode, respectively (*ibid*).

3.4.2.5. Glycine

There are more identifying bands attributed to glycine compared to the other molecules in this study. However, these characteristic and tentative bands are statistically less well constrained than the other molecules, because the statistical tests were only being performed on a duplicate sample rather than in triplicate as with the other molecules. Therefore, it is possible that some of the bands that are considered as identifying bands in this duplicate study may have been ruled out if they had been treated in triplicate. Hence, some caution should be applied when attempting to identify glycine using these defined bands. Nonetheless, the bands measured in both excitation wavelengths have a range of intensities from very weak to very strong, which could imply that identification of glycine may be easier than, for example, cysteine, which has only one very strong band and the other characteristic bands intensities are classified as weak or very weak.

The bond assignments for the characteristic bands for glycine are: the COO^- bend and CH_2 bend (501 cm^{-1}); the COOH bending mode is possibly associated with the 569 cm^{-1} band; the COOH bend is calculated for the 584 cm^{-1} band, but not empirically observed by Kumar *et al.* (2005); the NH_2 and CH_2 twist modes (888 cm^{-1}), a CH_2 deformation (1300 cm^{-1}), a mix of the NH_2 twist and the CH_2 twist (1327 cm^{-1}), the CH_2 scissor mode (1411 cm^{-1}); the CH_2 and OH bending modes (1495 cm^{-1}); and the 1598 cm^{-1} band is assigned to the NH_2 scissor mode (*ibid*).

3.4.3. Statistical comparison of band position and the relative wavenumber difference owing to excitation wavelength

In this study, the instrument consistency of the band position influences the designation of characteristic bands, so *t*-tests were performed to understand to what extent a difference in excitation wavelength contributed to the wavenumber position of the bands when using the same instrument setup. It was evident that there were some statistically significant differences in band positions for each of the samples studied. This is illustrated in Figure 3-5, which shows the difference in band positions of the 514 nm compared to the 473 nm laser spectra. In Figure 3-5, the intra-wavelength band positions were also examined, with the error bars representing the standard deviation in the wavenumber position of the band in the 473 nm triplicate map spectra.

The RWD for glycine, alanine and cysteine did not show a trend; the data generally lay within the instrument accuracy, with a few outliers; hence the difference in excitation wavelength had no effect on the consistency of the Raman band positions of these molecules. In comparison to the other molecules, the RWDs of aspartic acid showed a trend towards lower wavenumbers (see Figure 3-5) and glutamine showed the opposite trend to aspartic acid, towards higher wavenumbers.

As a result of the rigorous nature of the statistical testing, the characteristic bands of glycine that were subjected to the *t*-test failed more often than passed, which suggested that there was an effect because of the excitation wavelength; however, when the average of the means were compared, all but one band (167 cm^{-1}) were within the instrument accuracy, highlighting further that the Raman bands were not affected by the excitation wavelength. The mean positions of the band at 167 cm^{-1} were outside the instrument accuracy by 0.36 cm^{-1} (*i.e.*, the mean shift in band position was 1.34 cm^{-1}), which for many Raman

spectrometers is insignificant; in this respect, the band can still be considered as characteristic of glycine. Similarly, for the characteristic bands of alanine, all but one band originally failed the null hypothesis. Nonetheless, when means of the band positions in each excitation wavelength were compared they all were within the instrument accuracy; hence supporting that they were not affected by the excitation wavelength.

Half the characteristic bands for cysteine failed the *t*-tests, however all but two had their comparative means within the instrument accuracy. The two bands outside the instrument accuracy were 679 and 1142 cm^{-1}, with differences in their wavenumber position between excitation wavelength spectra of 1.88 and 1.04 cm^{-1}, respectively. These wavenumber differences are observable, and hence statistically significant, with Raman spectrometers with high resolution gratings, such as the one used in this study. However, Raman systems with lower resolution gratings such as those that are likely to be used on future planetary missions, would not measure such a difference and the bands would remain classified as characteristic.

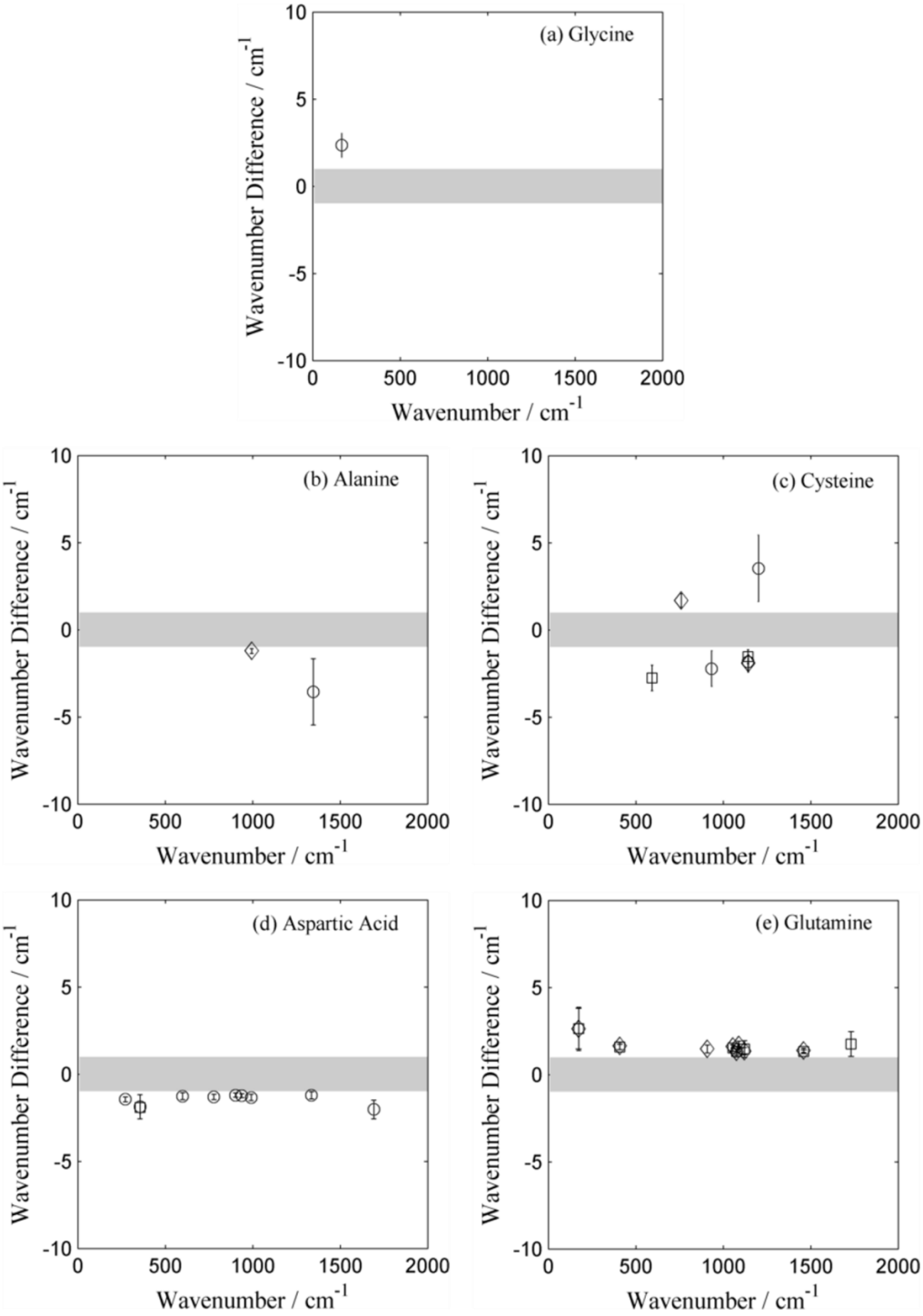

Figure 3-5: The relative wavenumber difference (RWD) in the position of the characteristic bands in the 514 nm excitation wavelength spectra relative to the 473 nm excitation wavelength spectra for (a) glycine; (b) L-alanine; (c) L-cysteine; (d) L-aspartic acid; (e) L-glutamine. The grey area represents the instrument accuracy. The error bars show the standard deviation of the bands from measurements of the samples in the 514 nm laser. Open circles represent band positions from map 1; open squares, map 2; and open diamonds, map 3. The RWD of some amino acids showed a trend to higher relative wavenumbers, some a trend to lower relative wavenumbers and others experience no observable trend (data for bands within the instrument accuracy and rejected bands not shown).

All the characteristic bands of aspartic acid failed the *t*-tests; the results demonstrated that the band positions were statistically significantly different from one another when compared across the two excitation wavelengths and supports the trend to lower wavenumbers seen in Figure 3-5. However, when the instrument accuracy is considered, most bands had mean wavenumber positions within the instrument accuracy, except those at 992, 1260, 1423 and 1692 cm^{-1}. These bands were outside of the instrument accuracy margin by 0.16, 0.11, 0.37 and 0.12 cm^{-1}, which is negligible for lower resolution Raman spectrometers, hence these bands should still be considered as characteristic of aspartic acid. For glutamine, the *p* values that resulted from the *t*-tests showed that the difference in the band positions between excitation wavelengths is statistically significant for the majority of bands. Nonetheless, all but three of the bands were within the instrument accuracy; the bands 409, 1090 and 1732 cm^{-1} were outside the error by 1.15, 1.08 and 1.16 cm^{-1}. For lower resolution Raman spectrometers, is not significant enough to remove these bands from the set of characteristic bands for glutamine, but should be considered with caution by higher resolution Raman spectrometer users. The recorded band positions in each excitation wavelength are listed in Table 3-2 and Table 3-3.

These tests showed that even when using the same instrument, there are minute, but statistically significant changes in wavenumber position of bands, because of differences in instrument characteristics, setup and calibration. Future studies should be aware of this when designating characteristic bands using a variety of excitation wavelengths. When considering future planetary missions that have excitation lasers extensively outside of the range 514 to 473 nm (*i.e.* red optical, IR or UV wavelengths), the same tests should be applied to laboratory measured Raman bands of target biomarkers to ensure which bands can be defined as characteristic as they may differ to the ones reported here.

Dispersion effects because of the crystal structure may account for differences in band position. This effect has been shown to occur in disordered carbons and graphites (Vidano *et al.*, 1981; Matthews *et al.*, 1999), where the positions of some of the bands are dependent on the excitation wavelength whereas other band positions are not. In carbon structures the major bands are the graphitic or G band and the disorder or D band; the RWD for the D band is relatively small (about 35 cm^{-1}) when examined over a wavelength range between 488 to 647.1 nm (Vidano *et al.*, 1981). This effect, though small, could explain the RWD between the two excitation wavelengths in this study. Matthews *et al.* (1999) present a model that describes how the dispersion of the D band is because of a resonant Raman process in which phonons and electrons experience a coupling within the Brillouin zone and are in resonance with the excitation wavelength. The C−C bonds and/or the increasing molecular size of the amino acids (*i.e.* increasing the number of phonons that could resonate with the excitation wavelength) could create a similar behaviour in the crystalline structures studied here. As the number of C−C bonds (glycine, two; alanine and cysteine, three; aspartic acid, four; and glutamine, five) and number of overall bonds increase, potentially allowing for the dispersion effect to occur more readily, increased scattering and trends in the difference of the wavenumber positions because of the excitation wavelength shifting to higher or lower wavenumbers are seen (Figure 3-5). For this resonance in the Brillouin zone with the excitation wavelength to be possible in amino acids, the group velocity of the acoustic phonons in the molecules and ratio of the difference in wavenumber position verses the difference in the laser wavelength would have to be similar, as discussed in the model for the dispersion effect in the D band by Matthews *et al.* (1999). These calculations are beyond the scope of this study, but a dispersion effect of this kind in amino acids crystals has not been previously reported.

3.5. Summary

This chapter has demonstrated that a statistical method can be developed to define rigorously a set of characteristic Raman bands for assisting in the identification of amino acids in an unknown sample. The use of a statistical method allowed the identification of the characteristic bands to be independent of the number of bands that are Raman active for each amino acid (Table 3-4) and their intensity, removing the need to define a generic minimum number of bands that may not be applicable across a wide range of biomarkers as general rule. The statistical method was readily able to define sets of characteristic bands for the amino acids alanine, aspartic acid, cysteine, glutamine and glycine that could be used as a reference for future planetary missions.

Amino Acid	Characteristic Bands (cm^{-1})
Alanine	**71**, 91, 124, 333, 760, **832**, 919, 995, 1114, 1346
Aspartic Acid	84, 272, 466, 551, 778, 872, **938**, 991, *1082*, 1336, 1360, 1408, 1423
Cysteine	68, 131, 159, 593, 608, **679**, 762, 866, 933, 1142, 1202, 1220
Glutamine	**96**, **112**, 122, 174, *323*, 409, *908*, 1055, 1076, **1090**, 1122, 1225, *1462*, 1732
Glycine	73, 137, 167, 501, 516, 569, 584, 860, **875**, 888, 914, 1104, 1130, 1300, 1327, 1411, 1450, 1495, 1598

Table 3-4: A summary of the characteristic bands statistically defined for the amino acids in this study. Bold indicates bands with a very strong intensity classification. Italics indicate tentatively assigned characteristic bands.

4. Amino Acid Exposure to Simulated Martian Conditions

4.1 Introduction

This chapter explores the potential for Raman signatures of amino acids to be detected after exposure to simulated martian conditions. The results will help with the interpretation of results from future missions that attempt to detect organic molecules that are used by life. The aim of this chapter is to explore whether exposure to a complement of martian surface and near surface (defined by, approximately, the first 2 m below the surface) conditions affect the Raman spectra of amino acids. Raman spectra of the amino acids were acquired pre- and post-exposure to understand any changes that might occur to amino acids once they are exposed to Mars-like surface and near surface conditions, including: temperature cycling to represent freeze-thaw cycles and simulated atmospheric composition, temperature, pressure and UV exposure.

Amino acids are essential to life on Earth. They are the 'building blocks' of proteins, form enzymes and participate in various chemical reactions. Specifically, there are twenty amino acids that are used by life to build proteins (*e.g.* Creighton, 1993), known as the natural, proteinogenic or α- amino acids. Plants and microbes can synthesise all the natural amino acids (Hardy, 1985). These amino acids are all α-amino acids as the functional groups are bonded to the alpha carbon atom. The functional groups are an amine ($-NH_2$) and a carboxylic acid ($-COOH$).

The neutral molecular structure of amino acids is NH_2–CHR–COOH (shown in Figure 4-1), but they are more often of zwitterion form NH_3^+–CHR–CO_2^-, especially in solid form (Taylor, 1971). R is representative of the side chain that defines each amino acid. The side chain can be, as in glycine, a single H atom to the more complex ring structures seen in aromatic α-amino acids such as tryptophan or phenylalanine.

Amino acids are enantiomers so can be 'right-handed' (D form) or 'left-handed' (L form) chiral molecules. Terrestrial life displays an enantiometric excess for L-amino acids and D-sugars (*e.g.* Morozov, 1979; Hardy, 1985). However, one exception to the rule is glycine, the only biologically selected amino acid that is achiral.

Five amino acids (~99% purity, supplied from Sigma Aldrich, UK), glycine, L-alanine, L-cysteine, L-aspartic acid and L-glutamine, were studied. Hereafter, the amino acids will be referred to as glycine, alanine, cysteine, aspartic acid and glutamine. This subset of the twenty natural amino acids was chosen as they are representative of the various sub-classes assigned to amino acids. Glycine is non-polar, can exist in hydrophobic or hydrophilic environments and is the only achiral amino acid that is used by biological functions. It is the simplest amino acid, with a single H atom as its R side chain, its molecular structure was determined by Jönsson and Kvick (1972) and Power *et al.* (1976). Alanine is aliphatic, non-polar and hydrophobic. The molecular structure was determined by Lehmann *et al.* (1972). It is the simplest of the biological laevorotatory amino acids, with a methyl group as its R side chain. Alanine is regarded as ambivalent, *i.e.* it can exist inside or outside the protein molecule. Cysteine is a sulphur-containing, hydrophilic, non-polar amino acid; its molecular structure was defined by Harding and Long (1968).

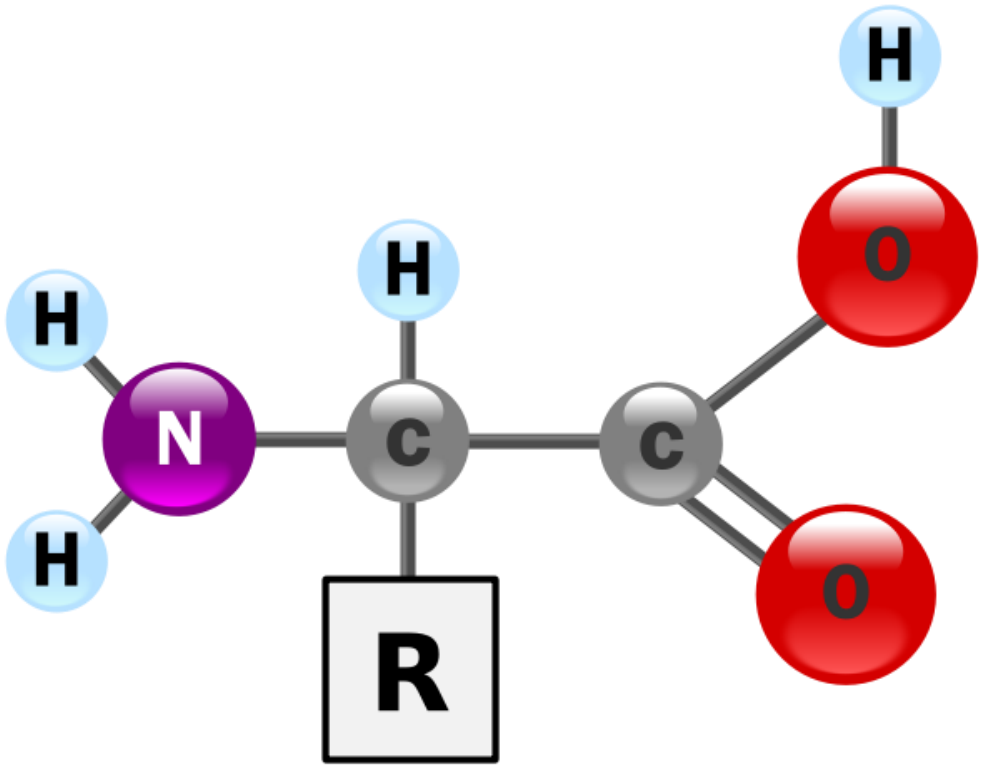

Figure 4-1: A basic cartoon of the molecular structure of an amino acid in its unionised form (created by: GYassineMrabetTalk https://commons.wikimedia.org/w/index.php?curid=2551977).

Aspartic acid is classed as acidic and hydrophilic with a negatively charged side chain, its molecular structure, determined by Derissen *et al.* (1968). Glutamine is polar, hydrophilic and its molecular structure was defined by neutron diffraction (Koetzle *et al.*, 1973).

Previously, there had been several attempts to detect organic molecules in the regolith on Mars, without success; though methane has been detected in the atmosphere (Webster *et al.*, 2014) and there must be a large daily influx of organic material from meteorites *etc.* (see Section 1.3.3). The Sample Analysis at Mars (SAM) instrument suite on the *Curiosity* rover has since found evidence of previously undiscovered nitrogen in regolith samples (Stern *et al.*, 2015); with molecules of nitric oxide, hydrogen cyanide and trifluoro-*N*-methyl-acetamide detected, though some of this could be contribution from

terrestrial contaminants (Stern *et al.*, 2014). Discovery of nitrogen in the regolith has implications for astrobiology as it is necessary for many biomolecules, including the amine functional group in amino acids. From this evidence it is possible that amino acids could exist on Mars, either at or in the near surface.

Amino acids have been exposed to simulated martian conditions in previous studies showing (extrapolated) longevity on the surface (current day expectation of sub-ppt levels) (ten Kate *et al.*, 2005); conversely the FTIR spectral features of samples flown on board the ISS for 1.5 yr were entirely diminished, suggesting total photodestruction (Noblet *et al.*, 2012). Where previous studies have used other detection methods to understand exposure of amino acids to martian conditions, this chapter reports the first use of Raman spectroscopy to attempt to detect the Raman signatures of amino acids post-exposure to coupled simulated martian conditions, and examined any changes that may have occurred as a result of this exposure.

In this chapter, martian simulation chambers and UV radiation sources were used to expose amino acid samples to a Mars-like surface and near surface environment. A Mars-like pressure of 6 to 10 mbar and an atmospheric composition of 95 % CO_2, 5 % N_2 was introduced into the chambers. Extended experiments where the samples were exposed to temperature of –18 °C and freeze-thaw cycling between –10 and 40 °C were conducted. For simulation of surface radiation UV source lamps were used (deuterium and xenon). The apparatus used for these simulations are described in Section 2.3.

The characteristic Raman bands of the amino acids, which were determined in Chapter 3, were used to determine the differences in the Raman spectra (if any) pre- and post-exposure to simulated martian conditions and hence, whether the amino acid samples still remain detectable after exposure. The 514 nm laser was used in these experiments, as it was the closest available wavelength to that selected for the *ExoMars* mission.

4.2 Results

4.2.1 Preliminary atmospheric composition and pressure tests

To establish how the martian environmental factors affected the amino acids, samples were placed in MSCs and exposed to isolated environmental factors in preliminary tests before exposure to a full analogue martian environment. These tests were conducted to constrain rigorously the contribution of each isolated environmental factor. Therefore, when experiments with coupled martian environmental factors were conducted, any changes in the Raman spectra could be understood more thoroughly. It was expected that the isolated atmospheric composition and pressure tests would yield no discernible changes to the amino acids and therefore, the Raman spectra of the amino acids.

Melchett-class MSCs (as described in Section 2.3.1.2) were used to conduct these preliminary tests. Samples of the amino acids (thin films on microscope slides, created as described in Section 2.4), alanine, aspartic acid, cysteine, glutamine and glycine, were placed for 167 and 170 days in a Mars-like atmospheric composition and pressure, respectively. The MSC for the atmospheric composition test was flushed several times with the Mars-like atmospheric composition before being sealed at a pressure of 1000 mbar. The Mars-like pressure was achieved by reducing the MSC pressure with a

terrestrial atmosphere to an initial pressure of 5.70 mbar. The *Melchett*-class chambers were leak-tested over five months, with an increase in pressure of 3.51 mbar. This was within the nominal martian atmospheric pressure range, so was acceptable over the course of experiments, which were approximately five months or less in length. The pressure readings over the course of the 170 day experiment were between 5.70 and 9.91 mbar.

In these experiments, the resulting spectra were an average of nine map points in a 300 μm × 300 μm area, where each point consisted of five 10 s repeats, all of which were baseline corrected and band fitted before analysis; the spectra were acquired pre- and post-exposure, returning to the same coordinates, for a direct comparison of those points on the samples; the data were collected as described in Section 2.2.3. In this and the following experiments, the spectra were processed using a custom MATLAB routine (part automatic, part user-led) that removed fluorescence and other noise, identified any bands in the spectra and created an individual *Excel* file for each map point with the raw, baseline corrected and, band intensity and position data. The individual map point *Excel* files were then combined into a master file (per experiment) containing the pre- and post-exposure data for manipulation to create the graphical figures in this chapter.

The results for these preliminary experiments were examined by comparing the pre- and post-exposure Raman intensity relatively (the strongest intensity characteristic band was set equal to 1), with the expectation that there was no difference in the relative intensities of all the bands before and after exposure (and hence, no change had occurred resulting from exposure). To examine this in more detail, the relative percentage differences in the intensity of the characteristic Raman bands were plotted for comparison; the smaller the percentage difference, the less significant the change in the relative intensity (*e.g.* a 20% difference equates to a 20% reduction in intensity in comparison to the pre-exposure

intensity) and hence, little or no significant change to the Raman spectra and furthermore the sample as a result of exposure to the simulated martian environment.

The results for the isolated atmospheric composition results are shown in Appendix A. All the amino acid samples mostly had the same averaged Raman spectra shape, *i.e.* in general no new bands form and no bands disappear or change wavenumber position. Exceptions to this were: the alanine and glutamine spectra, a band appeared at approximately 880 cm^{-1} and 875 cm^{-1}, respectively; the aspartic acid spectra, two bands at approximately 850 cm^{-1} and 1220 cm^{-1} disappeared.

The pre- and post-exposure Raman spectra for the pressure as an isolated environmental factor experiment are shown in Appendix A. Compared to the isolated atmospheric composition experiment the spectra were a bit more variable. For example, the results for alanine were that the strongest intensity decreased post-exposure relative to the pre-exposure intensity for the band at 832 cm^{-1}, whereas other bands appeared to be relatively increased in intensity, such as the 919 and 1114 cm^{-1} characteristic bands. There was some poor baseline fitting between approximately 280 and 530 cm^{-1}, which accounts for the apparent increase in intensity at 335 cm^{-1}. The bands for aspartic acid have an average relative percentage difference post-exposure of no more than 4 %, excluding the strongest band at 938 cm^{-1}, which has an average relative difference of 18 %. Cysteine showed the most difference following the exposure to a Mars-like pressure; though most the bands did not appear to have changed in intensity, there was a new band that has appeared at 500 cm^{-1}, where there was no band in the pre-exposure spectra and this band was not seen in the characterisation of the amino acid Raman spectra shown in Chapter 3. This band is associated with the amino acid cystine (note spelling: where cystine is the oxidised dimer form of cysteine); the band is the stretching of the S−S bond (Edsall *et al.*, 1950).

Regardless of the appearance of this new band the rest of the bands remain relatively similar in intensity pre- and post-exposure, with no change in relative Raman intensity greater than 9 %. The glutamine and glycine spectra have a consistent relative Raman intensity pre- and post-exposure.

4.2.2 Cold temperature environment exposure

The surface of Mars experiences a large temperature differential compared to the Earth because of its the thin atmosphere and its greater distance from the Sun. To establish whether amino acids samples were stable in a cold temperature environment, samples (thin films on microscope slides) were exposed at approximately –18 °C for an extended period of 55 days. The resulting spectra, collected pre- and post-exposure were an average of 16 map points in a 300 μm × 300 μm area, where each point consisted of five 10 s repeats, all of which were baseline corrected and band fitted before analysis.

The relative average changes to Raman intensity as a result of the exposure to an extended cold temperature environment are shown in Figure 4-2. Alanine showed a relative increase in intensity post-exposure, to an extent not seen in any of the other samples (see Section 4.3.1 for an explanation). The percentage difference for the characteristic Raman bands (shown in Figure 4-3) showed the average percentage difference for the strongest intensity characteristic band was approximately 43 %, whereas the other characteristic bands had a maximum percentage difference of 14 %. Cysteine did not show much difference in relative intensity, with the greatest average percentage difference of 11 %. Glycine was also relatively unchanged by the exposure, exhibiting a maximum of 21 % average percentage difference, a comparative maximum average percentage difference to those seen in the isolated atmospheric composition and pressure tests. The aspartic acid and

glutamine samples could not be analysed as the pre-exposure spectra were not as expected; the recorded spectra did not show the expected spectra (and therefore the characteristic bands) seen in Chapter 3 and hence, it was not possible to analyse or draw any conclusions from these samples.

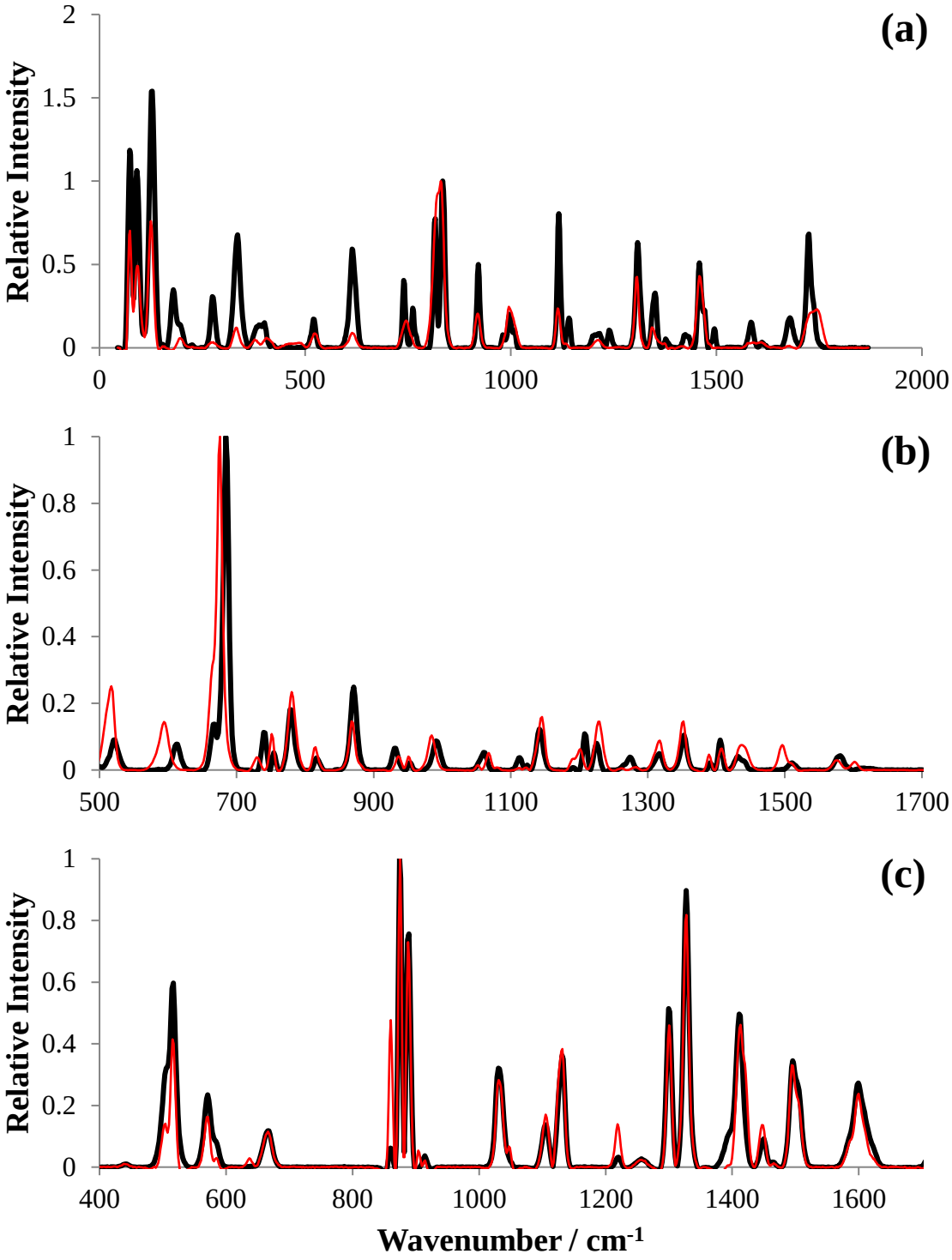

Figure 4-2: The pre- and post-exposure Raman spectra of the amino acids (a) alanine, (b) cysteine and (c) glycine (average of 16 spectra); samples were exposed to a cold temperature environment in a terrestrial atmospheric composition and pressure. The red line is the average pre-exposure spectrum and the black line is the post-exposure spectrum.

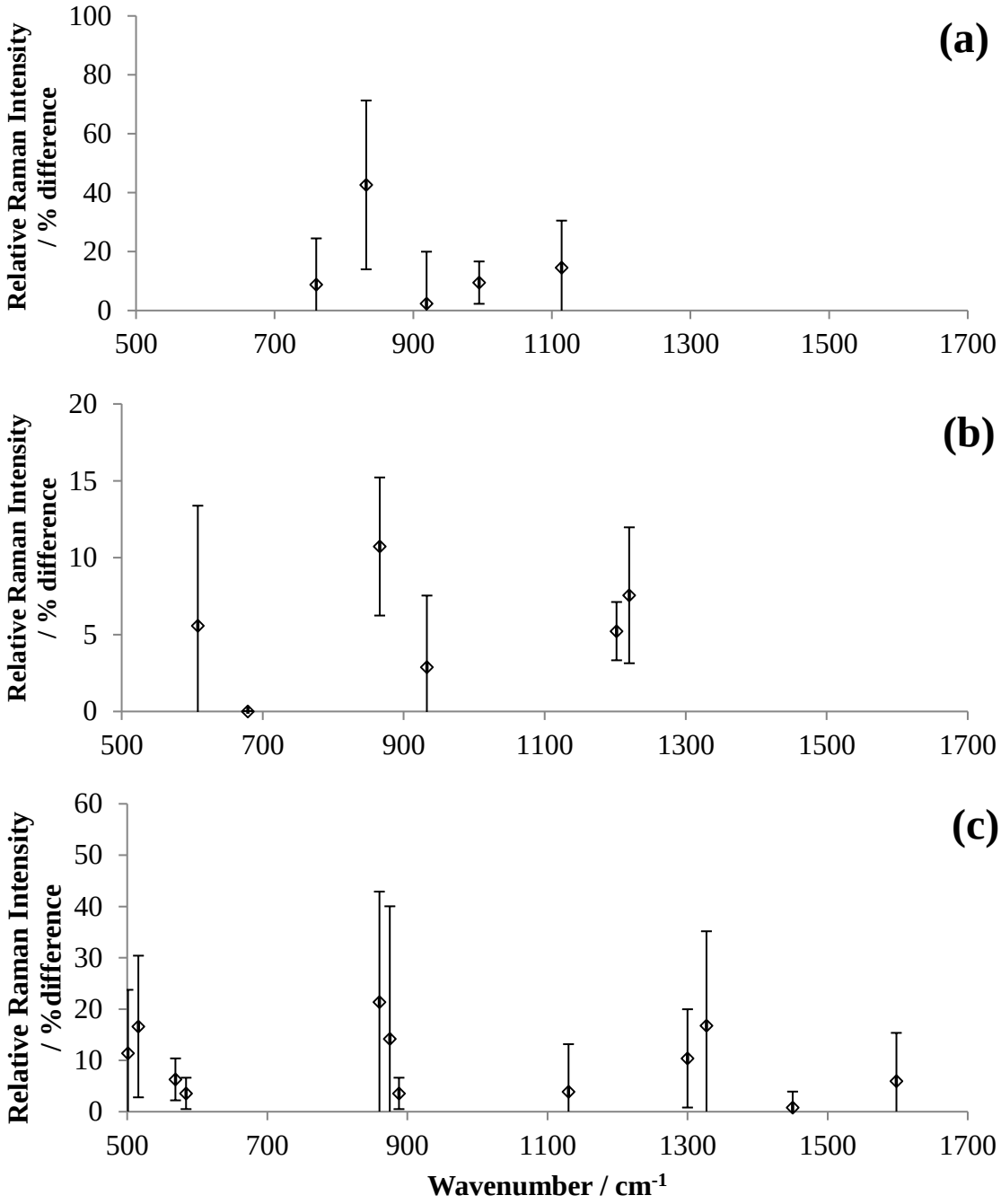

Figure 4-3: The average percentage difference in the relative Raman intensity for pre- and post-exposure to a cold temperature environment (in terrestrial atmospheric composition and pressure) for samples of (a) alanine, (b) cysteine and (c) glycine. The wavenumber range is the 'fingerprint' region 500 to 1700 cm^{-1}. Note: the percentage difference scale is different for each plot. The error bars represent one standard deviation.

4.2.3 Exposure of amino acids to freeze-thaw cycles

The previous section described samples being exposed to a continuous cold temperature environment below freezing (−18 °C). However, on Mars there is a diurnal freeze-thaw process. This freeze-thawing may have different effects to those seen when samples are kept at a constant sub-zero temperature. The diurnal temperature differential on Mars can range over at least 120 K (as described in Section 1.3.1.2). Simulation of this full temperature range was not possible with the apparatus available, but a Mars-like simulation was conducted. Using a temperature cycling oven as described in Section 2.3.2, a maximum range of 50 K was obtainable, simulating a diurnal temperature differential over 90 sols in nine days real time. Raman spectra of samples of amino acids as thin films on microscope slides were obtained before the samples were put in the MSC *Percy*, which, in turn, was placed in the oven. Before the temperature cycle was initiated the MSC was flushed with the Mars-like atmospheric composition and the pressure reduced to Mars-like range. After the exposure, Raman spectra were collected to analyse if there were any changes because of the environmental exposure. The resulting pre- and post-exposure spectra were an average of 16 map points in a 300 μm × 300 μm area, where each point consisted of five 10 s repeats, all of which were baseline corrected and band fitted before analysis. The averages of these spectral maps are shown in Figure 4-4 and the details of the percentage differences in the intensities of the characteristic bands are shown in Figure 4-5. The relative Raman intensity spectra exhibit little to no change in the relative intensities or shape of the bands for aspartic acid, cysteine and glycine, with alanine showing a slight decrease in relative intensity post-exposure. This was reflected when the percentage differences in the characteristic bands were assessed; with the exception of alanine the greatest average percentage difference was approximately 8 % (alanine had an average percentage difference for the 1114 cm^{-1} band of 17 %). The glutamine sample was not

analysed as the pre-exposure spectra were not consistent with the characteristic spectra recorded in Chapter 3.

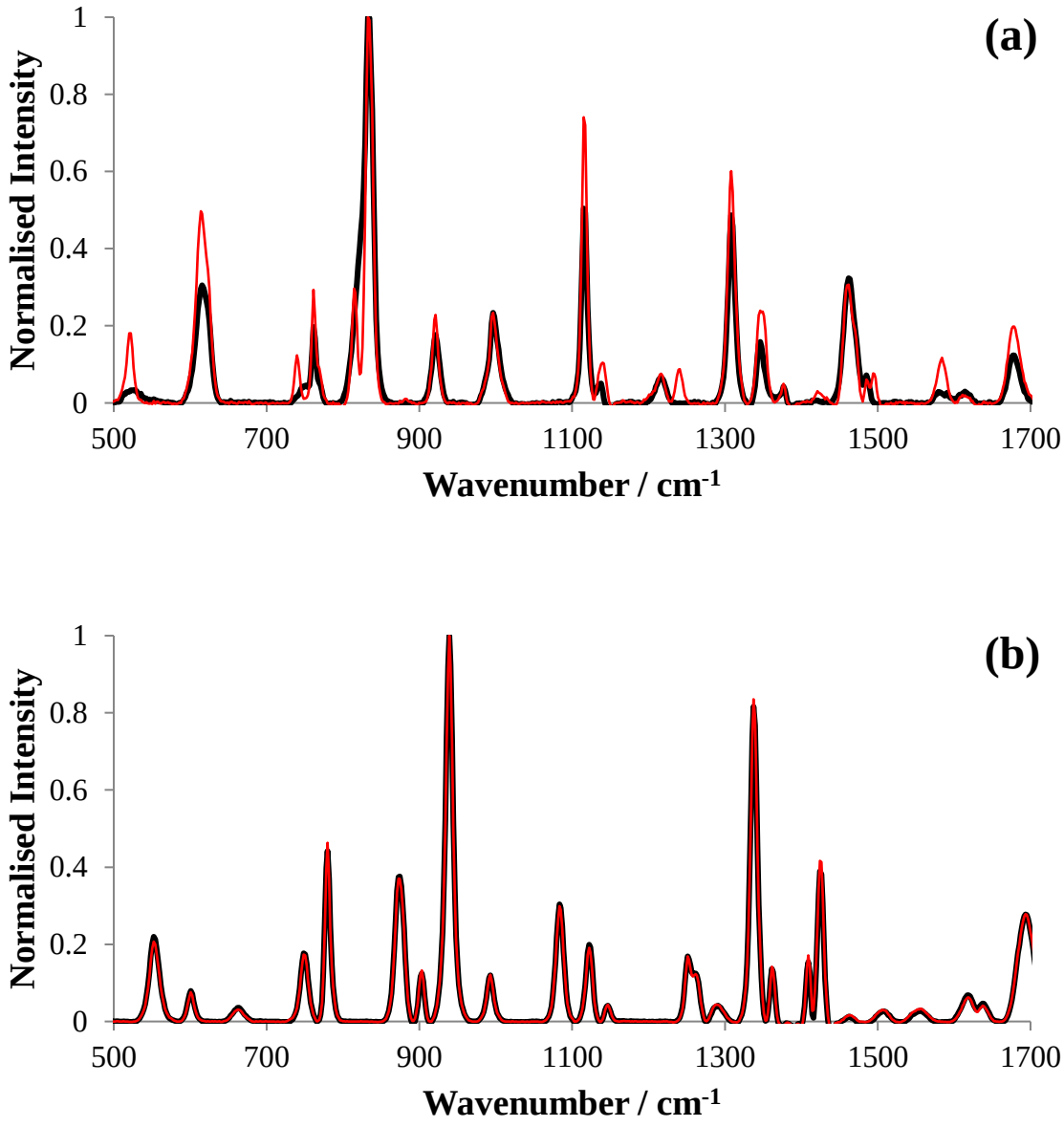

Figure 4-4: The pre- and post-exposure Raman spectra of the amino acids (a) alanine, (b) aspartic acid, (c) cysteine, (d) glycine (average of 16 spectra); samples were exposed to a Mars-like freeze-thaw cycle in a simulated martian atmospheric composition and pressure. The red line is the pre-exposure spectrum and the black line is the post-exposure spectrum.

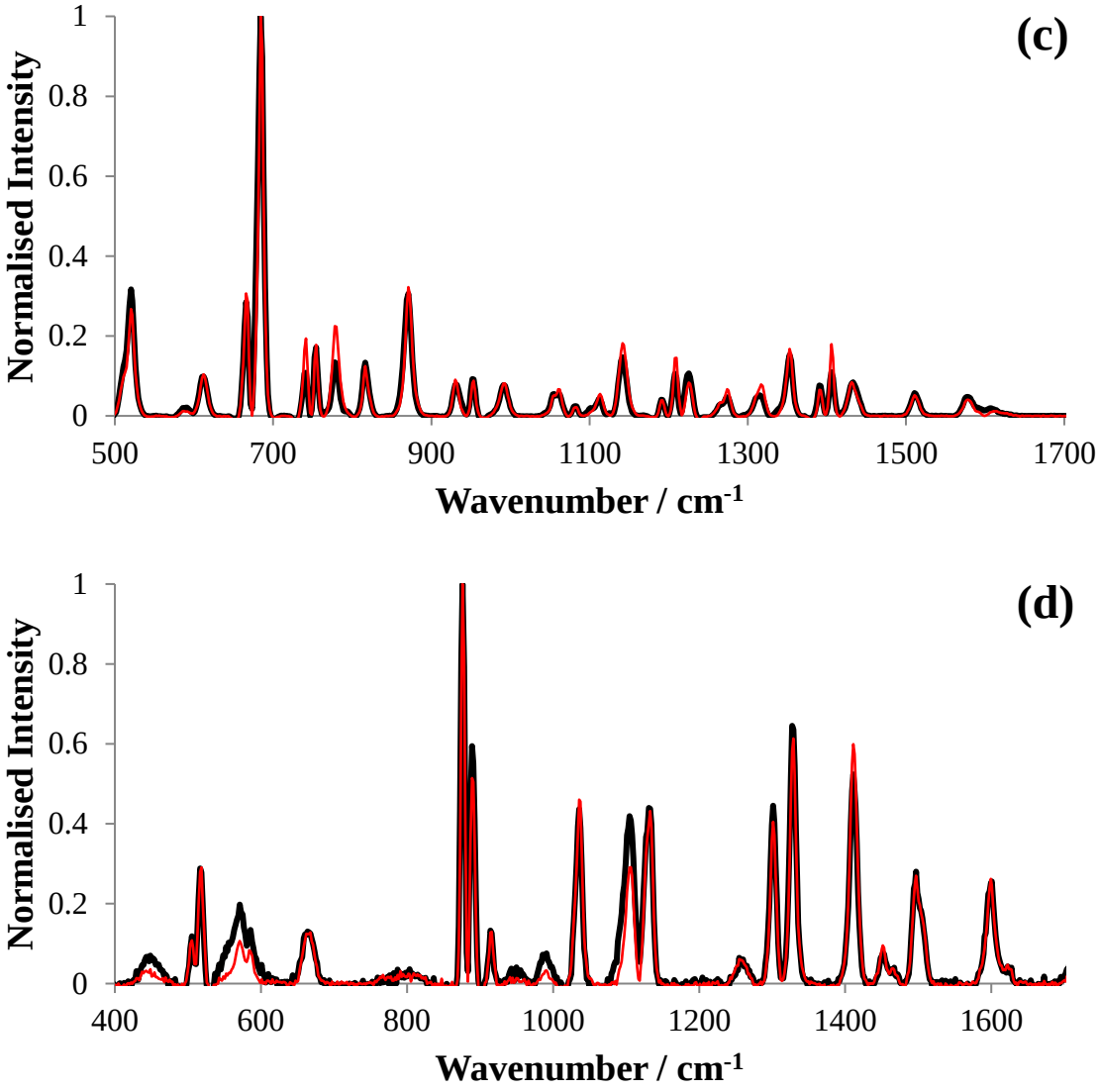

Figure 4-4 (cont.).

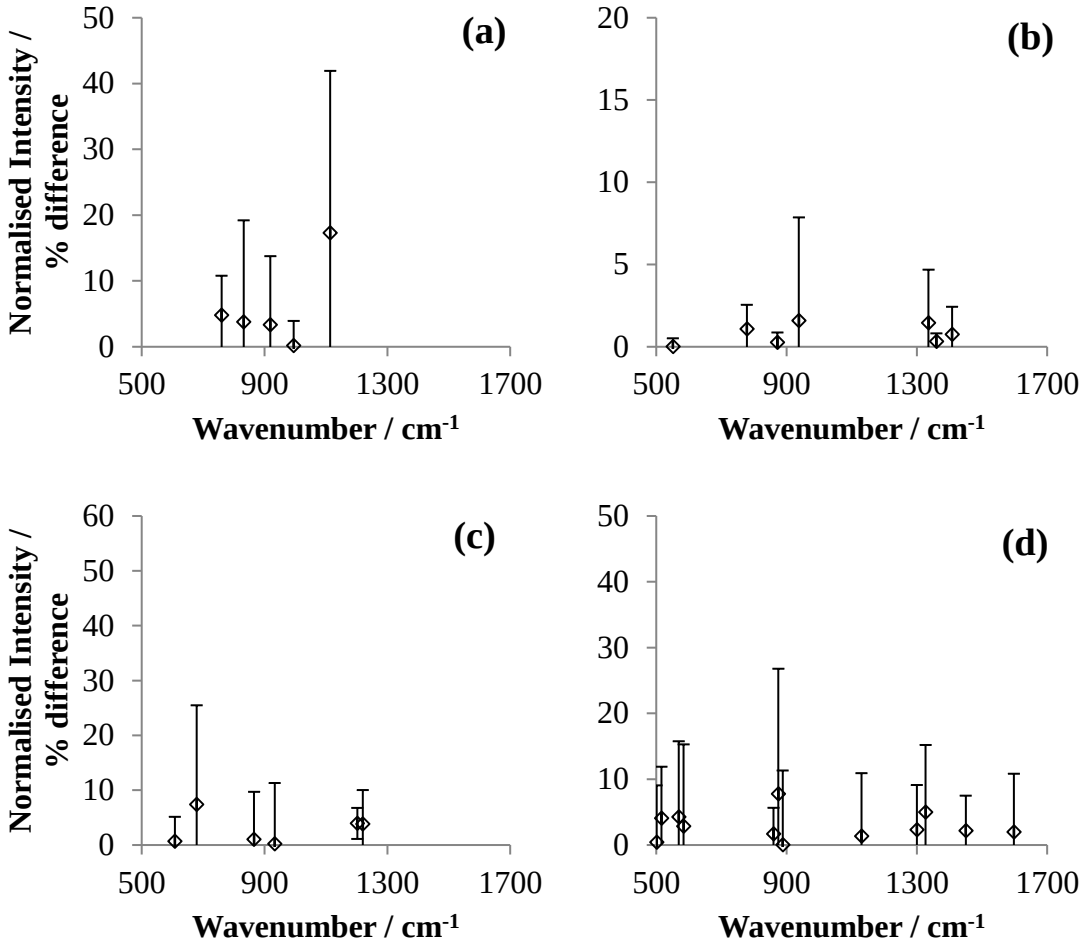

Figure 4-5: The average percentage difference in the relative Raman intensity for pre- and post-exposure to a Mars-like freeze-thaw cycles in simulated martian atmospheric composition and pressure of samples of (a) alanine, (b) aspartic acid, (c) cysteine and (d) glycine. The wavenumber range is the 'fingerprint' region 500 to 1700 cm^{-1}. Note: the percentage difference scale is different for each plot. The error bars represent one standard deviation.

4.2.4 Exposure of amino acids to ultraviolet radiation

As in previous experiments described above, amino acid samples were prepared as described in Section 2.4 and pre-exposure Raman spectra were collected. The resulting spectra were an average of 16 map points in a 300 μm × 300 μm area, where each point consisted of five 10 s repeats, all of which were baseline corrected and band fitted before analysis. The samples were exposed to a UV dose equivalent to a Mars-like sol of radiation using the Xe UV lamp (524 kJ m^{-2} per sol equivalent dose, described in Section 2.3.3) at ambient temperature (22.5 ± 0.4 °C), pressure and atmospheric composition, and follow up Raman spectra were recorded.

It was noted that after these experiments were conducted a discrepancy in the uniformity of the UV output of the Xe lamp was discovered. Figure 2-11 shows a cross-section of the output of the lamp. This non-uniform footprint allowed for the possibility that some samples may not have received the correct dose; however, examination of the images taken of the samples during their exposure to the lamp indicated that they were correctly exposed. An example placement of a sample is shown in Figure 4-6. Where amino acid samples were exposed one at a time, compared to other experiments (where three samples were exposed simultaneously, see Chapter 5), they were placed in the centre of the UV output.

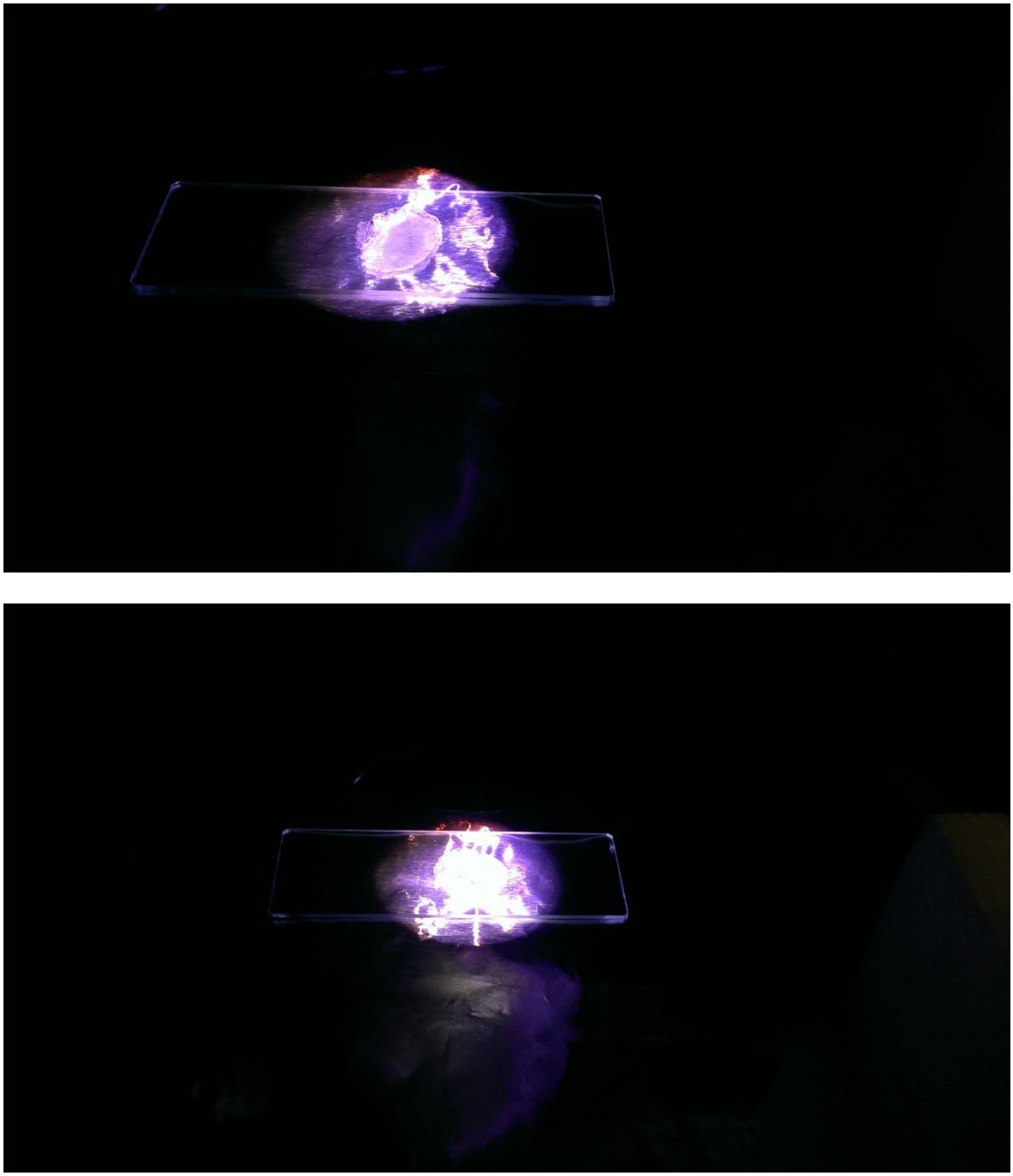

Figure 4-6: Examples of sample placement for amino acid UV exposure experiments. As samples were exposed one at time, they were placed in the centre of the UV output.

The UV exposures were repeated over five days, with the samples accumulating a sol equivalent dose of UV radiation exposure with each day. The 'fingerprint' region for organic molecules of the Raman spectra of the amino acids are displayed in Figure 4-7, which shows the pre-exposure spectra and the spectra after the final exposure to UV radiation, an accumulative dose of five sol equivalent doses, normalised to the intensity of the strongest characteristic band. The spectra for alanine are relatively unchanged, other than the band at 1305 cm^{-1}, which appeared to have increased intensity post-exposure (note: this is a non-characteristic band). The relative intensity of the aspartic acid bands showed little to no change. The cysteine pre- and post-exposure spectra exhibited the most difference. Cysteine has only one strong intensity band at 679 cm^{-1}, where all the other characteristic bands are classified as weak or very weak; nonetheless, the bands that are present pre-exposure appeared to remain at the same approximate relative intensity post-exposure. However, the band at 500 cm^{-1} recorded during the isolated pressure experiment (Section 4.2.1), was also recorded in these results. The relative intensities of the glutamine and glycine spectra displayed little to no change pre- and post-exposure.

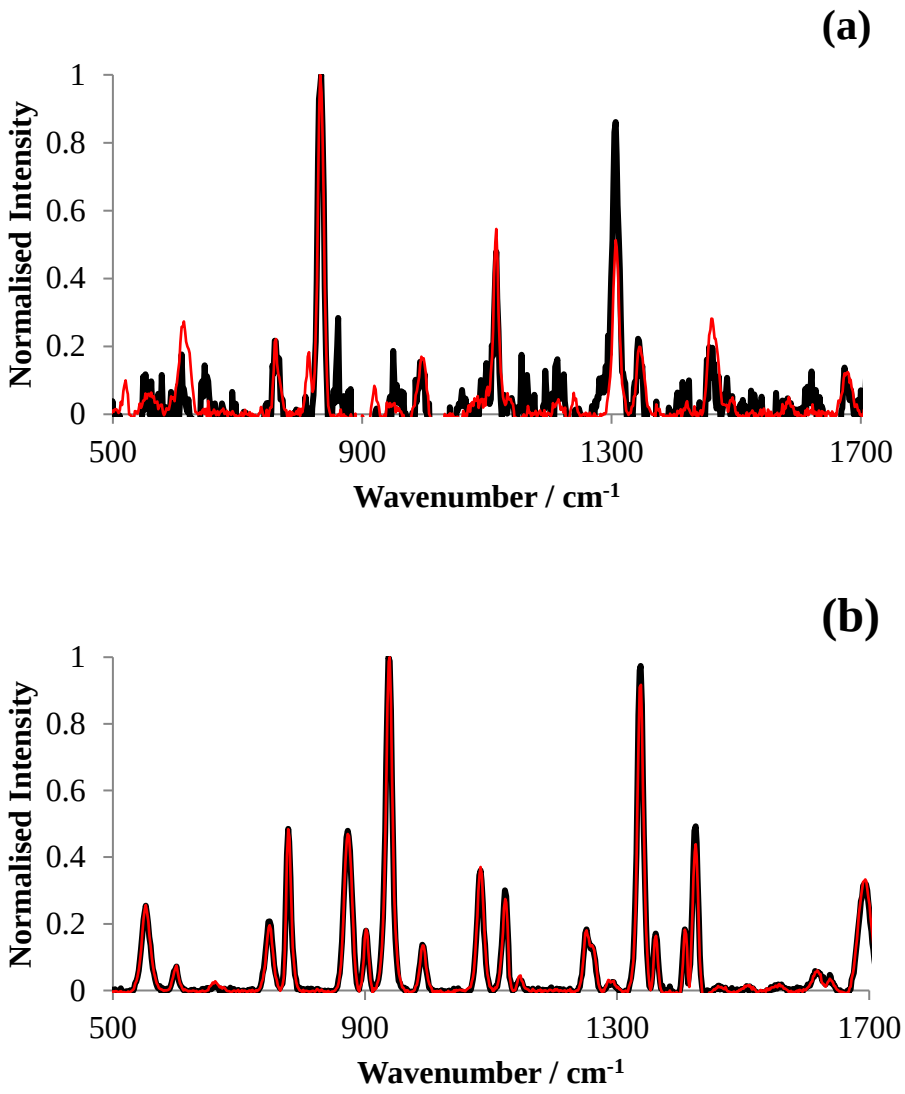

Figure 4-7: The pre- and post-exposure Raman spectra of the amino acids (a) alanine, (b) aspartic acid, (c) cysteine, (d) glutamine and (e) glycine (average of 16 spectra); samples were exposed to a Mars-like UV radiation. The red line is the pre-exposure spectrum and the black line is the post-exposure spectrum.

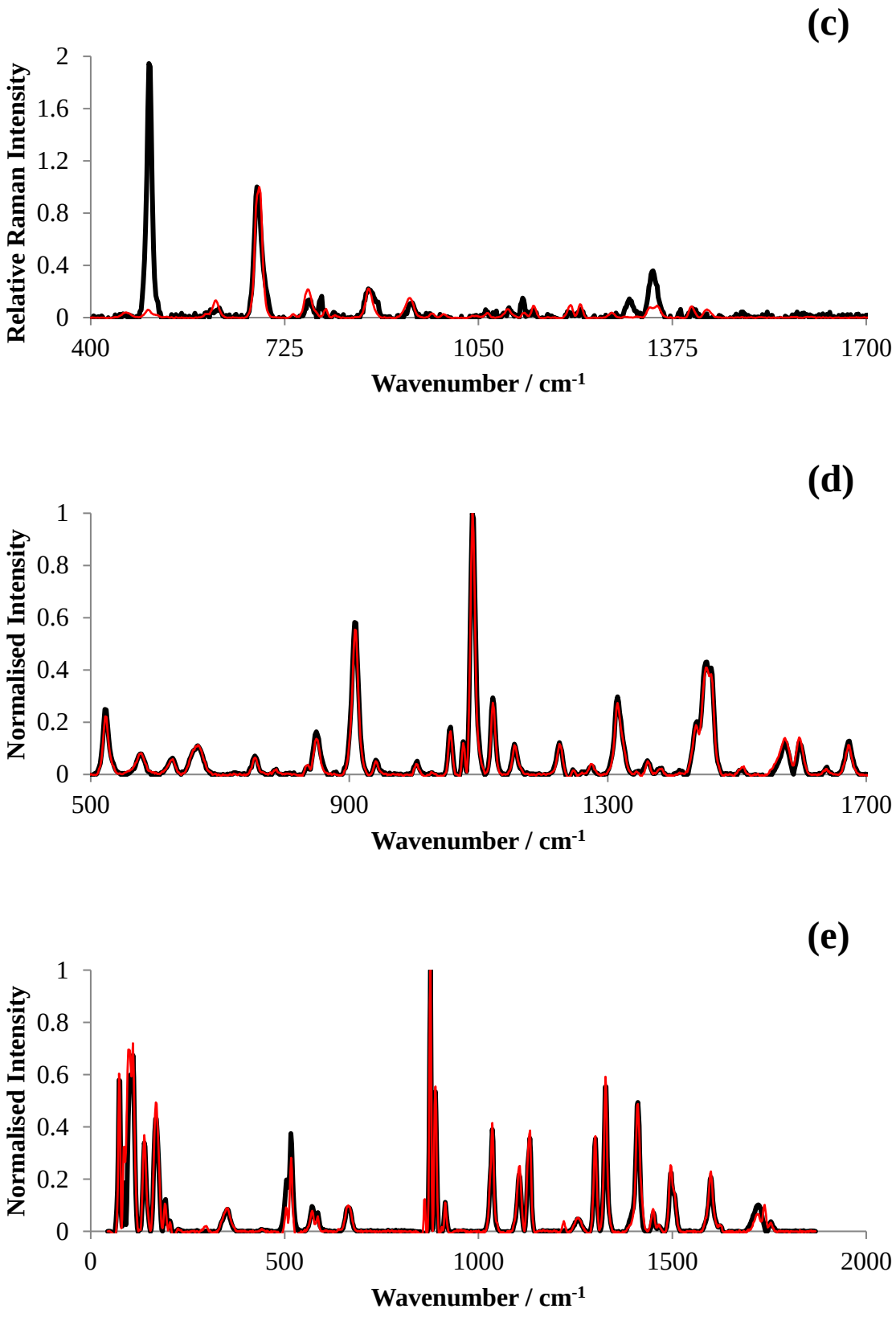

Figure 4-7 (cont.).

The following figures investigate the absolute intensity (*i.e.* the number of counts as recorded by the Raman spectrometer) of the samples for the duration of the accumulated UV doses. Figure 4-8 shows the average absolute intensity for the characteristic bands for alanine (as determined in Chapter 3) over the five sol equivalent dose of UV exposure. The average intensities of the bands were approximately similar, within the error of one standard deviation of one other as the dosage accumulated. The previous graphics represented the normalised intensity relative to the strongest characteristic band, so Figure 4-9 shows the absolute intensity change of the strongest characteristic band for alanine at 832 cm^{-1} as the UV dose accumulated. There is no definitive trend seen in the absolute intensity of this band, as the intensities remained fairly stable, within error of each other. Figure 4-10 shows the Raman intensity of the other characteristic bands, the range of the intensities were erratic, though there was no overall variation, *i.e.* they did not degrade over time as it might be expected if the molecule was being destroyed.

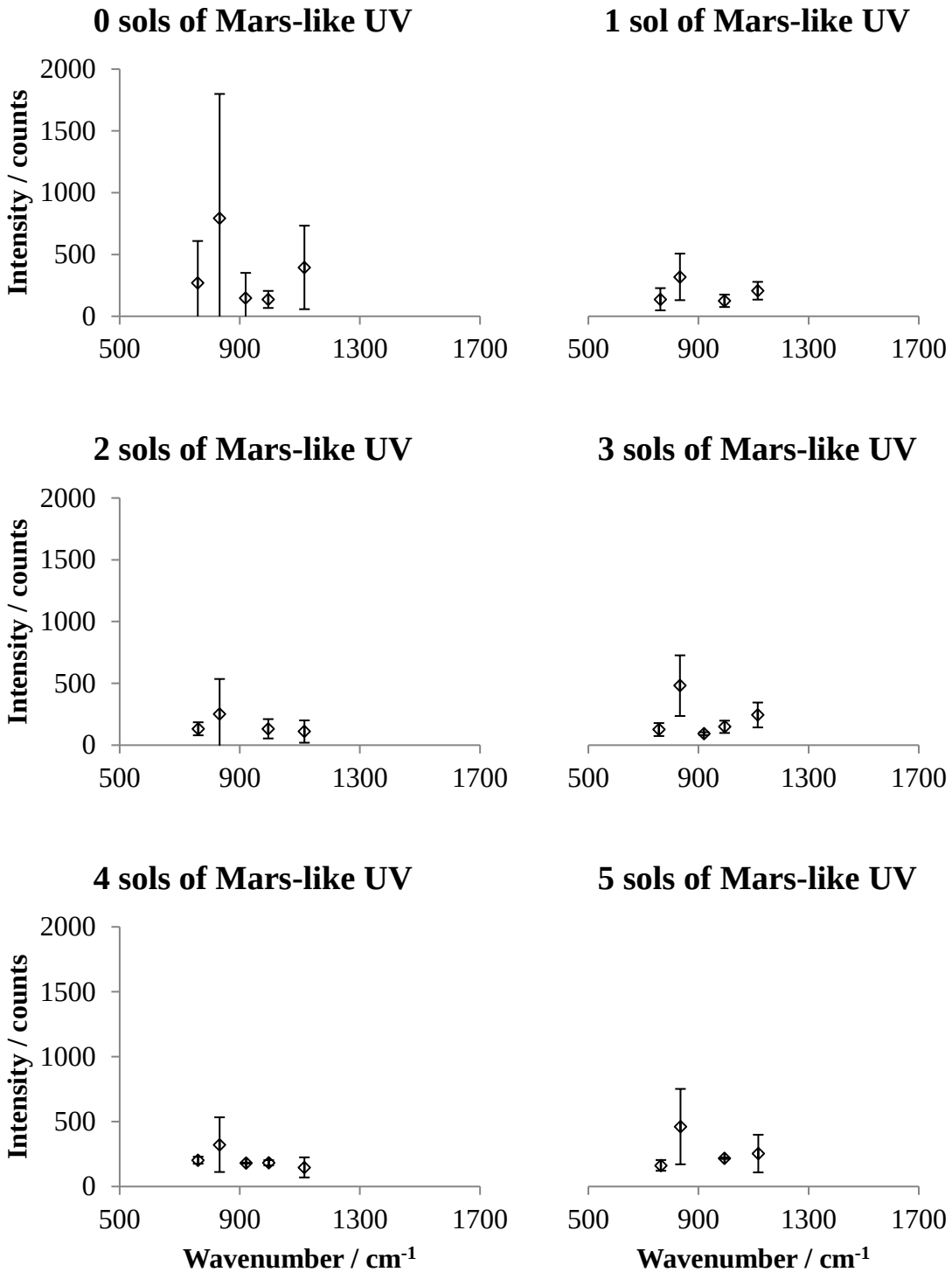

Figure 4-8: The average intensity of the characteristic bands for alanine for each sol of simulated UV exposure. The error bars represent one standard deviation.

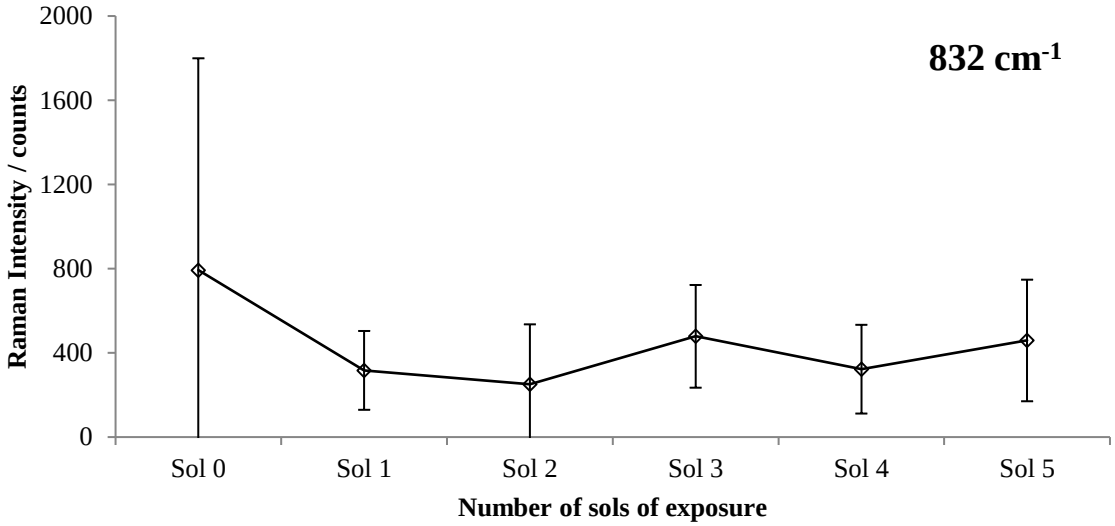

Figure 4-9: The Raman intensity of the strongest characteristic band for alanine at 832 cm^{-1} for each sol equivalent dose of exposure to UV radiation. The error bars represent one standard deviation.

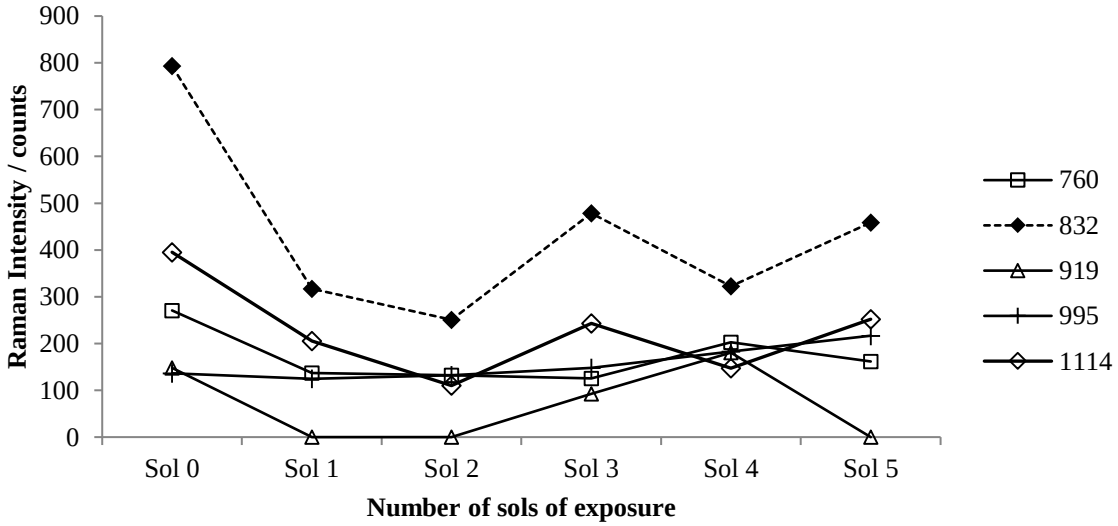

Figure 4-10: The Raman intensity of the other characteristic bands of alanine for each sol equivalent dose of exposure to UV radiation. The dashed line shows the strongest characteristic band.

The aspartic acid data for Sol 1 of exposure to the Mars-like UV was unfortunately lost, and hence not displayed. The aspartic acid characteristic bands were relatively stable in the absolute intensity, shown in Figure 4-11, with an apparent trend to a slight decrease in intensity after Sol 2. However, inspecting the bands individually with respect to number of sols of exposure (938 cm^{-1} band, Figure 4-12), the apparent trend of a decrease in the intensity is not conclusive as the intensities are all within error of one another. The other characteristic bands showed a consistent relationship with one another as the number of sols of exposure increased (see Figure 4-13), *i.e.* the intensity of all the bands changed consistently in comparison with the others, that some bands were not preferentially affected by the UV exposure.

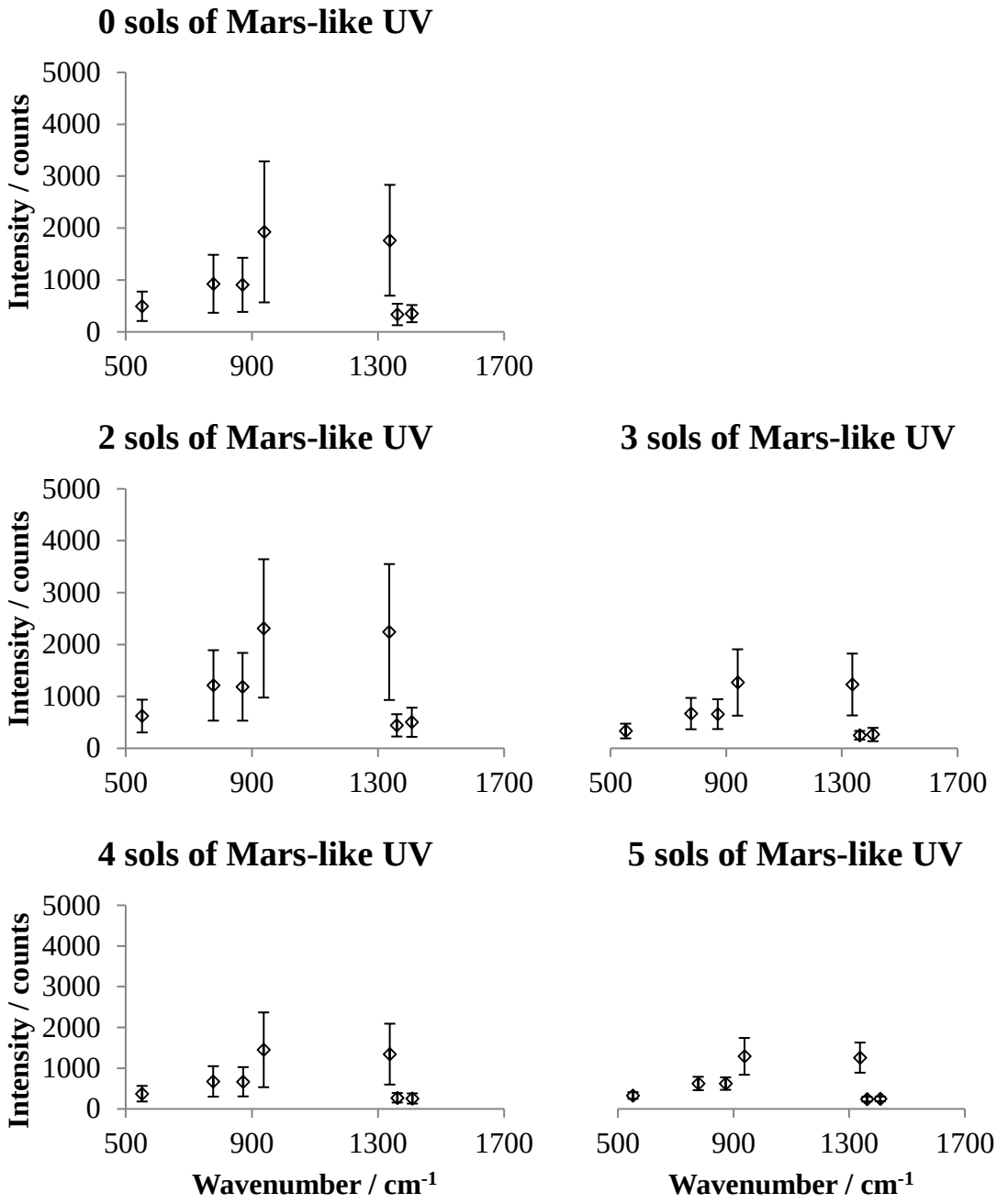

Figure 4-11: The average intensity of the characteristic bands for aspartic acid for each sol of simulated UV exposure. The error bars represent one standard deviation. The data for 1 sol of exposure was unfortunately lost.

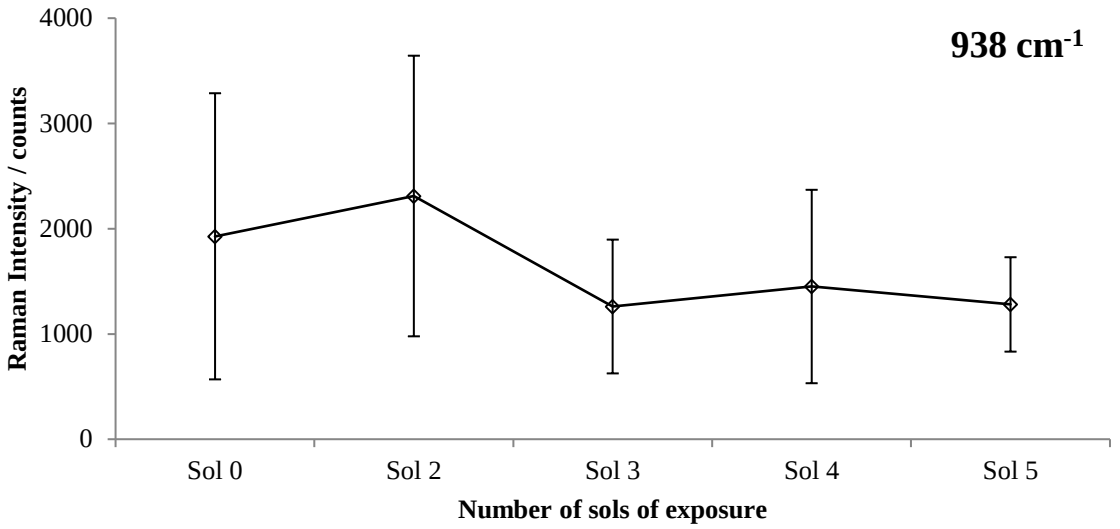

Figure 4-12: The Raman intensity of the strongest characteristic band for aspartic acid at 938 cm^{-1} for each sol equivalent dose of exposure to UV radiation. The error bars represent one standard deviation.

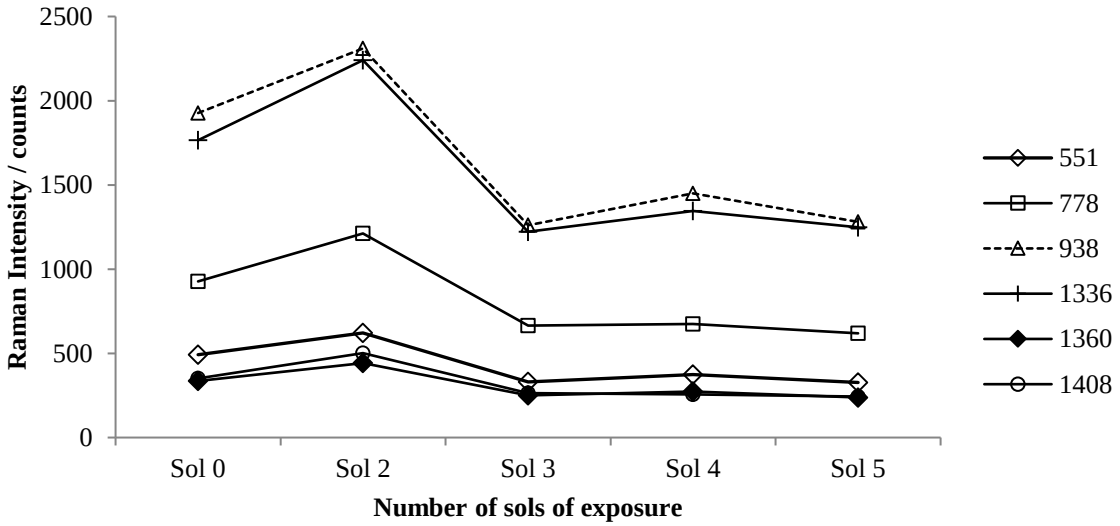

Figure 4-13: The Raman intensity of the other characteristic bands of aspartic acid for each sol equivalent dose of exposure to UV radiation. The dashed line shows the strongest characteristic band.

The absolute intensities recorded for the characteristic bands for cysteine are shown in Figure 4-14, as the dosage of UV increased, there was a notable reduction in the intensity of the bands. The cysteine results have an extra set of data "4a sols" plotted with the "4 sols" data; the cysteine sample began to emit a sulphurous smell after the fourth sol of UV radiation exposure, so before the fifth sol of exposure (approximately 24 hours later), Raman spectra of the sample were obtained to see if any changes were observed. The strongest intensity band appeared to increase slightly (though within error of the previous intensity measurement), but more notably there was a significant increase in the band at 500 cm^{-1}. Figure 4-15 and Figure 4-16 show the definitive reduction and increase in the absolute intensity of the 679 and 500 cm^{-1} bands. The 679 cm^{-1} band decreased by approximately 3000 counts over the first three sol equivalent doses of exposure, before remaining relatively steady at this reduced intensity. The 500 cm^{-1} band was highly variable for the duration of the experiment, but had an overall increasing trend. After an increase of approximately 1000 counts on average after the first sol equivalent dose of exposure, by Sol 4 the intensity declines back to the intensity level seen on Sol 0. Overnight, in real terms of time during the experiment, before the fifth sol equivalent dose of exposure, the Raman spectra of the cysteine sample showed an increase to the maximum level recorded in the 500 cm^{-1} band. The other characteristic bands decreased in intensity at approximately the same rate (the relationship to the intensity was consistent for all of the bands), as shown in Figure 4-17. The relative intensity of the 500 cm^{-1} band compared to the 679 cm^{-1} band is shown in Figure 4-18, demonstrating that the intensity of the 500 cm^{-1} band increased relatively to the intensity of the strongest characteristic band for the duration of the experiment.

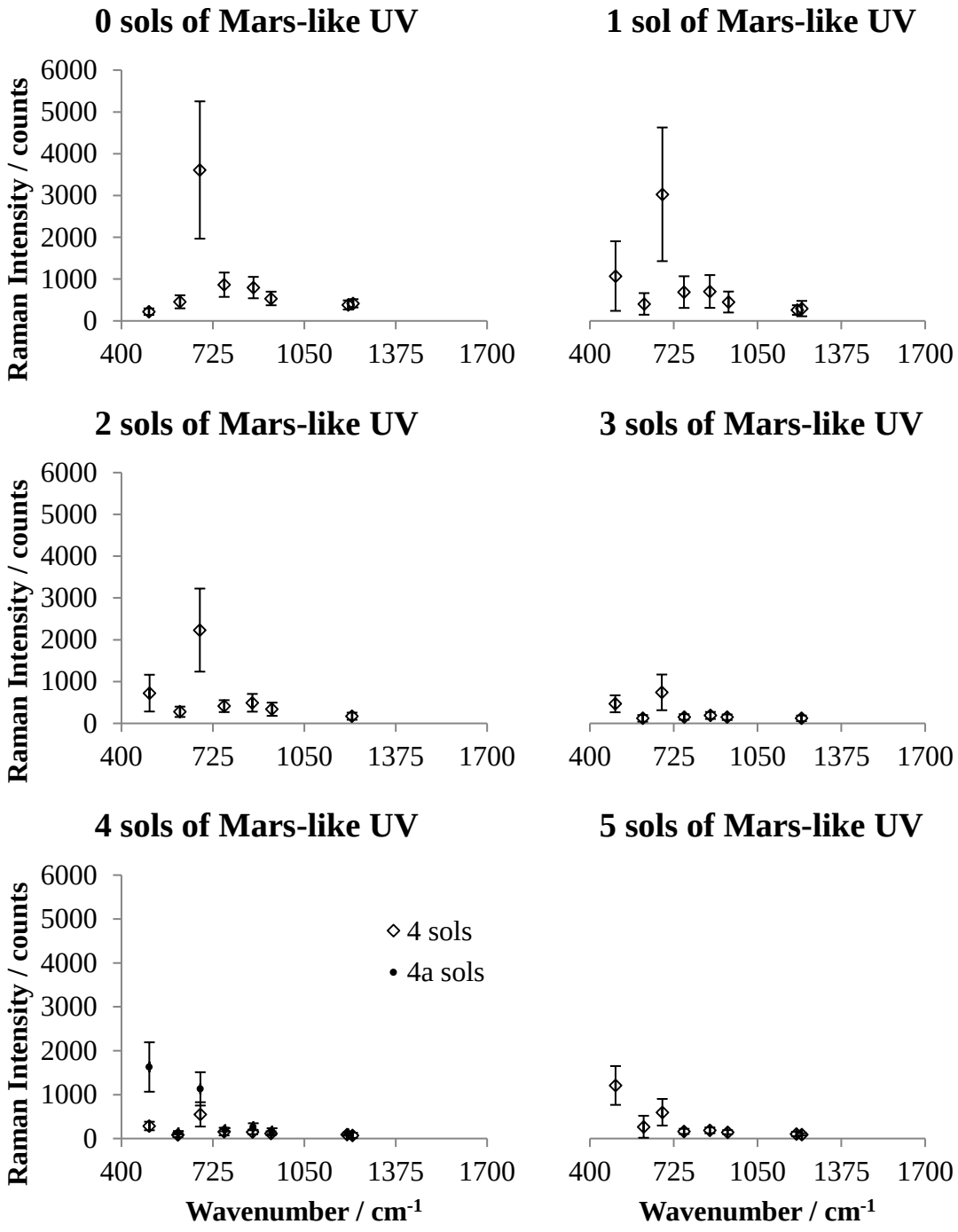

Figure 4-14: The average intensity of the characteristic bands for cysteine for each sol of simulated UV exposure. The error bars represent one standard deviation. The data marked "4a sols" is the average intensity of the characteristic bands 24 hours after being exposed to the 4th dose of UV (no extra UV dose was applied).

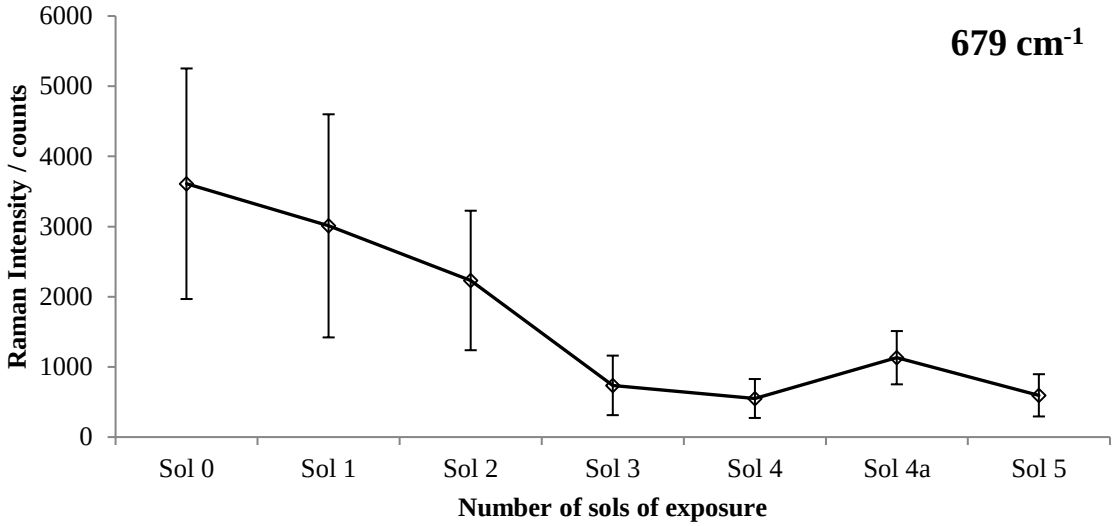

Figure 4-15: The Raman intensity of the strongest characteristic band for cysteine at 679 cm^{-1} for each sol equivalent dose of exposure to UV radiation. The error bars represent one standard deviation.

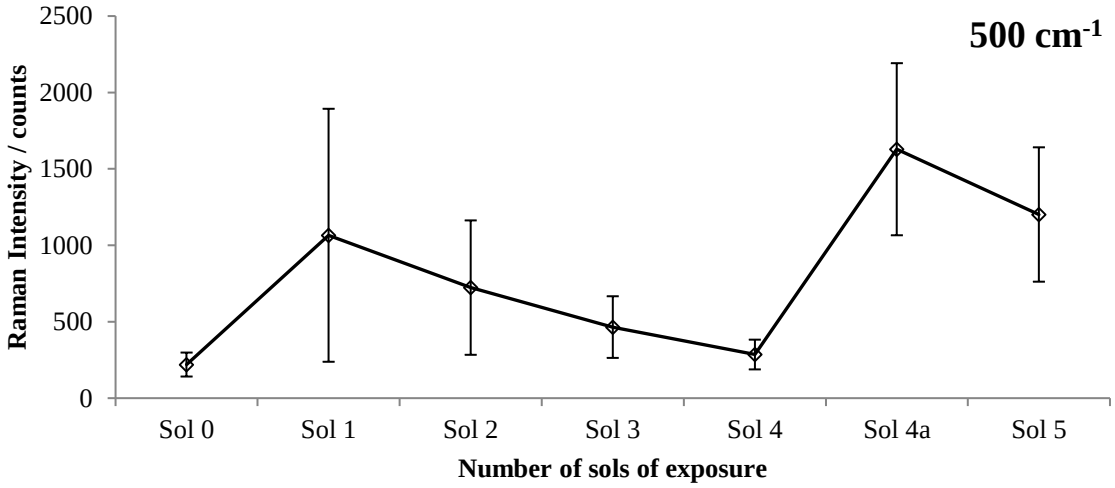

Figure 4-16: The Raman intensity of a band at for cysteine at 500 cm^{-1} for each sol equivalent dose of exposure to UV radiation. The error bars represent one standard deviation. The band is associated with a S−S bond in the amino acid cystine (note: spelling).

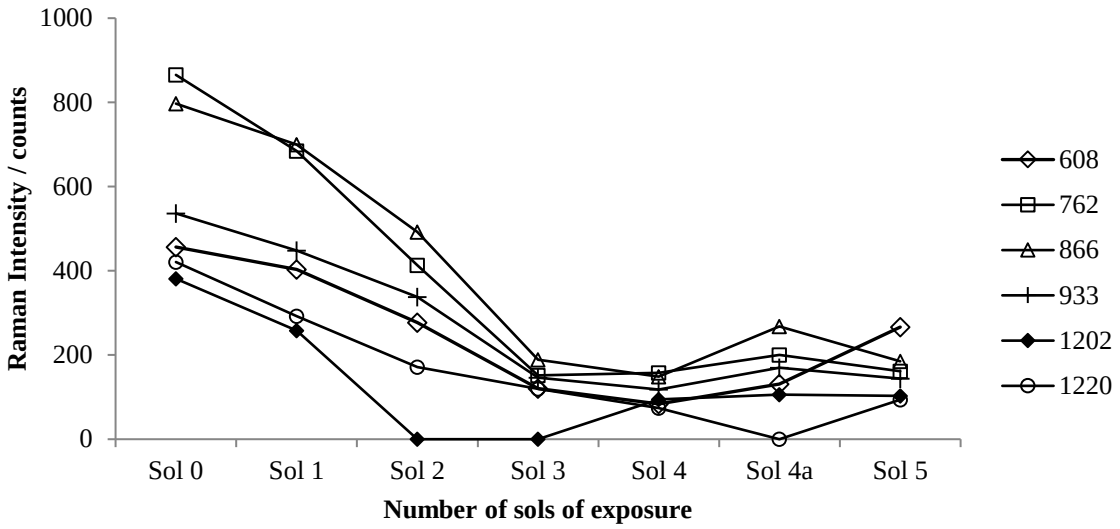

Figure 4-17: The Raman intensity of the other characteristic bands of cysteine for each of the sol equivalent dose of exposure to UV radiation.

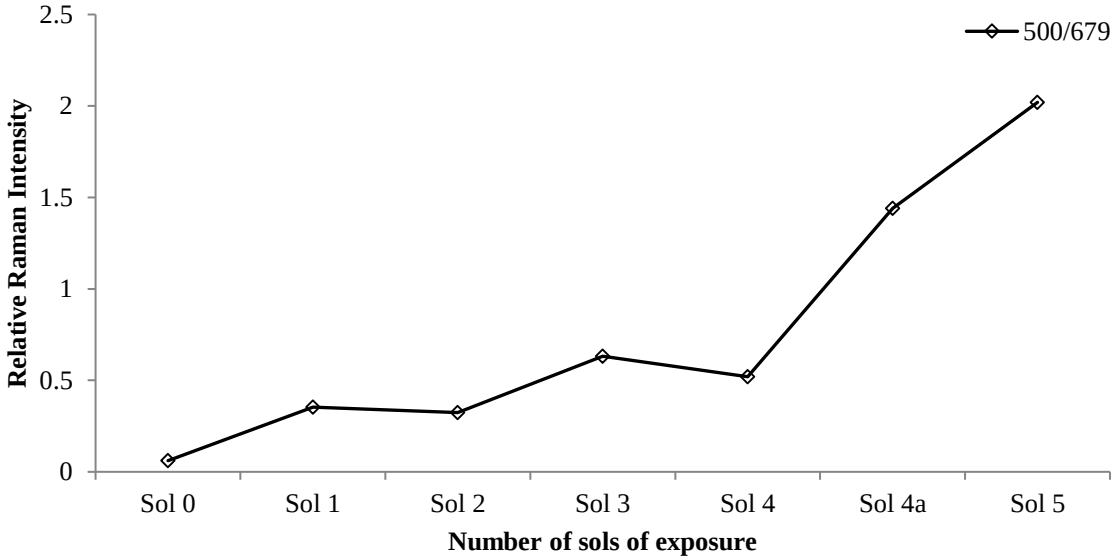

Figure 4-18: The relative Raman intensity of the 500 cm^{-1} band of cysteine compared to the strongest characteristic band at 679 cm^{-1} for each sol equivalent dose of exposure to UV radiation.

The characteristic bands of glutamine, remained stable in absolute intensity throughout the accumulative dosing of UV radiation, see Figure 4-19; this was reflected in the intensity profile of the strongest characteristic band, shown in Figure 4-20. The average intensity varied by less than 400 counts and, though large, the standard deviation was consistent, suggesting that the map points had varying but consistent intensities. Furthermore, the Raman intensities of the other characteristic bands remained steady throughout the experiment, see Figure 4-21.

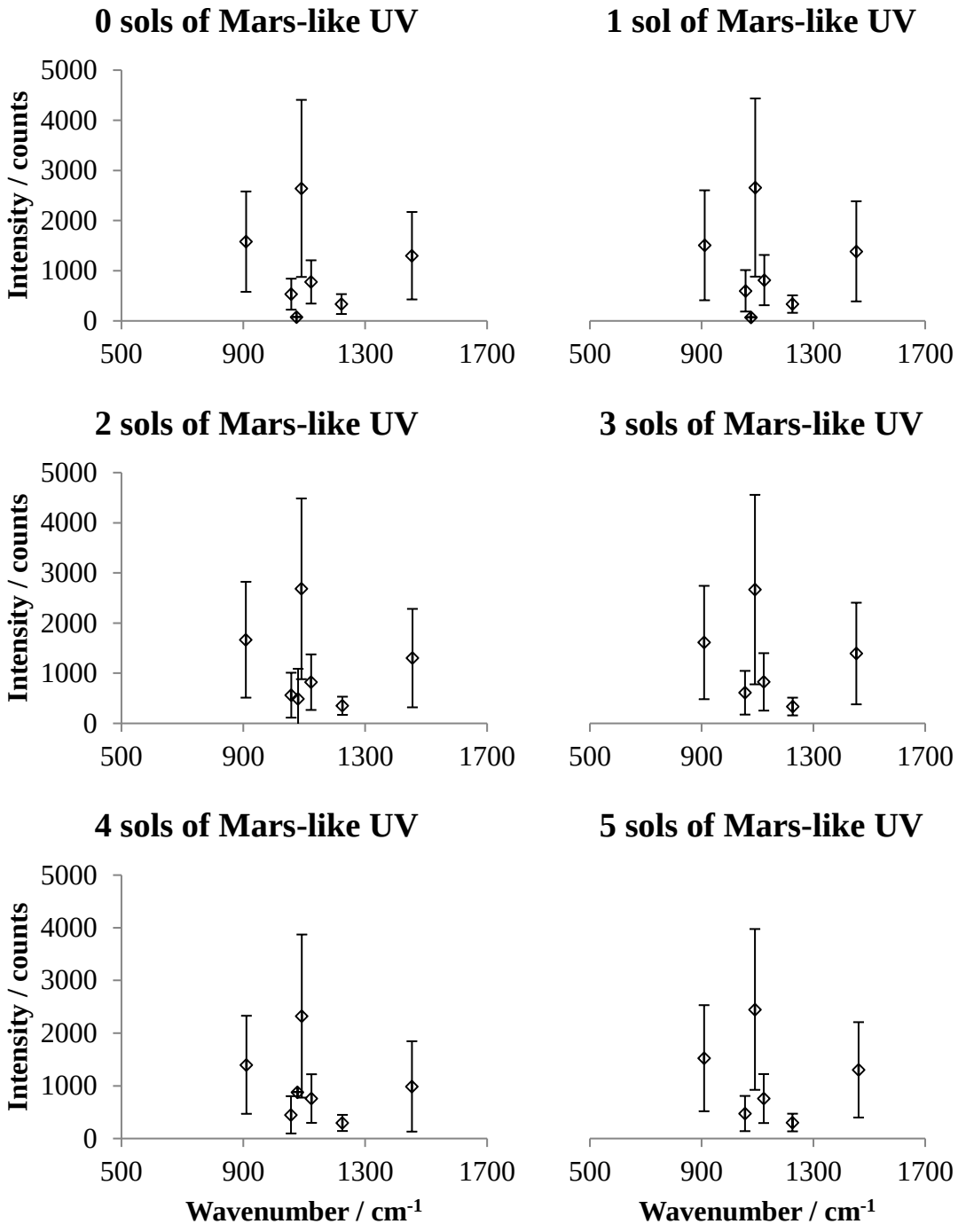

Figure 4-19: The average intensity of the characteristic bands for glutamine for each sol of simulated UV exposure. The error bars represent one standard deviation.

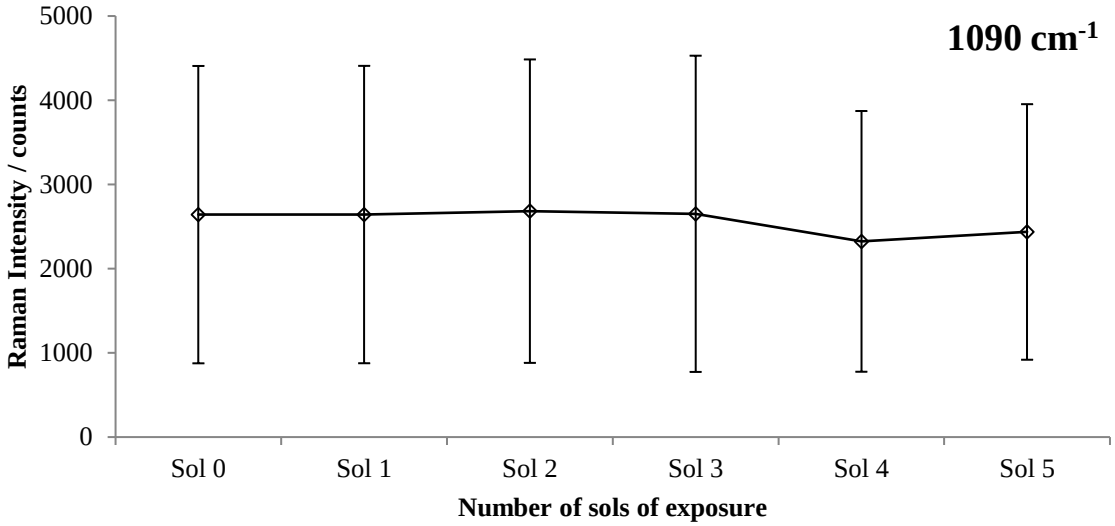

Figure 4-20: The Raman intensity of the strongest characteristic band for glutamine at 1090 cm^{-1} for each sol equivalent dose of exposure to UV radiation. The error bars represent one standard deviation.

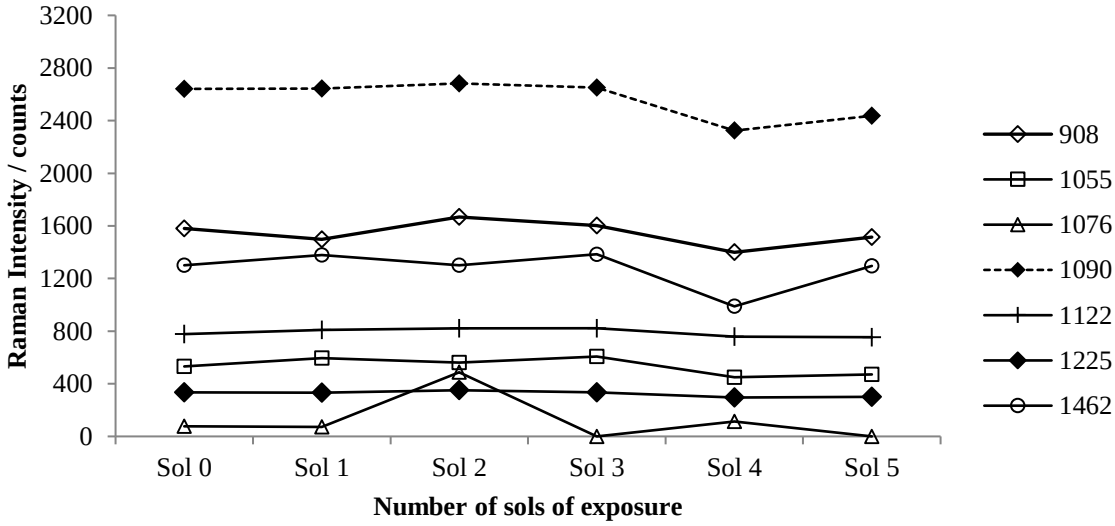

Figure 4-21: The Raman intensity of the other characteristic bands of glutamine for each of the sol equivalent dose of exposure to UV radiation. The dashed line shows the strongest characteristic band.

The intensity of the bands of glycine remained almost identical throughout the exposure to UV radiation, seen in Figure 4-22. The absolute intensity fluctuated slightly for the duration of the experiment, but the trend was relatively flat and within error, shown in Figure 4-23; this was also true for the intensities of the other characteristic bands associated with glycine, shown in Figure 4-24.

Overall, there was not a conclusive trend seen for all of the amino acids when exposed to simulated martian UV radiation; some of the amino acids appeared to survive relatively unaltered as a result of the exposure (glutamine and glycine), some showed minor but inconclusive changes (alanine and aspartic acid) and one was detrimentally affected (cysteine), with further exposure likely to continue to affect the molecular structure.

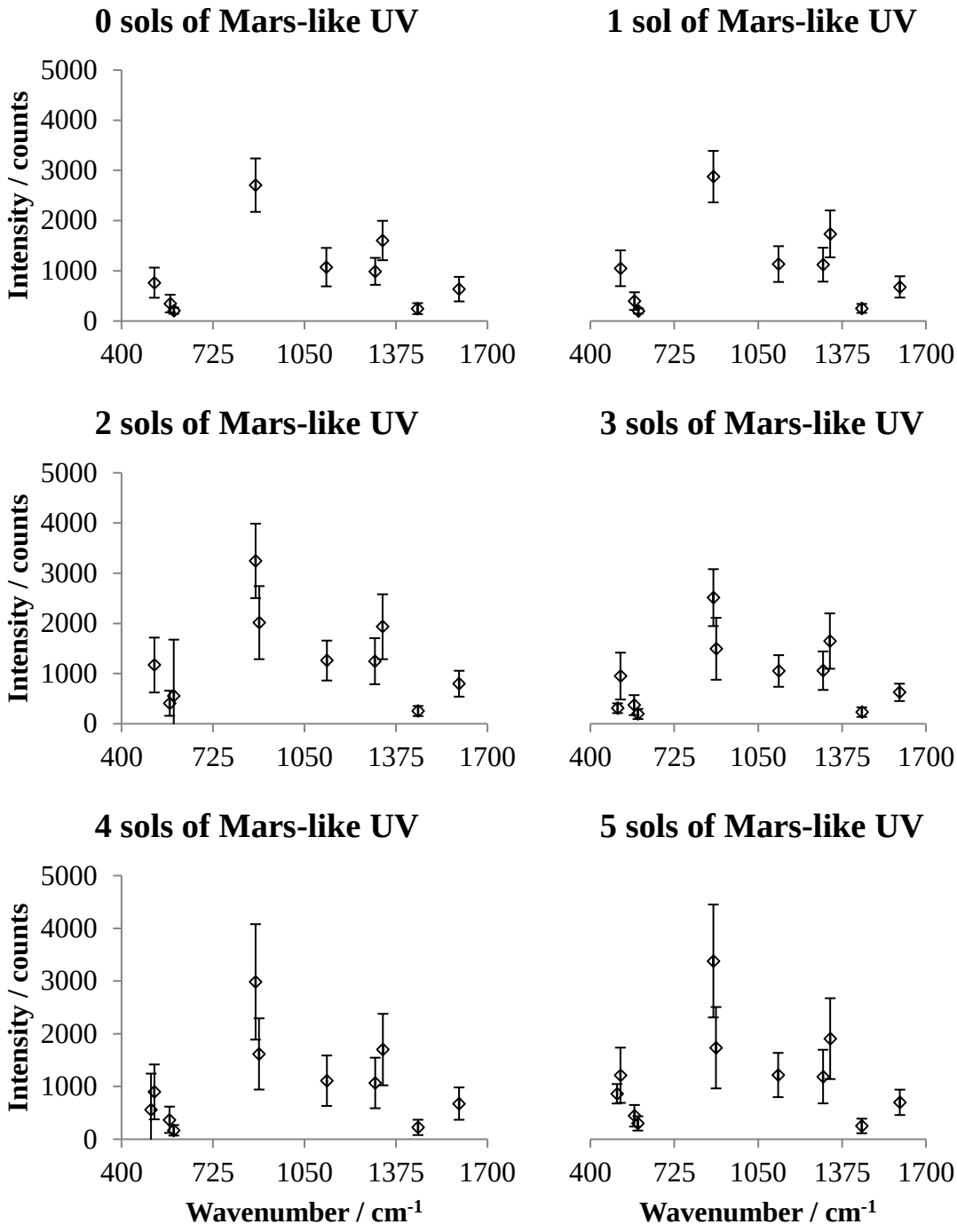

Figure 4-22: The average intensity of the characteristic bands for glycine for each sol of simulated UV exposure. The error bars represent one standard deviation.

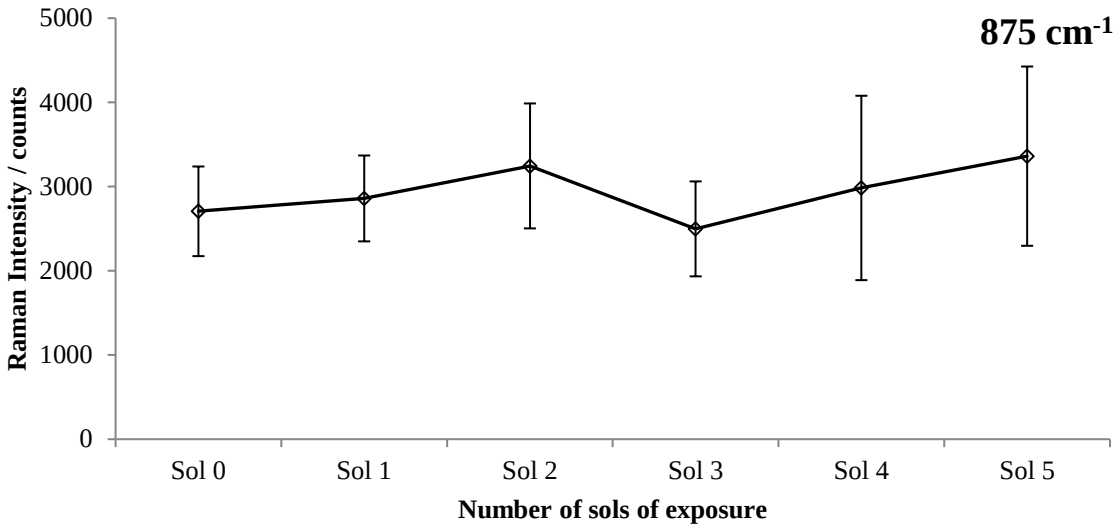

Figure 4-23: The Raman intensity of the strongest characteristic band for glycine at 875 cm^{-1} for each sol equivalent dose of exposure to UV radiation. The error bars represent one standard deviation.

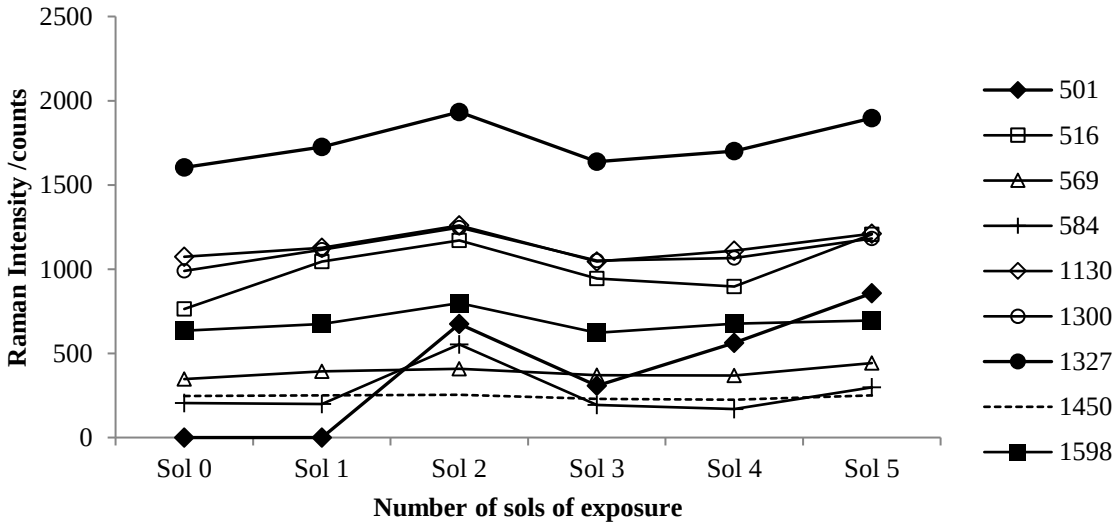

Figure 4-24: The Raman intensity of the other characteristic bands of glycine for each sol equivalent dose of exposure to UV radiation.

4.2.5 Martian analogue regoliths

The martian surface is composed of many different minerals. Though there have been robotic missions to Mars, any regolith that has been sampled by these missions only represents a minute percentage of the surface. Measurements have also been acquired from orbit, giving a wider understanding of the surface composition. To study the surface of Mars from Earth, terrestrial regolith of a similar composition can be used as an analogue for martian simulations.

The previous experiments have analysed the effects of simulated martian conditions on amino acids when placed on a glass base. The experiments presented in this section doped analogue regoliths with amino acids to perform a more complete martian simulation. Martian analogues are described in more detail in Section 2.3.4. Figure 4-25 shows microscope images, taken with the microscope camera on the Raman spectrometer, of the mineral hematite and two martian analogues, JSC Mars-1 and Salten Skov. The images show that the samples were not flat, that the areas chosen for Raman spectroscopy were difficult to select. Another martian analogue was used in this work was an unaltered basalt from Skye, UK, to be described in Section 4.2.5.1.

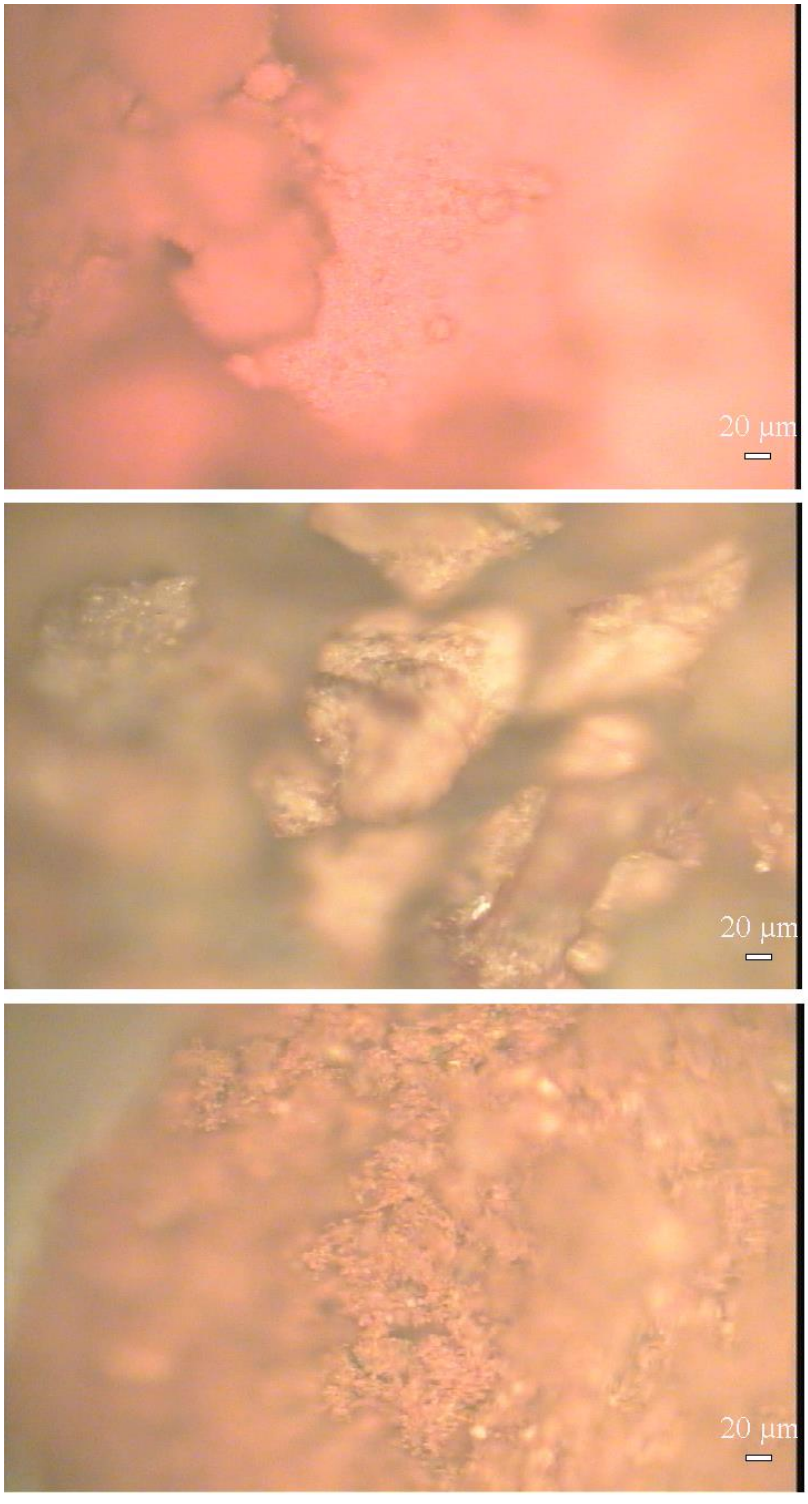

Figure 4-25: Microscope images (× 10 lens) of grains of (a) hematite, (b) JSC Mars-1 and (c) Salten Skov using the Raman spectrometer microscope camera. These are typical of the areas used to collect Raman spectra.

Figure 4-26 shows typical Raman spectra of martian analogue regoliths; JSC Mars-1, Salten Skov and pure hematite. JSC Mars-1 was planned for extensive use throughout this project (as a substrate for biomarkers to be exposed to simulated martian conditions) as a large quantity was readily available and it is spectrally similar to the bright regions on the surface of Mars in the infrared (IR) (Allen *et al.*, 1998). Nonetheless, it was determined that JSC Mars-1 was a poor analogue for use in experiments with Raman spectroscopy as the main analytical tool. As seen in Figure 4-26, a spectrum consisting of an average of three 5 s measurements created a highly fluorescent spectrum with no discernible features that would define the sample as JSC Mars-1. Amino acid samples required at least 20 s exposure times to obtain a good signal to noise ratio with bands suitable for analysis; spectra of JSC Mars-1 obtained for longer than 5 s led to over-exposure of the CCD because of fluorescence (*i.e.*64565 counts), so would have been impractical as a substrate for amino acid doping and simulated martian environment exposure. Furthermore, as no Raman spectra of JSC Mars-1 have been presented in the literature, this is the first report of its Raman signature.

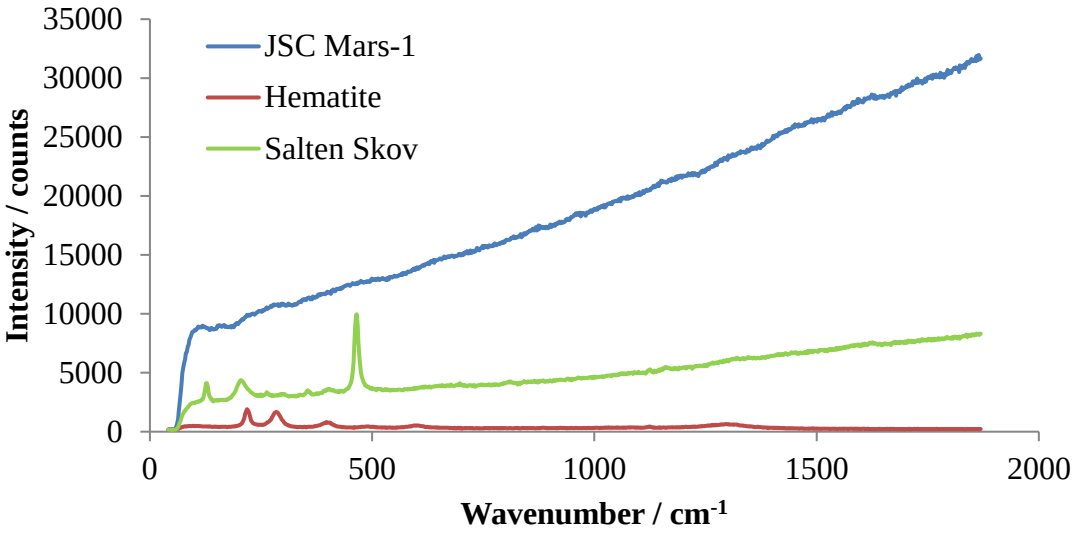

Figure 4-26: Typical Raman spectra of three martian analogue regolith samples.

Powdered samples of hematite and Salten Skov were tested to compare the Raman spectra of other regolith simulants; both returned fairly featureless, but unique Raman spectra with three or four defining bands denoting each sample. Salten Skov is meant for use as a dust simulant and not as a regolith simulant (Seiferlin *et al.*, 2008) and the hematite, though it produced a usable signature (where, if doped with amino acids, the bands would likely be distinguishable), was also a borrowed sample that was ground to a very fine grain size for use as a dust simulant. Following the result of the Raman spectra of JSC Mars-1, a different sample, an unaltered basalt, was sourced for use in regolith doping experiments.

4.2.5.1 Unaltered basalt from Skye, UK

To conduct some exposure experiments with an analogue martian regolith, a sample of unaltered basalt was obtained that had been previously collected from Skye, Scotland, UK for use on OU courses S260/276, which could be an analogue for the unaltered basalt environment on Mars. There were no known records of the mineralogy of the sample, so to understand the minerals that the sample was comprised of and confirm that it was a basalt, Raman spectroscopy, SEM and X-ray diffraction (XRD) analysis of the sample was performed. Figure 4-27 shows a typical area of the basalt sample used to collect Raman spectra, shown in Figure 4-28, which shows baseline corrected data; however, the raw data showed fluorescence and other noise included in the intensity of the unique bands of various minerals that are contained in the sample. The Raman spectra were an average of a 16 point map, where each spectral point is comprised of three 15 s acquisitions. At individual points, some of the Raman bands were stronger and some were weaker, or not present, depending on the mineral that was present at each map point. The major bands are at 178, 372, 518, 671, 876 and 1013 cm^{-1}.

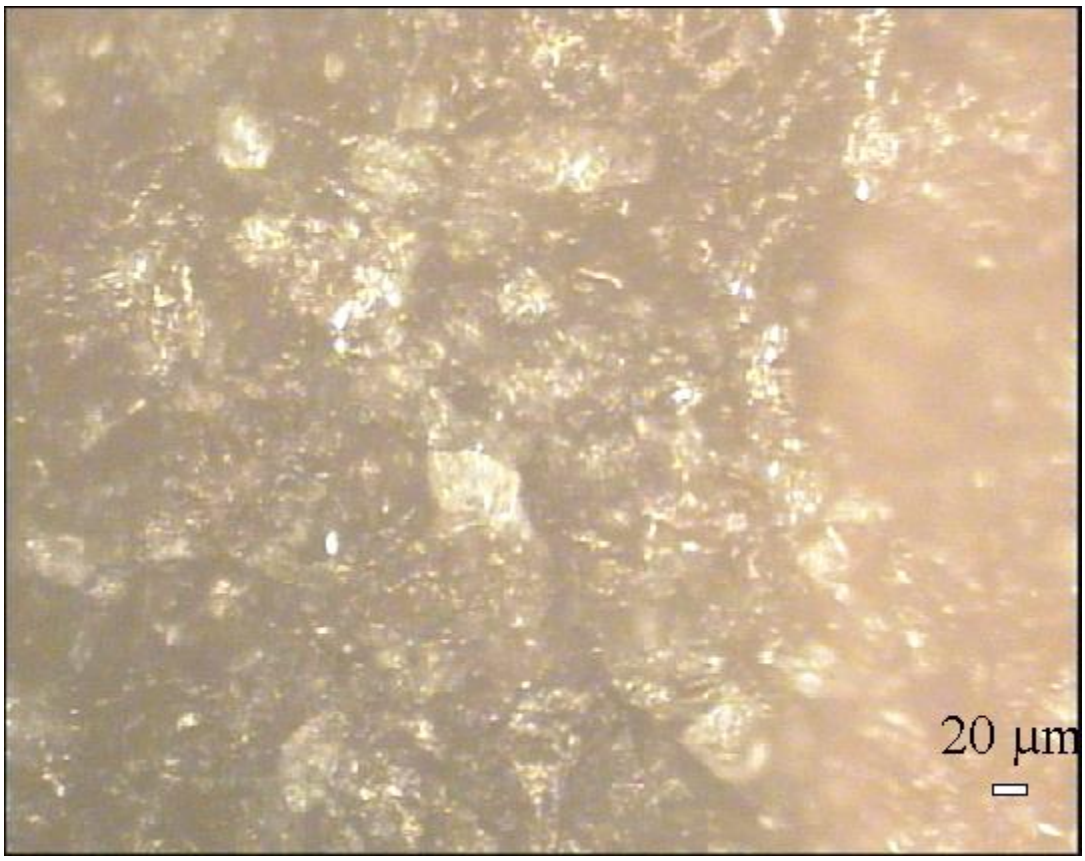

Figure 4-27: Microscope image (× 10 lens) of a chip of the basalt sample using the Raman spectrometer microscope camera. This is typical of the areas used to collect Raman spectra.

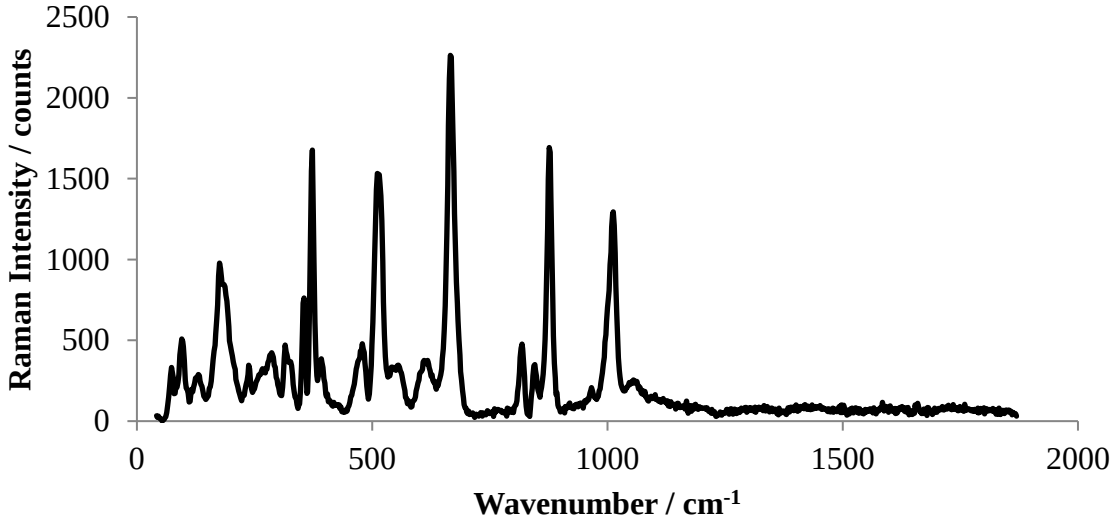

Figure 4-28: A typical Raman spectrum (average of a 16 point map) of the basalt used for a martian analogue.

Element analysis was performed using SEM, as described in Section 2.6. Figure 4-29 shows one of several areas that were imaged, all of which were similar to that seen in the figure displayed here. The major elements recorded in the sum spectrum of that area were silicon, magnesium, aluminium and calcium, shown in Figure 4-30. A small area was explored in greater detail, shown in Figure 4-31, where three point spectra were acquired for each varying but distinguished grey-scale area. Figure 4-32 shows the element data acquired at each of these points, A, B and C. Point A is dominated by silicon and secondly, relatively equally comprises of oxygen, magnesium and calcium, with smaller amounts of titanium and iron, and a few other trace elements. The majority of point B comprises of silicon and aluminium, followed by oxygen and iron, with smaller amounts of calcium, sodium and potassium. Finally, point C is dominated by titanium, followed by iron, manganese and oxygen, with some trace elements, such as cobalt.

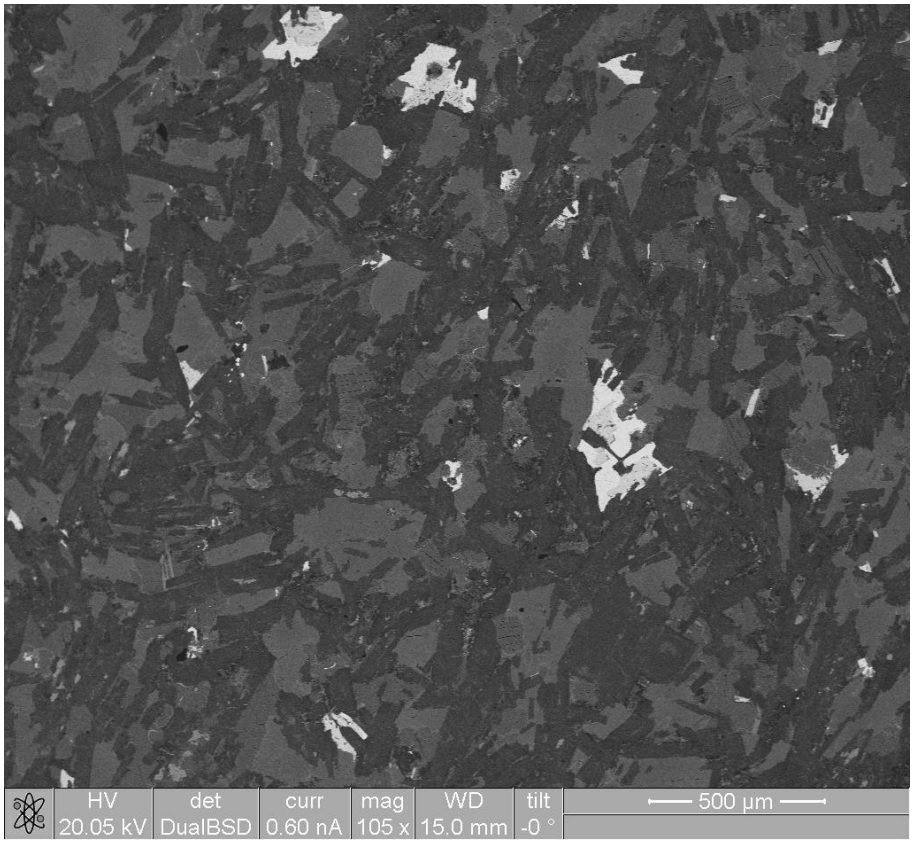

Figure 4-29: an area of the basalt sample imaged using SEM.

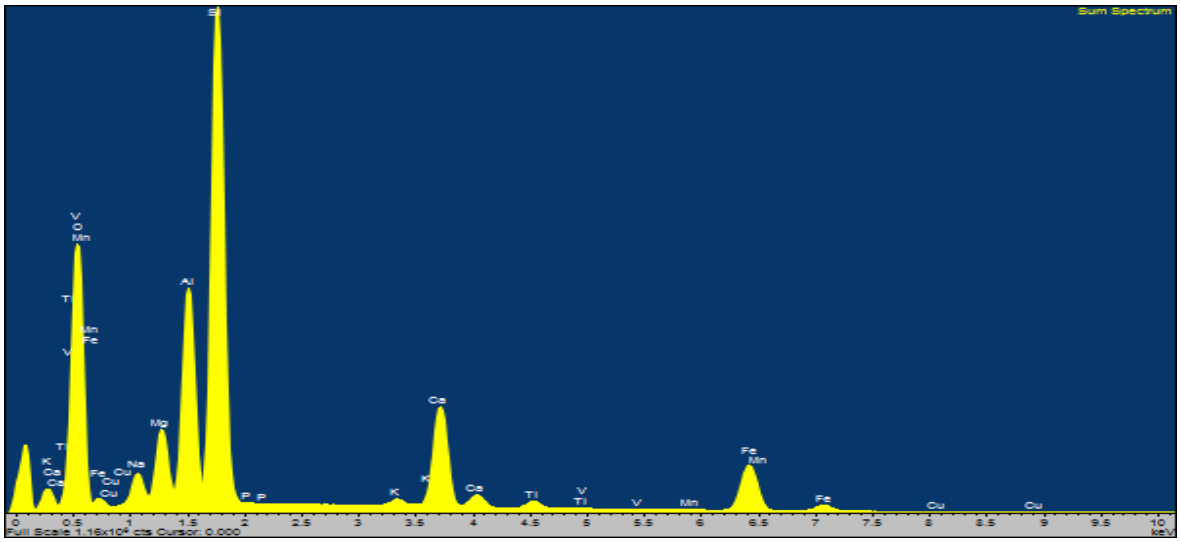

Figure 4-30: The sum spectrum of the area imaged in Figure 4-29. Major elements include silicon, magnesium, aluminium and calcium.

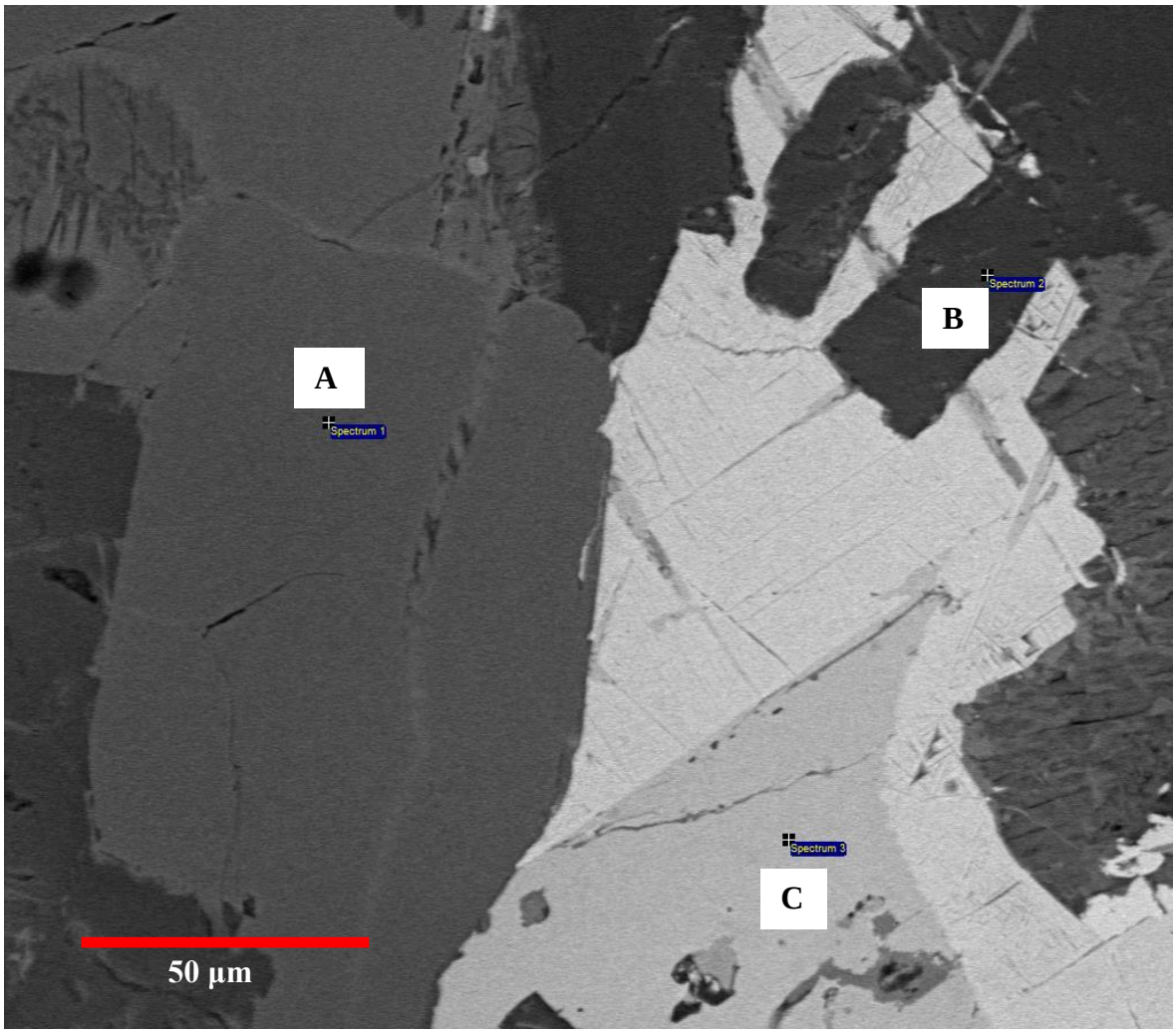

Figure 4-31: An enhanced area of the image shown in Figure 4-29, with three points where element spectra were acquired at A, B and C. The red line shows the scale of approximately 50 µm.

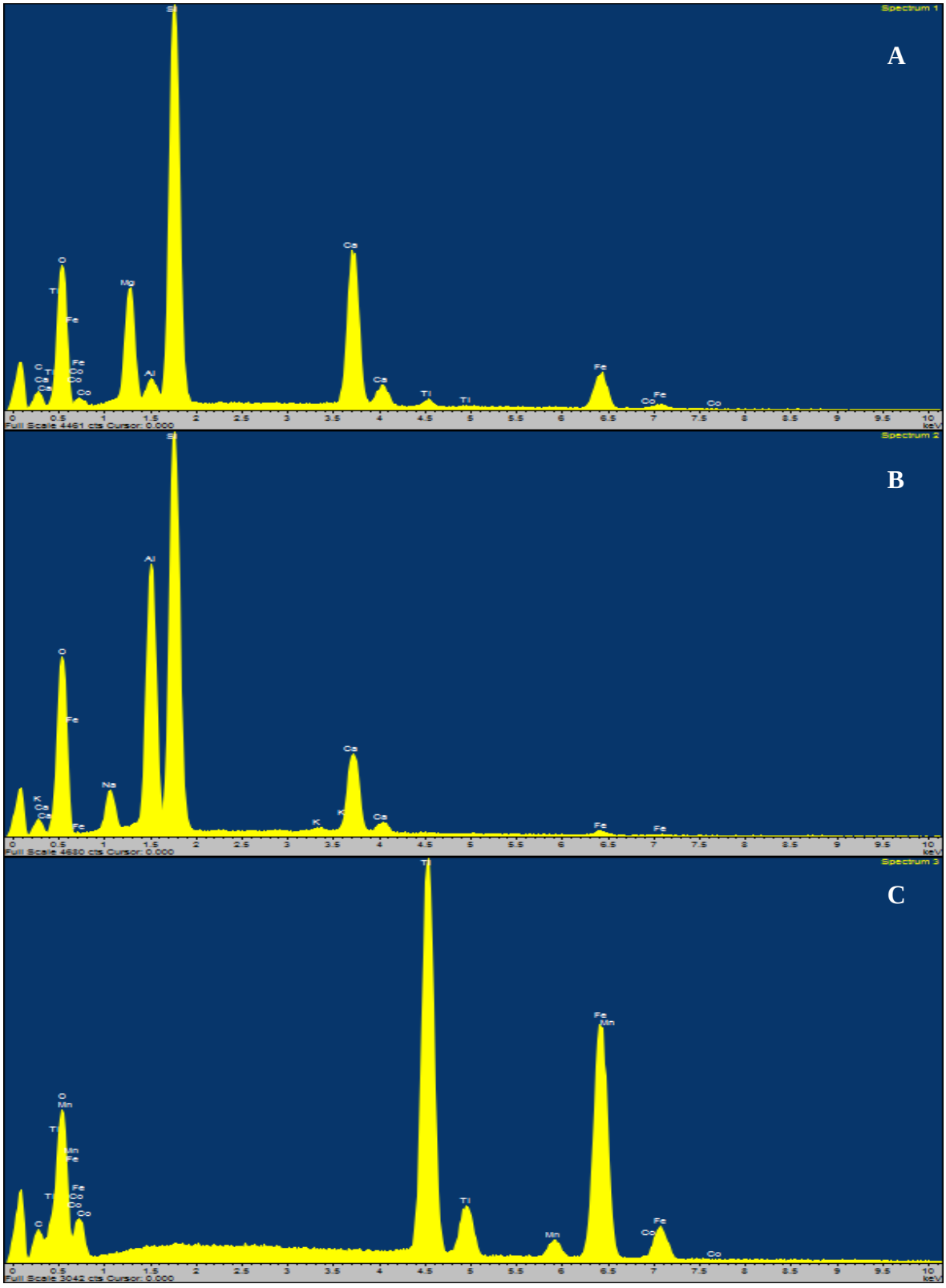

Figure 4-32: The spectra of the sample at the points A, B and C denoted in Figure 4-31.

For completeness, a sample of the basalt was sent for XRD analysis by Paul Schofield at the Natural History Museum, London, UK. The resulting spectrum is shown in Figure 4-33. The sample was confirmed as basalt with the following main phases identified (in no particular order): plagioclase, augite, amphibole (hornblende/richterite), +/− enstatite. Alteration products were also identified: clinochlore/chlorite, montmorillonite/smectite and talc.

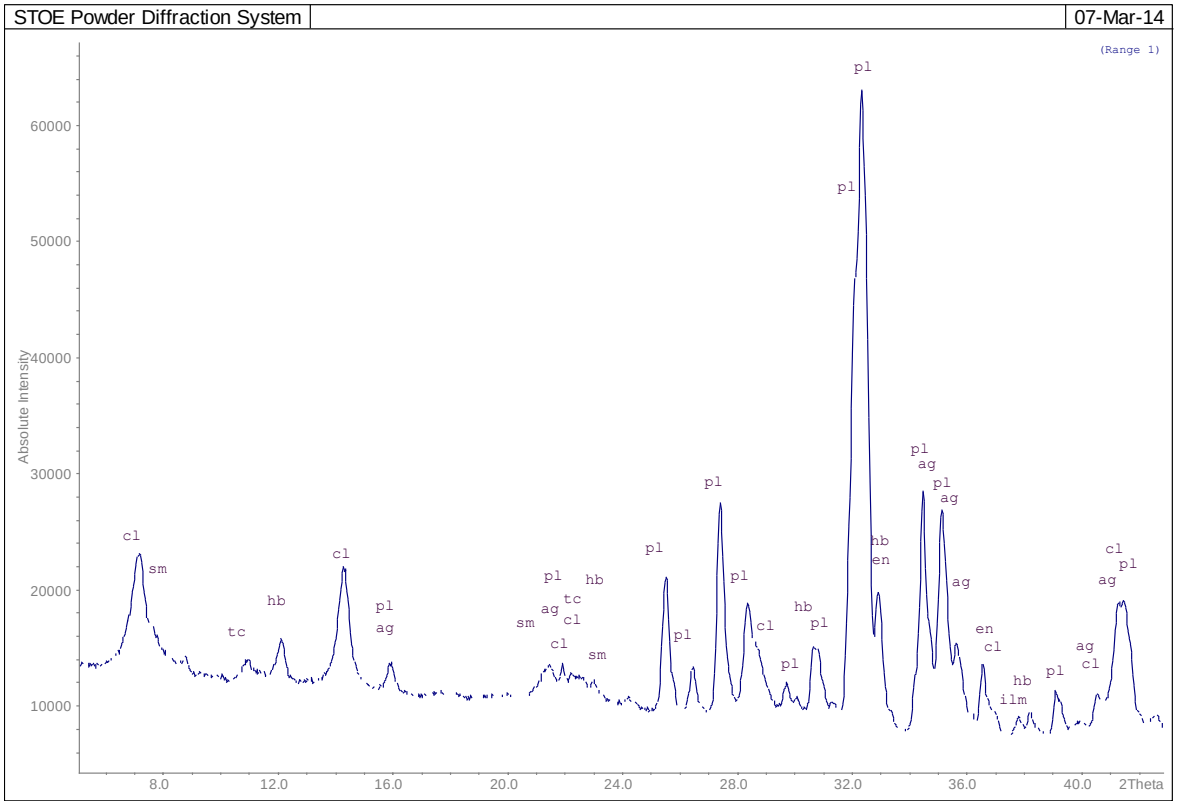

Figure 4-33: The XRD spectrum of the basalt from Skye, UK used an analogue martian substrate. The key for the peak labels are as follows: pl = plagioclase, hb = hornblende, cl = clinochlore/chlorite, tc = talc, sm = smectite/montmorillonite, ag = augite, en = enstatite and ilm = ilmenite.

4.2.5.2 Exposure of amino acid doped analogue regolith to simulated martian conditions

4.2.5.2.1 Pre-exposure examination of amino acid characteristic bands

Following the exposure to UV radiation on glass as described in Section 4.2.4, amino acids samples (same volume as used in the glass based experiments described above) were dried on the surface of approximately 1 cm^3 chips of the basalt, shown in Figure 4-34. Before the exposure, Raman spectra were acquired and analysed for which characteristic bands, determined in Chapter 3, were observable once the amino acids had been doped onto the basalt sample. The observed characteristic bands are reported in Table 4-1. The percentage of the characteristic bands that remained observable on the doped basalt were 44 % (alanine), 0 % (25) (aspartic acid), 33 % (44) (cysteine), 64 % (glutamine) and 53 % (glycine), where the bracketed values is the percentage if inconclusively observed bands are included.

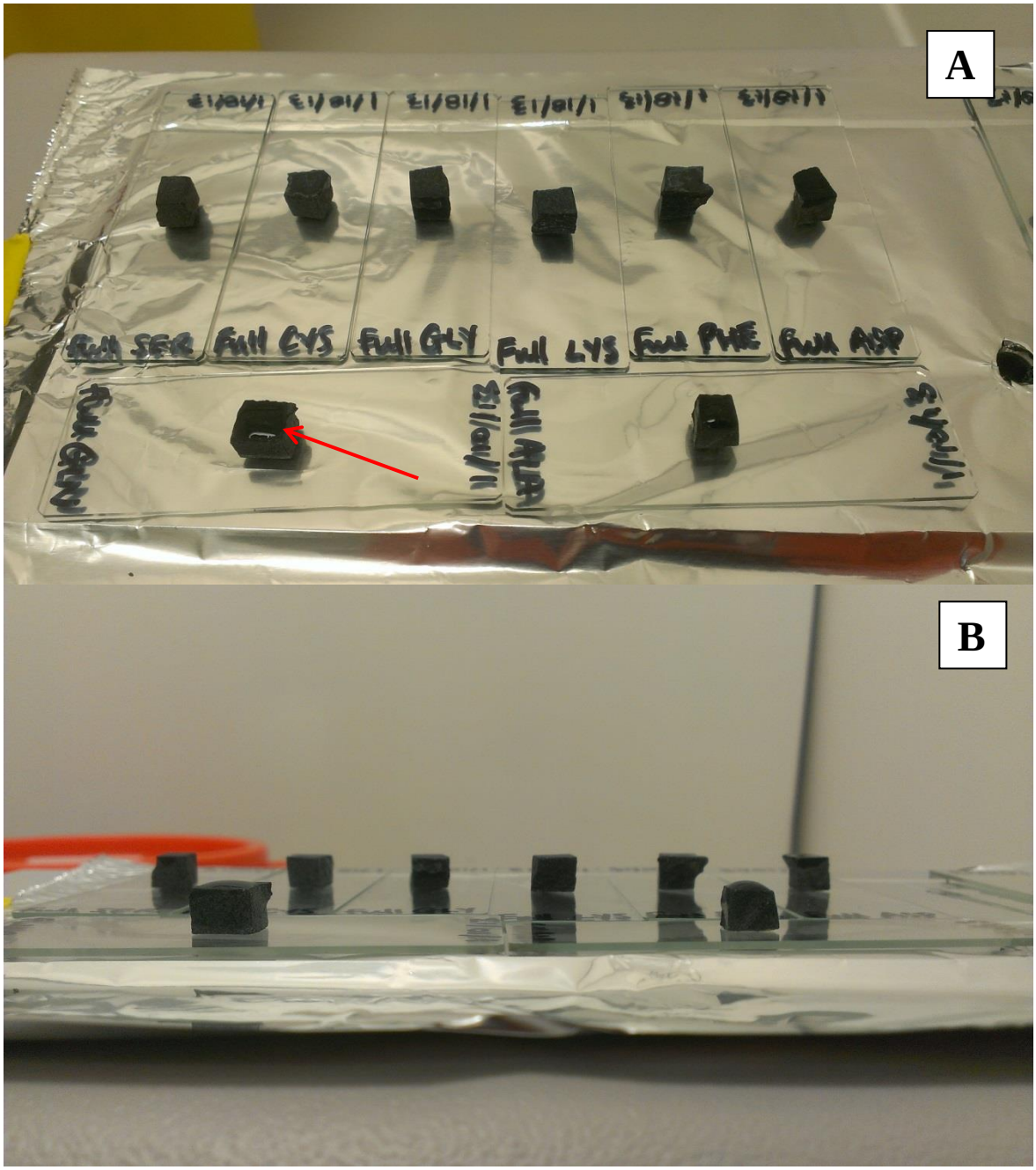

Figure 4-34: (A) shows the surface of the basalt chips to which the amino acid samples were administered. An arrow points to an example of the liquid phase of a sample before it had been left to dry overnight. (B) shows a side on view of the chip samples to show the shape.

Alanine Band / cm^{-1}	Obs.?	Aspartic Acid Band / cm^{-1}	Obs.?	Cysteine Band / cm^{-1}	Obs.?	Glutamine Band / cm^{-1}	Obs.?	Glycine Band / cm^{-1}	Obs.?
71	-	84	?	68	-	96	-	73	-
91	-	551	-	131	-	**112**	Y	137	-
124	-	778	-	608	Y	**122**	-	167	-
333	-	872	?	**679**	?	174	-	501	-
760	Y	**938**	-	762	Y	409	Y	516	-
832	Y	1336	-	866	-	1055	Y	569	Y
919	Y	1360	-	933	-	1076	-	584	-
995	-	1408	-	1202	Y	**1090**	Y	860	Y
1114	Y			1220	-	1122	Y	**875**	Y
						1462	Y	888	Y
						1732	Y	1130	Y
								1300	Y
								1327	Y
								1450	Y
								1598	-
% Obs.	44		0 (25)		33 (44)		64		53

Table 4-1: Indication of whether the characteristic bands of the amino acids were observed (obs.?) in amino acid doped basalt samples (chip). The strongest bands for each amino acid are highlighted in bold. Bands that were observed are marked 'Y', unobserved '-' and inconclusive '?'. The final row displays the percentage of the characteristic bands that were observed (plus inconclusive).

4.2.5.2.2 Mars-like environment simulation exposure

Once dried overnight, the samples were exposed to a Mars-like surface environment; using MSC *Bernard*, the samples experienced Mars-like atmospheric composition, pressure, temperature (using a bed of CO_2 ice) and UV radiation. As the results of the exposures to the UV lamp (Section 4.2.4) had shown an insignificant effect before four sol equivalent doses of exposure, the samples were exposed to four consecutive sols of UV radiation (84 min real time for Xe lamp output). Furthermore, this was approximately the limit of the CO_2 ice as it had mostly sublimated after this length of exposure.

The pressure was 8.0 ± 0.5 mbar, regulated by the automated vacuum system, which would have otherwise increased as the CO_2 ice sublimated and moreover, allowing the CO_2 ice to sublimate unchecked could have caused increased pressure within the chamber, with potentially unsafe consequences.

The resulting Raman spectra of the pre- and post-exposure are displayed in Figure 4-35. The Raman intensity was normalised to the band found in the basalt sample at approximately 518 cm^{-1} (*i.e.* the intensity of this band was set to 1), as the band was observed consistently in all the samples; it was not always the strongest band but had an approximate medium to strong intensity, it did not appear to deteriorate because of the UV exposure. The control sample (Figure 4-35a) showed a maximum of approximately 20 % degradation in one of the bands (671 cm^{-1}) and minimal relative difference in the other bands.

Note that the images of the samples during exposure were examined for any possible incorrect dose because of the non-uniform UV output of the lamp (described in Sections 2.3.3 and 4.2.4), but none were deemed to have been incorrectly exposed.

For the alanine/basalt sample (Figure 4-35b) four of the characteristic bands determined in Chapter 3 were observed in the pre-exposure spectra (indicated by the blue arrows: 760, 832, 919 and 1114 cm^{-1}), but were greatly reduced in the post-exposure and if it were an unknown sample, would not be detected. The sample of aspartic acid does not have any easily recognisable bands that are consistent with the characteristic bands previously categorised. The two arrows show possible tenuous bands that could be as a result of the aspartic acid sample on the basalt, though the first one (84 cm^{-1}) was overlapped by a band that is also observed in the basalt sample and the second (872 cm^{-1}) was very weak in this spectrum and was classified as a medium band in Chapter 3; hence, it was unusual that

there is no evidence of the strongest band for aspartic acid at 938 cm^{-1}. It was possible to observe some of the characteristic bands in the cysteine sample, though the strongest intensity band for cysteine (679 cm^{-1}) was overlaid by the band from the basalt sample seen at 671 cm^{-1} in the control sample. The other characteristic bands observed were 608, 762 and 1202 cm^{-1}. When the chamber was opened post-exposure, there was a noticeable sulphurous smell as had previously been observed in previous UV radiation exposures (Section 4.2.4). The band at 678 cm^{-1} was degraded by approximately 60 %. Due the data displayed here being an average of 16 point spectral map, there was some fluorescence that occurred post-exposure seen here between 1140 and 1660 cm^{-1}, but it was not present in all 16 spectral points; furthermore some of the spectral points had so much fluorescence that the CCD became overexposed from 1140 $cm^{-1}$and above. As all but the strongest characteristic band for cysteine are classified as weak or very weak and with the unfortunate overlapping of the band from this basalt sample at the position of the strongest characteristic band, cysteine would be very difficult to identify in an unknown sample of basalt (previously stated in Chapter 3). For glutamine, the characteristic bands that were identifiable from the basalt bands were 112, 409, 1055, 1090, 1122, 1462 and 1732 cm^{-1}. The normalised Raman intensity remained stable, except for a dramatic increase in intensity at approximately 112 cm^{-1} post-exposure. The characteristic bands that were observed on the glycine/basalt sample were 569, 860, 875, 888, 1130, 1300, 1327 and 1450 cm^{-1}. The strongest characteristic band at 875 cm^{-1} was approximately 60 % relative Raman intensity compared to the major basalt bands and the bands appeared to decrease in relative intensity, post-exposure. Nonetheless, the bands were still observable, and could likely be identified if this were an unknown sample.

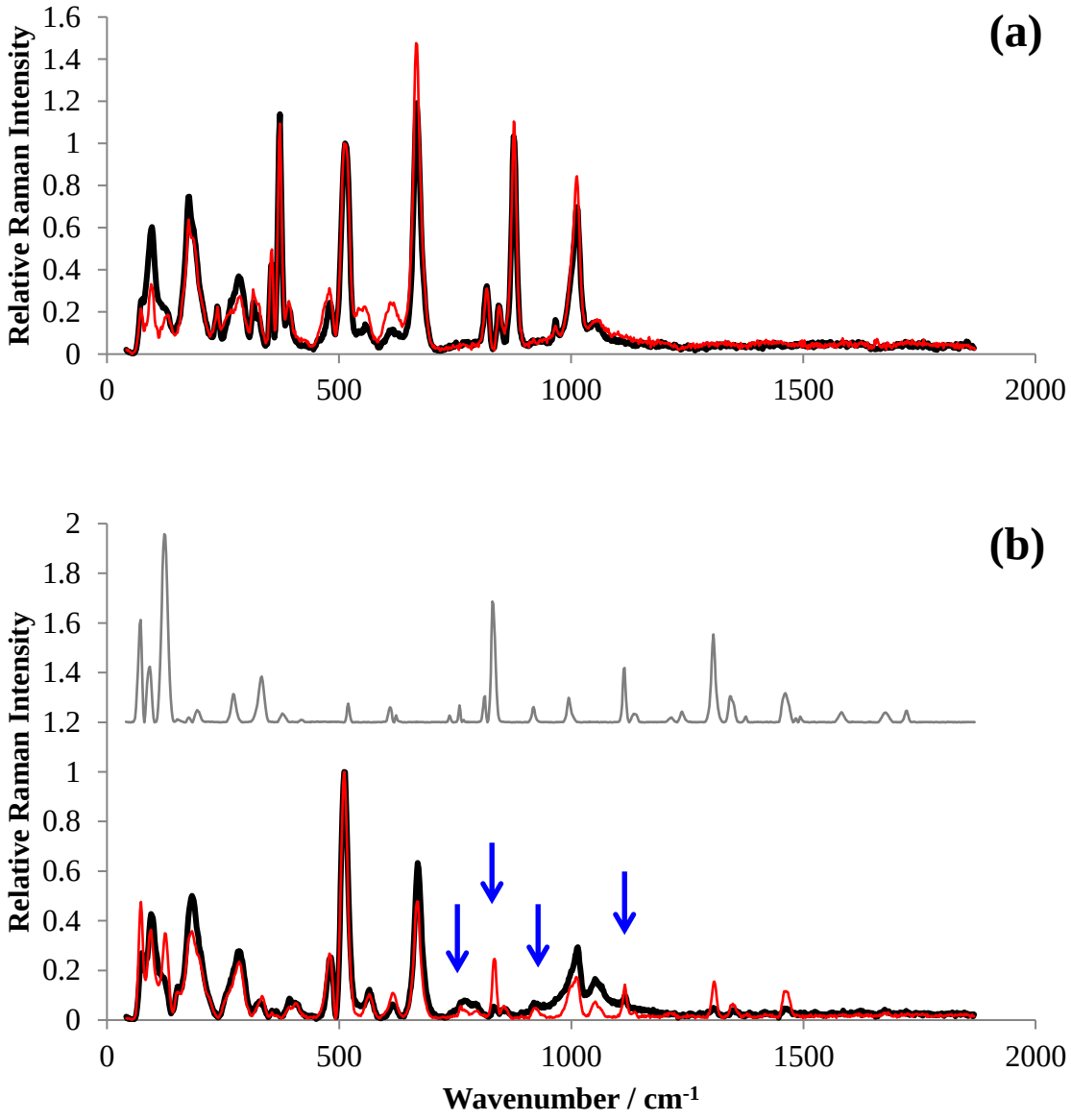

Figure 4-35: The pre- and post-exposure Raman spectra of the amino acid doped basalt chips (a) control (no amino acid), (b) alanine, (c) aspartic acid, (d) cysteine, (e) glutamine and (f) glycine (average of 16 spectra); samples were exposed to a Mars-like UV radiation, atmospheric composition, pressure and temperature. The red line is the pre-exposure spectrum and the black line is the post-exposure spectrum. The blue arrows indicate any bands that are characteristic to the amino acids observed in the sample.

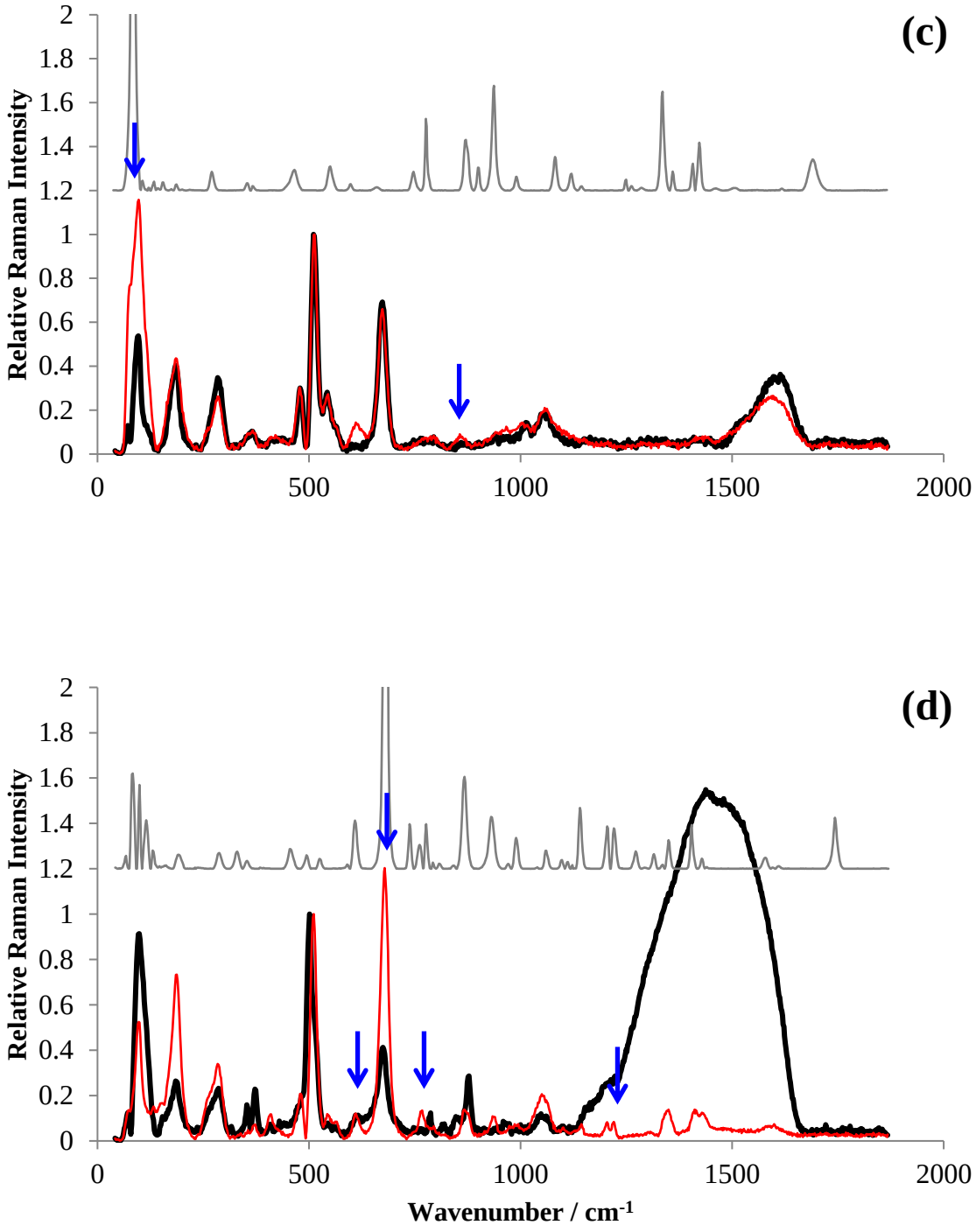

Figure 4-35 (cont.).

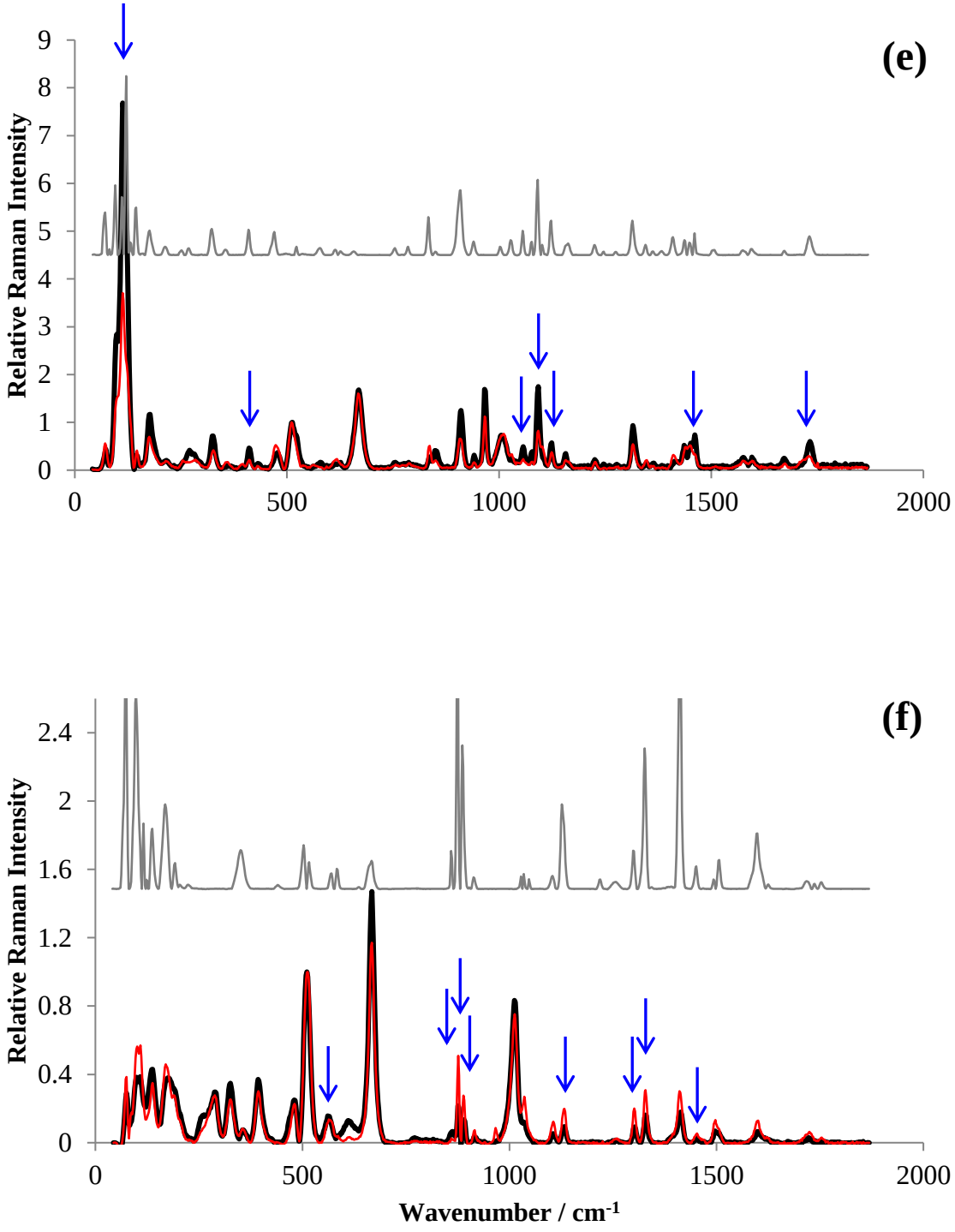

Figure 4-35 (cont.).

4.2.5.2.3 Powdered regolith samples

The *ExoMars* rover will powder samples that it collects to grain sizes in the range of 20 to 200 μm before it takes Raman spectra (Edwards *et al.*, 2012a). To replicate this, the basalt sample was crushed to a powder, doped with amino acids and Raman spectra were acquired. The powdered sample was prepared with the assistance of Marc Davies at the Open University. Chips of the sample were placed in an agate tema mill for approximately 10 min to reduce the sample to a fine powder. The mill was cleaned before and afterwards to minimise contamination, of this sample and for future users, by rinsing all the parts with hot water, which were left to partially dry before wiping with acetone and dried with compressed air. The mill was loaded with pure silica sand and run for five minutes before being washed again with hot water, acetone and compressed air.

When taking Raman spectra, the sample was used as a mixture of grain sizes as the *ExoMars* rover will not sieve for a certain grain size, but a portion of the sample was sieved here to determine the range of grain size. The sieves were rinsed with 15.2 Ω water from the back to reduce contamination and sonicated for 15 min before being placed in a drying cabinet. Once dry, the sample was put through the sieves, with mesh gradations of 10, 20, 40, 53, 63, 106 and 150 μm. The majority of the sample was in the range of 53 to 63 μm, with only approximately 10 % outside of this range (10 to < 53 μm and > 63 to 150 μm), shown in Figure 4-36.

Figure 4-36: An example of the powdered basalt (shown in the smaller and larger fractions, but these were mixed when used in the experiments).

Samples of 0.1 g of the powdered basalt were weighed out on glass slides and the samples were doped with 100 μl of the liquid amino acid and left to dry overnight. The Raman spectra of the samples before exposure to Mars-like surface environment are shown in Figure 4-37.

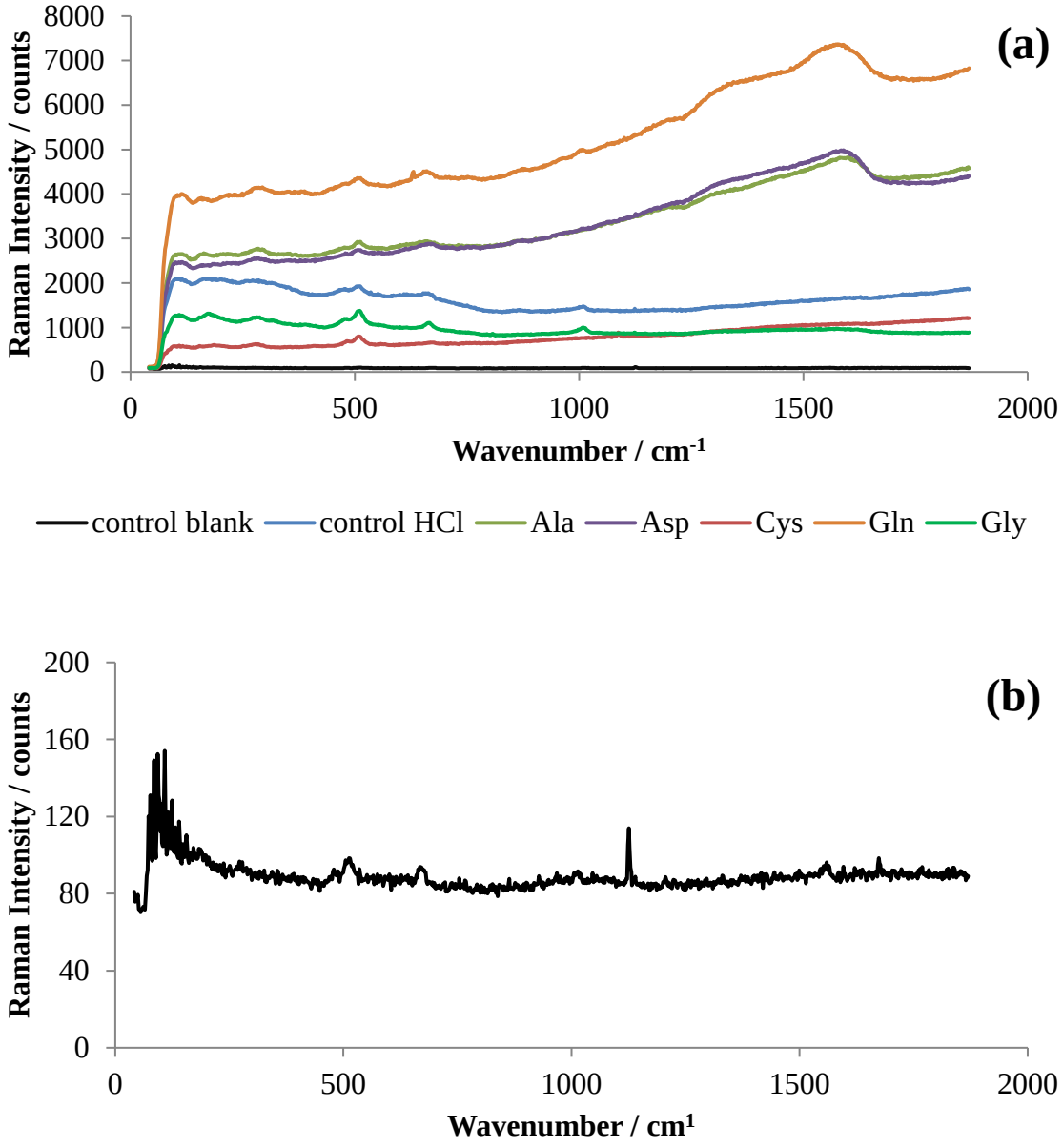

Figure 4-37: (a) The Raman spectra of powdered basalt samples doped with amino acids. (b) the 'control blank' sample spectra in detail. Small features at about 500 and 660 cm^{-1} are recorded in all the spectra.

The amino acids were dissolved in 0.1 % HCl and hence were doped onto the powdered basalt in liquid form, two control samples were examined, one of pure powdered basalt and one with the addition of 100 μl of 0.1 % HCl, to ensure there were no features that were because of the HCl, which there were not. The blank control sample (black line) appears to be featureless in the Figure 4-37 (a), but when plotted individually small features seen in the other Raman spectra are distinguishable in Figure 4-37 (b). The major features are at 285, 475, 509, 662, 1009 and 1580 cm^{-1}. The Raman spectra of the powdered sample has lost the defined bands of the 'chip' spectra and showed no evidence of the amino acid bands. All the features are broad; though the feature at 475 cm^{-1} could be the shoulder feature seen in the 'chip' spectra at the same position and the 509 cm^{-1} feature here, the 518 cm^{-1} band. The broad features at approximately 662 and 1009 cm^{-1} in the powdered sample could be related to the 671 and 1013 cm^{-1} 'chip' bands. The very broad feature peaking at 1580 cm^{-1} in the powdered sample could be a carbon G band (Matthews *et al.*, 1999) (defined in Section 3.4.3), it was seen as a small feature in the basalt chip, but in the powdered sample it is quite dominate in the higher wavenumber range.

4.3 Discussion

4.3.1 Exposure of amino acids to isolated Mars-like atmospheric composition, pressure and temperature (preliminary tests)

The results of the preliminary individual environmental factor tests showed that, generally, there were some minor, but not significant, changes to the intensity of the Raman bands post-exposure. On average, the greatest relative Raman intensity difference was approximately 18 % or one fifth. Therefore, in coupled experiments, the change in the spectra because of a Mars-like atmospheric composition or pressure would be expected to be no more than one fifth. If the samples exposed to a Mars-like atmospheric composition or pressure were unknown samples, they would still be distinguishable using standard identification molecule processes aided using the characteristic bands defined in Chapter 3. One major change in the spectra occurred to cysteine during exposure to a Mars-like pressure, where the formation of a new band at 500 cm^{-1} was observed. The changes in the bonds in cysteine because of high pressure (> 1×10^6 mbar) have been studied by, for example, Moggach *et al.* (2006) and Minkov *et al.* (2008) where the crystal phase has changed as a result of the compression and decompression of the molecule. Nonetheless, even though it was a Mars-like pressure, some terrestrial atmosphere was still available, so oxidation may have occurred independent of the pressure change. Future work would include using an inert atmospheric composition (*e.g.* argon) at Mars-like pressure to investigate whether the pressure was a contributing factor in the appearance of the 500 cm^{-1} band.

The samples that were exposed to a constant cold temperature environment (−18 °C) appeared to show larger changes in the wavenumber positions between pre- and post-exposure spectra in comparison to the atmospheric composition and pressure tests.

The bands for alanine had a maximum average of 43 % relative percentage difference in the intensities, this is thought to be because of the strongest intensity band at 832 cm^{-1} being recorded as a doublet band in the post-exposure compared to the more regularly measured singlet band (as seen in the pre-exposure spectra). When the spectra were being assessed for the characteristic bands reported in Chapter 3, it was noted that some spectra for alanine showed this doublet, bands at approximately 813 and 834 cm^{-1}. The band at 813 cm^{-1} did not appear in enough spectra to be considered for the categorisation as a characteristic band, but it was not unusual for this band to be observed. It was thought that the recording of the doublet (or not) was because of the resolution of the spectrometer, and perhaps as a combination of the angle at which the crystal was positioned and the read point along the wavenumber scale determined whether the band was recorded as (more commonly) a singlet or (more rarely) a doublet. For comparison, the normalised data were plotted using another characteristic band at 1114 cm^{-1} (where the pre- and post-exposure intensities are equal to 1), which showed there was a bias because of the doublet, shown in Figure 4-38.

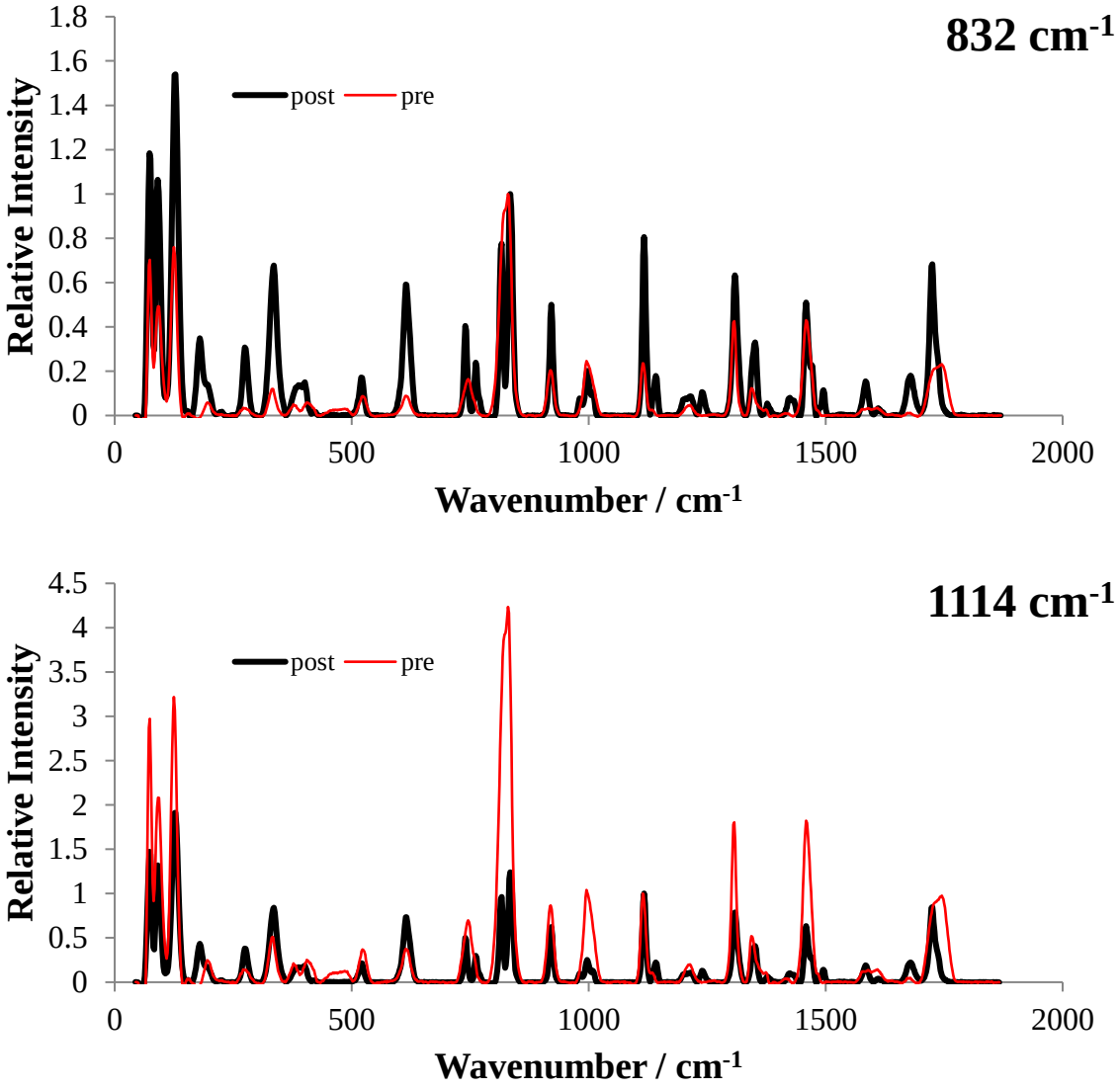

Figure 4-38: The intensities of alanine bands relative (equal to 1) to (a) the strongest intensity band at 832 cm^{-1} (repeated from Section 4.2.2) and (b) another characteristic band, 1114 cm^{-1} to show the relative differences because of the doublet band measured at approximately 832 cm^{-1} in the post-exposure data.

The results for aspartic acid and glutamine were not able to be analysed as the Raman spectra did not match the nominal band positions or shape; *i.e.* it was not that the spectra were, for example, 2 cm^{-1} or more different from the nominal spectra, but the same shape; the band position and shape were entirely different. Aspartic acid and glutamine are hydrophilic molecules and it was thought that because of this that the non-nominal sample could have had a hydrated component, changing the position of the bands because of extra atoms in the molecule. This extreme change in the shape of the Raman spectra because of the positions of the bands would render these amino acids unrecognisable if it was in an unknown sample (if these molecular forms were not catalogued).

4.3.2 Exposure of amino acids to freeze-thaw cycles

The resulting spectra from the samples exposed to a simulated diurnal temperature differential did not show any significant changes to the intensity for any of the amino acid samples. The maximum average percentage difference in the intensity of the bands was approximately 8 % (with the exception of one band with a percentage difference of approximately 17 %). Less than one tenth variation in the intensity of the bands would suggest that the amino acids tested were unaffected by the freeze-thaw cycle over 50 K and remained stable. Furthermore, the intensities remained within the relative percentage difference of one fifth that was established for the upper limit of intensity degradation when exposed to the Mars-like atmospheric composition and pressure. It should be noted that this was a relatively short simulation (especially in comparison to the length of the preliminary atmospheric composition and pressure tests) and it did not reach the minimum temperature seen at the martian surface. The important test during this experiment was the transition between freeze and thaw as previous work has examined amino acids at stable cold temperatures (*e.g.* Murli *et al.*, 2005). The samples were exposed to 90 freeze-thaw

transitions during the cycle. As the molecules were not destroyed, damaged or changed, this has longevity implications for sources of amino acids at or near the surface of Mars for potential pre-existing life to exploit, as well as for the emergence of life in the solar system where temperatures are wide ranging.

4.3.3 Exposure of amino acids to ultraviolet radiation

Overall, the resulting intensities of the characteristic bands of the amino acids after accumulated sol equivalent doses of exposure showed varying differences in each of the samples. The normalised intensity results for alanine are relatively stable but when the absolute intensity was examined some of the bands in the 'fingerprint' region for organic molecules appeared reduced. There are also fewer data points per band as the number of sols increases as a result of the bands becoming undetectable as they reduced in intensity into the noise. This can be understood more readily by examining the raw data. The band intensities plotted in Figure 4-7a are processed data that have had the baseline corrected to remove fluorescence and other noise; however, as the raw data shown in Figure 4-39 demonstrates, the quality of the alanine sample spectra was greatly reduced increasingly over the course of the experiment because of large counts of fluorescence. This was the cause for some of the bands disappearing in the spectra as the samples were exposed to UV for more sols; they are indistinguishable from the noise, though the intensity may also be reduced from the UV exposure. As a result of the shape of the fluorescent signature in the spectra, it caused a false bias that the bands at lower wavenumbers were unaffected or appeared increased in intensity compared to those that were at higher wavenumbers (*i.e.* a false reduction in intensity), whereas this was not the case, the fluorescence simply increased with wavenumber. This contrasted with, for example, the glycine sample, which was remarkably similar before and after UV exposure. It was possible that the band

intensities for alanine would have been stable, like glycine, if the samples were not affected by the fluorescence. Furthermore, the alanine Raman intensity counts were, at a maximum, about 2000 counts, which was not ideal; hence, weaker bands, such as the band at 919 cm^{-1}, would have been more difficult to observe and confidently band fit as the intensity of the band was similar to the noise level and the error on measurements was greater.

It is controversial to draw any conclusions from varying absolute intensity as it is a qualitative measurement. Furthermore, measurements cannot be compared between different Raman spectrometers as each system has different lasers and factors that contribute to noise in the spectra. It may be possible to draw conclusions from measurements made on the same Raman spectrometer. For example, Dartnell *et al.* (2012); Dartnell and Patel (2014) suggested that the intensity of the Raman bands of their samples were degraded as a result of exposure to ionising radiation.

The Raman spectra acquired for the experiments in this study were collected using the same Raman system, with consistencies in the settings, calibration technique, laser power and data processing routine to remove bias as a result of noise and to the best possible capability, geometric effects from the crystal, so that any degradation could be attributed to the simulated environmental effects, though caution should still be exercised.

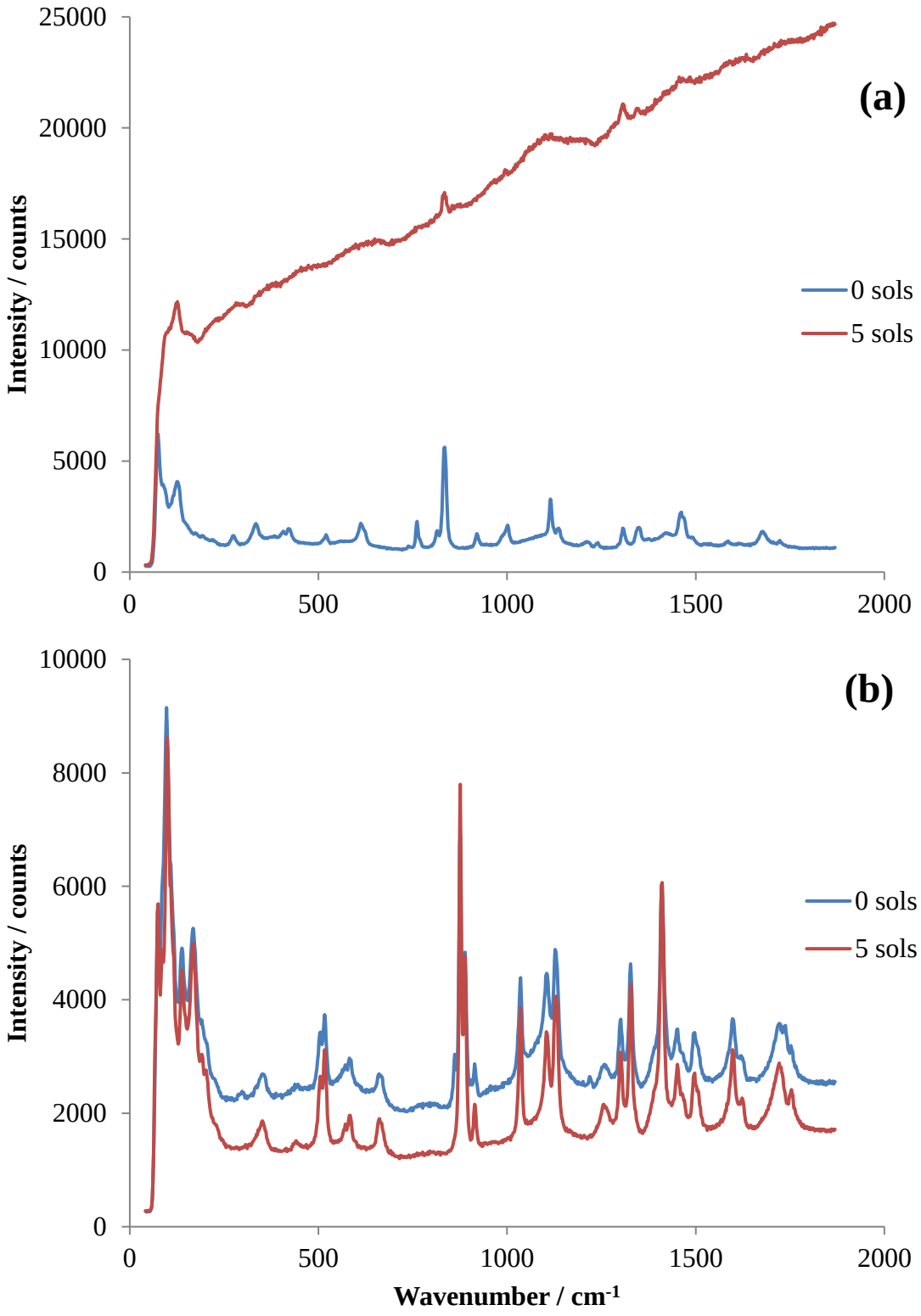

Figure 4-39: Typical Raman spectra of (a) alanine and (b) glycine after 0 sols (*i.e.* a control sample) (blue) and 5 sols (red) of exposure to simulated martian UV radiation.

The normalised spectra of cysteine showed no preferential degradation of the bands, and the band at approximately 500 cm^{-1} was not a characteristic band, but was seen to appear and increase as the UV radiation increased, so was plotted with the characteristic bands in Figure 4-14. In terms of absolute intensity measured, the strongest band (679 cm^{-1}) starts with a maximum of 8810 counts and after five sols of exposure has a maximum count of 1045, approximately 8.5 times less intense than the control sample. In contrast, the band at 500 cm^{-1} has a maximum starting count of 340 and a maximum of 2110 counts after five sols of UV exposure.

The band is associated with an S−S bond (*e.g.* Van Wart *et al.*, 1973), which is found in a molecule of cystine (note: spelling), formed by oxidation of the SH bond in two cysteine molecules. Cystine is readily formed along with reaction products H_2, H_2S and NH_3 when cysteine is exposed to γ radiation (Cataldo *et al.*, 2011). A similar reaction is thought to occur when cysteine is exposed to UV, with reaction products of cystine, H_2S, NH_3, CO_2 and CH_3CHO (acetaldehyde) and an interchange between cysteine and cystine, see Figure 4-40 (*e.g.* Obata and Tanaka, 1965) .

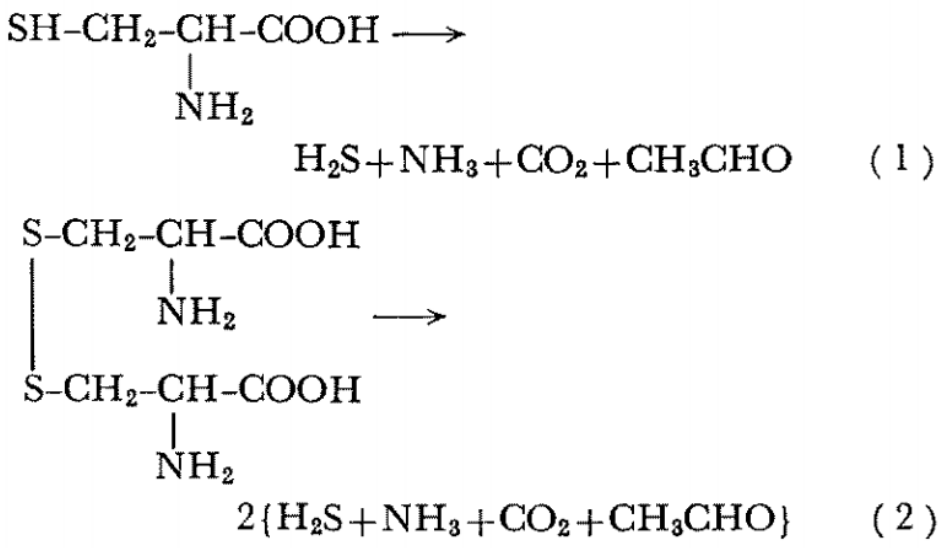

Figure 4-40: Possible reaction pathways for (1) cysteine and (2) cystine when exposed to UV radiation. From Obata and Tanaka (1965).

The cysteine sample was in the presence of oxygen in the experiments here (either in the terrestrial atmosphere or CO_2 in the Mars-like atmosphere), so the exposure to UV radiation could lead to the oxidation of the H atom from the cysteine molecule, leading to the formation of some cystine within the sample. On the fourth sol of exposure a sulphurous smell was noticeable from the sample, suggesting that the UV exposure was causing noticeable quantities of hydrogen sulphide to be released. Over the 24 hours before the next (fifth) exposure to UV, the band denoting the S−S bond (500 cm^{-1}), increased, while the bands at 608 and 679 cm^{-1} remained approximately steady in their intensities, furthermore suggesting that cystine was being formed between exposures, that the chemistry of the sample was changing while in the 'dark' stage of the exposures (samples were stored in a windowless, climate controlled room within a tin foil pouch).

The chemical reaction pathways for this process (if it was real, the standard deviation for the absolute intensities recorded on Sol 1, Sol 4a and Sol 5 are within error of one another) are beyond the scope of this thesis, but could be considered in further research into this interaction.

It was thought that the larger error bars on the absolute intensity data points, where the intensity was at higher intensities (Sol 1 and Sol 4a, Figure 4-16), was as a result of not measuring an increase in the intensity of the 500 cm^{-1} band in all the map points. This highlights that it was dependent on the position in the crystal and was not a ubiquitous change. To understand this further, more regular Raman spectra of the sample could be acquired during the exposures to confirm that the chemistry of the sample was changing throughout the 'dark' portion of the experiment, not just during exposure to UV radiation. After the fifth sol of exposure, the characteristic bands of cysteine continued to reduce in intensity, while the intensity of the band denoting the S−S bond increased, suggesting that cystine was continuing to form, along with hydrogen sulphide, which was still noticeable by smell.

Glutamine and glycine were very consistent, after each sol the band intensities were very similar to the pre-exposure spectra, no bands appeared or disappeared and the position of the bands were stable. This stability is supported by previous studies into the longevity of amino acids on the surface of Mars; *e.g.* ten Kate *et al.* (2005) extrapolated their environmental simulation results to the conclusion that glycine at a starting concentration of ppb would degrade to a concentration of ppt five to forty million years later. Although, ionising radiation has a devastating effect on amino acids, unless buried at least 1 m below the surface (Kminek and Bada, 2006).

The reduction of the intensities of the Raman bands because of exposure to radiation is also in agreement with previous studies that also observed a reduction of spectral intensity (and an increase in noise/fluorescence) (*e.g.* Ehrenfreund *et al.*, 2001a; Dartnell *et al.*, 2012; Dartnell and Patel, 2014), suggesting that the exposed molecules are being destroyed, though these studies did not observe the appearance/increase of another band indicating that a new bond was being formed within the sample.

4.3.4 Doped regolith samples

4.3.4.1 Basalt chips

In general, the doping of the amino acids onto basalt chips caused the Raman bands of the amino acids to be more difficult to observe; the number of characteristic bands that were measured was reduced by at least about 50 %, in one case up to 100 % of the bands were not observed. The minerals in the basalt produced a higher number of counts than the relatively small sample of amino acid applied to the basalt. Furthermore, the basalt caused some fluorescence that almost overwhelmed the signal from the amino acid pre-exposure, and hence, could overwhelm any signal from the amino acid that remained post-exposure.

It would be expected that a short exposure to UV radiation would cause minimal, if any, degradation to the Raman bands of the basalt (otherwise, the whole of the martian surface and the other terrestrial planets would have been destroyed by the solar UV environment!), which was the result here. For alanine, the characteristic bands that were observable pre-exposure became unobservable post-exposure as the intensity of the bands was reduced to a level below the intensity of the basalt signal. The aspartic acid/basalt sample did not feature any readily observable spectral feature from the aspartic acid, which would suggest that the amino acid would be near impossible to detect in a similar martian environment.

The possible band attributed to aspartic acid was more likely to be a band that was a result of a mineral structure in the basalt than from the amino acid as there was no evidence of the strongest band. It was also unfortunate that the strongest cysteine band was obstructed by a band that was from the basalt as the other characteristic bands of cysteine are classified as weak or very weak intensity, hence the possibility that cysteine would be near impossible to identify in basalt of mineralogical similarity. However, the band at approximately 679 cm^{-1} did degrade relative to the known basalt band, so this could be evidence of the cysteine component of that band being reduced while the basalt component remained. The large fluorescence signal after 1000 cm^{-1} engulfed any identifying features (the fluorescence is distorted by the baseline correction either side). It is a possibility, at the very surface of Mars, that the Raman signal would be hampered by fluorescence, but removal of a minute layer of the surface (UV only penetrates up to approximately 2 cm (Cockell and Raven, 2004)) and examination of the near surface would allow for less noisy results. Glutamine and glycine were likely to remain observable; the pre- and post-exposure spectra, with respect to absolute intensity, were approximately similar.

4.3.4.2 Basalt powder

The samples of the amino acids doped onto powdered basalt were not exposed to a simulated martian environment because of the extreme loss of information once the basalt had been powdered. All the samples showed minimal features verses high fluorescence, therefore it was deemed unnecessary to continue with the martian simulation. Foucher *et al.* (2013) also found that the recognition of minerals became increasingly difficult with decreasing grain size: background levels increased and as a consequence of the empty spaces between grains, there were fewer spectra per scan (*i.e.* the number of map positions

that gave a spectrum with information pertaining to a mineral). An unknown sample would be highly difficult to identify. One possible solution to this would be to perform a spectral line scan (opposed to a spectral map) across single grains to obtain some more detailed spectra. This is limited to the grain size with respect to the laser spot size where some minor mineral phases would not be detected. The powdering of the sample removed the context in which the minerals were formed and any potential to detect biomarkers was possibly compromised, which was seen here and by Foucher *et al.* (2013). Despite the potential for the use of specialist routines (*i.e.* line spectra) and thorough examination of the pre-crushed sample that could possibly give the best scientific return on data from the Raman Laser Spectrometer (RLS) on the *ExoMars* rover (*ibid*), from the data shown here it was impossible to detect biomarkers known to be doped onto a powdered basalt sample. Hence it is concluded that it will be highly challenging to detect not only the mineral phases of a sample but delicate biomarkers using the RLS.

4.4 Summary

In this chapter, amino acids samples were exposed to Mars-like environments to test the stability of the molecules under these conditions. Mars Simulation Chambers (MSCs) were used to simulate the extreme martian pressure environment, with additional apparatus, including: a Mars-like gas mixture, a –18 °C freezer, a temperature cycling oven and a UV radiation source to create a coupled, Mars-like surface or near surface environment. Raman spectroscopy was used to determine whether the molecules had been altered or destroyed once exposed to martian conditions.

Exposure to isolated environmental conditions, atmospheric composition and pressure, and freeze-thaw cycling (with Mars-like atmospheric composition and pressure) proved relatively non-destructive. Furthermore, though relatively non-destructive for most of the amino acids tested, it was ascertained that UV radiation changed and/or damaged and, ultimately, destroyed cysteine. This destruction began to occur in as little as one sol equivalent UV dose. This destruction was observed by the reduction in intensity of the Raman bands for the molecule.

Post-exposure analysis of Raman spectra using multiple characteristic bands to identify the amino acids after exposure to martian environmental conditions has proven the usefulness of identifying multiple characteristic bands, as described in Chapter 3, rather than using only the strongest band. If unknown samples became exposed to destructive surface conditions, the information that could be used to identify them will begin to be lost within a few sols of exposure; therefore, samples should be shielded from the UV radiation environment as soon as possible after extraction and analysis carried out within a reasonably short time frame to avoid the UV and ionising radiation environment.

It was determined that when observing amino acids doped onto basalt, some identifying amino acid Raman bands may be obscured by the basalt mineral bands, which will reduce the likelihood of certain amino acids being detected. Crushing the basalt sample removed contextual information and created spaces within the samples causing the Raman spectra to lose characteristic identifying features, which were replaced with broad features that were not necessarily related to identifying bands. Furthermore, any biomarker information would possibly become undetectable once the sample has been crushed.

5. Survivability of Halophiles in Simulated Martian Conditions: Implications for Life Detection

5.1 Introduction

Evidence of evaporite deposits, chlorides, sulphates and perchlorates, detected on the present-day surface of Mars have been interpreted as evidence of a water-rich evaporitic past (McKay, 1997; Gendrin *et al.*, 2005; Hecht *et al.*, 2009) (see Section 1.3.2). Despite the absence of direct measurements of modern, pure liquid water on the surface or subsurface of Mars, there is growing evidence that indicates that brines could have existed or still exist (McEwen *et al.*, 2011; Fischer *et al.*, 2014; Martín-Torres *et al.*, 2015); this is supported by experimental evidence indicating plausible brine forming conditions on Mars (Fischer *et al.*, 2014). *Curiosity* data indicate that conditions at Gale Crater were compatible with liquid brines, while observations of Recurring Slope Lineae (RSL) suggest the presence of transient near surface liquid water brines (McEwen *et al.*, 2011; Fischer *et al.*, 2014; Martin-Torres *et al.*, 2015).

Although halite (NaCl) has not definitively been recorded on the Mars surface, the *Opportunity* rover located possible NaCl in the form of cubic crystal polymorphs in the target rock "Lemon Rind", just north of Erebus crater (Squyres *et al.*, 2006). Furthermore, halite was found in the meteorite Nakhla, which is from the class of meteorites thought to

be of martian origin, known as the Shergotty-Nakhla-Chassigny (SNC) meteorites (Bridges and Grady, 1999). Crystals of halite found within the Nakhla meteorite were up to 400 μm in diameter, which corresponds to possibly one or more crystals (*ibid*).

It has been postulated that brines and evaporites on present day Mars are potential habitable environments (Rothschild and Mancinelli, 2001), where crystallised brines could be a day-to-day (or 'sol-to-sol') habitat but also a last resort location for survival when free-flowing liquid had become scarce on the surface. It is known that halite crystals contain fluid inclusions and that macromolecules and microorganisms are either entombed in fluid inclusions or excluded to hopper-enhanced surface and along discontinuities within the crystal (*i.e.* not incorporated into the crystal structure) (*e.g.* Pasteris *et al.*, 2006; Fendrihan *et al.*, 2009b; Stan-Lotter *et al.*, 2010; Fendrihan *et al.*, 2012). Exposure to Mars-like UV suggested that halophilic microorganisms could somewhat survive the detrimental effects at the surface of Mars. For example, the halophilic archaea, *H. sal* NRC-1, could survive irradiances of 0.7 kJ m^{-2} (cells in a liquid medium), 1.5 kJ m^{-2} (on agar plates) and at least 148 kJ m^{-2} (cells entombed in halite crystals) to D_{37} (dose with 37 % survival) (Fendrihan *et al.*, 2009a).

Halophiles, literally '*salt lovers*', are organisms that live in high saline environments and are found in the three domains of life (*e.g.* DasSarma and DasSarma, 2001). Research has suggested that halophilic archaea can survive between six months (laboratory conditions, Norton and Grant (1988)) and 260 million years entombed within ancient halite deposits; however, the longer time scale is controversial (Grant *et al.*, 1998). Halophiles are known to live in salt lakes and salterns (areas used for salt making); these deposits and other terrestrial environments are proposed analogues for the early and present martian environmental conditions (*e.g.* Wierzchos *et al.*, 2006; Preston and Dartnell, 2014).

To determine whether past or present life exists within the evaporitic deposits on Mars, Raman spectroscopy has been suggested as a life detection method (*e.g.* Edwards *et al.* (2012b), described in further detail in Section 1.5.3.2). Fendrihan *et al.* (2009b) examined Raman spectroscopy as a method for detecting extremely halophilic archaea in terrestrial halite, which could be applied to extraterrestrial samples (*in situ* or sample return). Their study indicated that Raman spectroscopy was able to detect bands that pertained to bonds in a carotenoid (which act as UV screening and DNA repair agents, see Section 1.2.3.4). The detection of halophiles by Raman spectroscopy (described in Section 5.2.3.2.1) comes from the major component of the cell (85 % of total) being comprised of a C_{50} carotenoid, bacterioruberin (molecular structure shown in Figure 1-4), found in, for example, the species *H. sal* NRC-1 (Kelly *et al.*, 1970).

The previous chapter examined the potential for amino acids to remain detectable by Raman spectroscopy after exposure to Mars-like conditions, the discovery of which are more likely to represent extinct life on Mars (*e.g.* Parnell *et al.*, 2007), though could constitute signals from extant life. This chapter will build on this, and the work described in Chapter 1, by studying the survivability, morphological alteration and the potential of using Raman spectroscopy as a life detection technique for halophilic microbes. This was achieved by exposing halophilic organisms to simulated martian conditions (freeze-thaw between –10 and 40 °C; Mars-like atmospheric composition 95 % CO_2, 5 % N_2; temperature approximately −80 °C, pressure approximately 6 to 10 mbar; and UV range 240 to 400 nm, as described in Section 2.3). The results of the exposures were examined using Raman spectroscopy and Transmission Electron Microscopy. The focus of this chapter are the known halophilic archaea, *Halobacterium salinarum* NRC-1, isolated by Helga Stan-Lotter, University of Salzburg (private communication, Terry McGenity, University of Essex) and two unclassified archaeal isolates that belong to the genera

Haloferax (N3.1) and *Haloarcula* (N4.1b), isolated from salterns, in Mallorca, by Terry McGenity, University of Essex (Figure 5-1). Hereafter, the isolates will be referred to as *H. sal* NRC-1, N3.1 and N4.1b, respectively. The microorganisms were entombed in halite crystals and exposed to Mars-like surface and near surface conditions to examine their survivability and to determine the feasibility of using the carotenoid Raman spectra for future life detection missions.

Figure 5-1: The salterns in Mallorca from which *Haloferax* (N3.1) and *Haloarcula* (N4.1b) were isolated. Image credit: Terry McGenity, University of Essex.

The aims of this chapter are as follows: (1) to determine whether halophilic microorganisms entombed within halite crystals can survive simulated Mars conditions. (2) To determine whether their Raman signatures remain detectable after exposure (*i.e.* Raman spectroscopy can be used as a life detection tool).

5.2 Results

5.2.1 Microbial growth in a liquid culture

For the controls, each of the isolates (n = 3) were grown in the medium described in Section 2.5.2 with a 1 % inoculum (this method was also used to culture samples to be entombed in halite, see later Sections). Growth was monitored with OD measurements, at 600 nm, as described in Section 2.5.4.2. Growth curves plotted using the OD_{600} values are shown in Figure 5-2. The error bars are much larger at the beginning of the growth curves because of the detection limits of the spectrometer at low values. *H. sal* NRC-1, N3.1 and N4.1b had distinct lag, log and stationary phases. The log phase for *H. sal* NRC-1 and N4.1b began at approximately 46 hours, whereas for N3.1 the log phase started at approximately 22 hours after inoculation. For all the isolates, the stationary phase was reached after 57 hours. The specific growth rate, μ, was calculated by finding the gradient of the graph during the exponential phase (see Section 2.5.6). These are the first reported μ values for N3.1 and N4.1b. The resulting μ were 0.064, 0.022 and 0.057 hr^{-1} for *H. sal* NRC-1, N3.1 and N4.1b, respectively. The plotted growth curves were an average of the three samples taken for each isolate, hence the associated standard deviation plotted on the graphs.

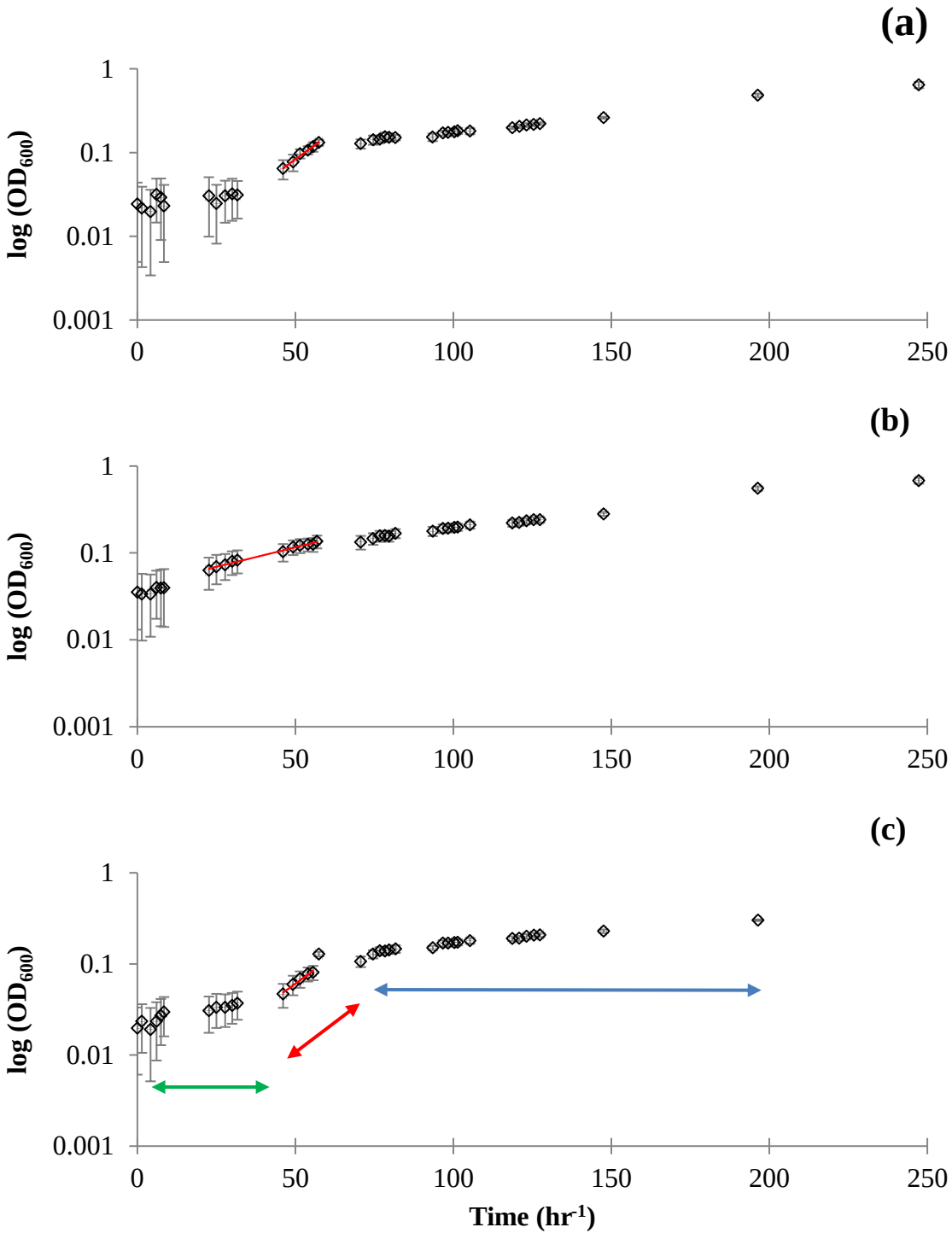

Figure 5-2: Growth of (a) *H. sal* NRC-1; (b) N3.1; (c) N4.1b, in ambient conditions in liquid media monitored by measuring the OD_{600}. The values reported are the mean of three independent experiments with the associated standard deviation. The red trend lines show the data from which the specific growth rate was calculated for each species. The lag (green arrow), logarithmic (red arrow) and stationary (blue arrow) phases of growth are demonstrated in the figure (c).

5.2.2 Survivability of entombed halophiles under simulated Mars conditions

To investigate the feasibility of halophilic microorganisms surviving on the surface of Mars, simulation chambers, as described in Section 2.5.5, were used. The isolates were entombed within artificial halite crystals, as described in Section 2.5.3 and exposed to freeze-thaw temperature cycling, and simulated martian near surface and surface conditions, as detailed in Table 5-1.

A 20 µl aliquot of the liquid suspension was allowed to dry overnight to produce the crystals, as shown in Figure 5-3. The crystals had a range of cell concentrations (depending on the number of crystals). For *H. sal* NRC-1 the cell numbers varied between 1.1×10^4 and 1.1×10^5; for N3.1, 1.0×10^4 and 3.2×10^5; and for N4.1b, 2.3×10^4 to 7.9×10^5 cells per crystal.

Figure 5-3: The resulting crystals from 20 µl aliquots of the liquid suspensions containing the isolates. N3.1 is notably lighter in colouration that *H. sal* NRC-1 and N4.1b.

As the crystals were allowed to dry slowly, *i.e.* overnight in ambient conditions, this resulted in crystals ranging in size between 300 and 1500 μm in the *x*- and *y*-axis (see Figure 1-11 (a) for coordinate diagram) and approximately 100 to 500 μm in the *z*-axis, where crystals with a larger *x,y* length would have a larger *z*-axis value as the general case. Visual examination of the crystals demonstrated that the microorganisms appeared ubiquitous throughout the crystal because of a general pink colouration; however, on inspection through a microscope, the fluid inclusions containing the microbes were clearly distinguished from the rest of the crystal structure, as seen in previous studies (*e.g.* Fendrihan *et al.*, 2009b and see Section 5.2.3.3.2).

Sample Type	*Description*
Control (ambient, agar)	Agar plate bound colonies that have experienced ambient terrestrial conditions, *i.e.*, • pressure: approximately 1000 mbar; • atmospheric composition: terrestrial atmosphere; • temperature: test conditions 20 ± 5 °C, grown in a dark incubator at 37 °C; • light conditions: dark.
Control (ambient, halite)	Halite entombed microbes that have experienced ambient terrestrial conditions, *i.e.*, • pressure: approximately 1000 mbar; • atmospheric composition: terrestrial atmosphere; • temperature: 20 ± 5 °C, grown in a dark incubator at 37 °C; • light conditions: diurnal terrestrial light cycle.
Near surface (control, no UV) OR surface (UV exposed)	Halite entombed microbes that were exposed to simulated martian conditions with (referred to as UV exposure) or without (referred to as near surface or dark) *i.e.*, • pressure: approximately 6 – 10 mbar; • atmospheric composition: 'rough Mars' mix (95 % CO_2, 5 % N_2); • temperature: approximately – 80 °C; • light conditions: dark accomplished by covering sample in tin foil OR UV exposed using Xenon UV lamp source (Section 2.3.3).
Freeze-thaw cycling	Halite entombed microbes that were exposed to temperature cycling to simulate freeze-thaw conditions, *i.e.*, • pressure: approximately 6 – 10 mbar; • atmospheric composition: 'rough Mars' mix (95 % CO_2, 5 % N_2); • temperature: cycled between – 40 °C to 10 °C (Section 2.3.2); • light conditions: dark.

Table 5-1: Descriptions of the conditions that various halophilic samples were exposed to.

5.2.2.1 Entombed isolates growth rate

To determine whether the microorganisms could grow after being entombed within halite crystals, the crystals were inoculated in the liquid medium (described in Section 2.5.2) and growth was monitored by measuring OD_{600} (these samples were subsequently used as ambient controls for the UV exposure experiments). The resulting μ were calculated as follows, 0.031, 0.022 and 0.015 for *H. sal* NRC-1, N3.1 and N4.1b, respectively. Entombment affected the μ for *H. sal* NRC-1 and N4.1b and the values were significantly less, compared to when they were grown in an idealised liquid media (approximately 0.5μ and 0.25μ, respectively) and there was no significant difference for N3.1. There are many possible reasons for the slowed rates, including, the microbes were in the stationary phase when they were entombed and took longer to adapt, the number of cells was different, increased salinity in the fluid inclusions, reduced nutrients and space that would have been available (*i.e.* the microbes were entombed in small fluid inclusions within the crystal). As the N3.1 μ values were similar for the cells in idealised liquid media and entombed cells, it is possible that this lower growth rate meant that this isolate was slow to adapt to both environments. These values provide a baseline for μ for comparison to microbes that were exposed to simulated martian conditions while entombed in halite crystals as described in the Sections 5.2.2.2, 5.2.2.3 and 5.2.2.4 below.

5.2.2.2 Near surface martian conditions

The near surface martian conditions are represented by a pressure of 6 to 10 mbar, a 'rough Mars' atmospheric composition (95 % CO_2, 5 % N_2) and a temperature of −80 °C, as described in Section 2.3, but no UV radiation (*i.e.* as though the samples were covered by at least a few millimetres of regolith, which has been shown to block UV radiation (Cockell and Raven, 2004)). For comparison, near surface samples were exposed at the same time as samples exposed to UV radiation, therefore, a sol equivalent dose (which has a dose of 524 kJ m^{-2}, equivalent to 21 min laboratory exposure) plus time to close and open the MSC, was a total exposure time of approximately 26 min. In parallel, control samples were covered in tinfoil and exposed to ambient conditions. After exposure the samples were incubated in the growth media and growth rates were measured using OD_{600}, as described in Section 2.5.4.2.2. The specific growth rates were 0.029, 0.013 and 0.011 for *H. sal* NRC-1, N3.1 and N4.1b, respectively, as shown in Figure 5-4. The respective OD measurements used to calculate μ are shown in Appendix B.1.

The μ values were used to analyse whether the exposure conditions affected microbial growth. To test whether these results were statistically significant, unpaired two-tailed *t*-tests were conducted on the means of the μ values for each test condition compared to the means of the μ values for the control (ambient, halite) samples. The results are displayed in Table 5-2, where a *p* value of ≥ 0.05 represents no statistically significant difference between the μ values, which would suggest that the log phase of the microbes was unaffected by the exposure experiments.

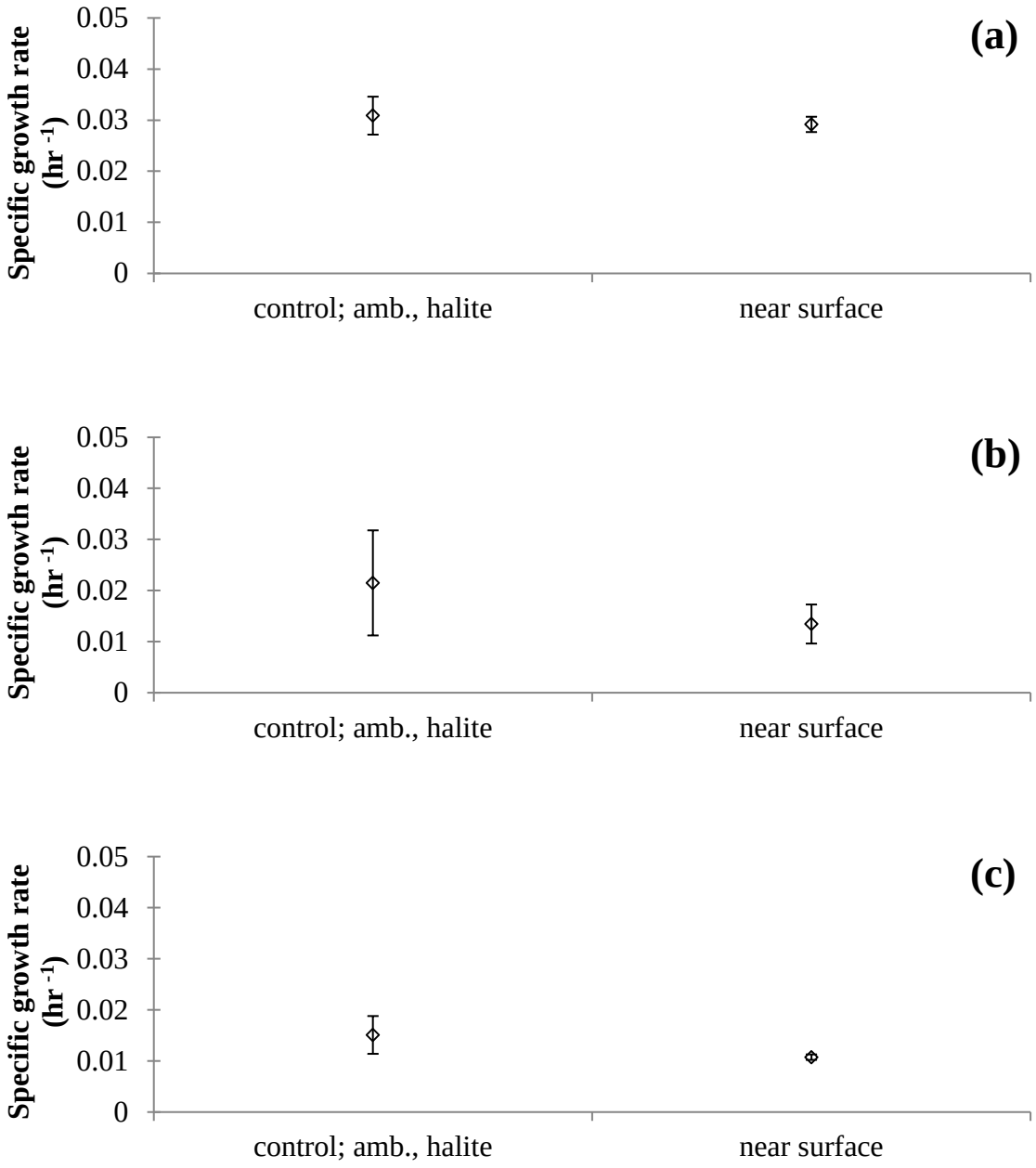

Figure 5-4: The specific growth rates, μ, of (a) *H. sal* NRC-1, (b) N3.1 and (c) N4.1b of control samples (n = 3) exposed to ambient conditions and near surface martian conditions.

Although the μ values were, on average, reduced, the result of the *t*-tests showed that there was no significant difference between the control (ambient, halite) and the samples exposed to simulated near surface conditions, *i.e.* all the *p* values were greater than 0.05. Furthermore, the number of cells that grew post-exposure were compared to the total number of cells in the control (ambient, halite) samples; on average, as a percentage of the control samples, total cell numbers in the near surface exposures were 102 ± 3 %, 103 ± 2 % and 77 ± 2 % for *H. sal* NRC-1, N3.1 and N4.1b, respectively.

Test	*t*	*df*	*p* (one-tailed)	*p* (two tailed)
		H. sal NRC-1		
Near surface	0.74	3	0.256	0.511
Freeze-thaw	8.06	4	< 0.001	0.001
20 kJ m^{-2}	5.92	3	0.005	0.010
30 kJ m^{-2}	4.83	4	0.004	0.008
50 kJ m^{-2}	5.53	3	0.006	0.012
250 kJ m^{-2}	11.31	2	0.004	0.008
524 kJ m^{-2}	11.40	3	0.001	0.001
		N3.1		
Near surface	1.27	3	0.147	0.294
Freeze-thaw	2.62	2	0.060	0.120
20 kJ m^{-2}	1.04	2	0.204	0.408
30 kJ m^{-2}	1.89	3	0.077	0.155
50 kJ m^{-2}	2.15	2	0.082	0.164
250 kJ m^{-2}	1.76	2	0.110	0.220
524 kJ m^{-2}	2.19	3	0.080	0.160
		N4.1b		
Near surface	2.02	2	0.091	0.181
Freeze-thaw	2.57	4	0.031	0.062
20 kJ m^{-2}	2.10	3	0.062	0.123
30 kJ m^{-2}	4.49	2	0.023	0.046
50 kJ m^{-2}	4.16	3	0.013	0.025
250 kJ m^{-2}	6.00	2	0.013	0.027
524 kJ m^{-2}	5.72	3	0.005	0.011

Table 5-2: The results of *t*-tests conducted on the μ of samples exposed to simulated martian conditions compared to the μ of the control (ambient, halite) samples for each of the isolates.

5.2.2.3 Martian surface conditions (including UV)

To examine the effect of simulated Mars surface conditions, halite entombed microbes (n = 3) were exposed to Mars-like atmospheric composition, pressure, temperature and UV radiation (240 to 400 nm) conditions for a maximum of a sol equivalent dose (which has a dose of 524 kJ m^{-2}, equivalent to 21 min simulated exposure) as described in Sections 2.5.5 and 2.3.1. Five different exposure times were used, where the equivalent doses were 20, 30, 50, 250 and 524 kJ m^{-2}. After exposure the samples were incubated in the growth media and the OD was measured using the method described in Section 2.5.4.2.2. To determine the effect of UV radiation exposure on the cells, the numbers of cells that grew as a result of incubation after the exposure was examined. The number of cells per ml of liquid media is related to the OD as shown in Figure 2-21. Figure 5-5 shows the total number of cells as a percentage of the total number of cells in control (ambient, halite) samples (*i.e.* 0 kJ m^{-2} of exposure to UV) for each of the dose rate tests.

Note that the UV Xe lamp used during these exposures was assumed to have a uniform UV output over the visible output footprint. However, because of some inconsistencies encountered in the results, as described below, the UV output of the lamp was investigated (also described in Section 4.2.4). This revealed that it was non-uniform (see Section 2.3.3 and Figure 2-11) and hence, some of the samples would not have received the expected dose of UV, contributing to the anomalous results. The measurements that were affected by the non-uniform behaviour of the lamp have been omitted from this analysis, since the dose received cannot be accurately determined, the justification for which is displayed in Appendix B.2.

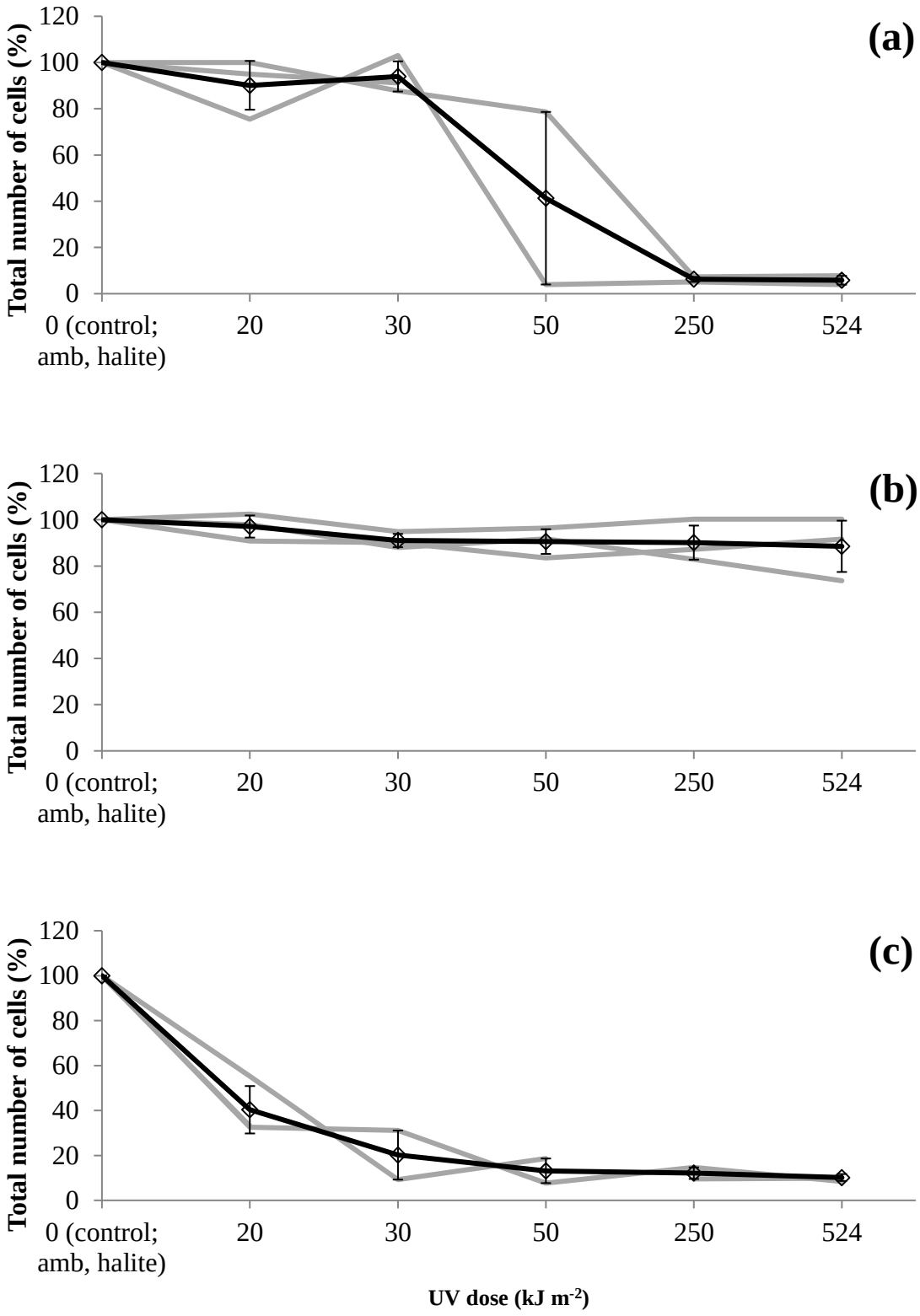

Figure 5-5: The total number of cells for each exposure test as a percentage of the total number of cells found in control (ambient, halite) samples for (a) *H. sal* NRC-1, (b) N3.1 and (c) N4.1b. Near surface samples were exposed to all simulated martian conditions except UV radiation. The black line shows the mean for each test and the error bars represent one standard deviation from the mean. The grey lines show the total cell numbers as a percentage for each of the samples tested (*n* = 3).

Figure 5-5 (a) showed that there was minimal decrease in viability of *H. sal* NRC-1 following exposure of up to 30 kJ m^{-2} (an average of approximately 90 % survival) and following exposure for one sol equivalent dose an average of approximately 5 % of cells were still viable. Three data points were not considered from one of the samples at 50, 250 and 524 kJ m^{-2} (where the total number of cells was 105, 93 and 80 %, respectively) because of the issue of non-uniform lamp output as described above, so at these points the samples are only in duplicate. The D_{37} dose for *H. sal* NRC-1 was approximately 237 kJ m^{-2}; where a D_{37} dose is the UV dose at which only a 37 % survival of the total number of cells is recorded, calculated by examining or extrapolating the survival curve using a trend line though available empirical data. By extrapolation, *H. sal* NRC-1 cells may be able to survive exposure to a dose of at least 1816 kJ m^{-2} or higher (approximately 3.5 sols). The survival of N3.1 is shown in Figure 5-5b, which after one sol equivalent dose of exposure had an average decrease in viability of 12 %. The D_{37} dose for N3.1 is, by extrapolation, approximately 1.2×10^{22} kJ m^{-2}, with complete destruction at a dose of approximately 2×10^{24} kJ m^{-2}; which, rudimentarily, is approximately 1×10^{19} yr. Figure 5-5c shows the decrease in viability of N4.1b to an average of 40 % after the smallest dose of 20 kJ m^{-2} and after one sol equivalent dose of exposure an average of approximately 10 % of cells were still viable. Some of the data points are only in duplicate, because of the removal of inconsistent points at 30, 50 and 250 kJ m^{-2} (where the total number of cells was 70, 53 and 30 %, respectively). The D_{37} was approximately 32 kJ m^{-2} and by extrapolation may be able to survive 1674 kJ m^{-2} (approximately 3.2 sols).

The μ of the exposed samples are presented in Figure 5-6. The OD measurements from which the values of the total numbers of cells per ml and μ were calculated are displayed in Appendix B.1. The μ values for all the isolates showed a trend of decreasing growth rate with increasing dose rate, though it is noted that the rates of the N3.1 isolate were all within error of each other as the dose increased, suggesting there may be no variation, *i.e.* the apparent decrease is not real.

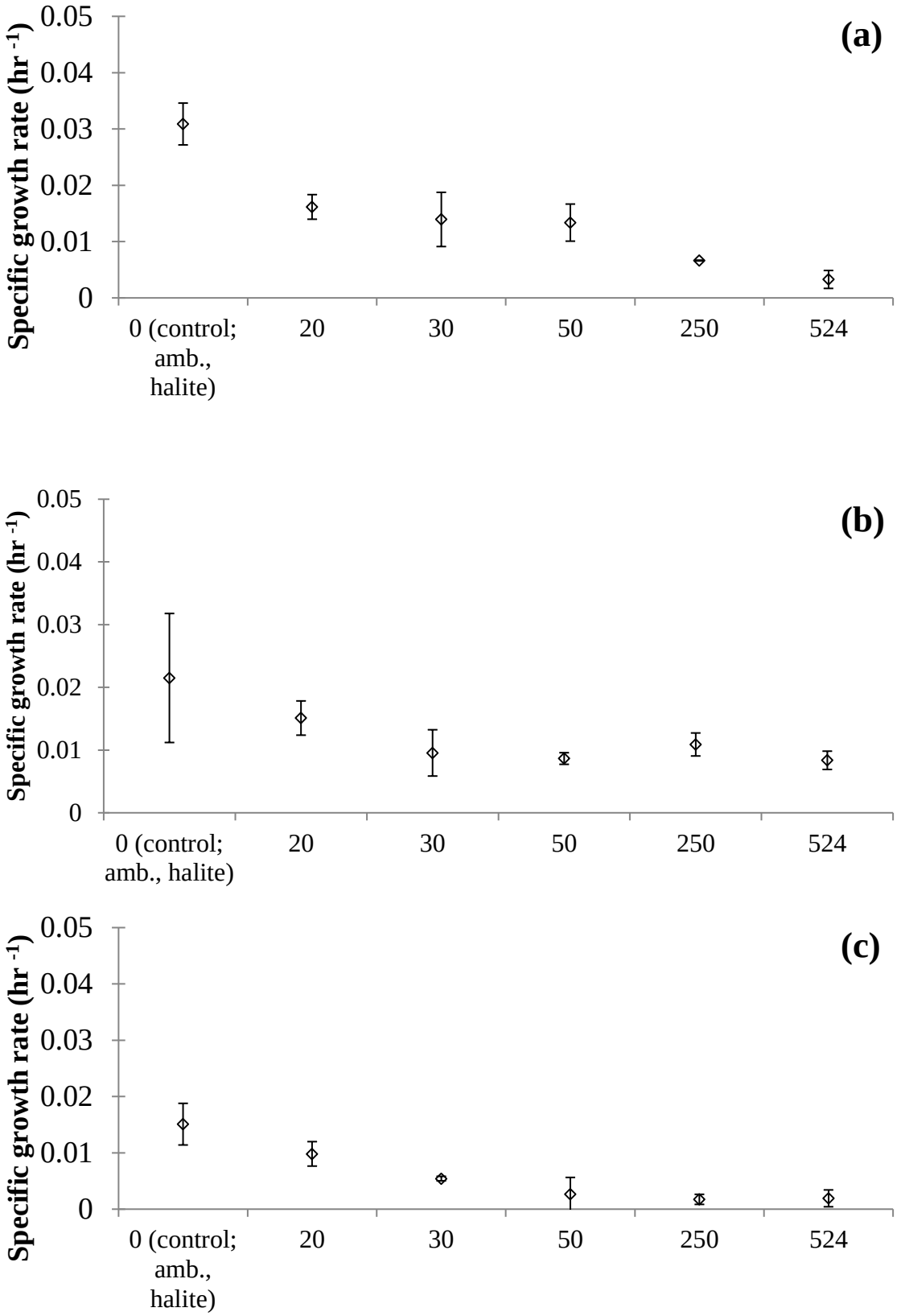

Figure 5-6: The specific growth rates, μ, of (a) H. sal NRC-1, (b) N3.1 and (c) N4.1b after UV irradiance of the samples in the MSCs.

The μ values of the *H. sal* NRC-1 samples exposed to UV radiation were statistically significantly different to those that did not experience UV exposure; all the *p* values were less than the α value of 0.05. The *p* values for the comparison of the N3.1 UV exposed samples to the control samples were not statistically significant, which reflects the results of the dosage curves, where approximately 80 % of comparable growth occurred after exposure to a sol equivalent dose of exposure. The N4.1b samples showed that the growth rate after exposure to 20 kJ m^{-2} was not statistically significant from the control sample μ, though increasing doses, 30, 50, 250 and 524 kJ m^{-2}, were significantly different to the control. Furthermore, some of the exposed samples had extended lag phases. The lag phases increased with the increasing dose rate, suggesting that the cells had been stressed by the exposure and took longer to adapt; the approximate lengths of the lag phases observed (if any) are displayed in Table 5-3.

n	*1*	*2*	*3*
Test	**Lag phase length (min)**		
	H. sal NRC-1		
Control (amb.)	-	-	-
Near surface	-	-	-
20 kJ m^{-2}	-	-	-
30 kJ m^{-2}	71	119	-
50 kJ m^{-2}	(119)	-	142
250 kJ m^{-2}	(166)	n/a	n/a
524 kJ m^{-2}	(142)	n/a	n/a
	N3.1		
Control (amb.)	-	-	-
Near surface	-	-	-
20 kJ m^{-2}	-	-	-
30 kJ m^{-2}	-	-	-
50 kJ m^{-2}	120	-	-
250 kJ m^{-2}	-	96	96
524 kJ m^{-2}	120	-	-
	N4.1b		
Control (amb.)	-	-	-
Near surface	-	-	-
20 kJ m^{-2}	524	333	333
30 kJ m^{-2}	(262)	n/a	422
50 kJ m^{-2}	(333)	743	n/a
250 kJ m^{-2}	n/a	(572)	n/a
524 kJ m^{-2}	n/a	n/a	n/a

Table 5-3: The length of the lag phases for samples exposed to UV radiation. These values are the minimum length of time before the log phase began. n/a represents samples for which there was no clear log phase observed. Bracketed data are those that did not receive the expected UV dose because of the non-uniform UV output of the lamp. A dash indicates that the log phase was observed from the first OD measurement, *i.e.* there was no lag phase. The lag phases were calculated from the OD measurements, shown in Appendix B.1.

5.2.2.4 Mars-like freeze-thaw temperature cycling

Freeze-thaw is a diurnal occurrence on Mars; alongside the other inhospitable environmental factors, it was important to discern whether the halophiles would survive repeated and extended freeze-thaw cycling. Crystals of each isolate (n = 5) were exposed to 90 freeze-thaw cycles between –40 and 10 °C, simulating a Mars-like summer season as described in Section 2.3.2. The μ values for these samples were 0.010, 0.006 and 0.009 for *H. sal* NRC-1, N3.1 and N4.1b, respectively; shown in Figure 5-7. The p value for *H. sal* NRC-1 shows the μ values for the freeze-thaw exposed samples were significantly different from the control sample; whereas the μ values for the freeze-thaw samples of N3.1 and N4.1b were not statistically significant *i.e.* there was no effect resulting from the freeze-thaw cycling on the μ values for these two isolates (see Table 5-2). Furthermore, though the growth rates were reduced for all the isolates, the aim of establishing whether or not the isolates were able to survive freeze-thaw cycles was achieved.

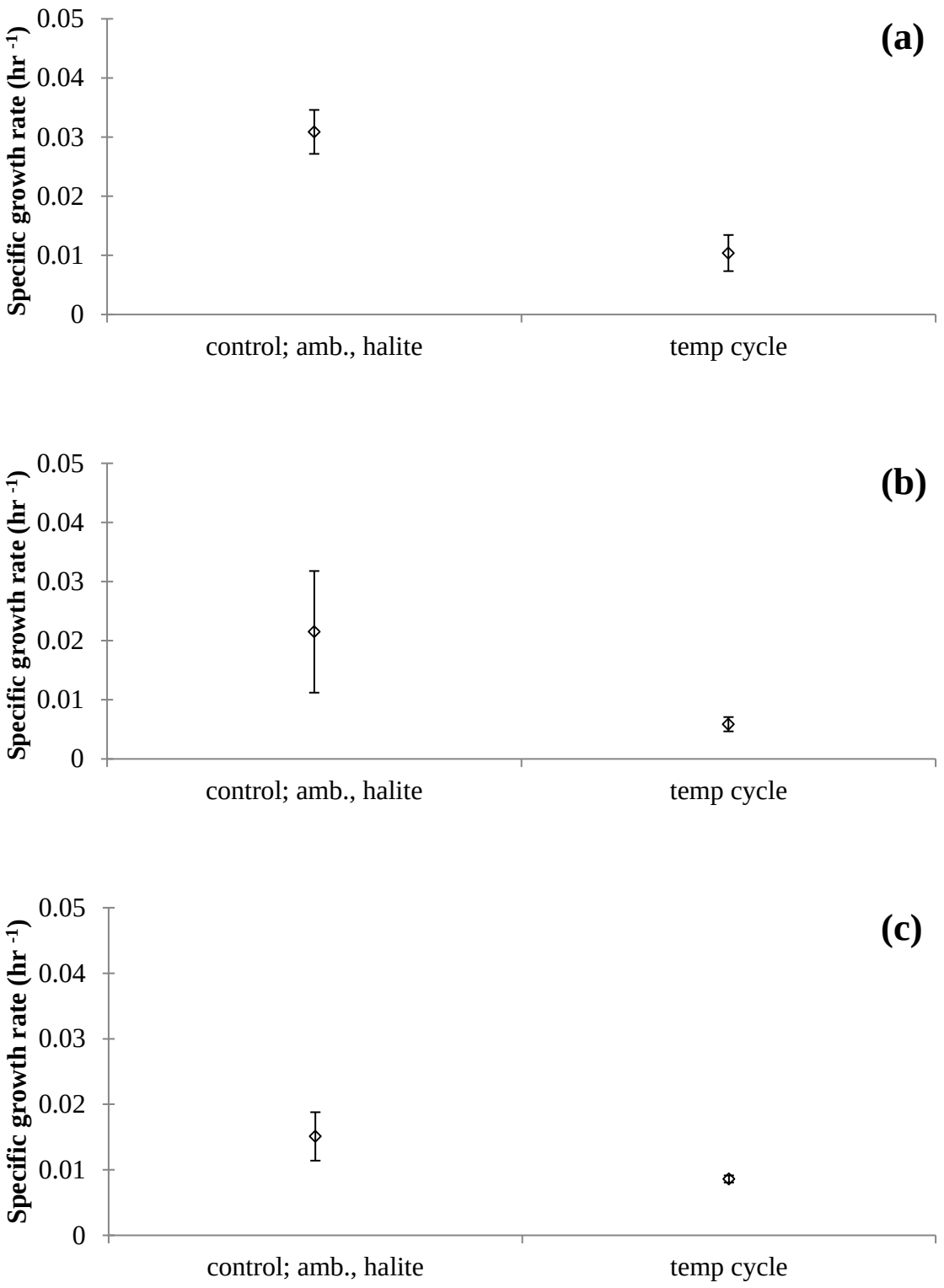

Figure 5-7: The specific growth rates, μ, of (a) *H. sal* NRC-1, (b) N3.1 and (c) N4.1b of control samples (n = 5) exposed to ambient conditions and freeze-thaw conditions.

5.2.3 Analysis of halophiles in context of future life detection

5.2.3.1 Morphological analysis of halophiles

To investigate any morphological alterations of the microorganism after exposure to Mars-like UV radiation, Transmission Electron Microscopy (TEM) was used, as described in Section 2.6. For the morphological analysis, the cells used were grown on agar plates, rather than entombed. This was because it was not possible to create a TEM section from halite crystals with entombed microbes. Therefore, the UV dose used was approximately half to ten times lower than in the lowest dose administered in the entombed experiments. Based on the finding by Fendrihan *et al.* (2009a), who recorded a D_{37} at 0.7 kJ m^{-2} for agar plate bound colonies of *H. sal* NRC-1, the cultures received a maximum of 10 kJ m^{-2} UV dosage (approximately a 24 s exposure in real time) to ensure that it was likely that all the microbes received a dose that would render them non-viable.

Figure 5-8 and Figure 5-9 show typical TEM images of N3.1 and N4.1b, respectively, of samples before and after exposure to Mars-like UV radiation created from aseptic scrapings from agar bound colonies, which were pelleted (for details on growth, see Table 5-4). The samples of *H. sal* NRC-1 prepared for TEM imaging were not as expected and did not provide adequate results to be able to draw any conclusions from; new sections would have to be examined in future work as time restraints did not allow for a repeat experiment.

Sample Type	*Description*
Colonies for TEM analysis	Agar plate bound colonies that have experienced simulated martian UV conditions only, but were otherwise kept in a tin foil wrapped Petri dish, *i.e.*, • pressure: approximately 1000 mbar; • atmospheric composition: terrestrial atmosphere; • temperature: 20 ± 5 °C, grown in a dark incubator at 37 °C; • light conditions (during experiment): simulated martian UV as described in Section 2.3.3.

Table 5-4: Descriptions of the conditions that the isolates used for TEM analysis were grown in and exposed to.

The controls were only exposed to ambient conditions. The N3.1 cells were typically coccoid in shape with a thick cell membrane, approximately 100 nm in thickness, as shown in Figure 5-8a. Furthermore, despite a grainy artefact across the image, the cytoplasm within the cell was visible. Some cells appeared elongated or rod shaped, but this was most likely as a result of the orientation of the cells rather than a true representation of their morphology, which is normally coccoid. Post-exposure to UV radiation showed the cells were misshapen and/or lysed, as demonstrated in Figure 5-8b.

Morphological examination of the controls demonstrated that approximately 14 % of the cells were lysed or damaged. In contrast, after exposure approximately 92 % of the cells were considered non-viable (full results displayed in Table 5-5 and counting method described in Section 2.6). Similarly, the image of the control sample of the N4.1b cells showed a tightly packed population with a largely coccoid morphology. The cytoplasm within the cells was distinguishable and the cell walls and membranes were readily visible as a darker feature of the cell, approximately 100 nm in thickness. Exposed cells showed evidence of morphology alteration and lysing, apparent cell enlargement and cytoplasm visibly forced out from within the cell when it lysed, see Figure 5-10 for an example.

Halophile species	Assumed viability of sample pre-exposure (%)	Assumed viability of sample post-exposure (%)
H. sal NRC-1	-	-
Haloferax N3.1	85.8 ± 3.4	8.0 ± 1.3
Haloarcula N4.1b	88.3 ± 1.1	0.0

Table 5-5: The viability of the halophilic archaea exposed to Mars-like UV radiation. Results from *H. sal* NRC-1 were inconclusive.

Much of the previously visible cytoplasm has been replaced with dark features, possibly a thickening of the cell wall (post-exposure thickness varies cell to cell; the average thickness is two to three times pre-exposure). The N4.1b control sample had approximately 12 % of the cells that appeared damaged and in the post-exposure sample 100 % of cells were regarded to be non-viable.

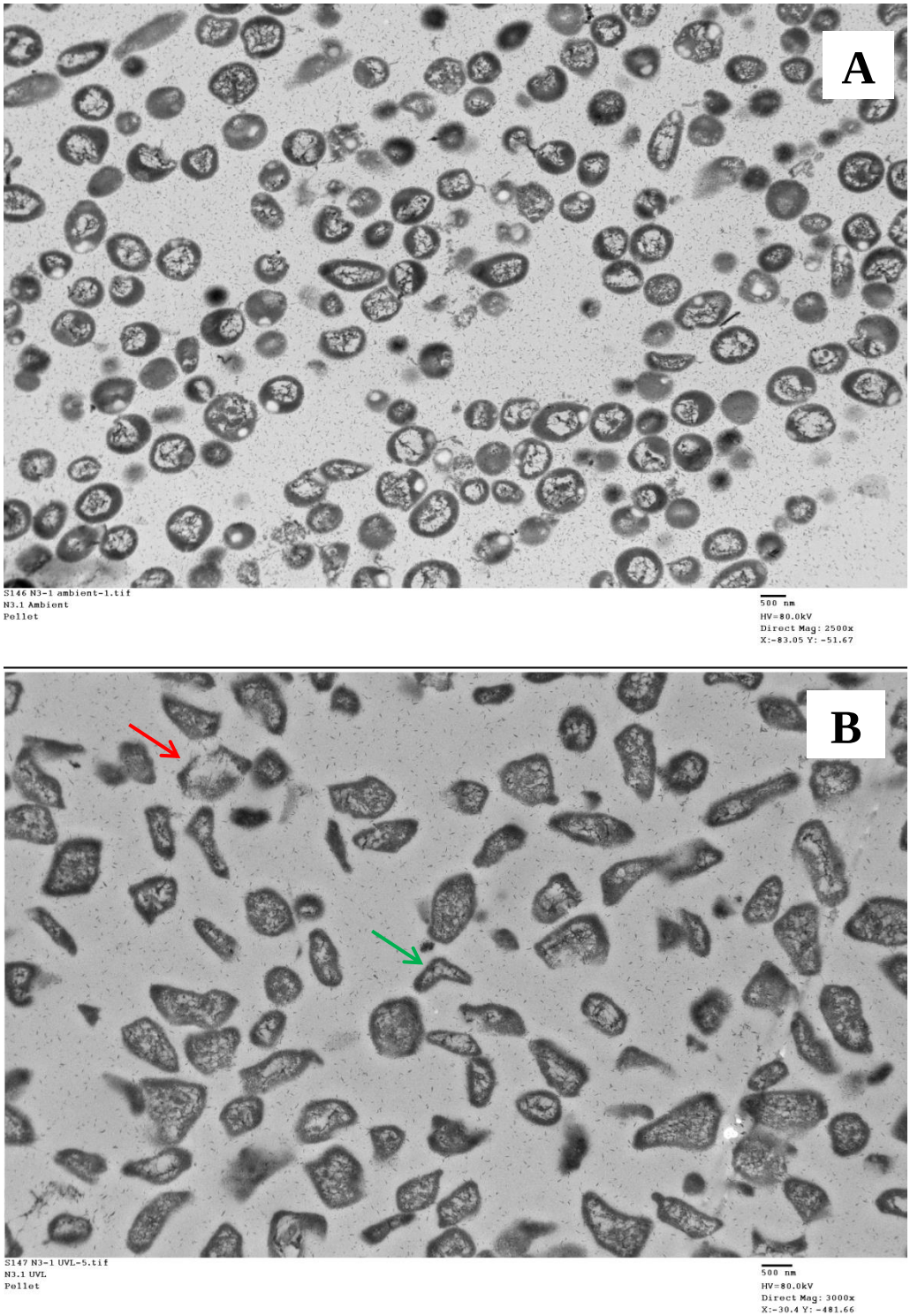

Figure 5-8: TEM images of the microbial strain N3.1, before (A) and after (B) exposure to UV radiation (between 2 to 10 kJ m^{-2}). Post exposure the cells are misshapen (*e.g.*, green arrow) and some cell walls are breached (*e.g.*, red arrow), rendering the cell non-viable. The scale bars (shown below each image) are 500 nm and the direct magnification is 3000×.

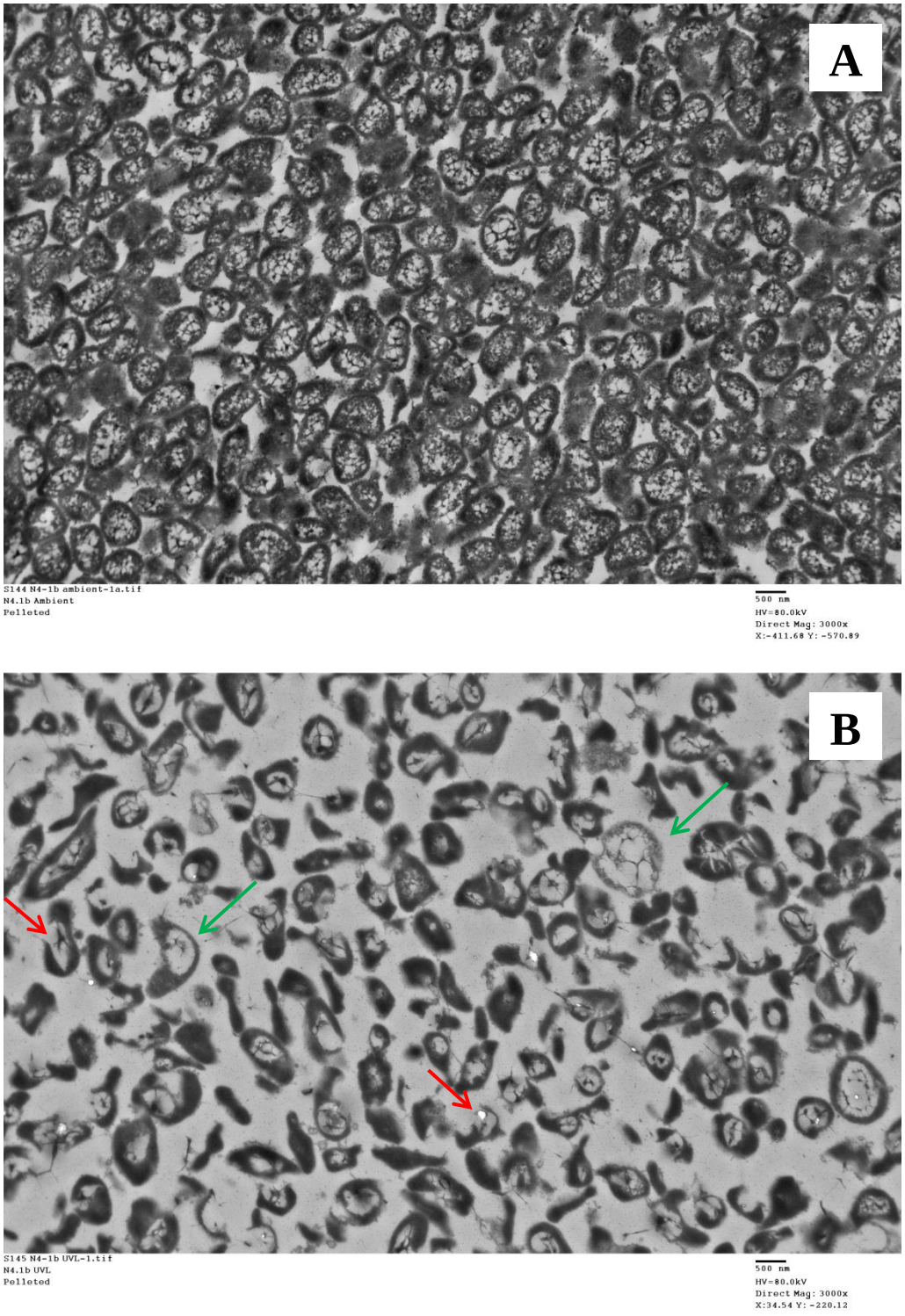

Figure 5-9: TEM images of the microbial strain N4.1b, before (A) and after (B) exposure to Mars-like UV radiation. The scale bars (shown below each image) are 500 nm and the direct magnification is 3000×. Post exposure the cells are misshapen (*e.g.*, green arrows) and some cell walls are breached (*e.g.*, red arrows), rendering the cell non-viable.

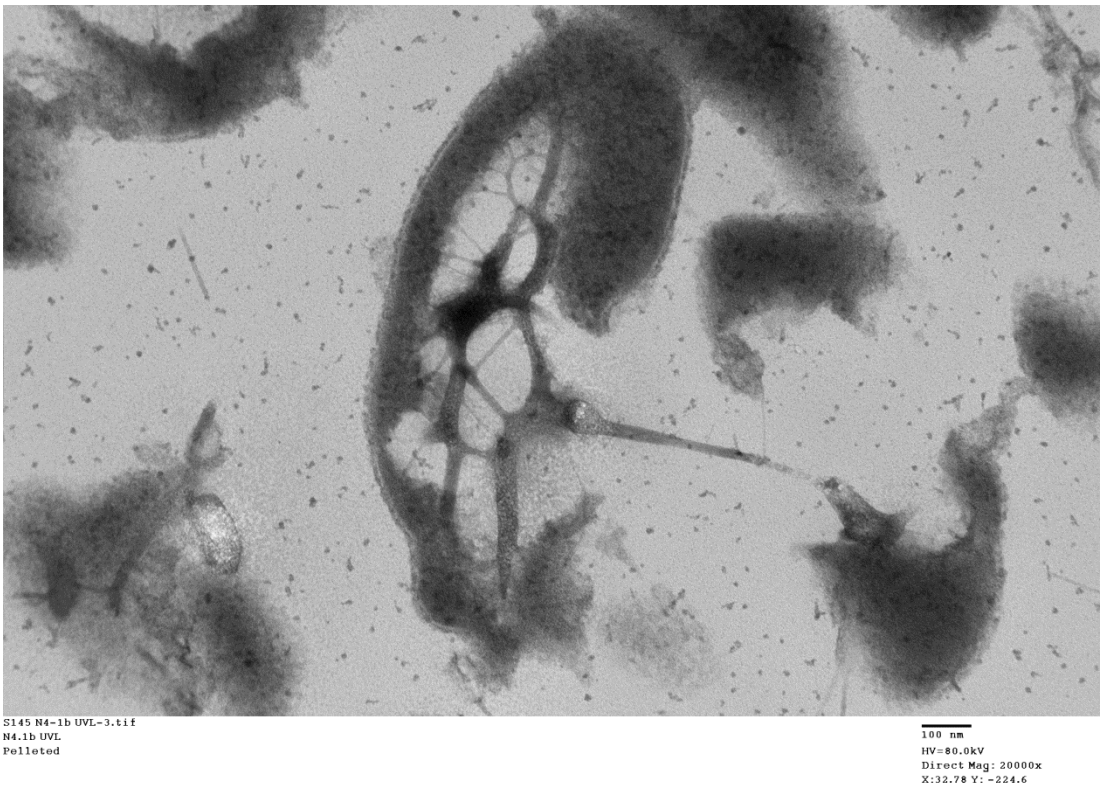

Figure 5-10: A lysed N4.1b cell having been exposed to simulated martian UV radiation. The cell wall has burst away, drawing some of the inner cytoplasm with it. The scale bar (shown below the image) is 100 nm and the direct magnification is 20,000×.

The pelleted samples gave an overview of the damage caused by the UV, but gave no structural information from the agar-bound colonies. Cross-sections of N4.1b colonies were prepared to investigate the effect of shielding from colony thickness in simulated martian UV conditions. Figure 5-11 (C) showed that there was a distinct area, 40 % of the thickness of the colony, in which the morphology of the cells was different in the upper part to that of the lower part of the colony, not seen in the control (ambient, agar) samples (Figure 5-11 (A) and (B)); it is noted that the control sample colonies were not as thick as the UV exposed colonies so this may have an effect on the interpretation of the exposed sample. The upper part of the UV exposed colony had a similar morphology to the

post-exposure pelleted cells, described above. The lower part of the colony does not appear to be as damaged, though it is assumed that the cells are viable, as, when compared to control colonies, many of them are misshapen and have a greater amount of the darker region surrounding them as seen in the upper part, but there are more cells with their cytoplasm visible.

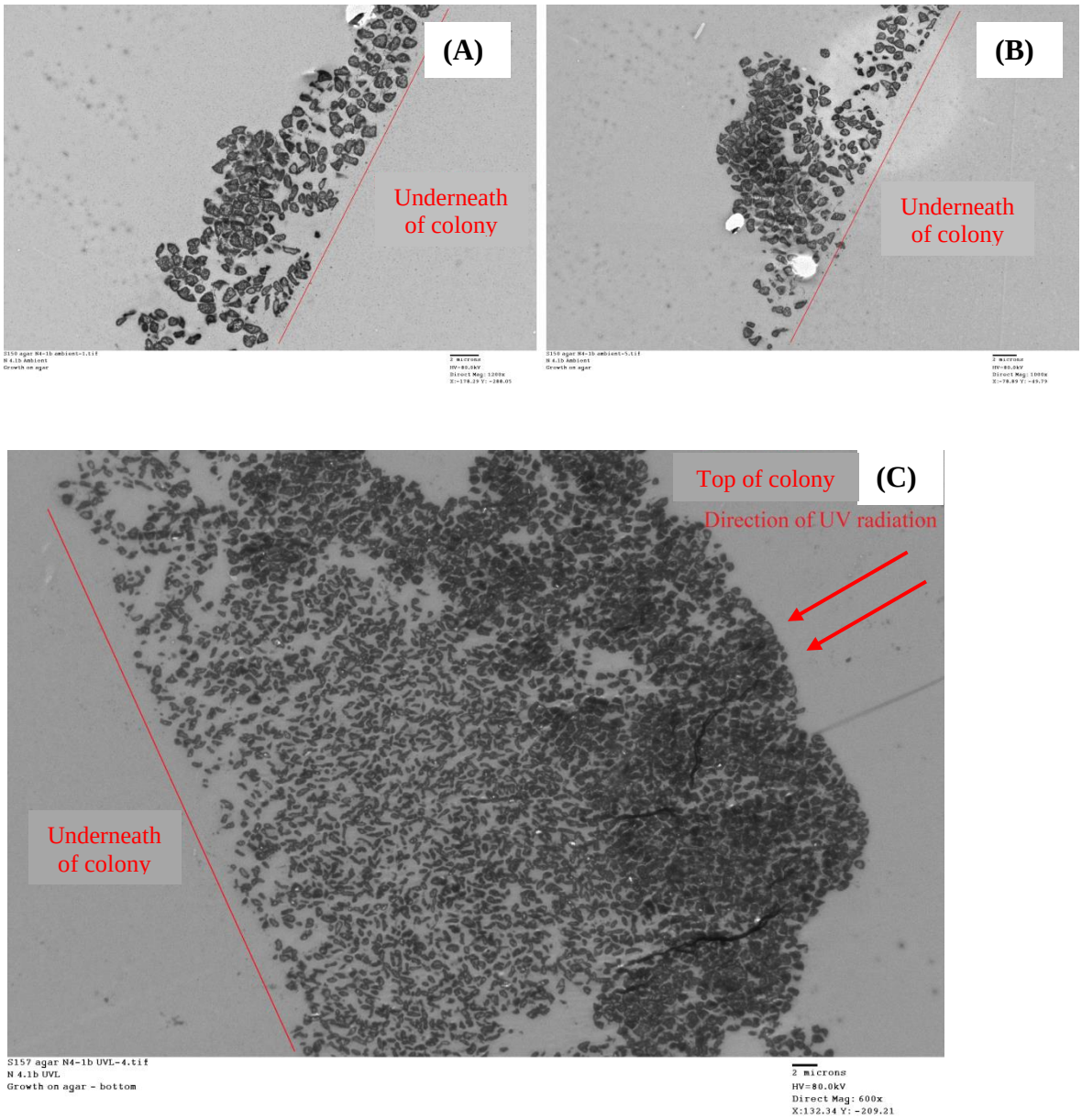

Figure 5-11: Cross-sections of N4.1b colonies grown on an agar plate that was exposed to (A) and (B) ambient conditions and (C) simulated martian UV radiation. The cross-sections are rotated from the original orientation because of the process of the creation of the thin section. The original underneath and top of the colony is marked with the direction of the UV radiation indicated where applicable. The scale bars for (A) and (B) (shown below the image) are 2 µm and the direct magnifications are 1200× and 1000×, respectively. The scale bar for (C) (shown below the image) is 2 µm and the direct magnification is 600×.

5.2.3.2 Detection of halophiles using Raman spectroscopy with implications for life on Mars

The focus of this section is the detection of halophilic microorganisms after exposure to simulated martian conditions, whether they remained detectable by Raman spectroscopy, and hence, have implications for future life detection missions, for example, the *ExoMars* rover. The Raman bands, as described in detail in Chapter 1, denote bond energies within molecules; a change in intensity would suggest a reduction in the number of bonds measured (*e.g.* Dartnell *et al.*, 2012; Dartnell and Patel, 2014) and a change in position would suggest the molecule is being destabilised or destroyed (*e.g.* Goodyear, 2013). As in the previous Chapter, the 514 nm laser was used in these experiments, as it was the closest available wavelength to that selected for the *ExoMars* mission.

5.2.3.2.1 Pre-exposure Raman spectra of the microbial species

Examples of Raman spectra of control samples of halite are shown in Figure 5-12, which were examined before the halite was doped with the halophiles. The halite spectrum was mostly featureless, the spectra recorded in this study were in agreement with accepted Raman spectra of halite (NaCl) (*e.g.* Lafuente *et al.*, 2015). Furthermore, once it had microbes entombed within it, the spectral features of the microbes overwhelmed any small features that the halite had. The small features seen in Figure 5-12 were thought to be contamination or impurities in the halite structure and as these bands are seen in only approximately 6 % or fewer of the spectra acquired, so were considered negligible.

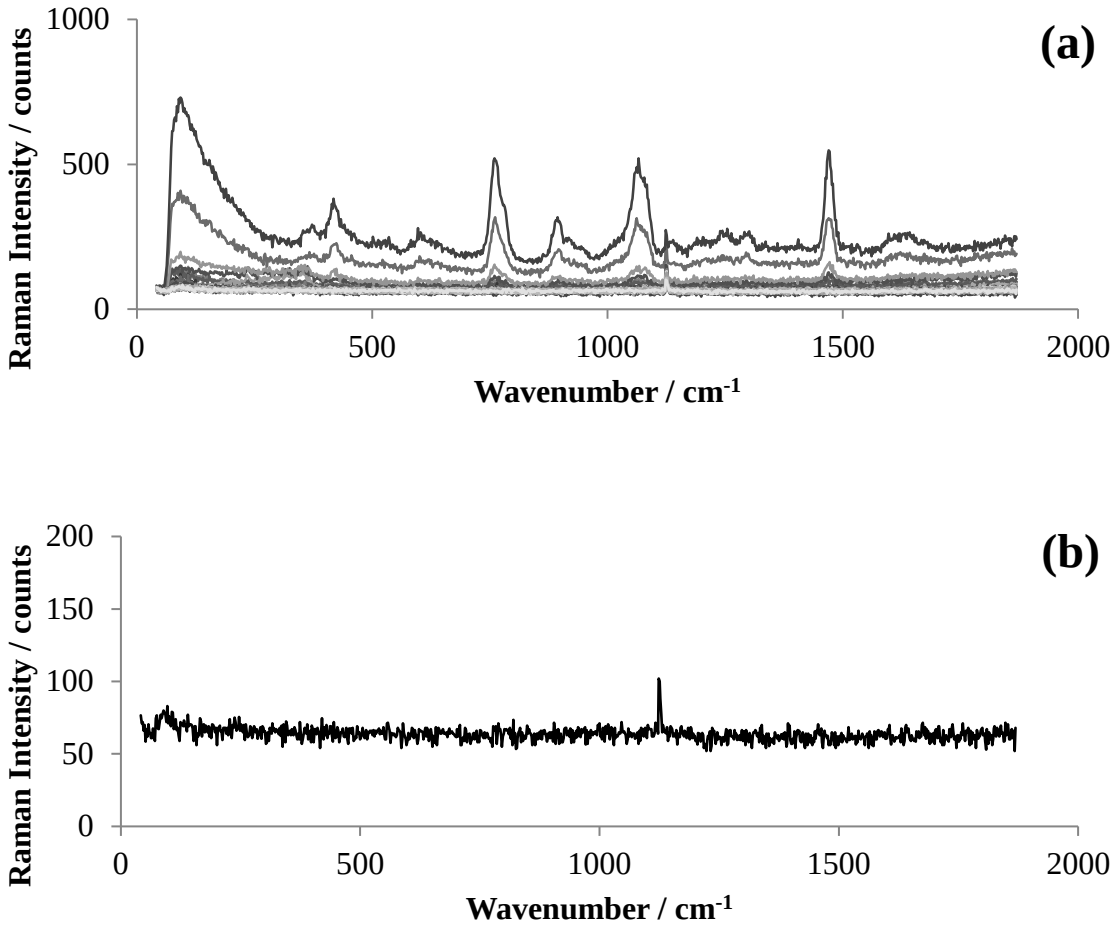

Figure 5-12: Raman spectra of halite used in this study. (a) shows a typical map of Raman spectra with a few spectra that may have impurities or contamination; for comparison, the *y*-axis is one tenth the intensity of the axis when the halophiles were entombed. (b) shows a single point on the map that is representative of the expected Raman spectrum of halite; for comparison, the *y*-axis is one order of magnitude less than the intensity of the axis when the halophiles were entombed and, therefore, any bands or features are negligible.

As a control, Raman spectra of the three microbial species were acquired from colonies grown in ambient conditions on agar plates. *H. sal* NRC-1 had three main bands at approximately 1002, 1152 and 1507 cm^{-1} (from 25 map points, the band positions are the average positions and in agreement with Marshall *et al.* (2007)) and some minor bands at approximately 1214, 1285, and 1356 cm^{-1}. The main bands for N3.1 were at approximately 1002, 1152 and 1507, with a minor band at approximately 1285 cm^{-1}. N4.1b had main bands at approximately 1002, 1152 and 1507 cm^{-1} and some minor bands at approximately 959, 1194, 1214, 1287, 1356, 1390 and 1444 cm^{-1}. Examples of the Raman spectra for each species are shown in Figure 5-13.

As the isolates N3.1 and N4.1b are novel isolates that have not been characterised in the literature, it was unknown which carotenoid they contained. For all the microbes the strongest band was 1507 cm^{-1}, followed by 1152 and 1002 cm^{-1}, respectively, suggesting N3.1 and N4.1b contained the same carotenoid as *H. sal* NRC-1. For the carotenoid, bacterioruberin, bands are assigned to the following bonds: 1507 and 1152 cm^{-1} to the C=C and C−C stretching vibrations, v_1 and v_2, of the polyene chain, respectively; and 1002 cm^{-1} to the in plane rocking modes of the CH_3 groups coupled to the C−C bonds (*ibid*). N3.1 generally produced a weaker signal than the other two isolates, which was assumed to be because of the comparatively paler pink colouring of N3.1, which is further assumed to result from less bacterioruberin.

For the entombed cells, Raman spectra of the crystals were acquired as a baseline comparison for the resulting spectra after exposure to experimental conditions was complete. Figure 5-14 shows examples of the Raman spectra of control (ambient, halite) samples of the isolates entombed in crystals. These spectra are near identical to those shown in Figure 5-13, with the biggest difference only seen in the raw data (not shown), before baseline correction, where fluorescence was several thousand counts more

pronounced in the spectra of the halite entombed samples most likely because of scattering and other interactions of the laser light with the halite crystals.

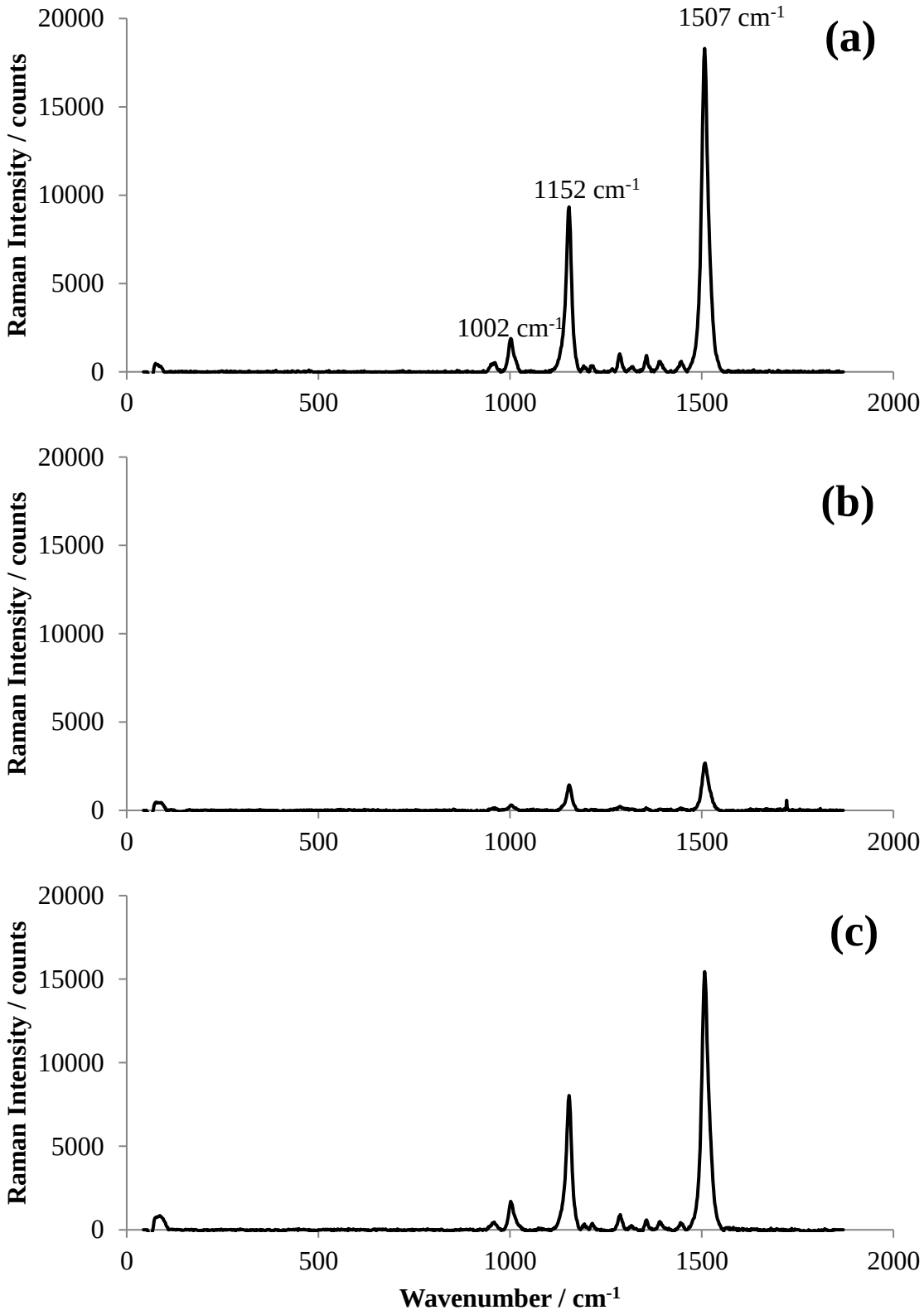

Figure 5-13: Typical Raman spectra of control (agar, ambient) samples of the three microbial species studied; (a) *H. sal* NRC-1, (b) N3.1 and (c) N4.1b.

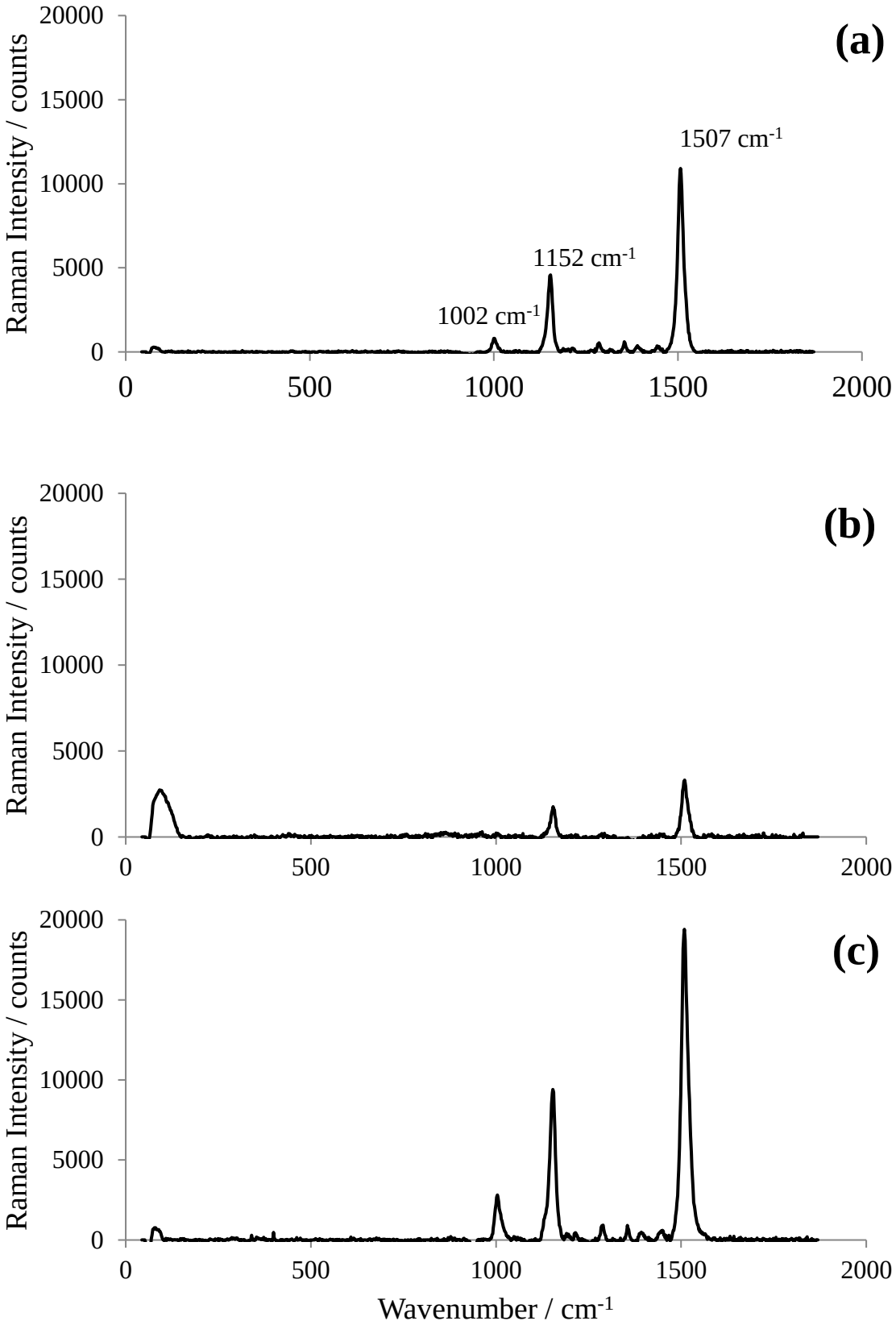

Figure 5-14: Typical Raman spectra of halite entombed samples of the three microbial species studied; (a) *H. sal* NRC-1, (b) N3.1 and (c) N4.1b.

5.2.3.2.2 Analysis of UV exposed microbes using Raman spectroscopy

To test whether there would be a change in the intensity of the bands as a result of exposure, samples of the isolates were grown on agar plates and exposed to UV radiation (the same samples used for the TEM analysis, receiving a maximum dose of 10 kJ m^{-2}). A 25 point *x-z* axis map was obtained to confirm whether the Raman intensity was reduced as a result of exposure to UV radiation. The Raman spectra pre- and post-exposure (average of the 25 points) are shown in Figure 5-15. The percentage difference in the pre- and post-exposure was examined, where (as stated in previously in Section 4.2.1) the smaller the percentage difference, the less significant the change in the relative intensity and hence, little or no significant change to the Raman spectra and therefore, the sample as a result of exposure to the simulated martian environment.

The Raman intensity for the strongest band for *H. sal* NRC-1 was reduced by up to 100 % (*i.e.* some points on the map recorded no bands) and by a minimum of 35.6 % and an average of 82.5 %. In the case of N3.1, in the majority of map points no bands were recorded post-exposure, suggesting that the carotenoid, and hence the microbes, was entirely destroyed by the UV exposure. The intensity of the 1507 cm^{-1} band was reduced by a minimum of 82.4 % and an average of 94.6 %. The Raman intensities for N4.1b were reduced by up to 99.6 % and by a minimum of 67.4 % and an average of 91.1 %. The details of the percentage differences are given in Table 5-6.

	Band intensity % difference pre-, post-exposure		
Raman Band / cm^{-1}	*H. sal* NRC-1	N3.1	N4.1b
1507	82.5 ± 17.5	94.6 ± 4.1	91.1 ± 8.4
1152	40.9 ± 11.2	49.8 ± 11.1	47.6 ± 6.8
1002	8.8 ± 3.4	4.3 ± 8.4	10.5 ± 3.8

Table 5-6: The percentage difference in band intensity for agar bound colonies pre- and post-exposure to Mars-like UV radiation.

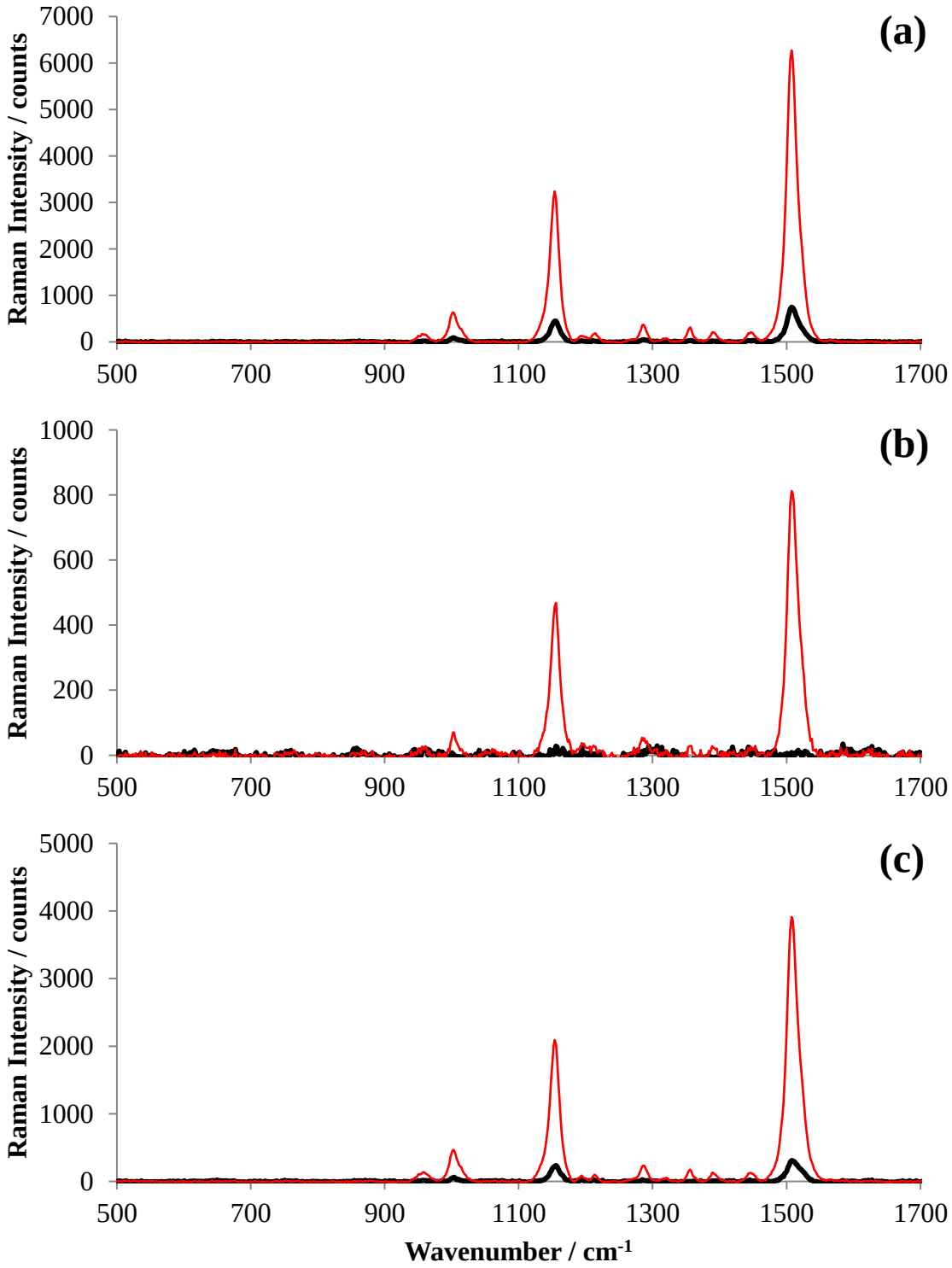

Figure 5-15: The Raman spectra of the isolates (a) *H. sal* NRC-1, (b) N3.1 and (c) N4.1b pre- (red solid line) and post-exposure (black solid line) to UV radiation (10 kJ m^{-2}). The Raman bands were completely destroyed for N3.1 in the post-exposure spectra, hence there are no bands. Note the scales are related to the maximum intensity counts for each isolate.

To investigate whether the bands were degrading relative to one another or if one band was degrading preferentially, the normalised intensity for the pre- and post-exposure data were plotted in Figure 5-16. There was a small relative difference in the 1152 cm^{-1} band compared to the 1507 cm^{-1} band for *H. sal* NRC-1, approximately 10 % and for N4.1b, approximately 20 %. The bands for N3.1 could not be compared relatively as they had been completely destroyed, also seen in Figure 5-15.

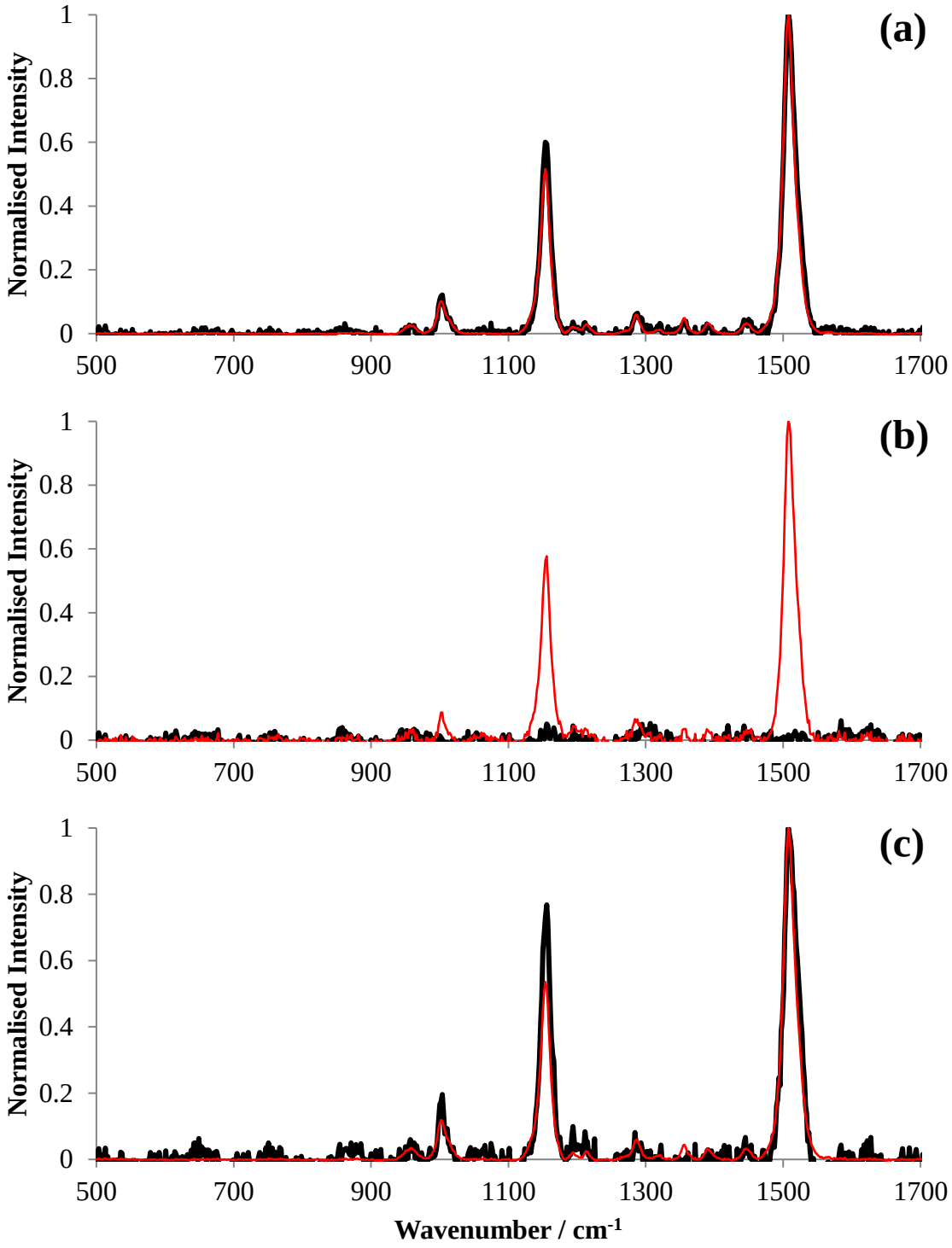

Figure 5-16: The normalised intensity of Raman bands for samples of (a) *H. sal* NRC-1, (b) N3.1 and (c) N4.1b, showing the relative degradation of the bands pre- (red solid line) and post-exposure (black solid line) to UV radiation (10 kJ m^{-2}).

5.2.3.2.3 Mars-like freeze-thaw temperature cycling

The Raman bands for the halophiles did not degrade to the same extent as seen in the UV exposure experiments when exposed to a freeze-thaw Mars-like simulation. Figure 5-17 shows the absolute intensities. The intensity of the strongest band had degraded by approximately 59 to 65 %, on average; the full percentage differences are given in Table 5-7. The normalised band intensities pre- and post-exposure were compared to determine if the bands were degraded at a relative or non-relative value to one another. The results are shown in Figure 5-18. The bands show minimal relative difference, with the 1152 cm^{-1} exhibiting a maximum of a 10 % difference between the pre- and post-exposure data.

	H. sal NRC-1	N3.1	N4.1b
Raman Band / cm^{-1}	Band intensity % difference pre-, post-exposure		
1507	59.1 ± 14.0	65.5 ± 6.6	65.5 ± 14.9
1152	25.1 ± 9.0	30.2 ± 3.9	35.8 ± 9.7
1002	10.1 ± 2.1	27.3 ± 1.9	8.2 ± 2.6

Table 5-7: The percentage difference in band intensity pre- and post-exposure to freeze-thaw cycles

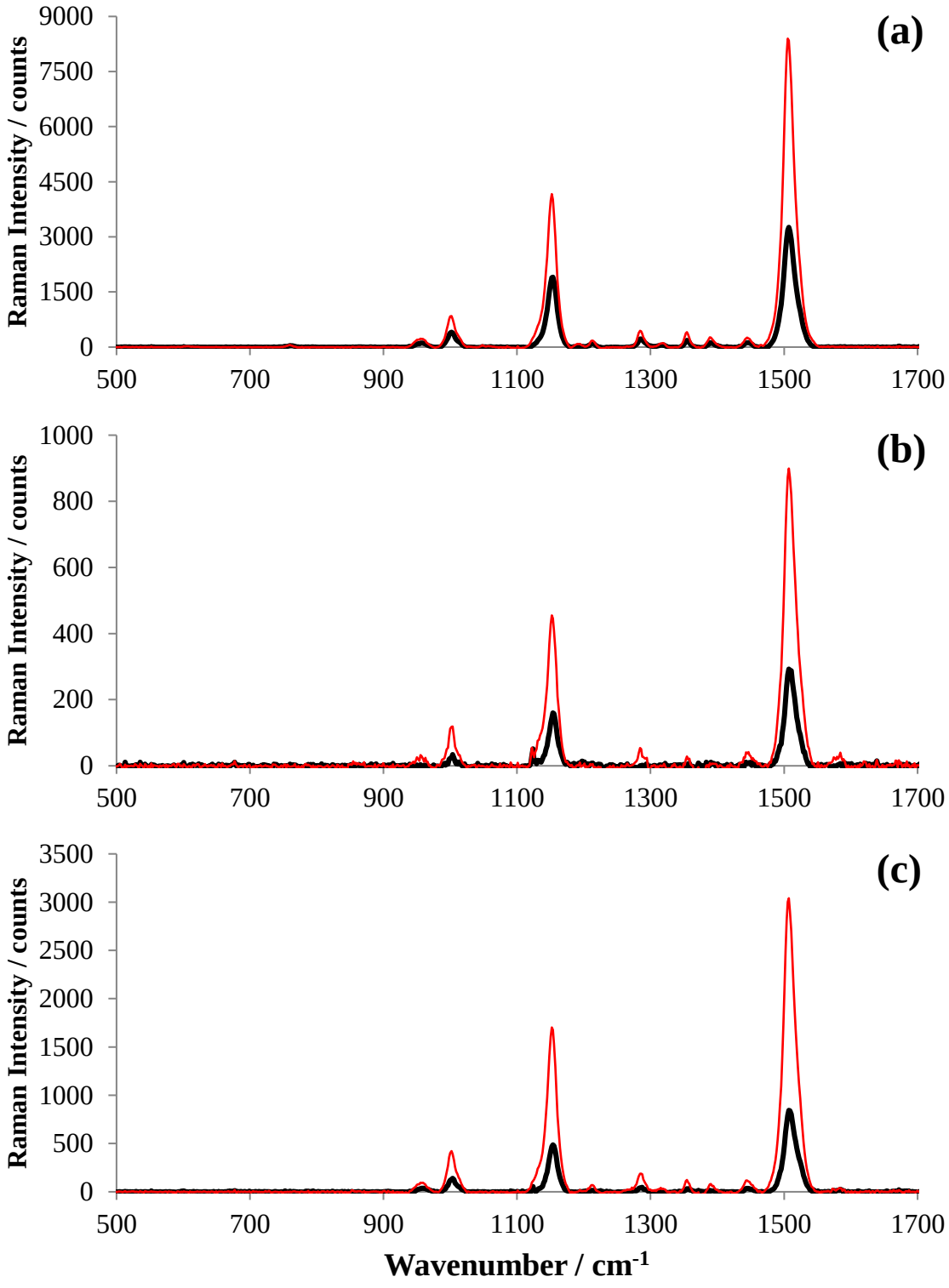

Figure 5-17: The intensities of the Raman spectra pre- (red solid line) and post-exposure (black solid line) to a simulated freeze-thaw cycle. All spectral features are relative to the strongest, pre-exposure band at 1507 cm^{-1}. Note the scales are related to the maximum intensity counts for each isolate.

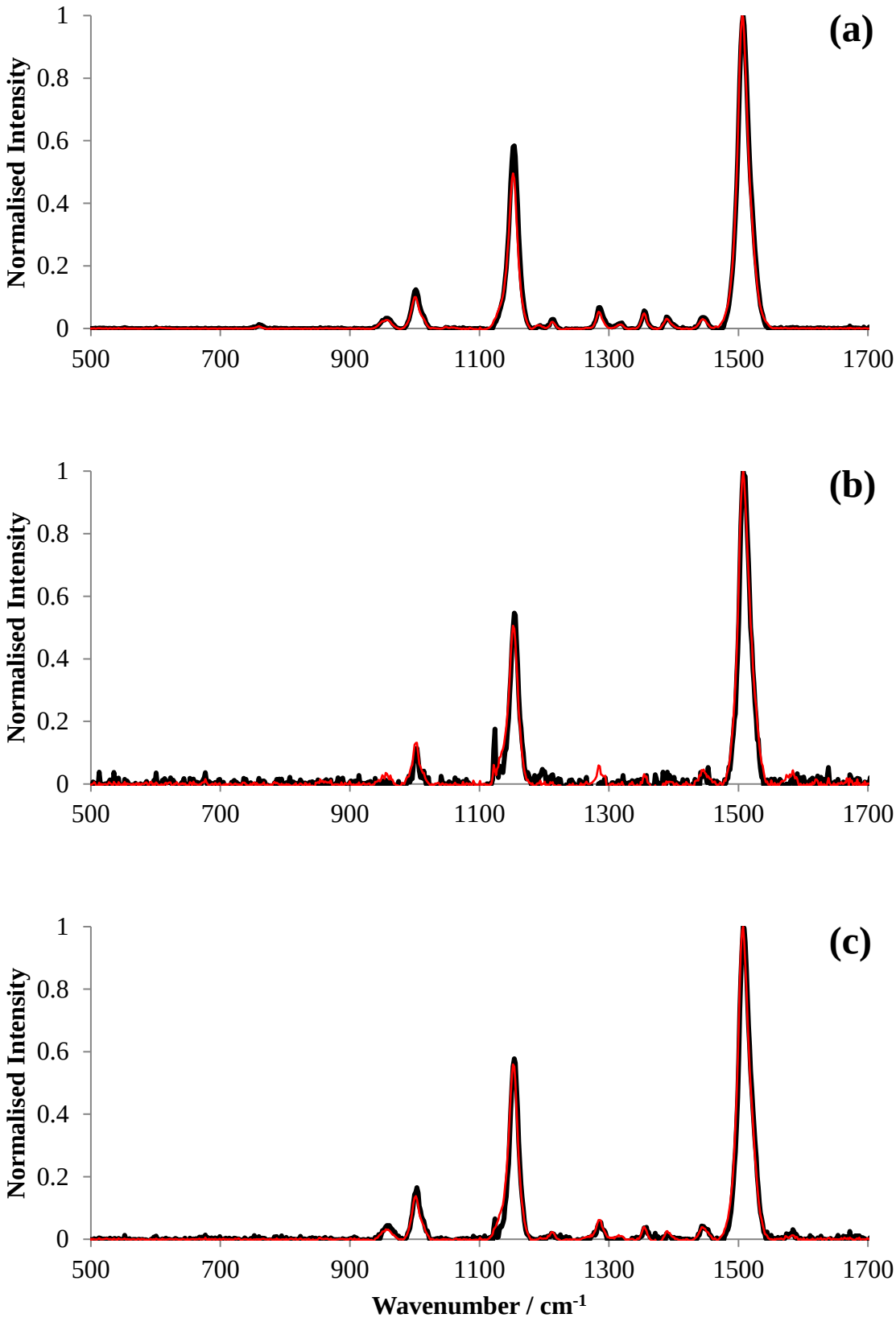

Figure 5-18: The normalised intensity of Raman bands for samples of (a) *H. sal* NRC-1, (b) N3.1 and (c) N4.1b, showing the relative degradation of the bands pre- (red solid line) and post-exposure (black solid line) to freeze-thaw cycling.

5.2.3.3 Halite crystal *z*-axis investigation

Halite is known to attenuate UV wavelengths by approximately 60 % (*e.g.* Kittel, 2005; Fendrihan *et al.*, 2009a), creating a partial shield for any microbial life that may be entombed within fluid inclusions in the structure of the crystal. Furthermore, the formation of fluid inclusions may occur in a manner where several are positioned above one another, so the cells themselves would provide shielding to others below them. Several methods were undertaken in an attempt to investigate the extent to which the position of the fluid inclusions can influence the survival of the microbes. The *z*-axis of the crystal is defined by the depth or thickness, shown in Figure 1-11(a).

5.2.3.3.1 Detection of LIVE/DEAD stained microbes using confocal microscopy

Confocal microscopy (described in Section 2.5.9) can be used to look at *x*-*y* cross-sections along the *z*-axis of a sample. To determine the viability of the microbes after exposure to simulated martian conditions at different points on the *z*-axis (and hence, whether any shielding occurred), the microbes were stained using LIVE/DEAD staining, described in Section 2.5.8. In a preliminary experiment, the entombed microbes were exposed to UV radiation using the xenon lamp and the dye was applied to the crystal afterwards with the intention that it would penetrate the crystal structure and stain the microbes while in the fluid inclusions.

However, the propidium iodide (PI), which causes the microbes to appear red (*i.e.* non-viable), was found to bind to the surface of the crystal and cause fluorescence; hence at lower *z* positions no information was recorded, forcing the conclusion that the dye had not penetrated the crystal. When increased amounts of the dye were added it caused destabilisation of the crystal structure, thus losing the structural information that was required. Nonetheless, pre-stained colonies of live cells were successfully imaged in fluid inclusions, shown in Figure 5-19.

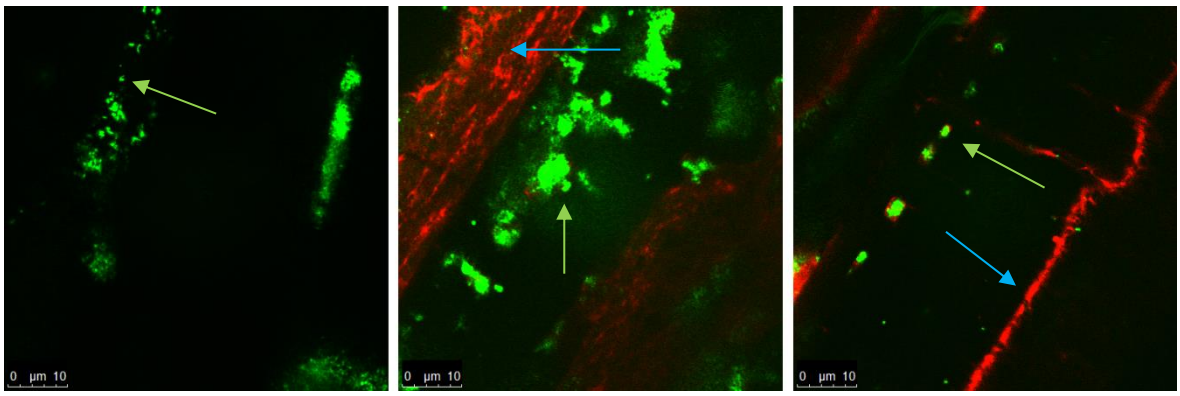

Figure 5-19: Confocal microscope images of LIVE/DEAD stained *H. sal* NRC-1 entombed in fluid inclusions within halite crystals. The green points are the microbial cells within fluid inclusions (examples highlighted by the green arrows), whereas the red areas are the halite crystal which has interacted with the PI stain (examples highlighted by the blue arrows).

5.2.3.3.2 Raman spectroscopy: z-axis mapping

As the confocal microscopy did not produce the expected results, detection of the isolates within fluid inclusions in the crystals using *z*-axis mapping Raman spectroscopy was attempted. The method is described in Section 2.5.7.1. Figure 5-20 shows a composite image of a halite crystal with fluid inclusions containing halophilic microbes, seen as pink areas. For analysis of the data, the definitions for band intensities were used, as suggested by Vandenabeele *et al.* (2012), described in detail in Section 3.1. To determine whether there was any correlation between UV exposure and *z*-axis, for each map, at a given band position the pre-exposure data were filtered by selecting only points that had intensities that related to a medium-weak intensity or above (where the lower limit of a medium-weak band was 35 % of the most intense band) to remove the weakest signals that may only be fringes of fluid inclusions.

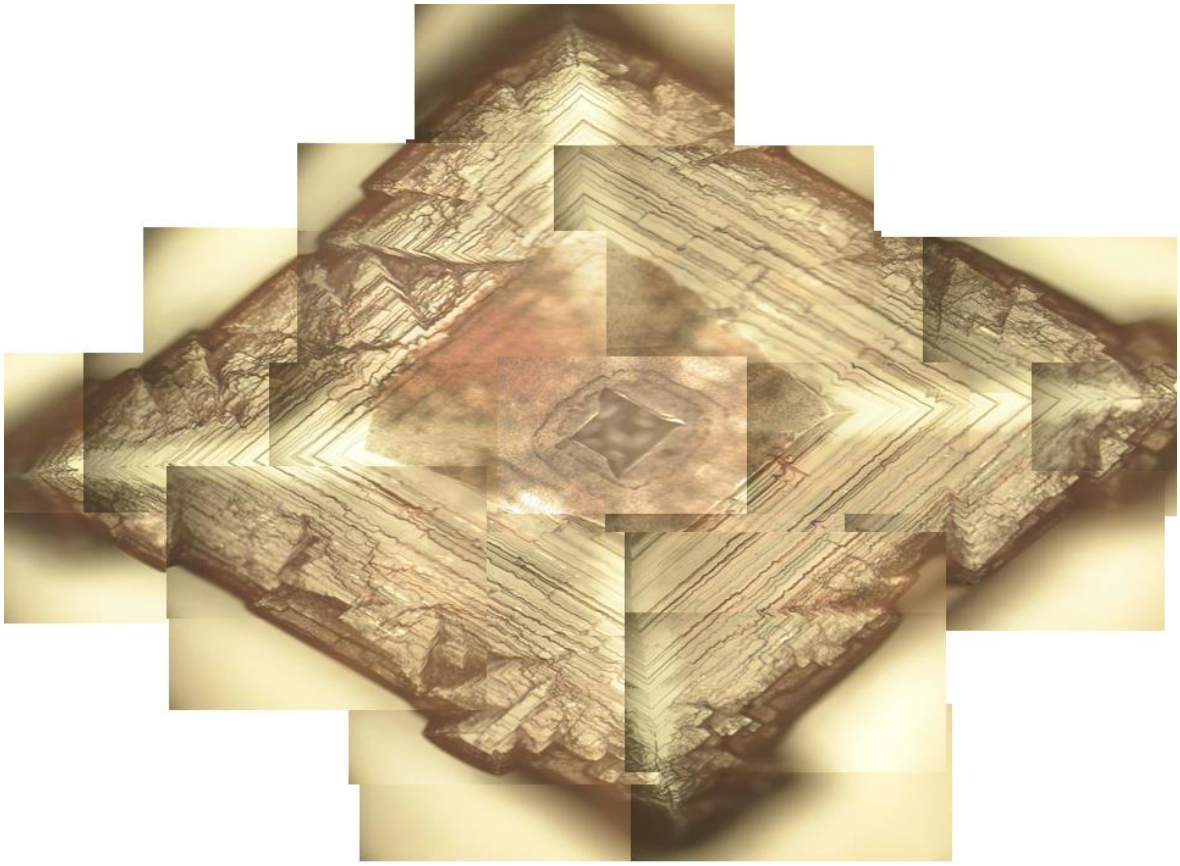

Figure 5-20: A composite image of a halite crystal containing fluid inclusions with entombed halophilic microbes. The hopper structure of the crystal is clearly visible. Each image was captured using the ×10 aperture lens on the Raman spectrometer. Image appears more like a diamond rather than the classic cubic shape expected, only because it is a composite image and the dimensions are irregular.

As a result of the filtering, of the data total acquired, 16, 13 and 13 % remained for *H. sal* NRC-1, N3.1 and N4.1b, respectively. As fluid inclusions were not the major structure of the crystal, these percentages related directly to the percentage of the crystal with fluid inclusions. From visual inspection of the microscope images from the Raman spectrometer, it was ascertained that these percentages corresponded approximately to the number of pink areas seen in the images. The pre-exposure intensity was compared to the post-exposure intensity, shown as a ratio in Figure 5-21.

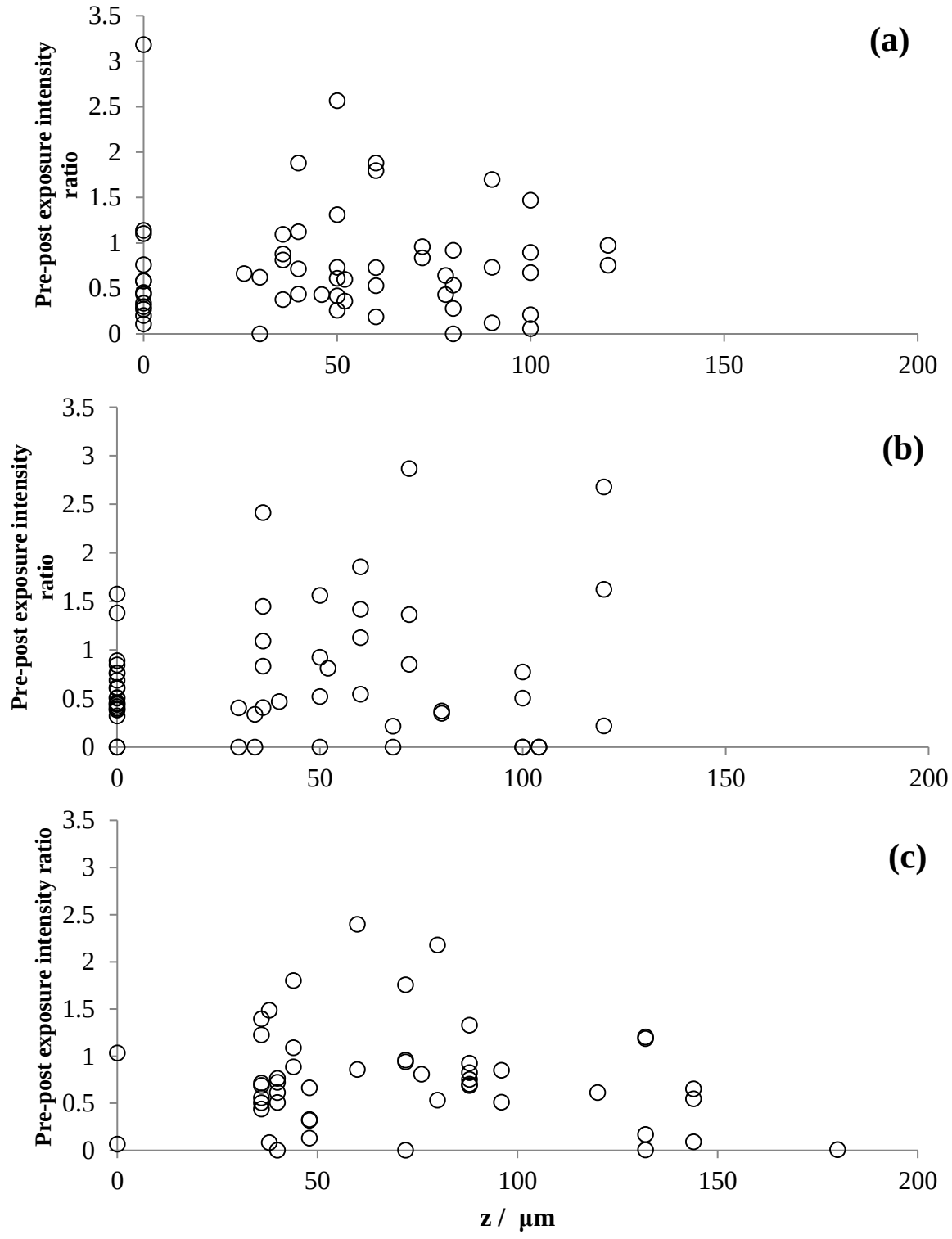

Figure 5-21: The ratio of the intensity of the Raman band 1507 cm^{-1} before and after exposure to martian conditions with respect to the depth of the microbes within the halite crystal. (a) *H. sal* NRC-1, (b) N3.1 and (c) N4.1b.

A majority of the bands recorded were reduced to 95 % or less of the original intensity (75.0 %, 71.7 % and 72.3 % of the *H. sal* NRC-1, N3.1 and N4.1b data, respectively), where 37.5 % (*H. sal* NRC-1), 34.7 % (N3.1) and 21.3 % (N4.1b) of the data were reduced to 50 % or less of their original intensity. Despite the majority of bands being reduced, and hence the assumption that some to all of the bacterioruberin pigment in the samples was destroyed by the UV, there appeared to be no correlation to suggest that crystals protect the microbial communities in the fluid inclusions to depths of up to 180 µm.

The relative changes in intensity, *i.e.* between the pre- and post-exposure data, were subjected to statistical *t*-tests to determine whether there was any statistical significance in the intensity of the bands with depth, the results are shown in Table 5-8. A paired *t*-test was used as the same crystal samples were investigated pre- and post-exposure and measurements were recorded at the same positions on each crystal. The significance level used was $\alpha = 0.05$ and the null hypothesis was that there would be no statistically significant difference between the intensity of the bands in relation to depth before and after exposure to simulated martian conditions.

Test	*t*	*df*	*p* (one-tailed)	*p* (two tailed)
		H. sal NRC-1		
0 to 200 nm	2.93	55	0.0025	0.005
0 nm	0.71	12	0.25	0.49
1 to 50 nm	1.62	17	0.06	0.12
51 to 100 nm	3.14	22	0.0024	0.0048
101 to 150 nm	1.60	1	0.018	0.36
		N3.1		
0 to 200 nm	2.72	55	0.0044	0.0087
0 nm	4.91	20	< 0.001	< 0.001
1 to 50 nm	0.90	13	0.19	0.38
51 to 100 nm	0.79	15	0.22	0.44
101 to 150 nm	−0.02	4	0.49	0.98
		N4.1b		
0 to 200 nm	3.71	48	< 0.001	< 0.001
0 nm	0.97	1	0.25	0.51
1 to 50 nm	2.43	18	0.013	0.026
51 to 100 nm	0.94	18	0.18	0.36
101 to 150 nm	2.51	7	0.02	0.04

Table 5-8: Results from *t*-tests on the relative intensity of the strongest Raman band pre- and post-exposure with respect to depth in a halite crystal. The *t*-test on the full depth of the crystal is highlighted in grey. The other tests were binned into 50 nm depth intervals.

The first row in the table (highlighted grey) for each isolate shows the overall *p* values for all the combined data collected for 12 halite crystals, each of which originally had an *x*-*z* map of 30 Raman spectra (total of 360 measurements); though, as described above, only the spectra that had Raman intensities that were classified medium-weak or above were used to denote the positions in the *x*-*z* maps of the fluid inclusions containing microbes in the crystals. This reduced the number of data points to 56, 56 and 49 spectra for *H. sal* NRC-1, N3.1 and N4.1b, respectively. The resulting *p* values were all less than the significance level of 0.05, suggesting that throughout the crystal there was a statistically significant difference in the intensity of the Raman band pre- and post-exposure to simulated martian conditions, with respect to depth in the crystal.

However, if *t*-tests were conducted on the relative intensities at varying depths in the crystal, the results showed there were some statistically significant differences depending on the depth. Note that as the position of the fluid inclusion was random, some were at a greater depth that others, this was reflected in the varying number of measurements seen at each depth for each isolate, *i.e.* the number of measurements for each isolate at different crystal depths was not comparable between the isolates.

For *H. sal* NRC-1 the null hypothesis (that there was no difference pre- and post-exposure) was not rejected at the surface of the crystal (0 nm) and between 1 to 50 nm, with *p* values of 0.49 and 0.12, respectively. At a deeper point in the crystal, between 51 to 100 nm, the *p* value was 0.0048. A sample size of two, at a depth of 101 to 150 nm, resulted in a *p* value of 0.36. This would suggest that microbes at the surface of the crystal were not damaged to the extent that it was statistically significant, while microbes deeper in the crystal showed that the intensities were statistically significant. The results for the *t*-tests for the crystals for N3.1 did reject the null hypothesis at the surface of the crystal (0 nm, $p > 0.001$), but throughout the rest of the depth of the crystal, there was no statistically significant difference at each depth tested. These results are opposite to those for *H. sal* NRC-1, suggesting that the surface microbes were affected by the exposure, but those deeper in the crystal were not. For N4.1b, there were only two sample points at the surface, resulting in a *p* value of 0.51, at lower depths the sample sizes increased and the *t*-tests resulted in *p* values of 0.026, 0.36 and 0.04 at 1 to 50, 51 to 100 and 101 to 150 nm, respectively. The null hypothesis was not rejected at the surface and at 51 to 100 nm, but there was a significant difference at 1 to 50 nm and 101 to 150 nm.

5.3 Discussion

The aims of this chapter were: (1) to determine whether halophilic microorganisms entombed within halite crystals can survive Mars simulated conditions, and (2) to determine whether their Raman signatures remained detectable after exposure (*i.e.* Raman spectroscopy can be used as a life detection tool). Mars-like near surface conditions were not overly detrimental to any of the isolates, though the longer that the samples were exposed to Mars-like surface conditions, the more difficult it became for the microbes to survive and for their Raman signature to be detected, as discussed in the Sections below.

Simply entombing cells in halite crystals had a detrimental effect on the specific growth rates of *H. sal* NRC-1 and N4.1b. The isolate N3.1 had a slower growth rate compared to the other two isolates in the liquid media and showed a similar growth rate after being entombed in halite. The growth rate in a liquid media for *H. sal* NRC-1 showed a preferential rate in comparison to previously reported growth rates (*e.g.* Joo and Kim, 2005; Ha *et al.*, 2007).

5.3.1 Survivability of halite entombed halophiles exposed to Mars-like conditions

5.3.1.1 Near surface martian conditions

Simulated exposure had a detrimental effect on growth compared to the ambient controls the μ was 0.001, 0.008 and 0.005 slower, for *H. sal* NRC-1, N3.1 and N4.1b, respectively. Smaller μ values, implied that the doubling time for the species had slowed as a result of a stressor (Egli, 2009), in this case, Mars-like near surface conditions.

For consistency with the UV exposure experiments the microorganisms were only exposed for approximately 26 min at the cold sublimation temperature of CO_2 ice at –80 °C.

Although the specific growth rates were slower after exposure, the total number of cells in stationary stage, compared to the controls, for *H. sal* NRC-1 and N3.1 were not significantly different. However, the total number of N4.1b cells were 25 % less compared to the total number of cells that grew in the control (ambient, halite) samples, indicating that the near surface conditions affected some of the microbes enough to reduce the total growth in the growth medium post-exposure; though there was no statistically significant difference in the μ values between the control (ambient, halite) samples and the near surface samples. Further testing would have to be conducted to confirm if this cell number reduction was repeatable, but a possible explanation could be that N4.1b was less able to adapt to the sudden cold (–80 °C) conditions. A sudden freezing of the cells could cause them to lyse more readily than if they had a longer time period (*i.e.* a slower freeze-thaw regime, see Section 5.3.1.3) to adapt by increasing their salt content and hence, decreasing their freezing point (*i.e.* a sudden freeze would cause any water within the cell to expand, possibly lysing the cell) (Mazur, 1984).

5.3.1.2 Martian surface conditions

This study demonstrated that microbial halophiles survived when entombed in halite and exposed to the simulated martian UV, pressure, atmospheric composition and temperature, which built on previous studies that exposed samples to UV in an otherwise terrestrial environment. From the results of this study, of particular interest is N3.1, the total cell numbers were not significantly different to the control (ambient, halite) samples; whereas for *H. sal* NRC-1 and N4.1b after a dose of 524 kJ m^{-2} the survival was reduced to 6 % and

10 % for *H. sal* NRC-1 and N4.1b, respectively. *H. sal* NRC-1 had a previously reported D_{37} of 148 kJ m^{-2} (Fendrihan *et al.*, 2009a), which was lower than the D_{37} recorded in this study by almost a factor of two, suggesting the microbes were able to survive higher dose rates in this study. Though there were a similar number of cells per aliquot, the volume of the aliquot used in this study was half to a third smaller than previously used, which led to smaller crystal sizes when solidified. Hence, fluid inclusions would have more cells per inclusion that those in previously reported data, which, in this study, could have provided more shielding and therefore a greater D_{37}. Furthermore, these samples were exposed to a higher dose of UV radiation (3.54 times the D_{37} dose for halite entombed *H. sal* NRC-1 (*ibid*)). Future work could study the effects of cell density in fluid inclusions relative to survival rates and could use analytical techniques such as TEM imaging to examine whether the cells were deformed or mutated post-exposure, which would explain the lower total cell number.

However, the paler colour of N3.1 (assumed to represent less bacterioruberin in the cells and hence, less UV protection) contradicts these results. Other than almost entirely adequate shielding occurring as a result of fluid inclusion stacking or an unknown secondary UV protection method (considering that the bacterioruberin Raman bands were entirely destroyed, see Section 5.2.3.2.2 and 5.3.4.1), a partial explanation could be the non-uniform UV footprint allowed for the possibility that some samples may not have received the correct dose (see Figure 2-11), however, the placement of these samples were not dissimilar to the other two isolates (*H. sal* NRC-1 and N4.1b) and would have received the same exposure (see Figure 5-22). Therefore, with the current data it was not possible to understand why the survival of N3.1 was relatively high, while paler in colouration compared to the other isolates, expectation was it would have less protection from UV.

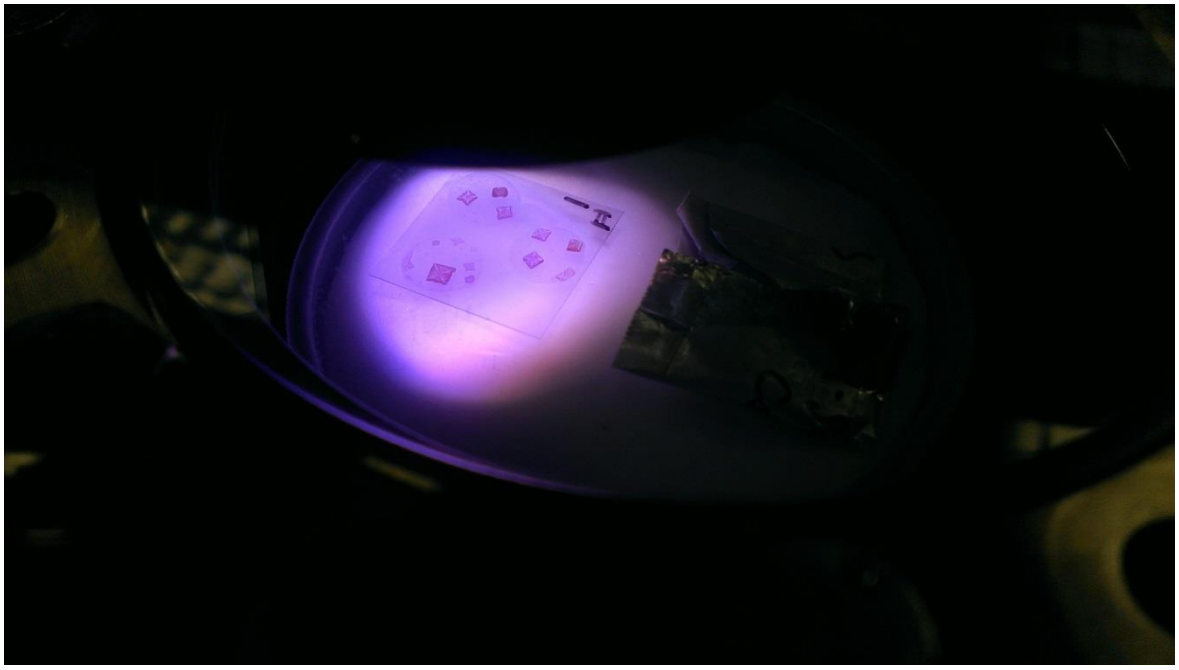

Figure 5-22: A typical placement of samples when conducting UV radiation exposure experiments.

Hence, to understand the resilience of this species, the survival experiments should be repeated, parallel to other investigations described in future work.

The extrapolation for the length of survival for *H. sal* NRC-1 and N4.1b yielded R^2 values (the fit of the trend line to the data) of 0.922 and 0.957, respectively; where a value of 1 would be an exact fit. However, because of the extremely large UV dose that would be required to administer the calculated D_{37} dose, the resulting R^2 value for the N3.1 data was 0.573; hence, the extrapolation must be considered with caution, especially as the calculated D_{37} dose was longer than the age of the Universe, let alone the Solar System (!).

The halite entombed isolates were monitored for growth after exposure by placing the coverslip glass to which the halite crystal was attached into a test tube of growth media. This was not an ideal method, it allowed for the glass potentially interfere with the OD measurement, which on occasion was evident when measurements were unusually high (*i.e.* the added thickness of the glass coverslip would increase the OD reading) and when

repeated with a more favourable placement of the glass coverslip in the test tube, gave a closer to expected measurement. When recording OD measurements, the coverslip shard was positioned so that it was 'side-on', *i.e.* parallel to the light beam in the spectrophotometer, and to one side of the test tube (always the same side to retain continuity), hence reducing the interference in the measurement. To ensure that OD measurements were not impeded by the coverslip glass, in future experiments the halite crystals could be dislodged from the coverslip using a scalpel (or similar) when inoculated into the growth medium, rather than placing the shard of coverslip into the medium with the halite crystal attached. Conversely, the advantage of placing the coverslip shard in the medium was that contamination was limited as no implement had touched the halite crystal since it was created.

Of 39 exposure experiments, 27 recovered (see Appendix B) post-exposure suggesting that small amounts of Mars-like UV radiation can be survived by halophiles, though this may result from a combination of shielding by stacked fluid inclusions and halite UV attenuation. Nonetheless, the fact that not all survived indicated that martian UV radiation can be fatal and damaging to the microbial communities. It is likely that those that did survive would not continue to survive with further exposure. Assuming similar microbial halophilic-like life could have evolved on Mars, the implication of the results from this study would mean for the best chance for survival, it would either have to rely on geological processes to keep it below the surface (or only expose it for a short period of time, a sol or less) or have evolved a much greater UV resistance than that which has evolved in terrestrial microbial halophiles, as UV exposure was the most damaging environmental factor of those tested here.

5.3.1.3 Mars-like freeze-thaw temperature cycling

All the microbial species studied here were able to survive a freeze-thaw cycle that was representative of a Mars-like environment. It was previously unknown whether N3.1 and N4.1b would tolerate a freeze-thaw cycle, and whether *H. sal* NRC-1 would tolerate freeze-thaw cycling in combination with other simulated martian conditions. The fact that *H. sal* NRC-1 survived the freeze-thaw cycles in this experiment is in agreement with the results found by Mancinelli *et al.* (2004). Mancinelli *et al.* (2004) air-dried samples of microbes, including *H. sal* NRC-1, onto quartz discs (the method was suggestive of crystal formation but never explicitly states this was the case, so the microbes may have been directly exposed to freezing conditions) and exposed them to ten freeze-thaw cycles (between –22 and 22 °C or –80 and 22 °C) over 144 days, which *H. sal* NRC-1 was able to survive.

This study showed that all the isolates showed signs of stress as a result of exposure, which was exhibited as a reduction in the growth rates (Figure 5-7); of which, the μ value of *H. sal* NRC-1 was statistically significant compared to the control (ambient, halite) samples, though the μ values for N3.1 and N4.1b were not. Nonetheless, the results are in agreement with previous freeze-thaw work with *H. sal* NRC-1 and this study demonstrated that the two unclassified species, N3.1 and N4.1b, were able to survive freeze-thaw conditions even though they were isolated from Mallorcan salterns, where the temperature rarely gets near 0 °C.

The results suggest, that if halophiles existed in the subsurface of Mars, they may possibly survive the freezing conditions, as demonstrated by the near surface simulation experiment, which demonstrated that they could survive brief exposure to near –80 °C. Furthermore, halophiles may have adapted as the climate of Mars changed and became

colder, adapting to the long-term to freezing temperatures experienced on present day Mars; similar to the microbial life that adapted to survive in an ice-sealed lake in Antarctica, which has a temperature of –13 °C, and is a closed ecosystem thought to have existed and been isolated for millennia (Murray *et al.*, 2012).

The presence of flowing liquid water at the surface of Mars, in the form of perchlorate brine (Ojha *et al.*, 2015), allows for the possibility of movement of nutrients and microbial cells to and from the surface and subsurface, which could also apply to possible halite brine reservoirs. Furthermore, martian salts contain fluid inclusions and have deliquescent and/or colligative properties (*ibid*). Survival of halophiles trapped within fluid inclusions in halite crystals exposed to a relatively rapid but prolonged freeze-thaw cycle in this experiment suggest that halophilic microbial entombed within halite may survive extended freeze-thaw processes.

5.3.2 Morphology of halophiles

TEM imaging showed a thickening of the cell wall (Figure 5-8b, Figure 5-9b), which was a distinct response to the UV radiation by the halophilic microbes, hence this study showed that an archaeal halophilic species exhibited a similar reaction as samples of cyanobacteria in a study by Olsson-Francis *et al.* (2013). The amount of bacterioruberin has evolved with the microbes to protect them from a telluric level of UV radiation (Shahmohammadi *et al.*, 1998); however, in this case, the microbes were exposed to a higher intensity and a wider range of biologically damaging UV wavelengths compared to the terrestrial range. Although most cells were damaged for all the species, it is possible that the colonies provided shielding for some of the lower cells and they remained viable. To test this, future experiments could use LIVE/DEAD staining (or similar) to confirm the viability of cells

after exposure. The morphology of the cells suggests that they are no longer viable, which is in agreement with the resulting growth (or lack thereof) of the microbes exposed to UV.

5.3.3 Raman spectra of control samples

The Raman spectra of the three microbial species were very similar (Figure 5-13, Figure 5-14); though the intensity of the bands varied, the microbes were indistinguishable as they all produced the same band pattern, which leads to the conclusion that they all have the same C_{50} carotenoid, bacterioruberin; known to be present in *H. sal* NRC-1 (Jehlička *et al.*, 2013), this was previously unknown for the isolates N3.1 and N4.1b. Furthermore, the Raman intensity from N3.1 was generally much weaker than the other two; this could be explained by the paler colour of the species as shown in Figure 5-23 and Figure 2-15, which suggests that this species does not have as much bacterioruberin as the other two species (which could be tested by examining the percentage component of the cell concerning bacterioruberin, by freezing then lysing the cells, allowing for the carotenoid to be extracted, similar to the method used by Kelly *et al.* (1970)). An expectation resulting from this was, compared to the other two species, N3.1 would be less likely to survive in martian surface conditions (*i.e.* a harsh UV environment). However, this expectation was contradicted in UV exposure survival tests (see Section 5.3.1.2).

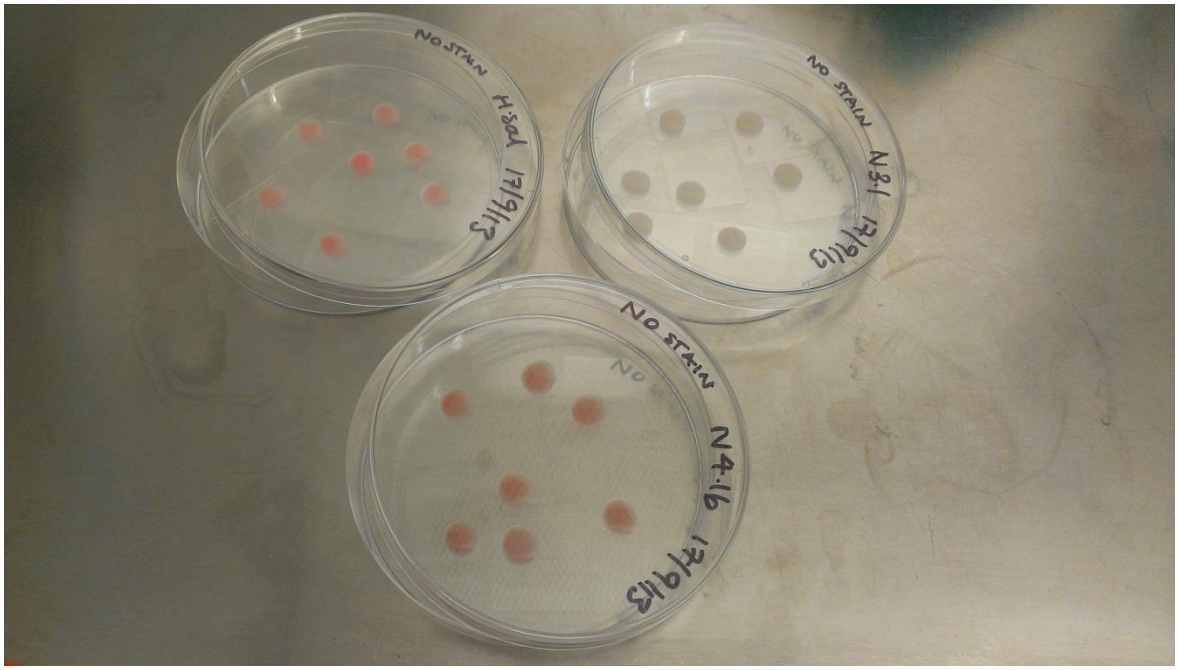

Figure 5-23: The media suspension of each of the microbial species as 20 µl aliquots on microscope cover slips in sterile Petri dishes in the laminar flow hood to be left to dry into halite crystals with the microbes trapped within fluid inclusions. Comparatively, N3.1 is much paler in colour than *H. sal* NRC-1 and N4.1b.

5.3.4 Life detection method using Raman spectroscopy

5.3.4.1 Analysis of UV exposed microbes using Raman spectroscopy

The reduction of the relative intensities of the Raman bands pre- and post-exposure shown in Figure 5-15 demonstrated that the Raman intensity is likely to be connected to the quantity of molecules as the intensity was reduced after exposure to UV radiation, which had probably destroyed the bacterioruberin molecules in the microbes. This is in agreement with Dartnell *et al.* (2012), who saw a reduction in the Raman intensity of biomarkers after exposure to ionising radiation. Previously, Vandenabeele *et al.* (2012) have alluded to a relationship between the quantity of a molecule and the intensity of the Raman spectrum, discussed in further detail in Section 1.5.4, though further work needs to be conducted to understand this relationship. Raman spectroscopy is often qualitative and interpreting the

Raman intensity as a quantitative measurement is difficult because, for example, of external factors such as influence from fluorescence created by ambient light, noise and offset from the CCD detector and other optical components; furthermore, a direct, quantitative comparison between spectra made on different Raman systems is difficult.

The complete or near destruction of the Raman bands in the N3.1 samples was contradictory to the (average) 88 % survival rate of entombed cells (Section 5.2.2.3) and extrapolated D_{37} dose of 1.2×10^{22} kJ m^{-2} of this isolate when exposed to UV. The assumption was that survival of cells was related to the destruction of the Raman signal, which appeared to hold true for *H. sal* NRC-1 and N4.1b. Hence, for N3.1, future work would investigate whether some other UV shielding (fluid inclusion stacking or halite attenuation) or DNA repair method had occurred.

5.3.4.2 Raman spectroscopy of samples exposed to freeze-thaw cycles

Little to no effect was seen in the relative intensities pre- and post-exposure (Figure 5-17), but the intensities of the Raman bands did reduce in the post-exposure spectra compared to the pre-exposure spectra (Figure 5-18), by approximately one third, which suggests that the freeze-thaw cycle was affecting the relative amount of the carotenoid molecule within the sample (*i.e.* the measured intensity did reduce but individual bands were not reducing at relatively different rates). It was possible that a portion of the cells were destroyed during the freeze-thaw and an extended freeze-thaw cycle may have seen total destruction of this Raman signal. As the microbes appeared to be relatively unaffected by the freeze-thaw cycles when detecting their carotenoid Raman signal and examining their survival (Section 5.3.1.3), it further supports the necessity to collect samples from the near surface during future missions, which could be a habitat for similar microbial life.

5.3.4.3 Halite crystal *z*-axis investigation

From the outcomes of the LIVE/DEAD experiments, issues with staining cells before exposure were highlighted: (1) to avoid the dye binding to the crystal structure, cells would have to be washed after being stained. However, once the cells were exposed to UV radiation, there would be no excess dye to stain those with damaged membranes and post-exposure staining would not work as discussed in Section 5.2.3.3.1. (2) The LIVE/DEAD kit uses fluorescent dyes; photobleaching because of extended exposure to UV radiation is likely to occur. However, even if it did not occur (the intensity of the LIVE/DEAD kit dyes did not appear to reduce significantly during examination with the confocal microscope, compared to a sample stained with SYBR® Green where photobleaching occurred almost instantly), the dye binding to the crystal structure meant this could not be tested effectively. In conclusion, it was not possible to examine successfully the structural information of a halite crystal with microbes entombed and determine whether they were viable or not after exposure to UV radiation.

Figure 5-21 showed the ratio of the intensity of the 1507 cm^{-1} band (the major band of the C_{50} carotenoid found in these microbial species) pre- and post-expose to Mars-like UV radiation. A reduction in intensity is assumed to be directly or proportionally related to the reduction of the molecule in the sample as a result of destruction by the UV radiation, though the relationship is not known. This is in agreement with previous research that has shown Raman bands to be reduced after exposure to ionising radiation (*e.g.* Dartnell *et al.*, 2012). By extrapolation of these results, it is possible to suggest that further exposure to martian conditions would erase any evidence of the carotenoid bands recorded in the Raman spectra.

The anomalous results, which accounted for 21.4, 26.1 and 25.5 % of the data, where the post-exposure band intensity was greater than the pre-exposure band intensity (Figure 5-21), could be explained by the possibility that the microbial culture within the fluid inclusions continued to multiply, using the nutrients available, increased their population and more carotenoid signal was available to be measured (between four and eight days passed between entombing and the final post-exposure Raman spectra were measured, which was because of the length of time it took to acquire the Raman spectra). Another possible explanation for a greater intensity band post-exposure could be that in defence of UV radiation exposure, the microbes were producing more bacterioruberin to counteract the production of damaging free radicals. There are numerous studies on the DNA repair mechanisms performed by *H. sal* NRC-1 (*e.g.* McCready, 1996; Shahmohammadi *et al.*, 1998; Asgarani *et al.*, 1999; DasSarma *et al.*, 2001; McCready and Marcello, 2003; Baliga *et al.*, 2004), but whether or not the UV stressor forces the production of bacterioruberin to increase, decrease or remain steady is not addressed. The measurement of a greater intensity of bacterioruberin bands could be evidence of increased production because of a UV stressor in the microbes exposed directly, *i.e.* those at the surface or at the top of a fluid inclusion stack.

When subjected to *t*-tests, the full set of data for each isolate entombed in halite showed that there was a statistically significant difference in the intensities of the Raman spectra pre- and post-exposure (Table 5-8). This would indicate that the halite did not provide enough shielding to prevent the microbes from being too damaged or destroyed. Though when the data were binned into 50 nm depth profiles, some data were, counter to expectation, not affected by the UV radiation at the surface of the crystal, but were affected deeper in the crystal. Furthermore, there was no overall variation in the ratios of the intensities, so it was difficult to make a meaningful interpretation from these data.

Some attenuation was expected, following the result from Fendrihan *et al.* (2009a), where the transmittance of the UV radiation was between about 40 and 70 % (*i.e.* reduced by up to 60 %) in the 200 to 400 nm range. The transmittance and reflectance in halite of the wavelength range 200 to 800 nm was measured, though the thickness of the crystals tested was not provided (*ibid*). However, as the crystals in this work were generally between 200 to 250 nm in thickness, future work would study a wider range of thicknesses in greater detail, using a spectrometer (*e.g.* like that described in Section 2.3.3) to measure the UV output at the surface of the crystal and the underside of the crystal to gain a better understanding of the attenuation provided by the halite, followed by halite crystals with halophile entombed to further understand the level of shielding provided by microbial colonies entombed within fluid inclusions. Furthermore, this would allow the testing of the possibility that the halite created focus points of UV at different depths and hence, why some depths the intensities were not significantly different and other were, contrary to expectation.

5.4 Summary

In this chapter, microbiological techniques were applied to three isolates of halophilic archaea: *Halobacterium salinarum* NRC-1, *Haloferax* N3.1 and *Haloarcula* N4.1b. Each isolate was grown in a liquid culture and was also entombed in artificial halite and exposed to ambient conditions (*i.e.* not exposed to simulated martian conditions) to obtain a baseline for its growth pattern and the approximate time at which its log phase of growth would occur and furthermore, their μ values. As an analogue for martian evaporitic environments, the isolates were entombed in halite crystals and tested for their survivability in simulated martian surface and near surface conditions. The halite entombed

microbes were exposed to simulated martian UV conditions of varying lengths, up to one sol of expected irradiance. After approximately half a sol of exposure or more, most of the samples did not recover when inoculated into a test tube of growth media. Those that did were suspected to either have had enough of the cells shielded as a result of a combination of shielding by other cells in the fluid inclusions and/or UV attenuation by the halite. Furthermore, those that did recover often had an extended lag phase and grew more slowly, indicating that the cells were stressed by the UV exposure by taking longer to start logarithmic growth and the doubling time is reduced once it does start. Despite failing to survive surface conditions, samples that were exposed to near surface (*i.e.* as though the samples were buried by a few mm of regolith) and Mars-like freeze-thaw cycles did survive.

Examination with TEM confirmed that the microbes were rendered unviable because of the exposure to UV radiation. Compared to cells that did not experience any UV radiation exposure, exposure caused changes to their morphological shape and there was evidence that the cell walls had thicken in response to the exposure. Furthermore, some cells had been lysed as a result of the exposure.

Having shown that these isolates, two of which are, at the time of writing, unclassified strains, were able to survive some simulated martian conditions, are they detectable by life detection apparatus? The *ExoMars* mission, due for launch in 2020, will carry a Raman spectrometer and a similar instrument is proposed for the NASA *Mars 2020* rover. Raman spectroscopy can identify minerals and organic molecules, as each has its own ‘fingerprint’ spectrum. A bench-top Raman spectrometer was used to identify the Raman bands of the microbes, originating from a molecule that provides protection from UV radiation and DNA repair: bacterioruberin. They were entombed in halite as there is some evidence for

halite crystals on Mars and halite has no Raman active bands in the ‘fingerprint’ region for organic molecules when excited with a 514 nm laser.

Exposure to freeze-thaw conditions reduced the overall intensity of the carotenoid biomarker but did not entirely destroy the Raman spectra of the microbes entombed in halite; hence, the cells remained detectable. As discussed above, exposure to UV rendered the microbes unviable and in many cases the entombed isolate samples were unable to re-establish a colony after exposure to up to a sol of simulated martian UV. However, when examined using a Raman spectrometer, the bands from halite entombed microbes were still detectable; suggesting that though the cells may be unviable, a biomarker from a UV protecting pigment, such as bacterioruberin, may still be detectable on the surface of Mars on future planetary missions with Raman spectroscopy.

6.Conclusions and Future Work

6.1. Introduction

The research questions that were set out to be answered in this thesis, as stated in Chapter 1, were:

RQ1. Using statistical techniques, can a set of characteristic Raman bands be rigorously defined for use as identifiers of amino acids?

RQ2. Does exposure to the martian near surface and surface conditions affect the Raman spectra of amino acids?

RQ3. Can halophilic microbial life entombed within halite crystals survive when exposed to coupled martian conditions and their Raman signatures remain detectable?

Each of these questions were answered in the results chapters: Chapter 3, 4 and 5, respectively. This chapter will present the conclusions of each of those chapters, which will address the research questions (Sections 6.2.1, 6.2.2 and 6.2.3, respectively). Following the conclusions, future work that could be conducted following the work in this study is presented.

6.2. Conclusions

6.2.1. Defining a set of characteristic Raman bands using a statistical method

In this study the need to define a set of identifying characteristic bands for astrobiologically relevant molecules, such as the proteinogenic amino acids, has been emphasised (opposed to the single strongest band to be used as an identifier). In previously published work, analysis of Raman spectra is often qualitative and conducted at one excitation wavelength across a number of different Raman spectrometer systems. This leads to discrepancies in the reporting of band positions, which, in an unknown sample may lead to an incorrect or non-identification of a particular molecule, especially as often only the strongest bands are acknowledged as an identifier of the molecule.

In this study the astrobiologically relevant amino acids L-alanine, L-aspartic acid, L-cysteine, L-glutamine and glycine were examined. Several bands per molecule have been quantitatively characterised that could be used to positively identify the amino acids (Table 3-2 and Table 3-3) in a future unknown sample. Comparing the 514 and 473 nm band positions did show a statistically significant difference in the relative wavenumber differences (RWDs) for some of the bands in the spectra as a result of minor differences in the Raman spectrometer – one to higher relative wavenumbers (glutamine) and one to lower relative wavenumbers (aspartic acid); the band positions of three of the molecules were consistent within the instrument accuracy of the spectrometer (glycine, alanine and cysteine), however an increase in the scattering of the data was observed, respectively. Nonetheless, the differences were small enough (< 2 cm^{-1}) that studies using lower resolution Raman spectrometers would be able to use the defined characteristic bands.

Any future missions using excitation wavelengths in the red optical, IR or UV should repeat the statistical method defined here to confirm the characteristic bands at these higher/lower excitation wavelengths as the Raman activity of bonds in a molecule and hence, intensity of bands can differ between excitation wavelengths; the characteristic bands could be different outside of the excitation wavelengths considered in this study.

Another factor that could affect the identification of a molecule in an unknown sample is the orientation or the angle of the crystal, which affects the intensity of the bands. This study has shown that the intensity of bands can differ by a factor of five because of the orientation of the sample. Hence, bands that could be characteristic of a molecule but had a reoccurring low intensity were not likely to be treated statistically, because of the criteria discussed in Section 3.2.3, *i.e.* the initial stage of the statistical method was to remove the bands that did not appear in the spectra within the upper quartile of frequency, so to remove bands that were too weak or potentially resulting from contamination. To reduce this effect, future studies defining characteristic bands for astrobiologically relevant molecules should take crystal orientation into account by rotating the sample or recording spectra at several points in the sample. The crushing system on board the *ExoMars* rover will crush samples in to a powder before Raman analysis is performed, with the intended grain sizes of approximately 20 to 200 μm (Edwards *et al.*, 2012a). The diameter of the spot size will be 50 μm (*ibid*), so the larger grains could potentially encounter issues with orientation effects of the minerals and possible biomarkers that may be contained in the sample (see Section 6.2.2 for related and further discussion on powdered samples).

Amino acids are a target in the search for life elsewhere in the Solar System and Raman spectroscopy could detect molecules pertaining to evidence for life. Future planetary surface missions that intend to use Raman spectroscopy, including that on board the *ExoMars* rover due for launch in 2020 and a NASA rover mission also scheduled for 2020,

may use differing excitation wavelengths. The grating used in this study has a high resolution in comparison to those likely to be used on future planetary missions. Hence, these results are providing an upper limit to the characteristic bands for use in identifying these amino acids in unknown samples, without having to define a minimal number of bands required to provide a positive identification of a molecule. The identification of substances relies on knowing accurately and unambiguously the band positions of potential target molecules in those spectra. Therefore, as an aid for identifying target molecules, defining the multiple characteristic bands using statistical methods of a molecule is crucial, otherwise an incorrect identification or a non-identification could occur of the minerals or organic molecules that are important in the search for evidence of life elsewhere in the Solar System. Hence, the work conducted here has answered RQ1, proving that a statistical method can be used to define rigorously a set of characteristic Raman bands for a given molecule and furthermore, this method does not need to rely on a minimal number of bands or the relative band intensity.

6.2.2. Detection of amino acids after exposure to simulated martian conditions

For (terrestrial) life, the environmental conditions on Mars are known to be relatively harsh in comparison to the Earth. Amino acids may be among the possible reserve of organic molecules that could exist on Mars. Exposure of biologically necessary amino acids to isolated and coupled simulated martian conditions in this work has shown it is possible for these molecules to remain detectable on (for at least a few sol equivalent UV doses) and near the surface of Mars.

The amino acids were not significantly affected by near surface conditions, which provided a shield to the harsher surface conditions and molecules appeared to be relatively stable. However, some of the amino acids were significantly affected by the Mars-like surface conditions, *i.e.* they were damaged or destroyed and became undetectable after a few sol equivalent UV doses, though some remained detectable throughout the experiments. Detecting amino acids (or biomarkers in general) at the surface of Mars will be highly challenging because of the UV radiation; though if geological or atmospheric processes (*e.g.* landslips, dust storms, dust devils) exposed previously unexposed regolith or rock that contained amino acids, they may be detectable. The amino acids may exist independently in the regolith or they could be generated by decomposing extinct or extant microbial communities. Overall, if amino acids ever formed on Mars, they may still be detectable (even if there was no current influx by external material or process of formation) if samples were retrieved from the near surface.

Having characterised the molecules in Chapter 3 and selected the characteristic Raman bands that could be used to identify unambiguously the amino acids in an unknown sample, the efficacy of this statistical method was proved when determining whether the amino acids could be detected amongst the mineralogical bands of a doped basalt. Upon doping onto the basalt surface, some of the characteristic bands were observable, and hence were able to be used as identifiers for the amino acids. However, not all the characteristic bands were observed, further enforcing the need for a set of characteristic bands that can be used to identify molecules in an unknown sample rather than just the strongest bands. Here, of the amino acids tested, some Raman bands of alanine, cysteine, glutamine and glycine were detectable, whereas no Raman bands for aspartic acid were observed.

These results, showing the stability of the molecules in near surface conditions, could help inform future missions with Raman spectroscopy, including the *ExoMars* rover. On future missions, samples that were removed from the near surface (and remained shielded or shielded as soon as possible, *i.e.* within one sol), would not be affected by UV exposure. However, though exposed to harsh surface conditions for at least five sol equivalent doses, some of the amino acids were still identifiable using the characteristic bands, even when doped onto a sample of basalt. Nonetheless, it is highly recommended that samples are shielded as quickly as possible to avoid harsh surface exposure to preserve any biomarker signature. It should be noted, though, that these experiments were conducted using a 1 % solution of amino acids, which is potentially a million to a billion times higher in concentration than what might be expected at the surface of Mars and, for example, in a terrestrial desert, samples contained a range from non-detectable to 100,000 ppb of amino acids when analysed by GCMS. It is not the case and it would not be realistic to assume a linear relationship between the number of counts recorded in a Raman spectrum and its concentration, as discussed in Section 1.5.4, however, if this broad assumption was made, the positive identification of amino acids made in this study would not translate to lower concentrations such as ppm or ppb. The instrument parameters used here would simply not detect the biomarker signal as the fluorescence present would cause the signal to be lost in the noise. Nonetheless, by changing some of the instrument parameters, such as decreasing the laser power and increasing spectral integration time, small concentrations of delicate organic material can be detected with the apparatus used in this study; for example, grains of interplanetary dust particles were successfully examined by Starkey *et al.* (2013) using the same apparatus. On future missions, it would be necessary to have an instrument able to detect minute concentrations (~ppm/ppb), this coupled with techniques such as sample mapping or line scanning and spectrum summation to increase the signal received from the

sample. It is possible that by sampling the near surface, where UV radiation would not affect biomolecules, concentrations would be higher.

On future missions, if a similar mineralogical composition of basalt was observed, from the results recorded here, alanine, glutamine and glycine could be unambiguously observed on Mars. Aspartic acid and cysteine would be difficult, if not impossible, to observe as they were either not detected (unambiguously) or had characteristic Raman bands obscured by the basalt bands. Note that this depends on the mineralogical composition of the regolith at any given sample point, different compositions could potentially obscure a different range of characteristic bands defined for the molecules.

Results from this study have crucially shown that the crushing of a regolith sample does not allow for the detection of geological or biomarker signatures (in this case, basalt and amino acids, respectively), which has also been observed in other recent studies. Crushing of samples regularly occurs for minerals such as pigments used in wall paintings (private communication, Jorge-Villar, Universidad de Burgos, 2017), so it may be the case that the extent of crushing has an effect, which would be explored in future work with respect to preparing for the *ExoMars* mission. On the *ExoMars* rover, if the design is fixed (*i.e.* it is not possible to allow for the Raman Laser Spectrometer (RLS) to engage with samples before they are crushed because of the instrument package design and layout), samples analysed by the RLS will have to use extremely specialist routines (detailed line spectra, pre-crush imaging, low power sample acquisition with extended iteration times and possibly spectra summation depending on the fluorescence that is measured) to be obtain meaningful information. However, the results of the tests in this study suggest that a significant amount of contextual information (mineralogical structures and biological signatures) would be lost once a sample is crushed. On future missions this may cause any biomarkers that exist in a sample to go undetected, hence it would be advisable to perform

Raman spectroscopy before a sample is crushed, as this would allow the most useful information that can be gained using this analytical technique to be acquired, even if other instruments on board require the sample to be crushed.

The results have achieved the aim of this chapter to use a Raman spectrometer as a biomarker (amino acid) detection tool for samples that have been exposed to a complement of simulated martian surface and near surface conditions. The overall result of asking RQ2 is that the Raman spectra were affected by the exposure to martian simulated conditions, though not so detrimentally (within a few sols) that they were rendered undetectable.

6.2.3. The survival and detection of halophiles in simulated martian conditions

The continued survival of all three test species (*H. sal* NRC-1, N3.1 and N4.1b) after exposure to coupled simulated martian conditions was previously unknown. The extent to which the near surface provided a potential habitat was encouraging for the search for life on Mars. Freeze-thaw cycles did not have a devastating effect upon survival, though exposure to sudden cold was more damaging. Exposure to the surface did bring on cell death fairly rapidly, though if life evolved on Mars, it is possible that the shielding techniques against UV would be more advanced than those present in terrestrial species (as the telluric UV wavelength range is smaller and less biologically damaging). Nonetheless, some Raman signal was still detectable after periods of exposure to UV, providing the possibility that a similar signal could be detected on Mars during future missions.

The presence of carotenoid such as bacterioruberin, which can be used for UV protection (*e.g.* Shahmohammadi *et al.*, 1998) is detectable by Raman spectroscopy and could be used towards confirming the existence of life on Mars as it is a molecule not found extensively

outside of biology. The Raman spectra of the microbial species, *H. sal* NRC-1, N3.1 and N4.1b, are indistinguishable from each other. Though detection with Raman spectroscopy of a carotenoid could initially help confirm (biomarker) signs of life on Mars, in the case of bacterioruberin-dominated species, future missions (including sample return) would have to apply other techniques (such as DNA sequencing) in parallel to Raman spectroscopy to differentiate any multiplicity of species that could exist on Mars.

Unless directly exposed to the surface conditions on Mars for a sol (or longer), which is fatally damaging, the entombed halophilic microbes exposed to martian conditions were fairly hardy and were shown to survive exposure to Mars-like surface, near surface and freeze-thaw conditions, with extrapolation to longer survival times in some cases. This study suggests that evaporitic environments at the surface are not likely to shelter halophilic microbes for longer than a sol or two of UV radiation exposure, though some longer survival could be possible if shielding occurs. As a lower limit, a halite crystal thickness of greater than 250 nm would be required for shielding (no conclusive evidence of shielding occurred up to this depth in this study) with the implication that any life that may exist at or near the surface of Mars would likely be fatally damaged if it was transported to this range of crystal thickness.

If microbial life could survive in the near surface, any future mission to Mars that raises samples to the surface should reduce exposure to UV conditions at the earliest possible opportunity to limit the effect of exposure on the Raman signal from carotenoid markers in the microbes. Ideally within a tenth of a daylight portion of a sol (approximately a dose of 50 kJ m^{-2}, which equates in real time on Mars to about 2.5 hr; to increase the time that a sample could be handled at the surface, extraction could begin after sunset). Freeze-thaw conditions showed a reduction in the intensity of the Raman spectra for bacterioruberin, but given the halophiles in this study have not evolved to withstand such a large range of

temperatures, it is probable that similar life on Mars would have had to have evolved to withstand these temperature cycles and the other near surface conditions. Future work could include the testing of polyextremophiles, in this case, a psychrohalophilic archaea, for example, *Halorubrum lacusprofundi* (Cavicchioli, 2006).

If life ever had an epoch on Mars, the evolution of halophilic life, pigments (such as carotenoids) though limited may be required for UV shielding for extant life at the near surface, *i.e.* if, on occasion, it is brought to the surface by geological or atmospheric processes such as landslips or dust storms. Mars is known to have evaporitic environments and free flowing brines (*e.g.* Squyres *et al.*, 2006; Ojha *et al.*, 2015) that are transported to and from the surface in a seasonal cycle, possibly diurnally on a localised scale. Furthermore, as halophiles are not directly reliant on photosynthesis, the implication of the near surface experiments suggest that similar microbial life could exist in the near surface or subsurface to escape the damaging UV radiation and to some extent the ionising radiation that interacts with the planet.

Evaporitic environments are wide-spread on Mars (Squyres *et al.*, 2006), providing many potential habitats (and/or last resorts for survival), therefore it is likely that they also exist in the subsurface. Some evidence for briny liquids at the surface is provided by Recurring Slope Lineae (RSL), which demonstrate the cycling of briny liquids to and from the surface. When the liquid retreats into the subsurface some remaining liquid may evaporate out into crystals trapping cells at or near the surface until the next cycle. Modelling has shown that deeper in the subsurface, as temperatures increase, liquids may be more common and free flowing (Monaghan, 2013), perhaps in aquifers, allowing the movement of nutrients and cells between locations. This work showed that cells could survive an environment similar to that of the martian near surface and could inhabit a near surface evaporitic environment such as RSL. However, there are some differences between the

simulation experiments conducted here and the martian environment that should be considered (which could be addressed in future work): the brine used here was a sodium-based brine, whereas the RSL brine was discovered to be perchlorate-based, this could have an effect on the habitability; previous studies have found that (sodium-based) halophiles were able to grow in low concentrations of perchlorate brine but at higher concentrations became damaged (Oren *et al.*, 2014). However, if perchlorate brines are dominant on Mars, any extant or extinct life may have evolved to live in perchlorate brine, hence, with no damaging effect at the higher concentrations (though it is likely that at an extreme concentration, as seen with terrestrial life, it would not survive).

The lifetime of an RSL at the surface is approximately one season; the freeze-thaw experiments here were approximated to one martian summer season, though the temperature range was not as wide as experienced on Mars (a minimum of −40 °C in the simulation compared to approximately −80 °C at the martian surface), hence survival of the microbes for the duration of the simulation would suggest that these isolates could survive at the near surface of Mars in an RSL, though further simulations would be required to test fully this, *e.g.* a martian temperature range, entombment in perchlorate-based crystals, longer temperature cycling (to simulate a martian year or longer), with and without exposure to some UV radiation to simulate the growth and decay of RSL at the surface. These differences between the simulations conducted here and the martian environment could be key in the true potential for any epoch of extant or extinct martian life.

The answer to RQ3 is two-fold: (1) the microbial species examined were able to survive martian simulated conditions, which for N3.1 and N4.1b was previously unknown and for *H. sal* NRC-1, the combination of martian conditions had not previously been explored. (2) On the basis that samples were not exposed for extended periods of time to martian surface conditions (greater than one sol), the Raman signature remained detectable, but soon deteriorated.

6.3. Future work

6.3.1. Amino acids

Though no definitive evidence of organic molecules has been found on Mars, missions at the martian surface are searching for indication that they exist, whether the origin is a native or external source. Amino acids are organic molecules that are necessary for terrestrial life and while searching for organic molecules, nitrogen bearing molecules have been detected by the *Curiosity* rover, where nitrogen is necessary for the structure of amino acids. To aid in the identification of astrobiologically relevant organic molecules on future planetary missions the following future work would be conducted.

Characterising the Raman spectra of the other 15 biologically relevant amino acids using the same statistical method that was developed in Chapter 3 would be the initial future work based on this study. This could then be expanded to other biologically relevant molecules, including carotenoids, DNA and ATP, which could be detected on Mars as signs of life, to create a database of sets of characteristic Raman bands (though this would be instrument relative).

Though a large percentage of the martian surface is basalt, there is evidence for clays and other water-altered minerals (which would be located in areas, for example, river beds, that life was potentially more likely to have started, remain extant or show evidence of extinct life). Determining the influence of other types of substrates when doped with amino acids and other potential biomarkers on their detectability and how the Raman bands react when exposed to simulated martian conditions would be of interest in future work.

Examining amino acids and other biomarkers with Raman spectroscopy, with a known concentration (and a known initial volume and mass), could be used to help determine the relationship between band intensity and concentration that is alluded to but with no studies yet having suggested one (this is non-trivial as the intensity of the bands in a spectrum rely on multiple factors). If a relationship between concentration and intensity was realised it would be possible to constrain more rigorously the survival of the amino acid molecules (with respect to the Raman band detectability) when exposed to extended periods of UV radiation. This would be important for understanding whether amino acids react at the surface of Mars or would need to be buried to survive over geological time periods; furthermore it would increase the understanding of the constraints needed to be placed on sample extraction and selection of collection sites when using Raman spectroscopy at the surface of Mars on future missions.

Constraining the energy requirements and chemical reactions that occur in the amino acid molecules, isolated and doped onto an analogue regolith, would be imperative to knowing whether life could harness any organic molecule reserves that may exist or existed on Mars (at the surface or in the subsurface). These calculations would be conducted in future work.

Terrestrial analogue samples containing naturally occurring biomarker molecules (and/or laboratory doped samples) could be analysed with Raman spectroscopy for biomarker signatures pre- and post-crushing. This would simulate the procedure to be performed on Mars by the *ExoMars* rover to determine the extent to which crushing may remove the ability to detect various biomarker signatures by Raman spectroscopy and whether, and to what degree, line spectra analyses or spectra summation would counteract the crushing of the sample.

6.3.2. Halophiles

The observation of RSL suggests the presence of transient near surface liquid water brines (McEwen *et al.*, 2011; 2013; Ojha *et al.*, 2015). There is speculation that these briny liquids could be a habitat for microbial halophilic life. Further probing with orbital and *in situ* measurements will reveal the extent of the brine reservoirs. Furthermore, evaporitic environments appear to be ubiquitous in areas previously known to have flowing liquid, such as Gale Crater currently being explored by the *Curiosity* rover. The RLS and other instruments on the *ExoMars* rover mission will be the first life detection instruments to search for biomarkers on Mars since the Viking missions in the 1970s. As a result of the geochemical evidence of brines, halophiles are an ideal analogue for studying life on early and present day Mars. Isolation and characterisation of halophilic microorganisms may increase our understanding of the physiological requirements for life on Mars.

The isolates N3.1 and N4.1b that were used in this study have not been classified (they could be classified via 16S RNA screening among other characterisation techniques, *e.g.* Jackman (2012)). Future work should be carried out to understand and characterise their growth in more detail and how they physiologically adapt to environmental stresses, such as UV radiation, low pressure and cold temperatures. The time at which the isolates would be exposed to near surface conditions could be extended to constrain the length of time that they could survive in low temperature and pressure environment, hence whether the survival at the near surface on Mars would be feasible and furthermore, whether microbial life could be detected there.

The microbes in this study, when exposed to the longer dose rates tended to experience a longer lag phase before entering the log phase, suggesting that they were stressed and took longer to adapt to their environment post-exposure. The lag phase is one of the most understudied areas in microbial studies (Rolfe *et al.*, 2012). In future work, it would be of

interest to study the stressed microbes that reside in the lag phase for an extended period of time, to understand the damage and/or recovery that the culture is experiencing because of the exposure to UV radiation and hence, why it is in the lag phase for that length of time but eventually is able to recover. Raman spectroscopy could be used to determine if the bacterioruberin is reduced during this stage and then recovers to a pre-exposure level. TEM imaging could be used to examine whether these microbes are mutated in anyway but are viable, hence able to reproduce and recover the colony many days after inoculation into the growth medium post-exposure.

To understand further the reasons for an extended lag phase and other changes, the physiological adaptations of the cells could be examined using transcriptomics and/or proteomics. These analyses can compare pre- and post-exposure cells to examine which genes are expressed at a given time and hence, if the exposure affects this. When a gene is switched on, it is transcribed into messenger RNA (mRNA), which is then used to make a protein; transcriptomics would analyse which mRNA are present and the relative abundances, and therefore whether the production of certain proteins is being affected. Proteomics would, in parallel, measure which proteins are present and their relative abundance. Therefore, for example, if the protein levels are reduced, but the gene mRNA is unchanged, the gene expression and/or transcription are not affected but could suggest that the proteins were being degraded post-exposure, which would show that the exposure was not affecting ability of the cell to produce certain molecules but only that the proteins or other molecules were being damaged, potentially leading to cell death. Also of interest would be building on previous work (*e.g.* El-Sayed *et al.*, 2002; Yang *et al.*, 2015) by comparing the transcriptomics and proteomic analyses which may expose changes to protein degradation; for example, if the mRNA levels for a specific gene are unchanged

post-exposure, but the corresponding protein levels have been reduced, this could suggest that protein degradation pathways have been triggered by the exposure.

Future work could also focus on further characterising the carotenoids with Raman spectroscopy and determining how they affect survival. If halophilic microbes are the most likely form of near surface microbial life that may exist on Mars today then identifying and characterising key carotenoids (other than and including bacterioruberin) is important for understanding RLS data from the *ExoMars* mission.

It was inconclusive as to the level of shielding that the artificial halite created for this work provided for the microbes. To improve on this, a combination of the LIVE/DEAD staining, confocal microscopy and the *z*-axis Raman spectroscopy investigation could be conducted. The cells could be LIVE/DEAD stained, then, following entombment in halite, confocal microscopy could be used to map the fluid inclusions throughout the crystal. The crystals would then be exposed to the UV radiation (after which photobleaching of the LIVE/DEAD staining would have likely occurred and the cells would have been washed so that it would be unlikely that there would be any of the propidium iodide (PI) to bind to any non-viable cells; nonetheless, *z*-axis Raman maps could be correlated to the position of fluid inclusions and levels of shielding could be more readily determined. A further improvement would be to create much thicker crystals (thicker than the 200 to 250 nm crystals used in this study) and after exposure to martian conditions a *z*-axis cross-section could be placed in the *x*-*y* plane of the Raman spectrometer rather than using the limited focusing depth (*z*-axis) of the spectrometer. Another examination technique could use thin layers of crystals (it is possible to create sections in the range of approximately 5 μm to 100 nm) created with FIB-SEM which could be placed successively on top of the microorganisms, to determine how thick the crystal needs to be for life to survive, *i.e.* this

technique would be characterising the transmission properties of halite crystals with respect to UV wavelengths.

In some cases the normalised Raman spectra appeared to show an increase in the intensity of the bacterioruberin after the initial measurement. It is possible that a population increase could explain the relatively higher Raman signal. To determine whether this is the reason halite crystals could be dissolved in a known volume of NaCl buffer solution and a cell count conducted to determine whether population growth was the cause of the increase in signal. Furthermore, the samples could be subjected to additional exposure to martian conditions, followed by acquiring Raman spectra at regular intervals (after each increment of exposure, *e.g.* a sol), would determine whether the signal increased was followed by a decrease as the UV destroyed the carotenoid signal or whether there was some other trend.

Expanding on the simulations of the martian evaporitic environment; other evaporitic minerals and brines have been found on Mars, for example gypsum and perchlorate brine. For example, isolating and characterising the microorganisms in gypsum crystals and determining whether sulphate crystals, since they are more abundant than chloride minerals, can provide a better shielding environment for the microorganisms. Furthermore, by comparing minerals, it may demonstrate that some minerals are more conducive to survivability than others. This would link to future site selection for lander missions and selection of sampling sites on Mars, *i.e.* the known mineralogy of the surface and near surface could inform selection committees as to which is more likely to contain biomarkers that can be detected using Raman spectroscopy.

Moreover, with the confirmation of liquid brine RSL at the surface of Mars, the simulation of localised brine transport within a regolith would be an important analogue for potential habitats at and near the surface of Mars. This could be achieved by doping regolith with

increasing amounts of brine (to find the brine concentration that would be analogous to the growth and decay of surface brine observed on Mars, informed by martian fluid modelling (Schwenzer *et al.*, 2016)) and exposing it to a freeze-thaw regime with UV cycles, with the potential to expand this using a sub-regolith reservoir of brine and creating an incline in the regolith to attempt to simulate an RSL. Further to this, the introduction of microbes to this type of simulation could be used to understand the viability of the cells after exposure to such a system. As RSL consist of perchlorate-based brine, perchlorate-reducing microbes (*e.g. Dechloromonas aromatica* (Coates and Achenbach, 2004)) could be used in these simulations, which could provide a better understanding of survival than a Na-based microbe that has been placed outside its normal nutrient environment and habitat.

Overall, for amino acids (and in general, organic molecules) and microbes, given that UV radiation is greatly damaging to the survivability of the molecule/microbe and therefore, the Raman biomarker signal, further work on extended exposure to low temperatures, pressures and freeze-thaw conditions should be studied as subsurface samples are more likely to contain organic molecule reserves and viable microbial life (*i.e.* several months, seasons, years, simulated, as, in this study, a simulated martian freeze-thaw season was survived with relatively little damage to the cell population).

Finally, increasing the understanding into the crucial factors which impact the destruction of Raman bands as biomarkers and the survival and growth of halophiles on Mars, can be achieved by using simulated environments and life detection techniques such as those described in this thesis.

Appendix A

Results from the experiments discussed in Section 4.2.1 and 4.3.1 are displayed in this appendix. For the preliminary atmospheric composition experiment samples were exposed to a ‘rough Mars’ gas mixture at a pressure of 1 bar. For the preliminary pressure experiment samples were exposed to a Mars-like pressure, with a nominal terrestrial atmospheric composition.

Preliminary atmospheric composition exposure results

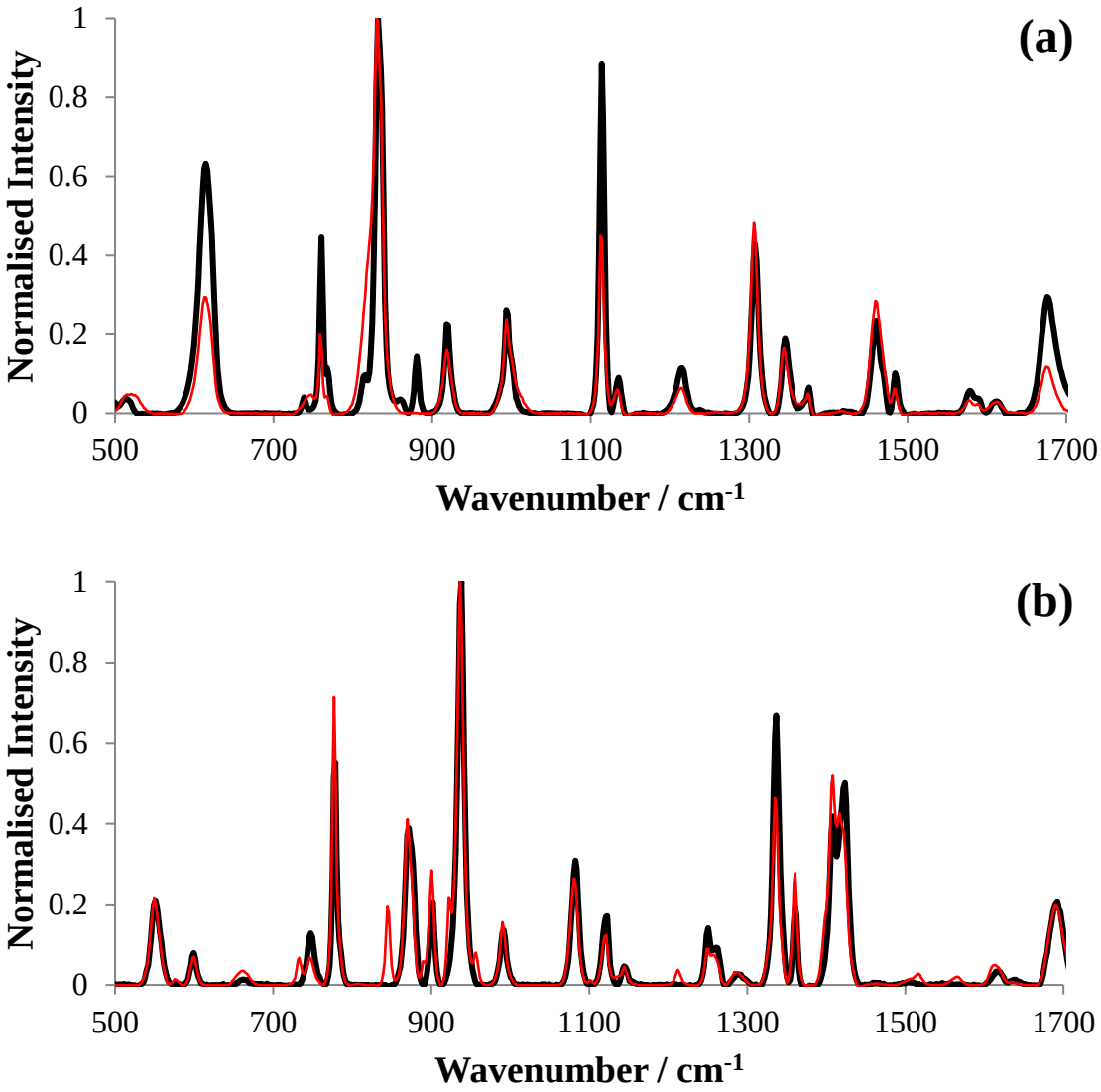

Figure A-1: The pre- and post-exposure Raman spectra of the amino acids (a) alanine, (b) aspartic acid, (c) cysteine, (d) glutamine and (e) glycine (average of nine spectra); samples were exposed to a Mars-like atmospheric composition at a pressure of 1 bar. The red line is the pre-exposure spectrum and the black line is the post-exposure spectrum.

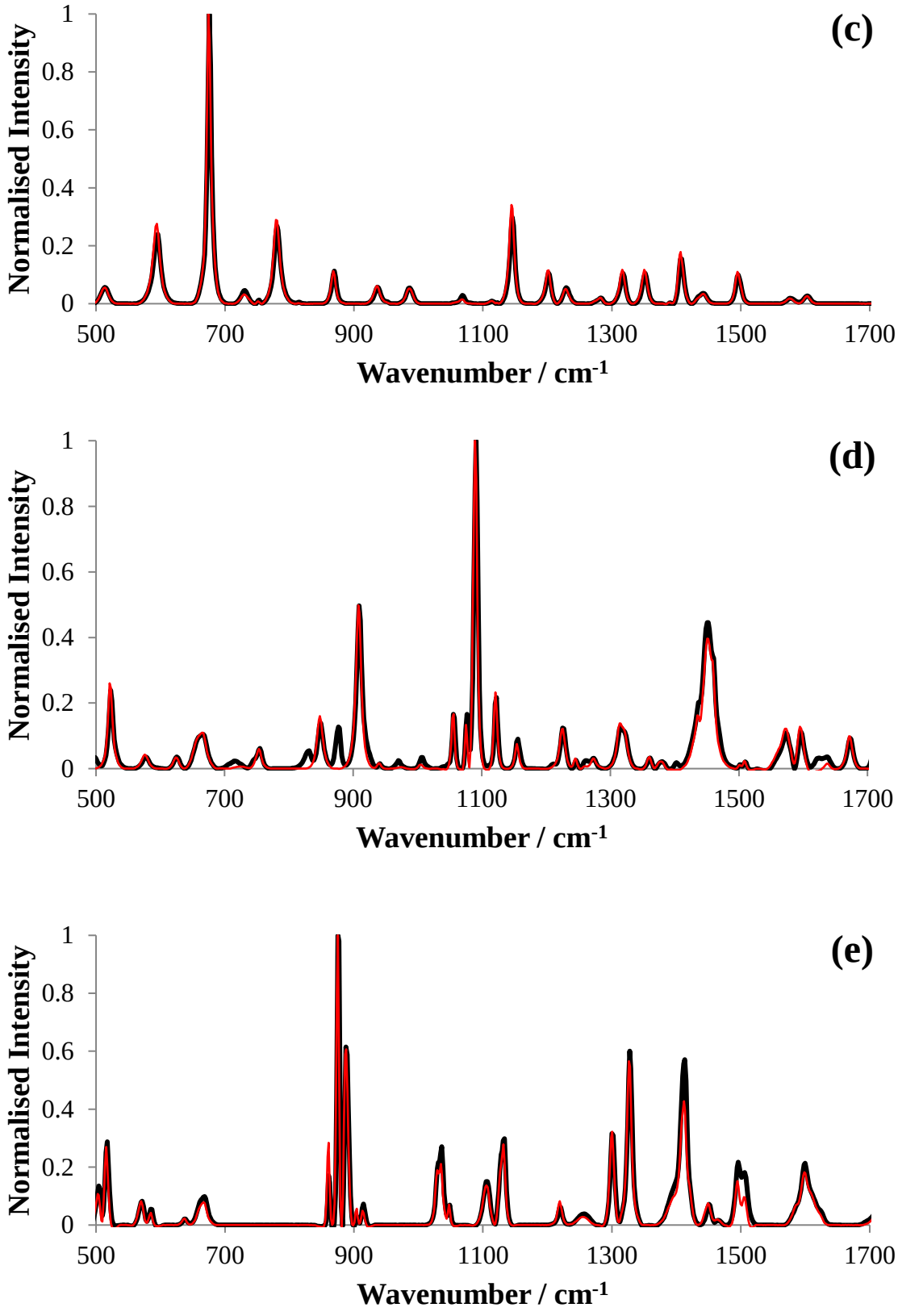

Figure A-1 (cont.).

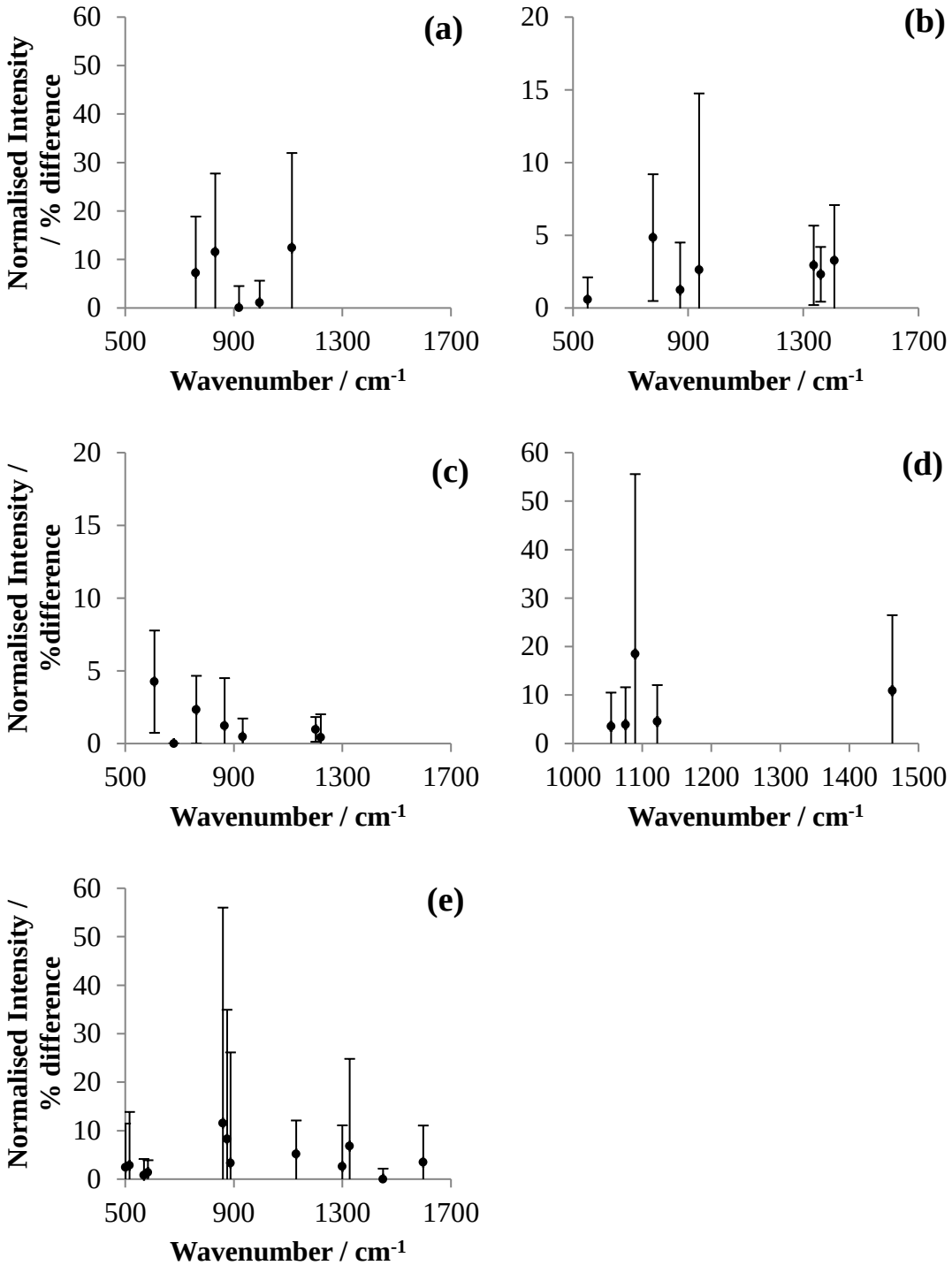

Figure A-2: The average percentage difference in the relative Raman intensity for pre- and post-exposure to a Mars-like atmospheric composition (at a pressure of 1 bar) for samples of (a) alanine, (b) aspartic acid, (c) cysteine, (d) glutamine and (e) glycine. The wavenumber range is the 'fingerprint' region 500 to 1700 cm^{-1}. Note: 1) the wavenumber range for (d) is 1000 to 1500 cm^{-1} because of several characteristic bands being in close proximity to one another; 2) the percentage difference scale is different for each plot. The error bars represent one standard deviation.

Preliminary pressure exposure results

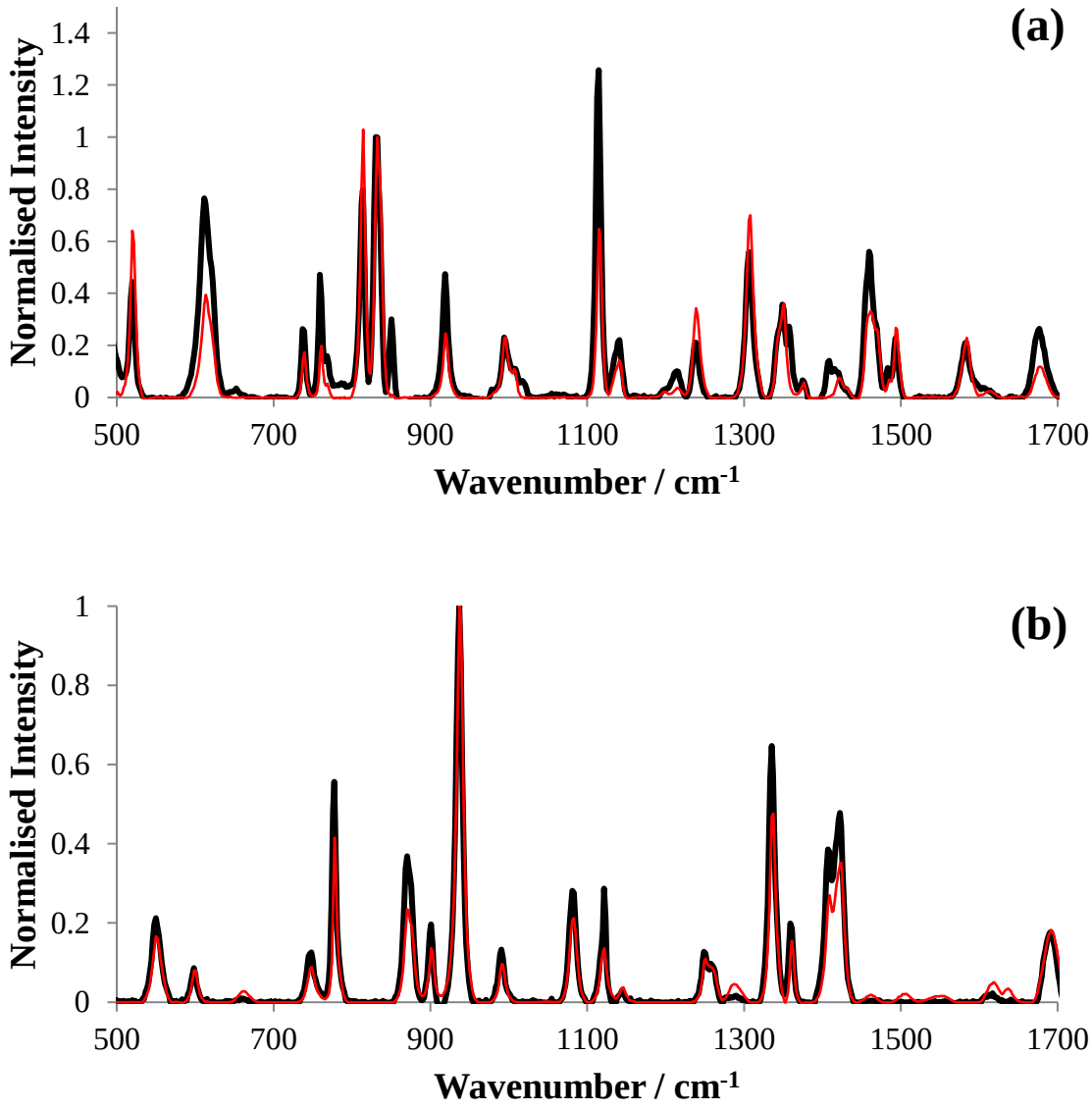

Figure A-3: The pre- and post-exposure Raman spectra of the amino acids (a) alanine, (b) aspartic acid, (c) cysteine, (d) glutamine and (e) glycine (average of nine spectra); samples were exposed to a Mars-like pressure in a terrestrial atmosphere. The red line is the pre-exposure spectrum and the black line is the post-exposure spectrum.

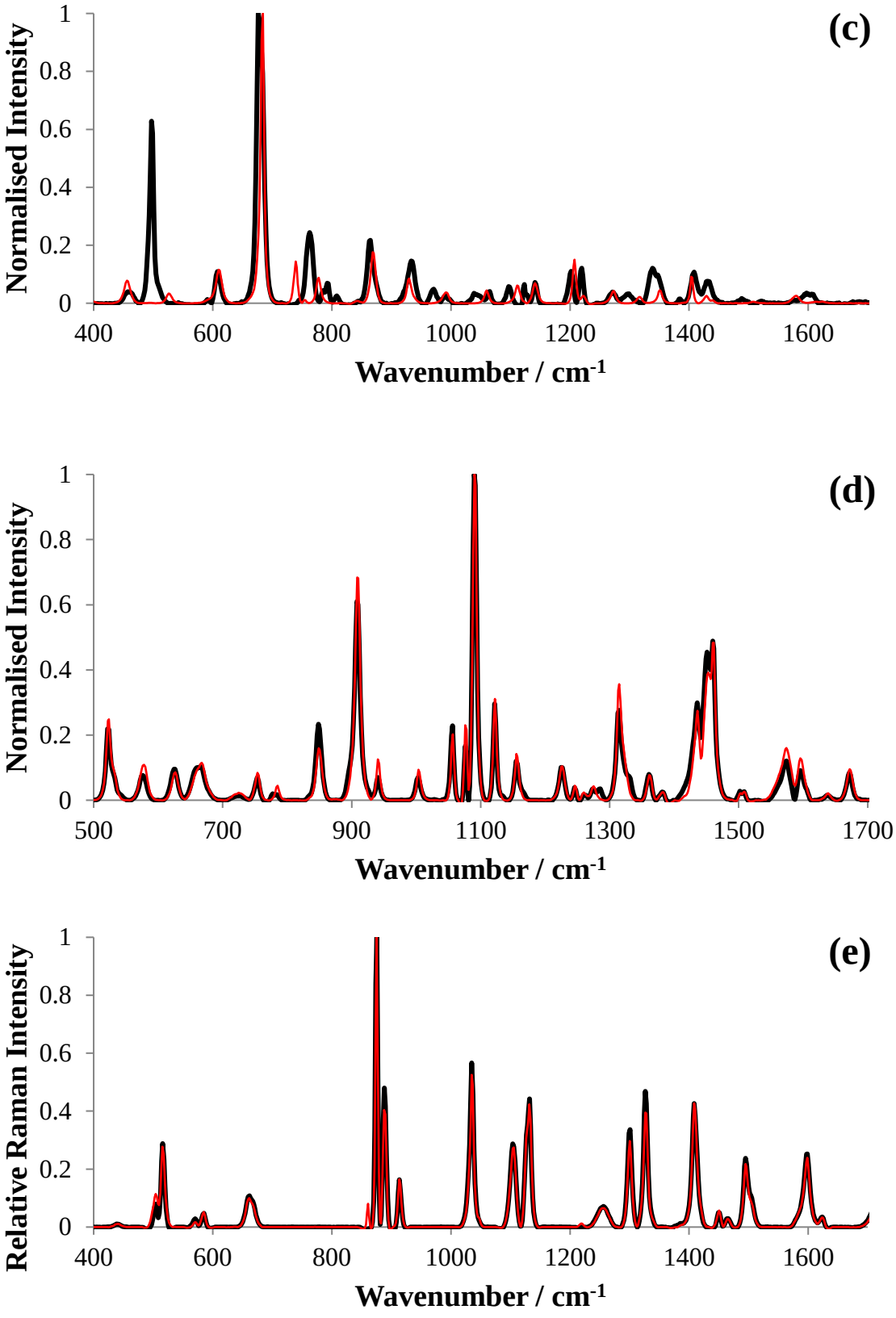

Figure A-3 (cont.).

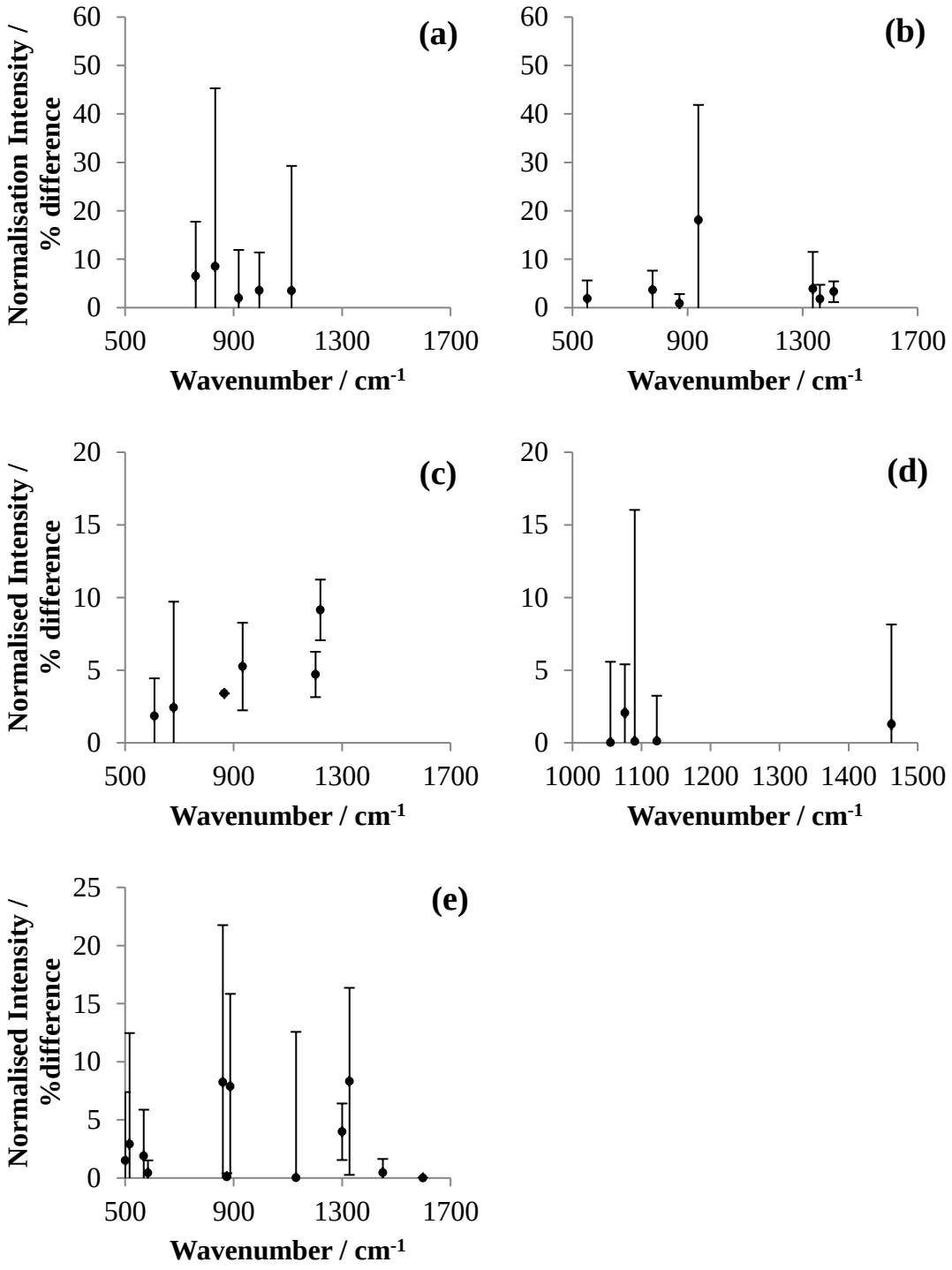

Figure A-4: The average percentage difference in the relative Raman intensity for pre- and post-exposure to a Mars-like pressure (in a terrestrial atmosphere) for samples of (a) alanine, (b) aspartic acid, (c) cysteine, (d) glutamine and (e) glycine. The wavenumber range is the 'fingerprint' region 500 to 1700 cm^{-1}. Note: 1) the wavenumber range for (d) is 1000 to 1500 cm^{-1} because of several characteristic bands being in close proximity to one another; 2) the percentage difference scale is different for each plot. The error bars represent one standard deviation.

Appendix B

B.1. OD_{600} growth curves

This appendix contains the OD growth curves used to calculate the μ values for the microbial isolates *H. sal* NRC-1, N3.1 and N4.1b in the various exposure experiments conducted: ambient controls, Mars-like near-surface and surface conditions, and temperature cycling. The line of best fit shows the range of data that was regarded as the log phase of growth.

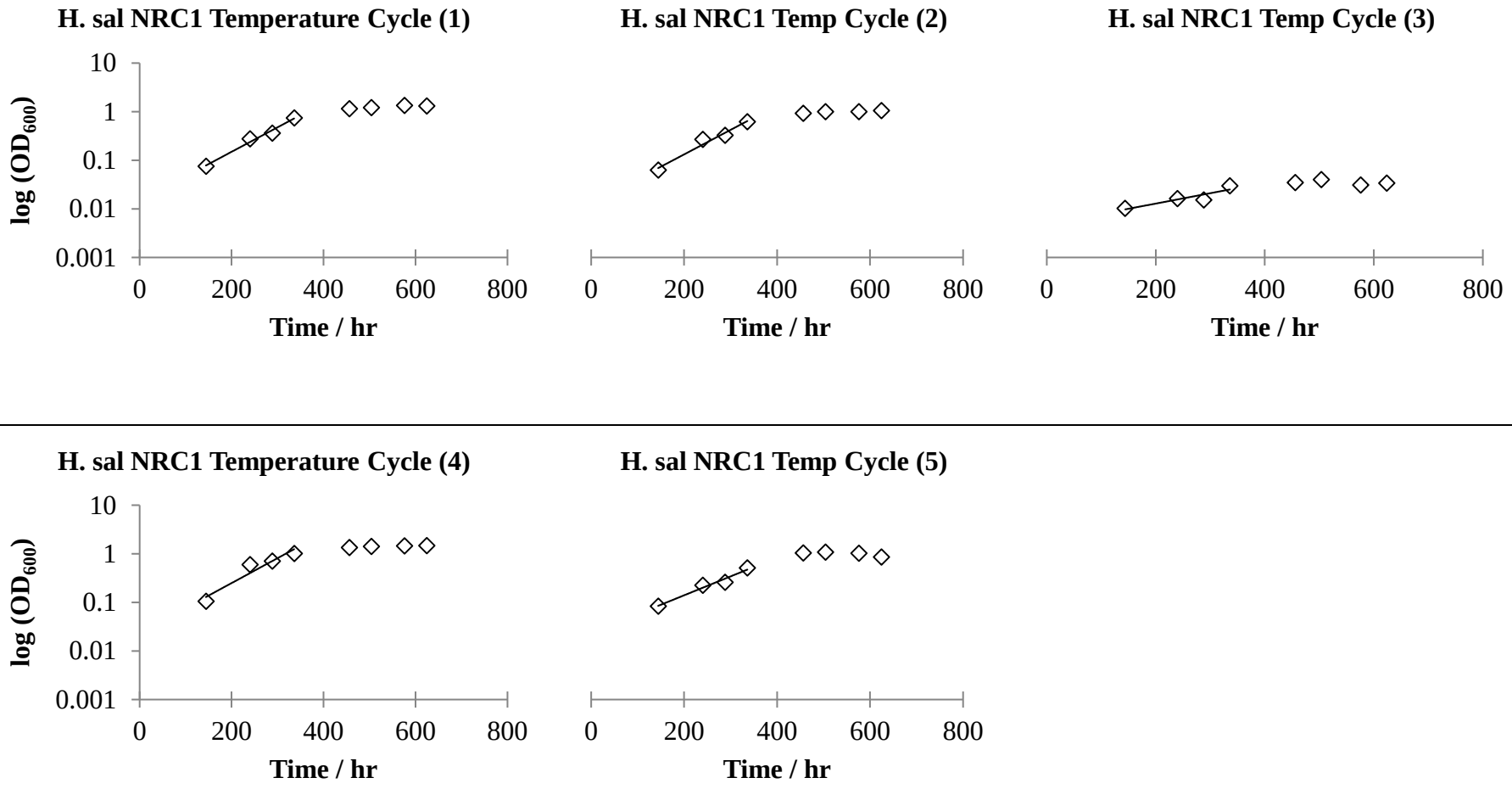

Figure B-1: The growth curves of samples of *H. sal* NRC-1 that were exposed to a Mars-like freeze-thaw cycle.

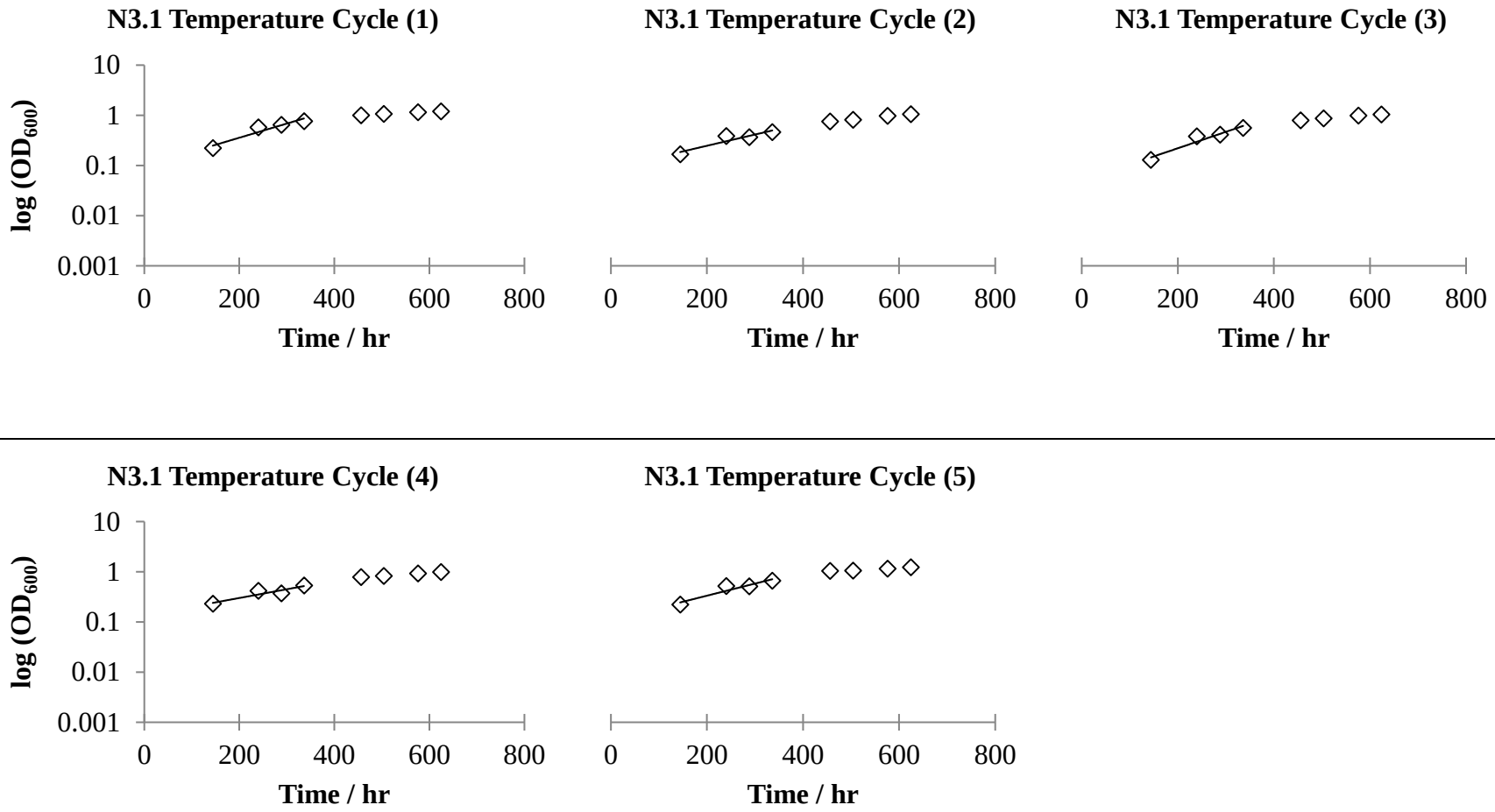

Figure B-2: The growth curves of samples of N3.1 that were exposed to a Mars-like freeze-thaw cycle.

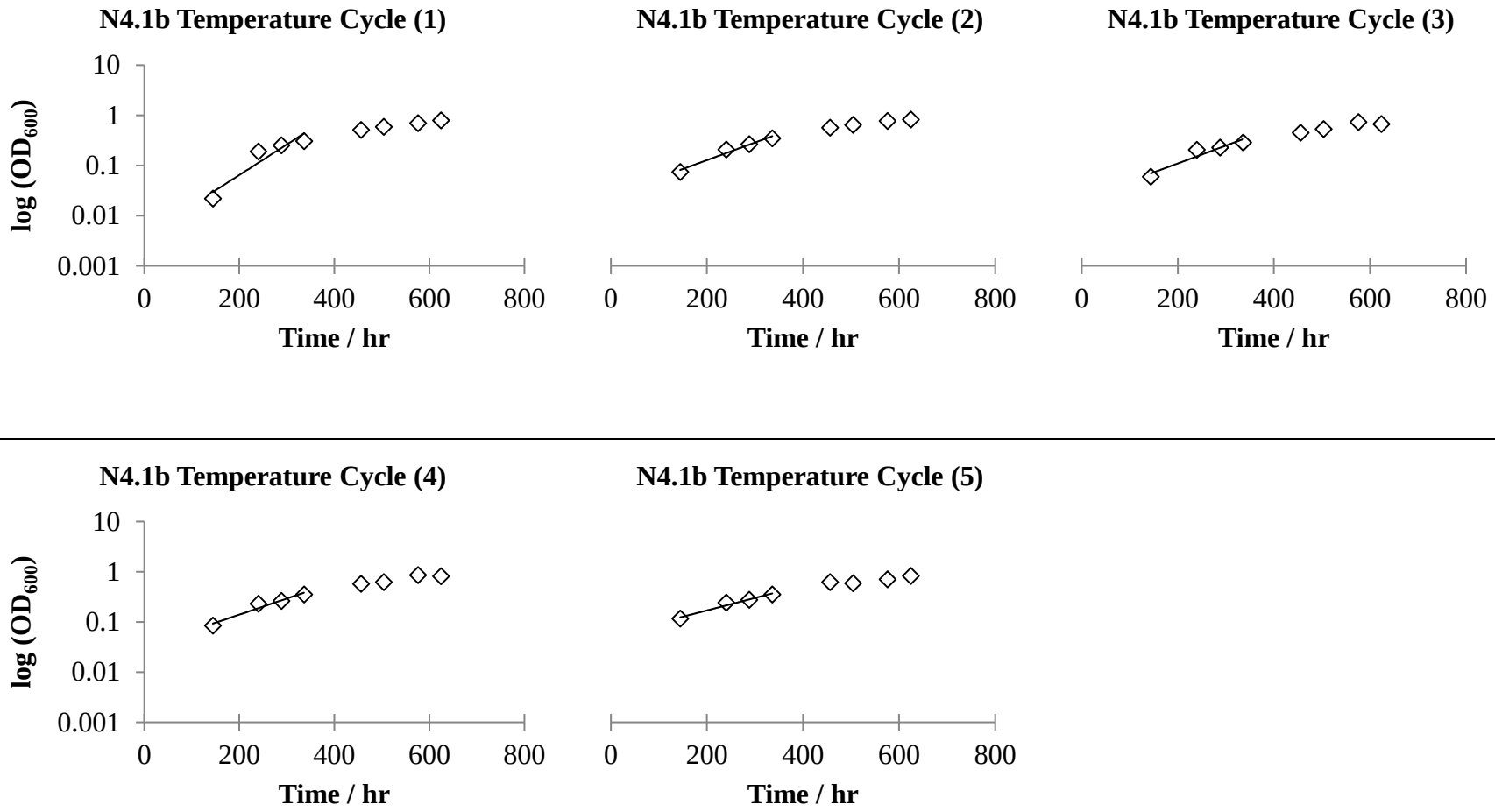

Figure B-3: The growth curves of samples of N4.1b that were exposed to a Mars-like freeze-thaw cycle.

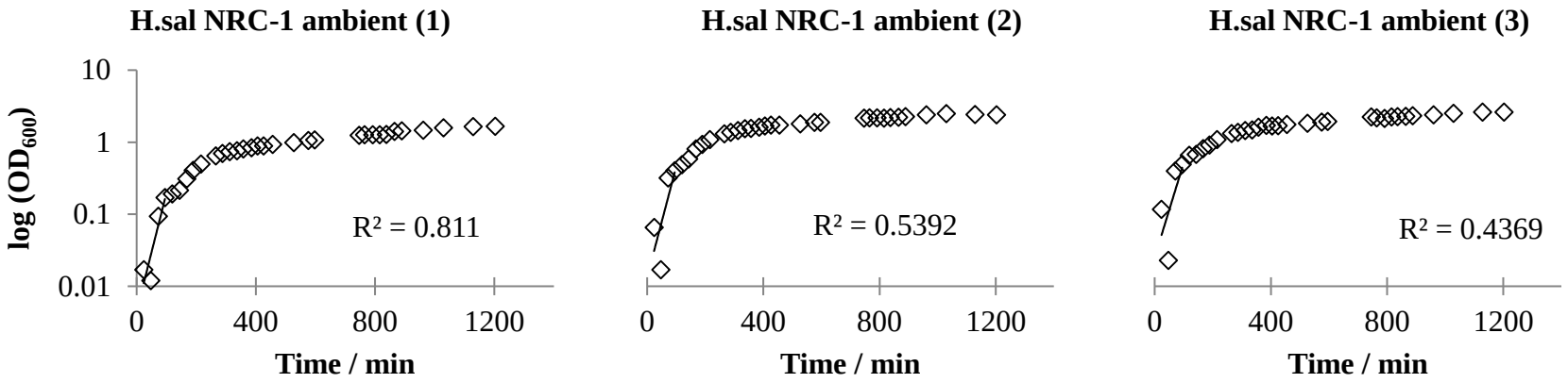

Figure B-4 **(a)**

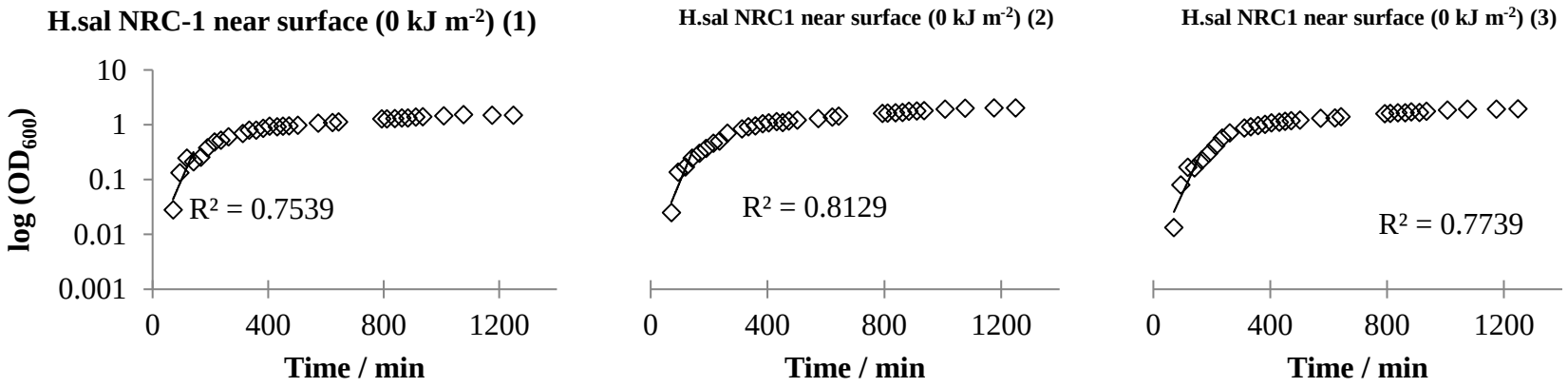

Figure B-4 **(b)**

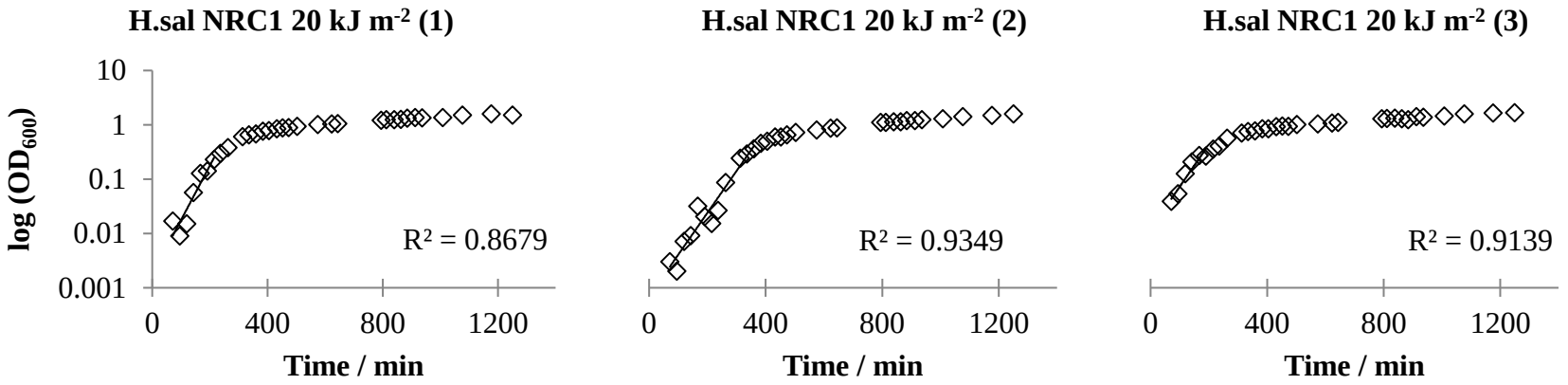

Figure B-4 **(c)**

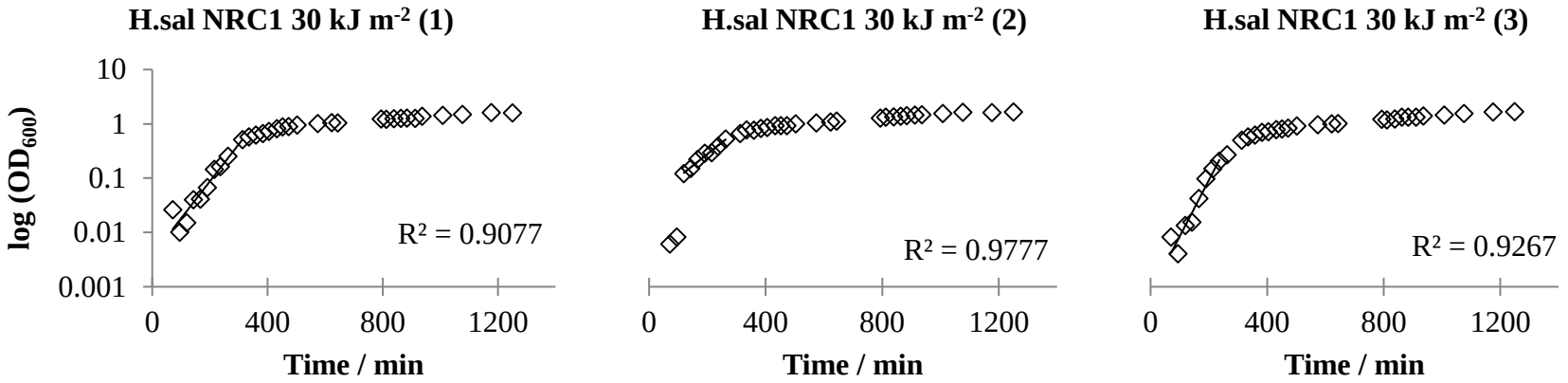

Figure B-4 **(d)**

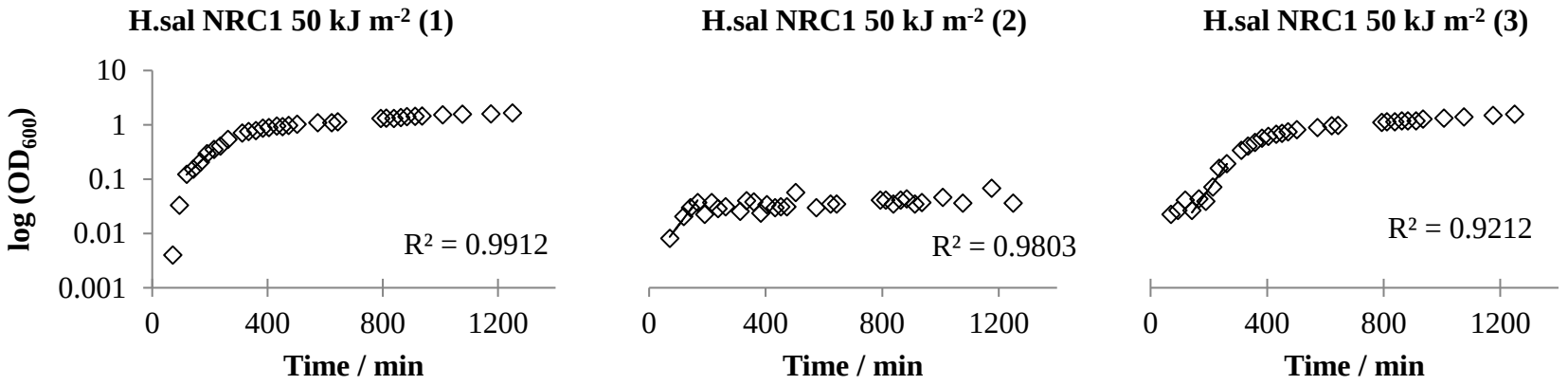

Figure B-4 **(e)**

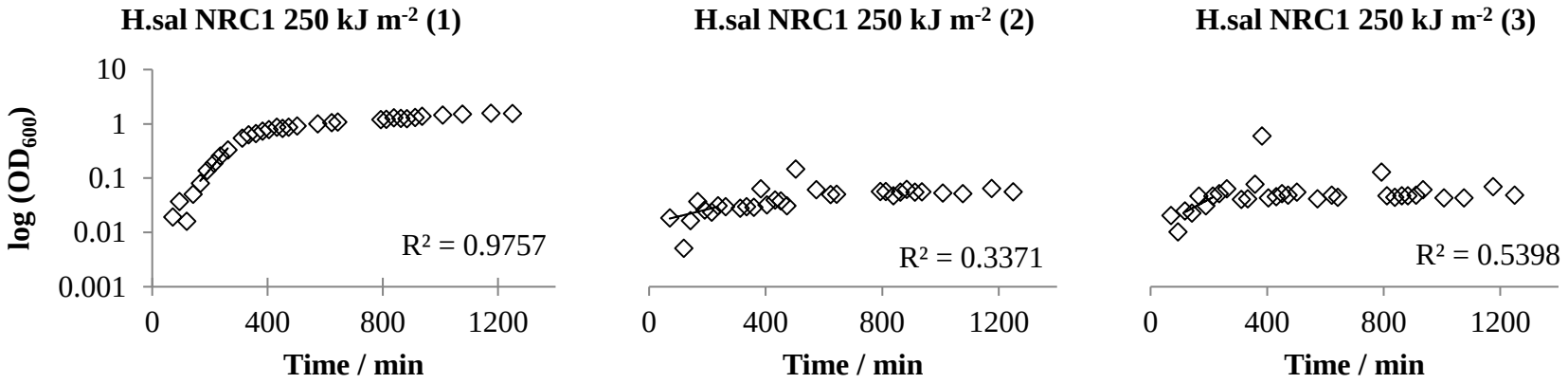

Figure B-4 **(f)**

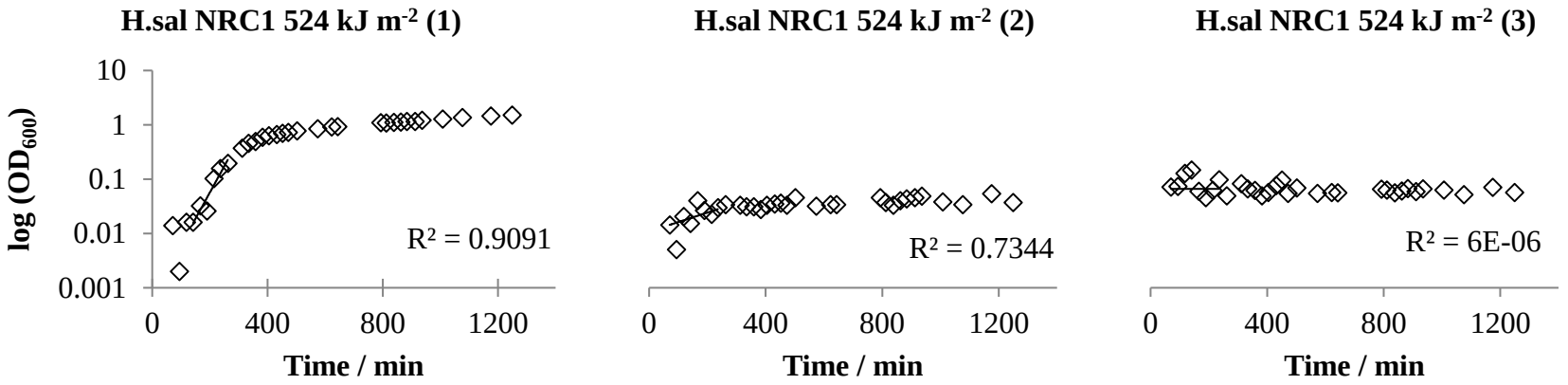

Figure B-4 **(g)**

Figure B-4: The growth curves of *H. sal* NRC-1 in (a) ambient conditions; (b) martian near surface conditions, *i.e.* exposure to Mars-like temperatures, atmospheric composition and pressure but blocked from any UV exposure; (c – g) Mars-like conditions with increasing UV doses, respectively.

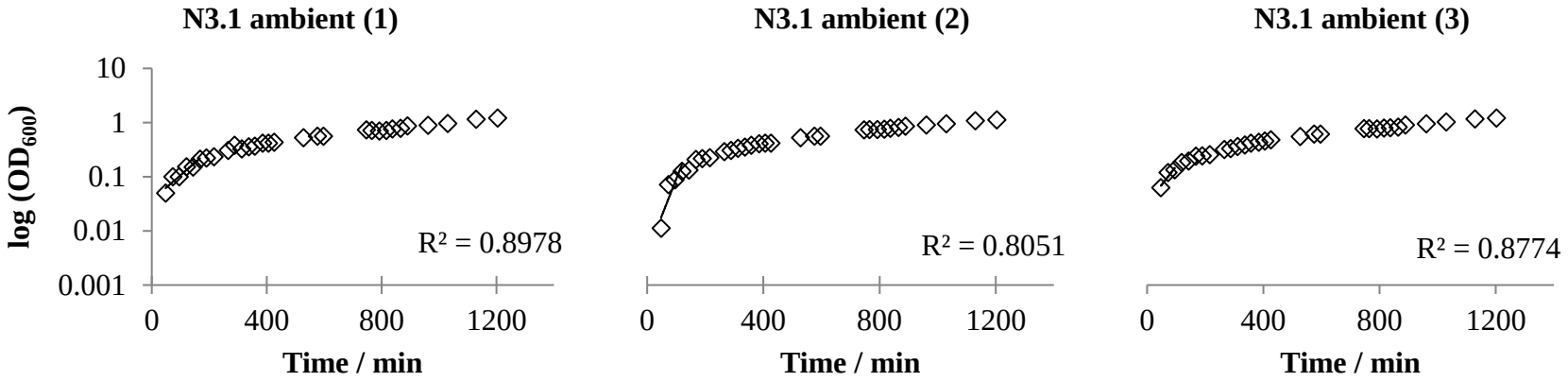

Figure B-5 **(a)**

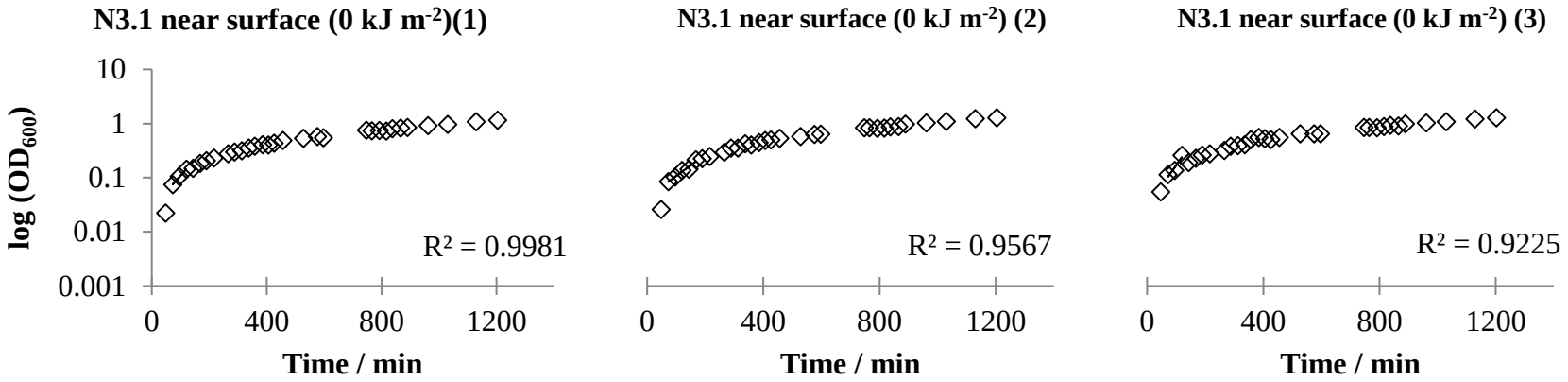

Figure B-5 **(b)**

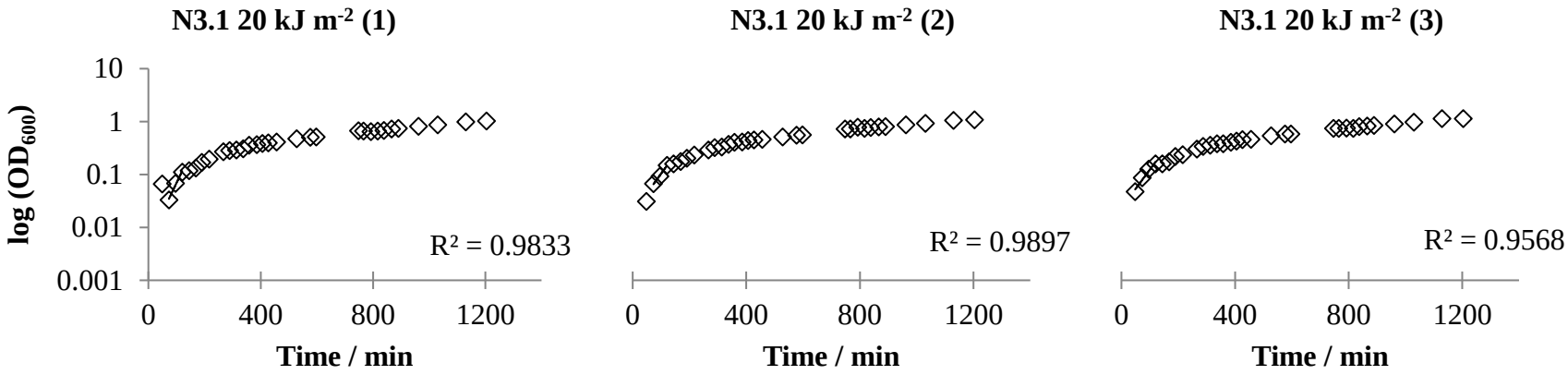

Figure B-5 **(c)**

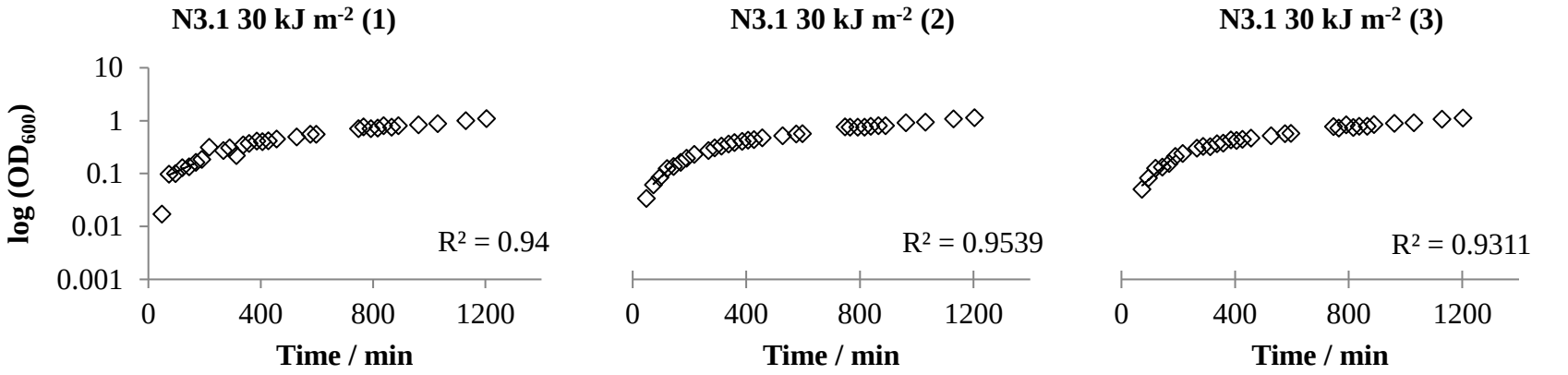

Figure B-5 **(d)**

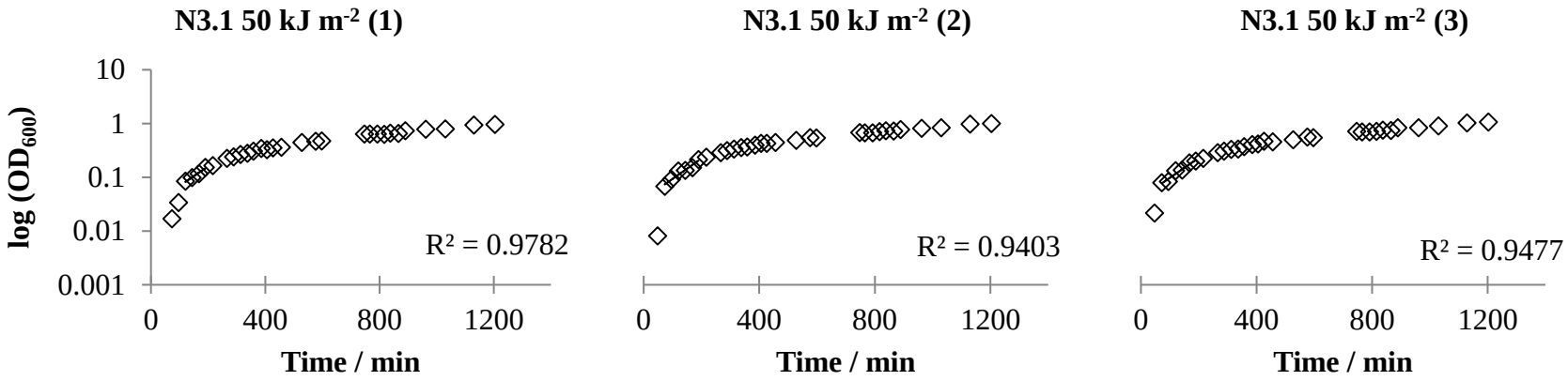

Figure B-5 **(e)**

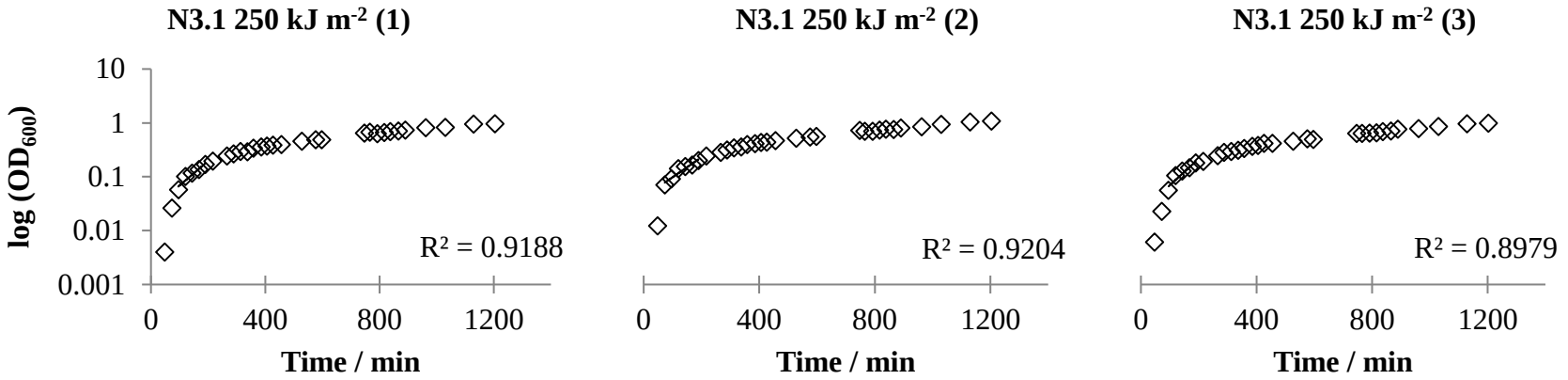

Figure B-5 **(f)**

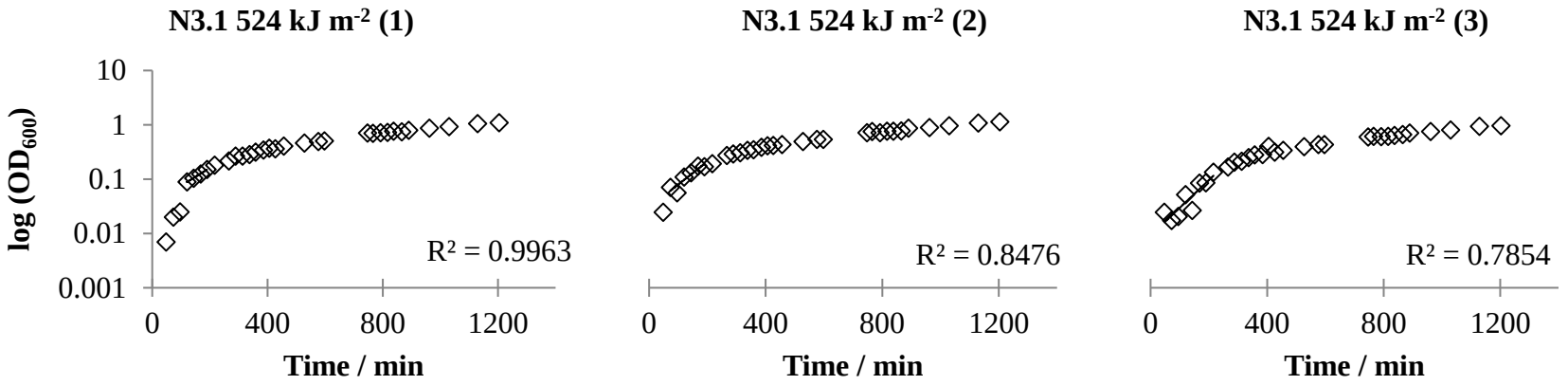

Figure B-5 **(g)**

Figure B-5: The growth curves of N3.1 in (a) ambient conditions; (b) martian near surface conditions, *i.e.* exposure to Mars-like temperatures, atmospheric composition and pressure but blocked from any UV exposure; (c – g) Mars-like conditions with increasing UV doses, respectively.

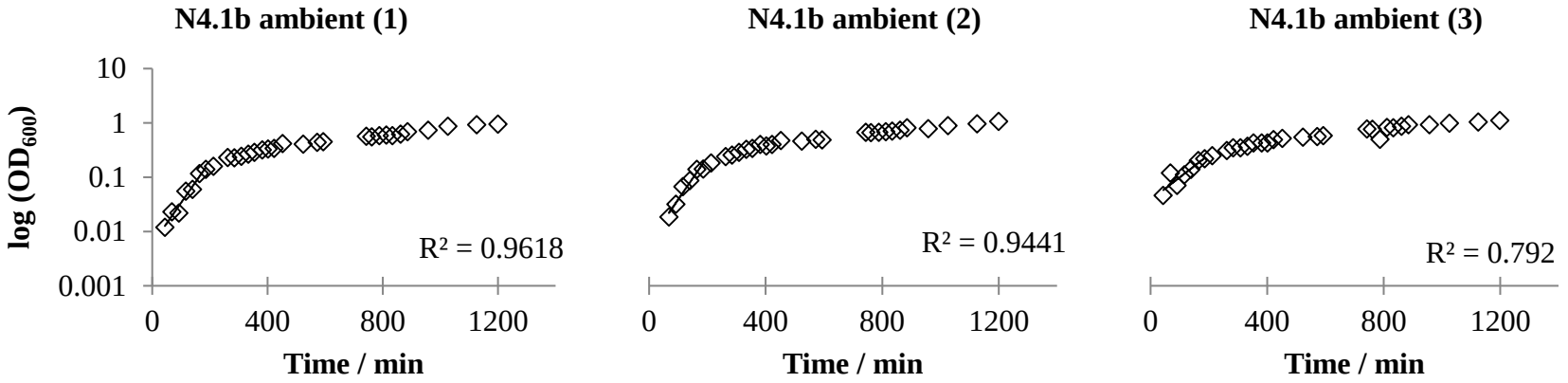

Figure B-6 **(a)**

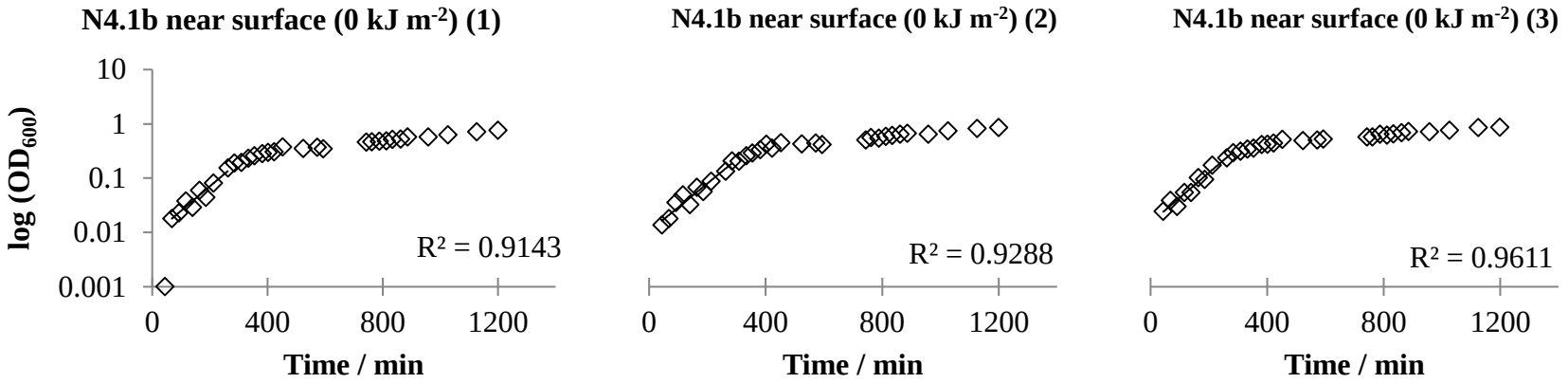

Figure B-6 **(b)**

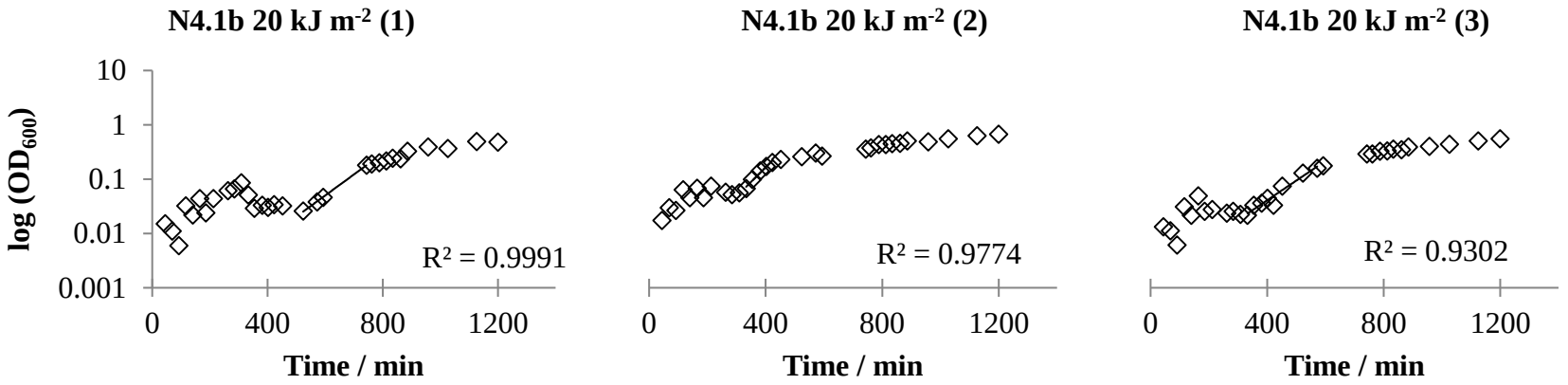

Figure B-6 **(c)**

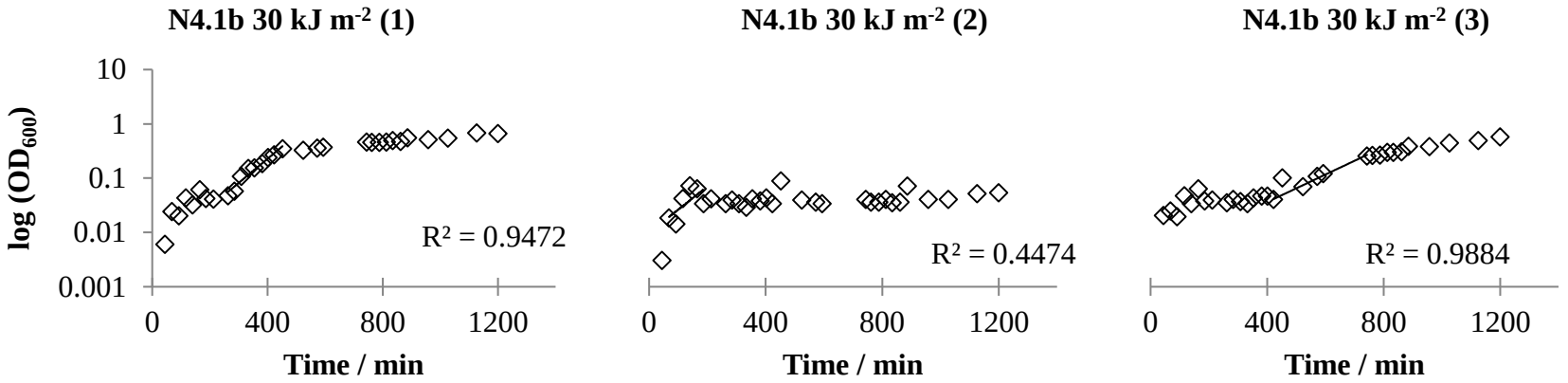

Figure B-6 **(d)**

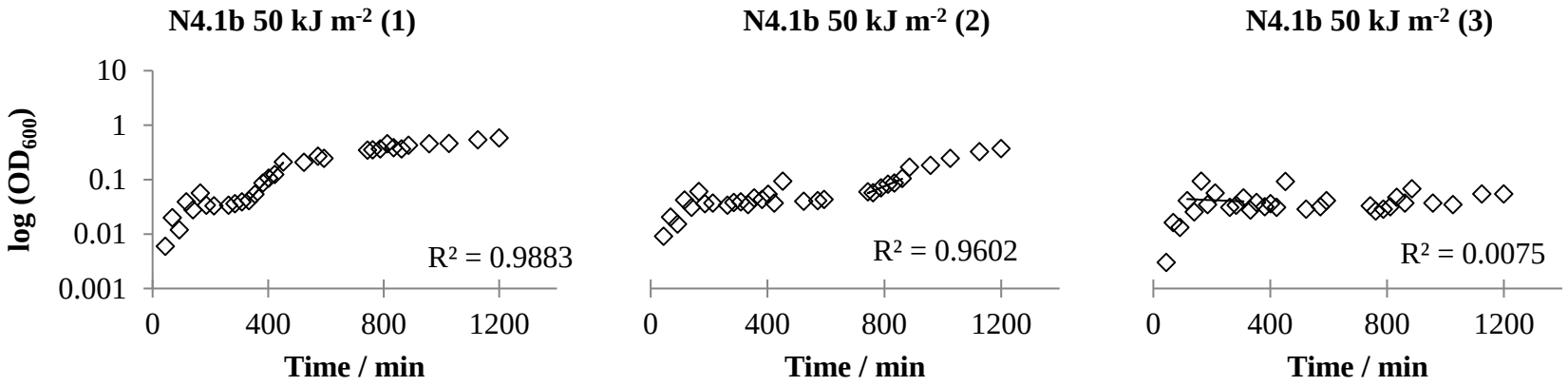

Figure B-6 **(e)**

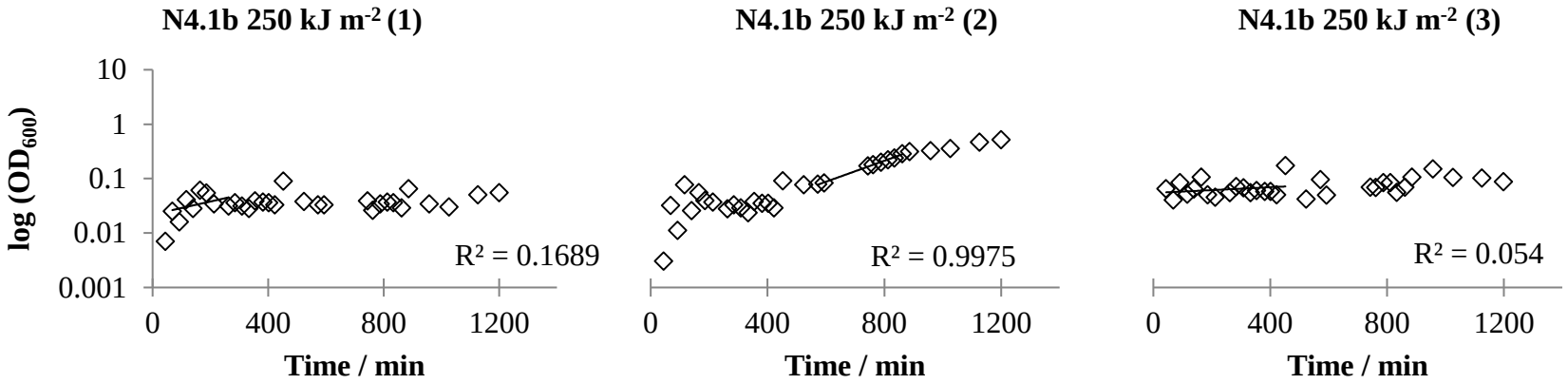

Figure B-6 **(f)**

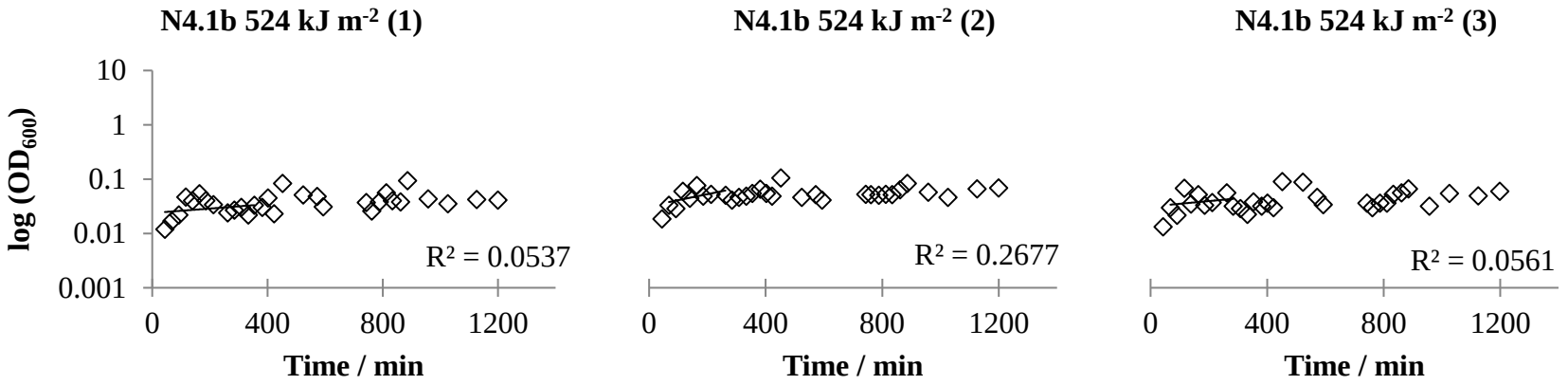

Figure B-6 **(g)**

Figure B-6: The growth curves of N4.1b in (a) ambient conditions; (b) martian near surface conditions, *i.e.* exposure to Mars-like temperatures, atmospheric composition and pressure but blocked from any UV exposure; (c – g) Mars-like conditions with increasing UV doses, respectively.

B.2. Examination of UV output: removal of data because of non-uniform UV output

In Section 5.2.2.3, where samples were exposed to a full complement of martian conditions, some data were removed because of the UV output of the lamp later being found to be non-uniform across the visible footprint. The images of the experiments used to justify the removal of these data are shown here. The orientation of the image differs with respect to the orientation of the coordinate system used to measure the UV output, so the affected sample(s) are circled in red for clarity.

***H. sal* NRC-1, dose rate: 50 kJ m^{-2}**

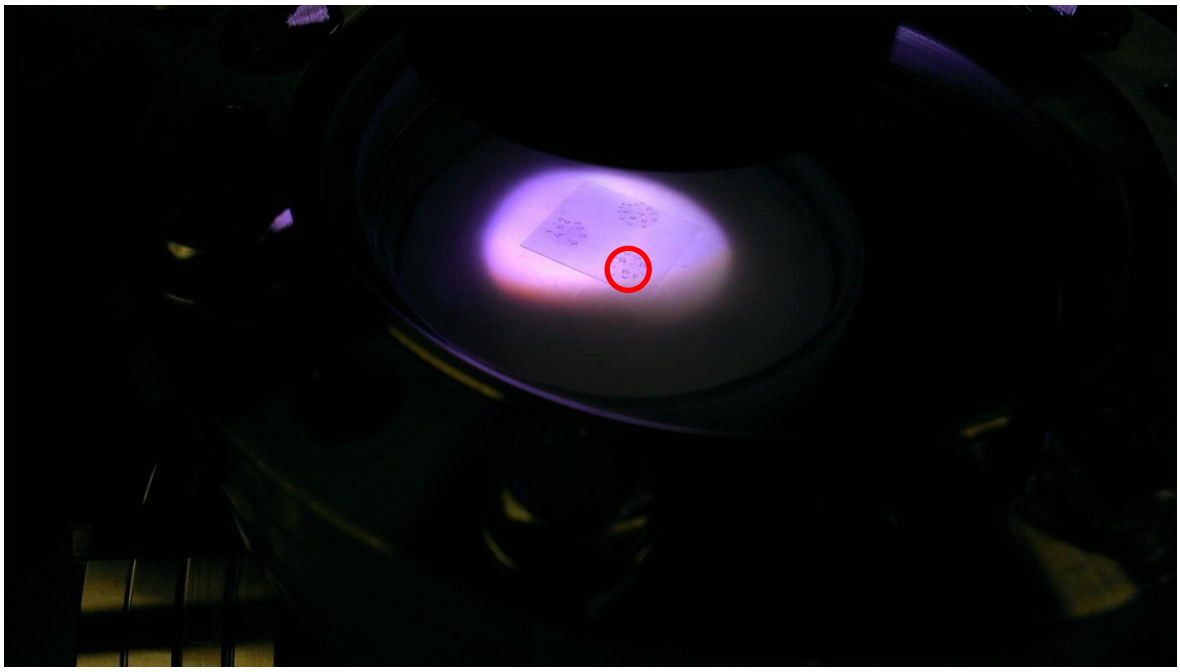

***H. sal* NRC-1, dose rate: 250 kJ m^{-2}**

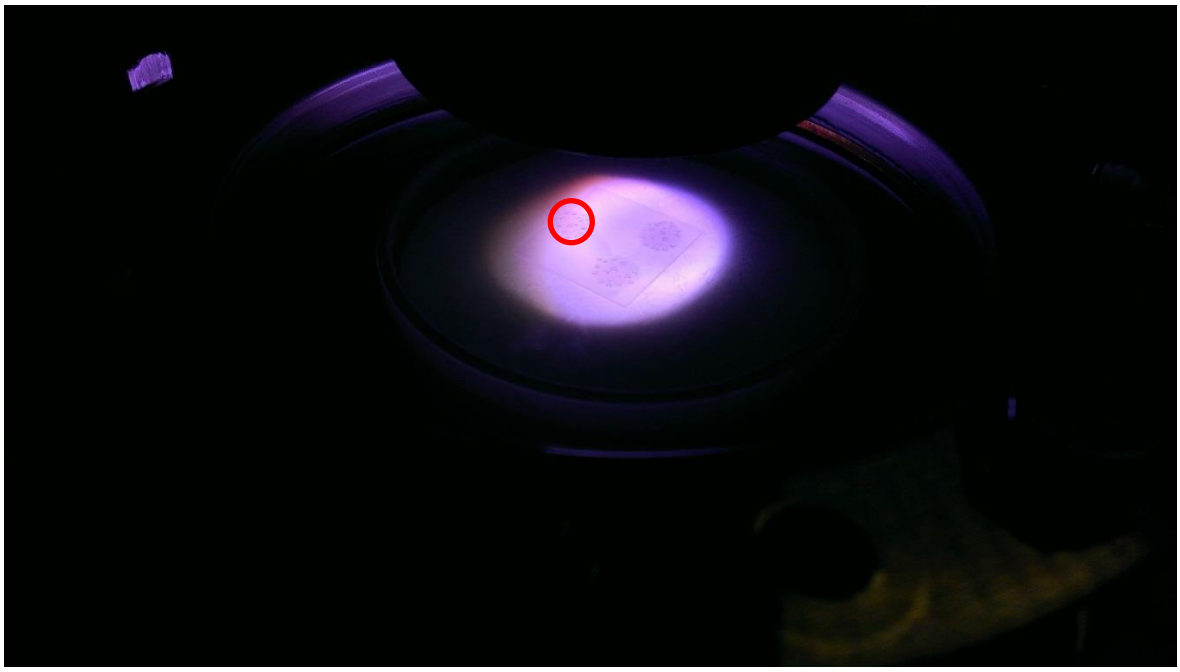

***H. sal* NRC-1, dose rate: 524 kJ m^{-2}**

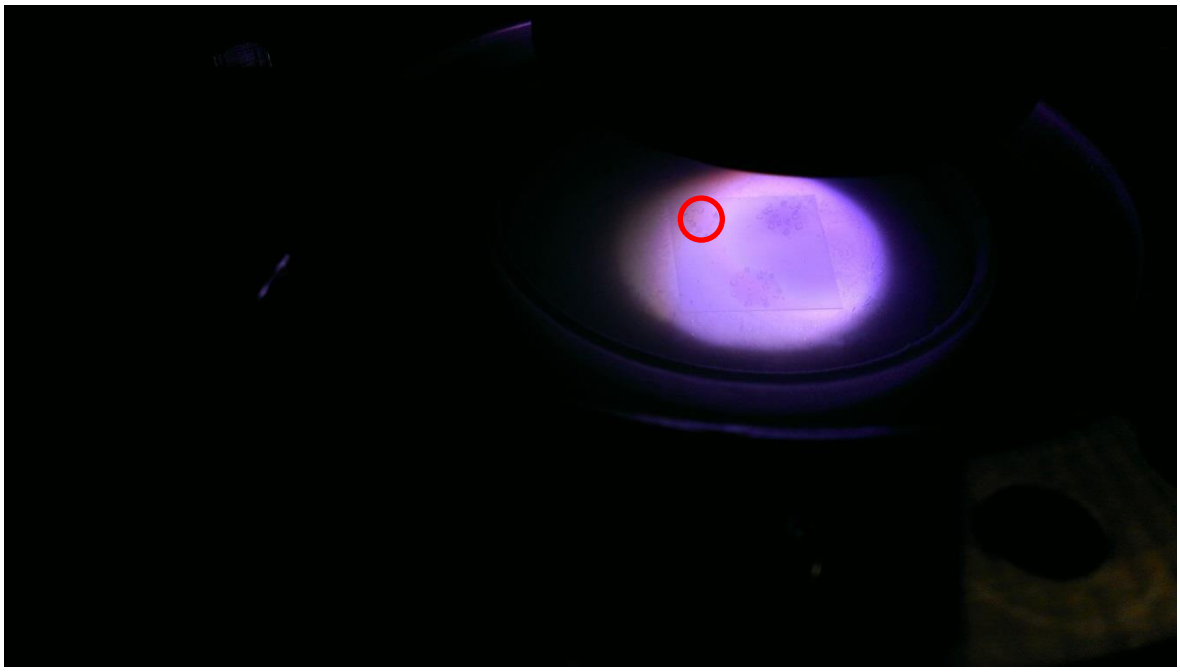

N4.1b, dose rate: 30 kJ m^{-2}

N4.1b, dose rate: 50 kJ m^{-2}

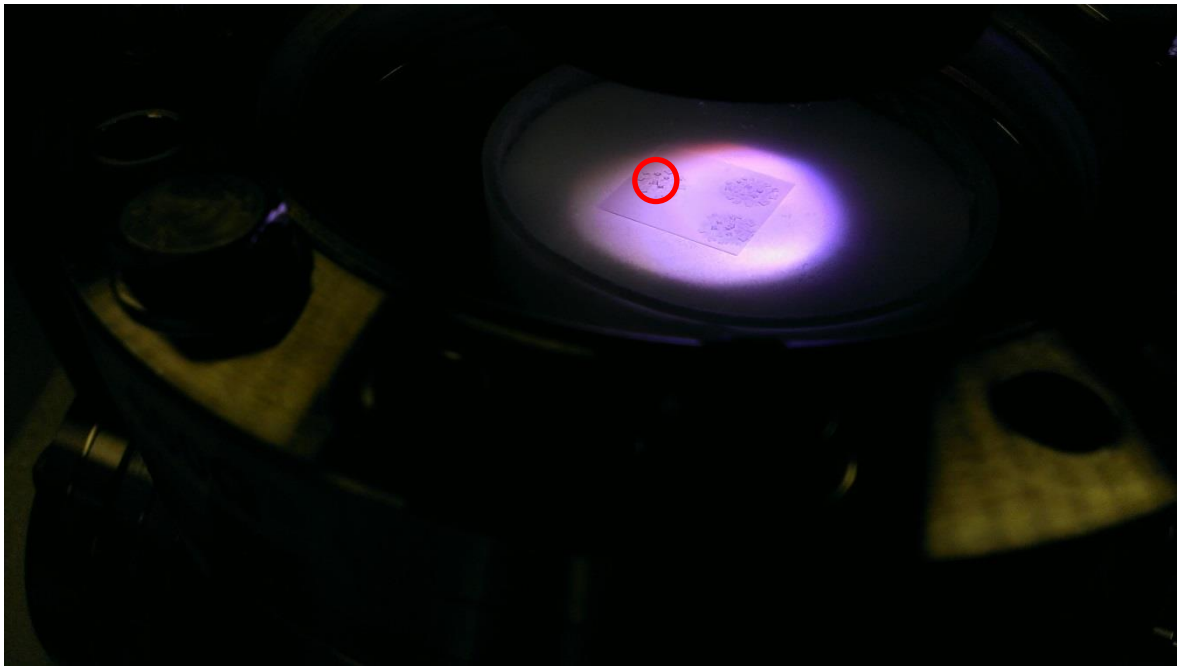

N4.1b, dose rate: 250 kJ m^{-2}

References

Adamski, J. C., Roberts, J. A. & Goldstein, R. H. 2006. Entrapment of Bacteria in Fluid Inclusions in Laboratory-Grown Halite. *Astrobiology,* 6**,** 552-562.

Aerts, J., Röling, W., Elsaesser, A. & Ehrenfreund, P. 2014. Biota and Biomolecules in Extreme Environments on Earth: Implications for Life Detection on Mars. *Life,* 4**,** 535-565.

Alajtal, A. I., Edwards, H. G. M., Elbagerma, M. A. & Scowen, I. J. 2010. The effect of laser wavelength on the Raman Spectra of phenanthrene, chrysene, and tetracene: Implications for extra-terrestrial detection of polyaromatic hydrocarbons. *Spectrochimica Acta Part A: Molecular and Biomolecular Spectroscopy,* 76**,** 1-5.

Allen, C. C., Jager, K. M., Morris, R. V., Lindstrom, D. J., Lindtsrom, M. M. & Lockwood, J. P. 1998. Martian soil simulant available for scientific, educational study. *Eos Trans. AGU,* 79**,** 405-409.

Allen, C. C. & Morris, R. V. 1999. Reply [to "Comment on 'Martian soil simulant available for scientific, educational study'"] Caution advised on suitability of a Mars soil simulant. *Eos, Transactions American Geophysical Union,* 80**,** 169-169.

Almeida, F. M., Freire, P. T. C., Lima, R. J. C., Remédios, C. M. R., Mendes Filho, J. & Melo, F. E. A. 2006. Raman spectra of L-isoleucine crystals. *Journal of Raman Spectroscopy,* 37**,** 1296-1301.

Archer, P. D., Franz, H. B., Sutter, B., Arevalo, R. D., Coll, P., Eigenbrode, J. L., Glavin, D. P., Jones, J. J., Leshin, L. A., Mahaffy, P. R., McAdam, A. C., McKay, C. P., Ming, D. W., Morris, R. V., Navarro-González, R., Niles, P. B., Pavlov, A., Squyres, S. W., Stern, J. C., Steele, A. & Wray, J. J. 2014. Abundances and implications of volatile-bearing species from evolved gas analysis of the Rocknest

aeolian deposit, Gale Crater, Mars. *Journal of Geophysical Research: Planets,* 119**,** 2013JE004493.

Arvidson, R. E., Squyres, S. W., Iii, J. F. B., Catalano, J. G., Clark, B. C., Crumpler, L. S., Jr., P. a. D. S., Fairén, A. G., Farrand, W. H., Fox, V. K., Gellert, R., Ghosh, A., Golombek, M. P., Grotzinger, J. P., Guinness, E. A., Herkenhoff, K. E., Jolliff, B. L., Knoll, A. H., Li, R., McLennan, S. M., Ming, D. W., Mittlefehldt, D. W., Moore, J. M., Morris, R. V., Murchie, S. L., Parker, T. J., Paulsen, G., Rice, J. W., Ruff, S. W., Smith, M. D. & Wolff, M. J. 2014. Ancient Aqueous Environments at Endeavour Crater, Mars. *Science,* 343.

Asgarani, E., Funamizu, H., Saito, T., Terato, H., Ohyama, Y., Yamamoto, O. & Ide, H. 1999. Mechanisms of DNA protection in Halobacterium salinarium, an extremely halophilic bacterium. *Microbiological Research,* 154**,** 185-190.

Auer, B. M. & Skinner, J. L. 2008. IR and Raman spectra of liquid water: Theory and interpretation. *The Journal of Chemical Physics,* 128**,** 224511-12.

Bada, J. L. & McDonald, G. D. 1995. Amino Acid Racemization on Mars: Implications for the Preservation of Biomolecules from an Extinct Martian Biota. *Icarus,* 114**,** 139-143.

Baliga, N., Bjork, S., Bonneau, R., Pan, M., Iloanusi, C., Kottemann, M., Hood, L. & Diruggiero, J. 2004. Systems level insights into the stress response to UV radiation in the halophilic archaeon Halobacterium NRC-1. *Genome Res,* 14**,** 1025 - 1035.

Barlow, N. G. 2008. *Mars: An Introduction to its Interior, Surface and Atmosphere,* New York, Cambridge University Press.

Bauermeister, A., Bentchikou, E., Moeller, R. & Rettberg, P. 2009. Roles of PprA, IrrE, and RecA in the resistance of Deinococcus radiodurans to germicidal and environmentally relevant UV radiation. *Archives of Microbiology,* 191**,** 913-918.

Beegle, L. W., Bhartia, R., DeFlores, L., Darrach, M., Kidd, R. D., Abbey, W., Asher, S., Burton, A., Clegg, S., Conrad, P. G., Edgett, K., Ehlmann, B., Langenhorst, F., Fries, M., Hug, W., Nealson, K., Popp, J., Sorbon, P., Steele, A., Wiens, R. & Williford, K. 2014. SHERLOC: Scanning Habitable Environments with Raman and Luminescence for Organics and Chemicals, an Investigation for 2020. *45th Lunar and Planetary Science Conference.* 2835. Houston: Lunar and Planetary Institute.

Bernstein, M. P., Dworkin, J. P., Sandford, S. A., Cooper, G. W. & Allamandola, L. J. 2002. Racemic amino acids from the ultraviolet photolysis of interstellar ice analogues. *Nature,* 416**,** 401-403.

Bertrand, M., Chabin, A., Brack, A., Cottin, H., Chaput, D. & Westall, F. 2012. The PROCESS Experiment: Exposure of Amino Acids in the EXPOSE-E Experiment on the International Space Station and in Laboratory Simulations. *Astrobiology,* 12**,** 426-435.

Bibring, J.-P., Langevin, Y., Mustard, J. F., Poulet, F., Arvidson, R., Gendrin, A., Gondet, B., Mangold, N., Pinet, P., Forget, F., The, O. T., Berthé, M., Gomez, C., Jouglet, D., Soufflot, A., Vincendon, M., Combes, M., Drossart, P., Encrenaz, T., Fouchet, T., Merchiorri, R., Belluci, G., Altieri, F., Formisano, V., Capaccioni, F., Cerroni, P., Coradini, A., Fonti, S., Korablev, O., Kottsov, V., Ignatiev, N., Moroz, V., Titov, D., Zasova, L., Loiseau, D., Pinet, P., Douté, S., Schmitt, B., Sotin, C., Hauber, E., Hoffmann, H., Jaumann, R., Keller, U., Arvidson, R., Duxbury, T., Forget, F. & Neukum, G. 2006. Global Mineralogical and Aqueous Mars History Derived from OMEGA/Mars Express Data. *Science,* 312**,** 400-404.

Bibring, J.-P., Langevin, Y., Poulet, F., Gendrin, A., Gondet, B., Berthe, M., Soufflot, A., Drossart, P., Combes, M., Bellucci, G., Moroz, V., Mangold, N., Schmitt, B. & Omega Team, T. 2004. Perennial water ice identified in the south polar cap of Mars. *Nature,* 428**,** 627-630.

Biemann, K. & Bada, J. L. 2011. Comment on "Reanalysis of the Viking results suggests perchlorate and organics at midlatitudes on Mars" by Rafael Navarro-González et al. *Journal of Geophysical Research: Planets,* 116**,** E12001.

Biemann, K., Oro, J., Iii, P. T., Orgel, L. E., Nier, A. O., Anderson, D. M., Simmonds, P. G., Flory, D., Diaz, A. V., Rushneck, D. R. & Biller, J. A. 1976. Search for Organic and Volatile Inorganic Compounds in Two Surface Samples from the Chryse Planitia Region of Mars. *Science,* 194**,** 72-76.

Biemann, K., Oro, J., Toulmin, P., Iii, Orgel, L. E., Nier, A. O., Anderson, D. M., Simmonds, P. G., Flory, D., Diaz, A. V., Rushneck, D. R., Biller, J. E. & Lafleur, A. L. 1977. The Search for Organic Substances and Inorganic Volatile Compounds in the Surface of Mars. *J. Geophys. Res.,* 82**,** 4641-4658.

Binder, A. B., Arvidson, R. E., Guinness, E. A., Jones, K. L., Morris, E. C., Mutch, T. A., Pieri, D. C. & Sagan, C. 1977. The Geology of the Viking Lander 1 Site. *J. Geophys. Res.,* 82**,** 4439-4451.

Blöchl, E., Rachel, R., Burggraf, S., Hafenbradl, D., Jannasch, H. W. & Stetter, K. O. 1997. *Pyrolobus fumarii,* gen. and sp. nov., represents a novel group of archaea, extending the upper temperature limit for life to 113°C. *Extremophiles,* 1**,** 14 - 21.

Böttger, U., De Vera, J. P., Fritz, J., Weber, I., Hübers, H. W. & Schulze-Makuch, D. 2012. Optimizing the detection of carotene in cyanobacteria in a martian regolith analogue with a Raman spectrometer for the ExoMars mission. *Planetary and Space Science,* 60**,** 356-362.

Boulos, L., Prévost, M., Barbeau, B., Coallier, J. & Desjardins, R. 1999. LIVE/DEAD® BacLight™: application of a new rapid staining method for direct enumeration of viable and total bacteria in drinking water. *Journal of Microbiological Methods,* 37**,** 77-86.

Bowman, J. P., McCammon, S. A. & Skerratt, J. H. 1997. *Methylosphaera hansonii* gen. nov., sp. nov., a psychrophilic, group I methanotroph from Antarctic marine-salinity, meromictic lakes *Microbiology,* 143**,** 1451 - 1459.

Bridges, J. C. & Grady, M. M. 1999. A halite-siderite-anhydrite-chlorapatite assemblage in Nakhla: Mineralogical evidence for evaporites on Mars. *Meteoritics & Planetary Science,* 34**,** 407-415.

Carter, J., Loizeau, D., Mangold, N., Poulet, F. & Bibring, J.-P. 2015. Widespread surface weathering on early Mars: A case for a warmer and wetter climate. *Icarus,* 248**,** 373-382.

Cataldo, F., Ragni, P., Iglesias-Groth, S. & Manchado, A. 2011. Solid state radiolysis of sulphur-containing amino acids: cysteine, cystine and methionine. *Journal of Radioanalytical and Nuclear Chemistry,* 287**,** 573-580.

Cavicchioli, R. 2006. Cold-adapted archaea. *Nat Rev Micro,* 4**,** 331-343.

Chyba, C. & Sagan, C. 1992. Endogenous production, exogenous delivery and impact-shock synthesis of organic molecules: an inventory for the origins of life. *Nature,* 355**,** 125-132.

Clayton, R. N. & Mayeda, T. K. 1996. Oxygen isotope studies of achondrites. *Geochimica et Cosmochimica Acta,* 60**,** 1999-2017.

Coates, J. D. & Achenbach, L. A. 2004. Microbial perchlorate reduction: rocket-fuelled metabolism. *Nat Rev Micro,* 2**,** 569-580.

Cockell, C. S., Balme, M., Bridges, J. C., Davila, A. & Schwenzer, S. P. 2012. Uninhabited habitats on Mars. *Icarus,* 217**,** 184-193.

Cockell, C. S., Catling, D. C., Davis, W. L., Snook, K., Kepner, R. L., Lee, P. & McKay, C. P. 2000. The Ultraviolet Environment of Mars: Biological Implications Past, Present, and Future. *Icarus,* 146**,** 343-359.

Cockell, C. S. & Raven, J. A. 2004. Zones of photosynthetic potential on Mars and the early Earth. *Icarus,* 169**,** 300-310.

Cook, A. M., Mattioda, A. L., Ricco, A. J., Quinn, R. C., Elsaesser, A., Ehrenfreund, P., Ricca, A., Jones, N. C. & Hoffmann, S. V. 2014. The Organism/Organic Exposure to Orbital Stresses (O/OREOS) Satellite: Radiation Exposure in Low-Earth Orbit and Supporting Laboratory Studies of Iron Tetraphenylporphyrin Chloride. *Astrobiology,* 14**,** 87-101.

Courtin, R. 2009. Europa, Enceladus and Titan as possible sites for life. *Proceedings of the International Astronomical Union,* 5**,** 676 - 677.

Craddock, R. A. & Howard, A. D. 2002. The case for rainfall on a warm, wet early Mars. *Journal of Geophysical Research: Planets,* 107**,** 5111.

Creighton, T. H. 1993. *Proteins: structures and molecular properties.,* San Francisco, W. H. Freeman.

Cronin, J. R., Cooper, G. W. & Pizzarello, S. 1995. Characteristics and formation of amino acids and hydroxy acids of the Murchison meteorite. *Advances in Space Research,* 15**,** 91-97.

Crovisier, J. 2005. The Molecular Complexity of Comets. *In:* Ehrenfreund, P., Irvine, W., Owen, T., Becker, L., Blank, J., Brucato, J., Colangeli, L., Derenne, S., Dutrey, A., Despois, D., Lazcano, A. & Robert, F. (eds.) *Astrobiology: Future Perspectives.* Netherlands, Springer.

Crowley, D., Boubriak, I., Berquist, B., Clark, M., Richard, E., Sullivan, L., DasSarma, S. & McCready, S. 2006. The uvrA, uvrB and uvrC genes are required for repair of ultraviolet light induced DNA photoproducts in Halobacterium sp. NRC-1. *Saline Systems,* 2**,** 11.

Culka, A., Jehlicka, J. & Edwards, H. G. M. 2010. Acquisition of Raman spectra of amino acids using portable instruments: Outdoor measurements and comparison.

Spectrochimica Acta Part A: Molecular and Biomolecular Spectroscopy, 77**,** 978-983.

Culka, A., Jehlička, J. & Strnad, L. 2012. Testing a portable Raman instrument: The detection of biomarkers in gypsum powdered matrix under gypsum crystals. *Spectrochimica Acta Part A: Molecular and Biomolecular Spectroscopy,* 86**,** 347-350.

Culka, A., Jehlička, J., Vandenabeele, P. & Edwards, H. G. M. 2011. The detection of biomarkers in evaporite matrices using a portable Raman instrument under Alpine conditions. *Spectrochimica Acta Part A: Molecular and Biomolecular Spectroscopy,* 80**,** 8-13.

Dartnell, L., Page, K., Jorge-Villar, S., Wright, G., Munshi, T., Scowen, I., Ward, J. & Edwards, H. 2012. Destruction of Raman biosignatures by ionising radiation and the implications for life detection on Mars. *Analytical and Bioanalytical Chemistry,* 403**,** 131-144.

Dartnell, L. R., Desorgher, L., Ward, J. M. & Coates, A. J. 2007. Modelling the surface and subsurface Martian radiation environment: Implications for astrobiology. *Geophys. Res. Lett.,* 34**,** L02207.

Dartnell, L. R. & Patel, M. R. 2014. Degradation of microbial fluorescence biosignatures by solar ultraviolet radiation on Mars. *International Journal of Astrobiology,* 13**,** 112-123.

DasSarma, S. & DasSarma, P. 2001. Halophiles. *Encyclopedia of Life Sciences.* John Wiley & Sons, Ltd.

DasSarma, S., Kennedy, S., Berquist, B., Victor Ng, W., Baliga, N., Spudich, J., Krebs, M., Eisen, J., Johnson, C. & Hood, L. 2001. Genomic perspective on the photobiology of Halobacterium species NRC-1, a phototrophic, phototactic, and UV-tolerant haloarchaeon. *Photosynth Res,* 70**,** 3 - 17.

Day, J. S., Edwards, H. G. M., Dobrowski, S. A. & Voice, A. M. 2004. The detection of drugs of abuse in fingerprints using Raman spectroscopy I: latent fingerprints. *Spectrochimica Acta Part A: Molecular and Biomolecular Spectroscopy,* 60**,** 563-568.

De Gelder, J., De Gussem, K., Vandenabeele, P. & Moens, L. 2007. Reference database of Raman spectra of biological molecules. *Journal of Raman Spectroscopy,* 38**,** 1133-1147.

Derissen, J. L., Endeman, H. J. & Peerdeman, A. F. 1968. The crystal and molecular structure of l-aspartic acid. *Acta Crystallographica Section B,* 24**,** 1349-1354.

Des Marais, D. J., Harwit, M. O., Jucks, K. W., Kasting, J. F., Lin, D. N. C., Lunine, J. I., Schneider, J., Seager, S., Traub, W. A. & Woolf, N. J. 2002. Remote Sensing of Planetary Properties and Biosignatures on Extrasolar Terrestrial Planets. *Astrobiology,* 2**,** 153-181.

Des Marais, D. J., Nuth, J. A., Allamandola, L. J., Boss, A. P., Farmer, J. D., Hoehler, T. M., Jakosky, B. M., Meadows, V. S., Pohorille, A., Runnegar, B. & Spormann, A. M. 2008. The NASA Astrobiology Roadmap. *Astrobiology,* 8**,** 715-730.

Dhamelincourt, P. & Ramirez, F. J. 1993. Polarized Micro-Raman and FT-IR Spectra of L-Glutamine. *Appl. Spectrosc.,* 47**,** 446-451.

Dhamelincourt, P. & Ramírez, F. J. 1991. Polarized micro-Raman and Fourier transform infrared spectra of L-glutamic acid. *Journal of Raman Spectroscopy,* 22**,** 577-582.

Dollish, F. R., Fateley, W. G. & Bentley, F. F. 1974. *Characteristic Raman Frequencies of Organic Compounds,* New York, John Wiley & Sons.

Edsall, J. T., Otvos, J. W. & Rich, A. 1950. Raman Spectra of Amino Acids and Related Compounds. VII. Glycylglycine, Cysteine, Cystine and Other Amino Acids. *Journal of the American Chemical Society,* 72**,** 474-477.

Edwards, H. G. M., Hutchinson, I. & Ingley, R. 2012a. The ExoMars Raman spectrometer and the identification of biogeological spectroscopic signatures using a flight-like prototype. *Analytical and Bioanalytical Chemistry,* 404**,** 1723-1731.

Edwards, H. G. M., Hutchinson, I. B. & Ingley, R. 2012b. Raman spectroscopy and the search for life signatures in the ExoMars Mission. *International Journal of Astrobiology,* 11**,** 269-278.

Egli, T. 2009. Growth Kinetics, Bacterial. *In:* Schaechter, M. (ed.) *Encyclopedia of Microbiology (Third Edition).* Oxford: Academic Press.

Eglinton, G., Scott, P. M., Belsky, T., Burlingame, A. L. & Calvin, M. 1964. Hydrocarbons of Biological Origin from a One-Billion-Year-Old Sediment. *Science,* 145**,** 263-264.

Ehrenfreund, P., Bernstein, M. P., Dworkin, J. P., Sandford, S. A. & Allamandola, L. J. 2001a. The Photostability of Amino Acids in Space. *The Astrophysical Journal Letters,* 550**,** L95.

Ehrenfreund, P. & Charnley, S. B. 2000. Organic Molecules In The Interstellar Medium, Comets, And Meteorites: A Voyage from Dark Clouds to the Early Earth. *Annual Review of Astronomy and Astrophysics,* 38**,** 427-483.

Ehrenfreund, P., Glavin, D. P., Botta, O., Cooper, G. & Bada, J. L. 2001b. Extraterrestrial amino acids in Orgueil and Ivuna: Tracing the parent body of CI type carbonaceous chondrites. *Proceedings of the National Academy of Sciences,* 98**,** 2138-2141.

El-Sayed, W. S. M., Takaichi, S., Saida, H., Kamekura, M., Abu-Shady, M., Seki, H. & Kuwabara, T. 2002. Effects of Light and Low Oxygen Tension on Pigment Biosynthesis in Halobacterium salinarum, Revealed by a Novel Method to Quantify Both Retinal and Carotenoids. *Plant and Cell Physiology,* 43**,** 379-383.

ESA. 2014. *ExoMars Trace Gas Orbiter Instruments* [Online]. Available: http://exploration.esa.int/mars/48523-trace-gas-orbiter-instruments/, retrieved 28/05/2014.

Fendrihan, S., Bérces, A., Lammer, H., Musso, M., Rontó, G., Polacsek, T. K., Holzinger, A., Kolb, C. & Stan-Lotter, H. 2009a. Investigating the Effects of Simulated Martian Ultraviolet Radiation on Halococcus dombrowskii and Other Extremely Halophilic Archaebacteria. *Astrobiology,* 9**,** 104-112.

Fendrihan, S., Dornmayr-Pfaffenhuemer, M., Gerbl, F. W., Holzinger, A., Grösbacher, M., Briza, P., Erler, A., Gruber, C., Plätzer, K. & Stan-Lotter, H. 2012. Spherical particles of halophilic archaea correlate with exposure to low water activity – implications for microbial survival in fluid inclusions of ancient halite. *Geobiology,* 10**,** 424-433.

Fendrihan, S., Musso, M. & Stan-Lotter, H. 2009b. Raman spectroscopy as a potential method for the detection of extremely halophilic archaea embedded in halite in terrestrial and possibly extraterrestrial samples. *Journal of Raman Spectroscopy,* 40**,** 1996-2003.

Ferraro, J. R., Nakamoto, K. & Brown, C. W. 2003. *Introductory Raman Spectroscopy*. San Diego, Academic Press.

Fischer, E., Martínez, G. M., Elliott, H. M. & Rennó, N. O. 2014. Experimental evidence for the formation of liquid saline water on Mars. *Geophysical Research Letters,* 41**,** 4456-4462.

Flynn, G. J. 1996. The delivery of organic matter from asteroids and comets to the early surface of Mars. *Earth, Moon, and Planets,* 72**,** 469-474.

Formisano, V., Atreya, S., Encrenaz, T., Ignatiev, N. & Giuranna, M. 2004. Detection of Methane in the Atmosphere of Mars. *Science,* 306**,** 1758-1761.

Foucher, F., Lopes-Reyes, G., Bost, N., Rull-Perez, F. & Rüßmann, P. 2013. Effect of grain size distribution on Raman analyses and the consequences for in situ planetary missions. *Journal of Raman Spectroscopy,* 44**,** 916-925.

Freissinet, C., Buch, A., Szopa, C. & Sternberg, R. 2013. Enantiomeric separation of volatile organics by gas chromatography for the in situ analysis of extraterrestrial materials: Kinetics and thermodynamics investigation of various chiral stationary phases. *Journal of Chromatography A,* 1306**,** 59-71.

Garry, J. R. C., Ten Kate, I. L., Martins, Z., Nørnberg, P. & Ehrenfreund, P. 2006. Analysis and survival of amino acids in Martian regolith analogs. *Meteoritics & Planetary Science,* 41**,** 391-405.

Gellert, R., Rieder, R., Anderson, R. C., Brückner, J., Clark, B. C., Dreibus, G., Economou, T., Klingelhöfer, G., Lugmair, G. W., Ming, D. W., Squyres, S. W., D'uston, C., Wänke, H., Yen, A. & Zipfel, J. 2004. Chemistry of Rocks and Soils in Gusev Crater from the Alpha Particle X-ray Spectrometer. *Science,* 305**,** 829-832.

Gendrin, A., Mangold, N., Bibring, J.-P., Langevin, Y., Gondet, B., Poulet, F., Bonello, G., Quantin, C., Mustard, J., Arvidson, R. & Lemouélic, S. 2005. Sulfates in Martian Layered Terrains: The OMEGA/Mars Express View. *Science,* 307**,** 1587-1591.

Gilmour, I. 2003. 1.10 - Structural and Isotopic Analysis of Organic Matter in Carbonaceous Chondrites. *In:* Heinrich, D. H. & Karl, K. T. (eds.) *Treatise on Geochemistry.* Oxford: Pergamon.

Goguen, J. D., Clancy, R. T., Wolff, M. J. & James, P. B. 2003. UV Optical Properties of Aerosol Dust from HST STIS Spectra of Mars during the 2001 Dust Storm. *American Astronomical Society, DPS meeting #35, #03.09; Bulletin of the American Astronomical Society* [Online], 35. Available: http://adsabs.harvard.edu/abs/2003DPS....35.0309G.

Golyshina, O. V., Pivovarova, T. A., Karavaiko, G. I., Kondrat'eva, T. F., Moore, E. R. B., Abraham, W.-R., Lünsdorf, H., Timmis, K. N., Yakimov, M. M. & Golyshin, P. N. 2000. *Ferroplasma acidiphilum* gen. nov., sp. nov., an acidophilic, autotrophic, ferrous-iron-oxidizing, cell-wall-lacking, mesophilic member of the *Ferroplasmaceae* fam. nov., comprising a distinct lineage of the *Archaea*. *International Journal of Systematic and Evolutionary Microbiology,* 50**,** 997 - 1006.

Gómez-Elvira, J., Armiens, C., Carrasco, I., Genzer, M., Gómez, F., Haberle, R., Hamilton, V. E., Harri, A.-M., Kahanpää, H., Kemppinen, O., Lepinette, A., Martín Soler, J., Martín-Torres, J., Martínez-Frías, J., Mischna, M., Mora, L., Navarro, S., Newman, C., De Pablo, M. A., Peinado, V., Polkko, J., Rafkin, S. C. R., Ramos, M., Rennó, N. O., Richardson, M., Rodríguez-Manfredi, J. A., Romeral Planelló, J. J., Sebastián, E., De La Torre Juárez, M., Torres, J., Urquí, R., Vasavada, A. R., Verdasca, J. & Zorzano, M.-P. 2014. Curiosity's rover environmental monitoring station: Overview of the first 100 sols. *Journal of Geophysical Research: Planets,* 119**,** 2013JE004576.

Goodyear, M. D. 2013. *Organic chemistry and mineral interactions in the solar system.* PhD, The Open University.

Gramain, A. 2009. *Entombment and survival of extreme halophiles in halite.* Doctor of Philosophy, University of Essex.

Grant, W. D., Gemmell, R. T. & McGenity, T. J. 1998. Halobacteria: the evidence for longevity. *Extremophiles,* 2**,** 279-287.

Grotzinger, J., Crisp, J., Vasavada, A., Anderson, R., Baker, C., Barry, R., Blake, D., Conrad, P., Edgett, K., Ferdowski, B., Gellert, R., Gilbert, J., Golombek, M., Gómez-Elvira, J., Hassler, D., Jandura, L., Litvak, M., Mahaffy, P., Maki, J., Meyer, M., Malin, M., Mitrofanov, I., Simmonds, J., Vaniman, D., Welch, R. &

Wiens, R. 2012. Mars Science Laboratory Mission and Science Investigation. *Space Science Reviews,* 170**,** 5-56.

Grotzinger, J. P., Sumner, D. Y., Kah, L. C., Stack, K., Gupta, S., Edgar, L., Rubin, D., Lewis, K., Schieber, J., Mangold, N., Milliken, R., Conrad, P. G., Desmarais, D., Farmer, J., Siebach, K., Iii, F. C., Hurowitz, J., McLennan, S. M., Ming, D., Vaniman, D., Crisp, J., Vasavada, A., Edgett, K. S., Malin, M., Blake, D., Gellert, R., Mahaffy, P., Wiens, R. C., Maurice, S., Grant, J. A., Wilson, S., Anderson, R. C., Beegle, L., Arvidson, R., Hallet, B., Sletten, R. S., Rice, M., Iii, J. B., Griffes, J., Ehlmann, B., Anderson, R. B., Bristow, T. F., Dietrich, W. E., Dromart, G., Eigenbrode, J., Fraeman, A., Hardgrove, C., Herkenhoff, K., Jandura, L., Kocurek, G., Lee, S., Leshin, L. A., Leveille, R., Limonadi, D., Maki, J., McCloskey, S., Meyer, M., Minitti, M., Newsom, H., Oehler, D., Okon, A., Palucis, M., Parker, T., Rowland, S., Schmidt, M., Squyres, S., Steele, A., Stolper, E., Summons, R., Treiman, A., Williams, R., Yingst, A., Team, M. S., Kemppinen, O., Bridges, N., Johnson, J. R., Cremers, D., Godber, A., Wadhwa, M., Wellington, D., McEwan, I., Newman, C., Richardson, M., Charpentier, A., Peret, L., King, P., Blank, J., Weigle, G., Li, S., Robertson, K., Sun, V., Baker, M., Edwards, C., Farley, K., Miller, H., Newcombe, M., Pilorget, C., Brunet, C., Hipkin, V., Léveillé, R., et al. 2014. A Habitable Fluvio-Lacustrine Environment at Yellowknife Bay, Gale Crater, Mars. *Science*, 343.

Gruber, C., Legat, A., Pfaffenhuemer, M., Radax, C., Weidler, G., Busse, H.-J. & Stan-Lotter, H. 2004. Halobacterium noricense sp. nov., an archaeal isolate from a bore core of an alpine Permian salt deposit, classification of Halobacterium sp. NRC-1 as a strain H. salinarum and emended description of H. salinarum. *Extremophiles,* 8**,** 431-439.

Gu, C.-H. & Grant, D. J. W. 2006. Physical properties and enantiomeric composition. *In:* Busch, K. W. & Busch, M. A. (eds.) *Chiral Analysis.* Oxford: Elsevier.

Gulick, V. C. & Baker, V. R. 1990. Origin and evolution of valleys on Martian volcanoes. *Journal of Geophysical Research: Solid Earth,* 95**,** 14325-14344.

Ha, D.-J., Joo, W.-A., Han, G.-Y. & Kim, C.-W. 2007. Proteome analysis of Halobacterium salinarum and characterization of proteins related to the degradation of isopropyl alcohol. *Biochimica et Biophysica Acta (BBA) - Proteins and Proteomics,* 1774**,** 44-50.

Haberle, R. M., McKay, C. P., Schaeffer, J., Cabrol, N. A., Grin, E. A., Zent, A. P. & Quinn, R. 2001. On the possibility of liquid water on present-day Mars. *Journal of Geophysical Research: Planets,* 106**,** 23317-23326.

Harding, M. M. & Long, H. A. 1968. The crystal and molecular structure of L-cysteine. *Acta Crystallographica Section B,* 24**,** 1096-1102.

Hardy, P. M. 1985. The Protein Amino Acids. *In:* Barrett, G. C. (ed.) *Chemistry and Biochemistry of the Amino Acids.* London: Chapman and Hall Ltd.

Hargraves, R. B., Knudsen, J. M. & Madsen, M. B. 1999. [Comment on "Martian soil simulant available for scientific, educational study"] Caution advised on suitability of a Mars soil simulant. *Eos, Transactions American Geophysical Union,* 80**,** 168-169.

Harri, A. M., Genzer, M., Kemppinen, O., Kahanpää, H., Gomez-Elvira, J., Rodriguez-Manfredi, J. A., Haberle, R., Polkko, J., Schmidt, W., Savijärvi, H., Kauhanen, J., Atlaskin, E., Richardson, M., Siili, T., Paton, M., De La Torre Juarez, M., Newman, C., Rafkin, S., Lemmon, M. T., Mischna, M., Merikallio, S., Haukka, H., Martin-Torres, J., Zorzano, M. P., Peinado, V., Urqui, R., Lapinette, A., Scodary, A., Mäkinen, T., Vazquez, L., Rennó, N. & The, R. M. S. L. S. T. 2014. Pressure

observations by the Curiosity rover: Initial results. *Journal of Geophysical Research: Planets,* 119**,** 82-92.

Hartman, A. L., Norais, C., Badger, J. H., Delmas, S., Haldenby, S., Madupu, R., Robinson, J., Khouri, H., Ren, Q., Lowe, T. M., Maupin-Furlow, J., Pohlschroder, M., Daniels, C., Pfeiffer, F., Allers, T. & Eisen, J. A. 2010. The Complete Genome Sequence of *Haloferax volcanii* DS2, a Model Archaeon. *PLoS ONE,* 5**,** e9605.

Hartmann, W. K. 2005. Martian cratering 8: Isochron refinement and the chronology of Mars. *Icarus,* 174, 294-320.

Hecht, M. H., Kounaves, S. P., Quinn, R. C., West, S. J., Young, S. M. M., Ming, D. W., Catling, D. C., Clark, B. C., Boynton, W. V., Hoffman, J., DeFlores, L. P., Gospodinova, K., Kapit, J. & Smith, P. H. 2009. Detection of Perchlorate and the Soluble Chemistry of Martian Soil at the Phoenix Lander Site. *Science,* 325**,** 64-67.

Hegde, S., Paulino-Lima, I. G., Kent, R., Kaltenegger, L. & Rothschild, L. 2015. Surface biosignatures of exo-Earths: Remote detection of extraterrestrial life. *Proceedings of the National Academy of Sciences,* 112**,** 3886-3891.

Hess, S. L., Ryan, J. A., Tillman, J. E., Henry, R. M. & Leovy, C. B. 1980. The annual cycle of pressure on Mars measured by Viking Landers 1 and 2. *Geophys. Res. Lett.,* 7**,** 197-200.

Horowitz, N. H., Hobby, G. L. & Hubbard, J. S. 1977. Viking on Mars: The carbon assimilation experiments. *Journal of Geophysical Research,* 82**,** 4659-4662.

Hutchinson, I. B., Ingley, R., Edwards, H. G. M., Harris, L., McHugh, M., Malherbe, C. & Parnell, J. 2014. Raman spectroscopy on Mars: identification of geological and bio-geological signatures in Martian analogues using miniaturized Raman spectrometers. *Philosophical Transactions of the Royal Society A: Mathematical, Physical and Engineering Sciences,* 372.

Hynek, B. M., Beach, M. & Hoke, M. R. T. 2010. Updated global map of Martian valley networks and implications for climate and hydrologic processes. *J. Geophys. Res.,* 115**,** E09008.

Izawa, M., Applin, D. & Cloutis, E. Detection Limits of Polycyclic Aromatic Hydrocarbons (PAHs) in Martian Soil Simulant JSC-Mars-1. *Lunar and Planetary Science Conference,* 2014. 1572.

Jackman, J. 2012. The Microbe: The Basics of Structure, Morphology, and Physiology as They Relate to Microbial Characterization and Attribution. *In:* Cliff, B. J., Kreuzer, W. H., Ehrhardt, J. C. & Wunschel, S. D. (eds.) *Chemical and Physical Signatures for Microbial Forensics.* New York, NY: Springer New York.

Jehlička, J., Edwards, H. G. M. & Oren, A. 2013. Bacterioruberin and salinixanthin carotenoids of extremely halophilic Archaea and Bacteria: A Raman spectroscopic study. *Spectrochimica Acta Part A: Molecular and Biomolecular Spectroscopy,* 106**,** 99-103.

Jenkins, A. L., Larsen, R. A. & Williams, T. B. 2005. Characterization of amino acids using Raman spectroscopy. *Spectrochimica Acta Part A: Molecular and Biomolecular Spectroscopy,* 61**,** 1585-1594.

Johnson, A. P., Pratt, L. M., Vishnivetskaya, T., Pfiffner, S., Bryan, R. A., Dadachova, E., Whyte, L., Radtke, K., Chan, E., Tronick, S., Borgonie, G., Mancinelli, R. L., Rothschild, L. J., Rogoff, D. A., Horikawa, D. D. & Onstott, T. C. 2011. Extended survival of several organisms and amino acids under simulated martian surface conditions. *Icarus,* 211**,** 1162-1178.

Johnson, P. V., Hodyss, R., Chernow, V. F., Lipscomb, D. M. & Goguen, J. D. 2012. Ultraviolet photolysis of amino acids on the surface of icy Solar System bodies. *Icarus,* 221**,** 800-805.

Jönsson, P. G. & Kvick, Å. 1972. Precision neutron diffraction structure determination of protein and nucleic acid components. III. The crystal and molecular structure of the amino acid [alpha]-glycine. *Acta Crystallographica Section B,* 28**,** 1827-1833.

Joo, W.-A. & Kim, C.-W. 2005. Proteomics of Halophilic archaea. *Journal of Chromatography B,* 815**,** 237-250.

Jorge Villar, S. & Edwards, H. 2006. Raman spectroscopy in astrobiology. *Analytical and Bioanalytical Chemistry,* 384**,** 100-113.

Jorge Villar, S. E., Edwards, H. & Worland, M. 2005. Comparative Evaluation Of Raman Spectroscopy At Different Wavelengths For Extremophile Exemplars. *Origins of Life and Evolution of Biospheres,* 35**,** 489-506.

Kelly, M., Norgård, S. & Synnøve, L.-J. 1970. Bacterial Carotenoids. 31. C_{50}-carotenoids. Carotenoids of *Halobacterium salinarium*, especially bacterioruberin. *Acta Chemica Scandinavica,* 24**,** 2169-2182.

Kieffer, H. H., Christensen, P. R., Martin, T. Z., Miner, E. D. & Palluconi, F. D. 1976. Temperatures of the Martian Surface and Atmosphere: Viking Observation of Diurnal and Geometric Variations. *Science,* 194**,** 1346-1351.

Kittel, C. 2005. Chapter 20: Point Defects. *Introduction to Solid State Physics.* Eighth ed. USA: John Wiley & Sons, Inc.

Klein, H. P. 1974. Automated Life-Detection Experiments for the Viking Mission to Mars. *In:* Oró, J., Miller, S. L., Ponnamperuma, C. & Young, R. S. (eds.) *Cosmochemical Evolution and the Origins of Life.* Netherlands, Springer.

Klein, H. P. 1977. The Viking Biological Investigation: General aspects. *Journal of Geophysical Research,* 82**,** 4677-4680.

Kminek, G. & Bada, J. L. 2006. The effect of ionizing radiation on the preservation of amino acids on Mars. *Earth and Planetary Science Letters,* 245**,** 1-5.

Koenig, J. L. 1972. Raman spectroscopy of biological molecules: A review. *Journal of Polymer Science: Macromolecular Reviews,* 6**,** 59-177.

Koetzle, T. F., Frey, M. N., Lehmann, M. S. & Hamilton, W. C. 1973. Precision neutron diffraction structure determination of protein and nucleic acid components. XIII. Molecular and crystal structure of the amino acid L-glutamine. *Acta Crystallographica Section B,* 29**,** 2571-2575.

Krasnopolsky, V. A., Maillard, J. P. & Owen, T. C. 2004. Detection of methane in the martian atmosphere: evidence for life? *Icarus,* 172**,** 537-547.

Kumar, S., Kumar Rai, A., Rai, S. B., Rai, D. K., Singh, A. N. & Singh, V. B. 2006. Infrared, Raman and electronic spectra of alanine: A comparison with ab intio calculation. *Journal of Molecular Structure,* 791**,** 23-29.

Kumar, S., Rai, A. K., Singh, V. B. & Rai, S. B. 2005. Vibrational spectrum of glycine molecule. *Spectrochimica Acta Part A: Molecular and Biomolecular Spectroscopy,* 61**,** 2741-2746.

Kvenvolden, K., Lawless, J., Pering, K., Peterson, E., Flores, J., Ponnamperuma, C., Kaplan, I. R. & Moore, C. 1970. Evidence for Extraterrestrial Amino-acids and Hydrocarbons in the Murchison Meteorite. *Nature,* 228**,** 923-926.

Kvenvolden, K. A., Lawless, J. G. & Ponnamperuma, C. 1971. Nonprotein Amino Acids in the Murchison Meteorite. *Proceedings of the National Academy of Sciences,* 68**,** 486-490.

Lafuente, B., Downs, R. T., Yang, H. & Stone, N. 2015. *The power of databases: the RRUFF project. In: Highlights in Mineralogical Crystallography, pp 1-30* [Online]. Berlin, Germany: W. De Gruyter. Available: http://rruff.info/about/downloads/HMC1-30.pdf [Accessed 7th June 2016].

Lage, C. a. S., Dalmaso, G. Z. L., Teixeira, L. C. R. S., Bendia, A. G., Paulino-Lima, I. G., Galante, D., Janot-Pacheco, E., Abrevaya, X. C., Azúa-Bustos, A., Pelizzari, V. H.

& Rosado, A. S. 2012. Mini-Review: Probing the limits of extremophilic life in extraterrestrial environment-simulated experiments. *International Journal of Astrobiology,* 11**,** 251-256.

Lawless, J. G., Kvenvolden, K. A., Peterson, E., Ponnamperuma, C. & Moore, C. 1971. Amino Acids Indigenous to the Murray Meteorite. *Science,* 173**,** 626-627.

Lehmann, M. S., Koetzle, T. F. & Hamilton, W. C. 1972. Precision neutron diffraction structure determination of protein and nucleic acid components. I. Crystal and molecular structure of the amino acid L-alanine. *Journal of the American Chemical Society,* 94**,** 2657-2660.

Leshin, L. A., Mahaffy, P. R., Webster, C. R., Cabane, M., Coll, P., Conrad, P. G., Archer, P. D., Atreya, S. K., Brunner, A. E., Buch, A., Eigenbrode, J. L., Flesch, G. J., Franz, H. B., Freissinet, C., Glavin, D. P., McAdam, A. C., Miller, K. E., Ming, D. W., Morris, R. V., Navarro-González, R., Niles, P. B., Owen, T., Pepin, R. O., Squyres, S., Steele, A., Stern, J. C., Summons, R. E., Sumner, D. Y., Sutter, B., Szopa, C., Teinturier, S., Trainer, M. G., Wray, J. J., Grotzinger, J. P. & Team, M. S. 2013. Volatile, Isotope, and Organic Analysis of Martian Fines with the Mars Curiosity Rover. *Science,* 341.

Leuko, S., Legat, A., Fendrihan, S. & Stan-Lotter, H. 2004. Evaluation of the LIVE/DEAD BacLight Kit for Detection of Extremophilic Archaea and Visualization of Microorganisms in Environmental Hypersaline Samples. *Applied and Environmental Microbiology,* 70**,** 6884-6886.

Lima, J. A., Freire, P. T. C., Lima, R. J. C., Moreno, A. J. D., Mendes Filho, J. & Melo, F. E. A. 2005. Raman scattering of L-valine crystals. *Journal of Raman Spectroscopy,* 36**,** 1076-1081.

Long, D. A. 1977. *Raman Spectroscopy,* Great Britian, McGraw-Hill International Book Company.

Lunine, J. I. 2005. Necessary Concepts III: The Chemistry of Life. *Astrobiology A Multidisciplinary Approach.* San Francisco: Pearson Education Inc.

Magrum, L., Luehrsen, K. & Woese, C. 1978. Are extreme halophiles actually "bacteria"? *Journal of Molecular Evolution,* 11**,** 1-8.

Mahaffy, P. R., Webster, C. R., Atreya, S. K., Franz, H., Wong, M., Conrad, P. G., Harpold, D., Jones, J. J., Leshin, L. A., Manning, H., Owen, T., Pepin, R. O., Squyres, S., Trainer, M. & Team, M. S. 2013. Abundance and Isotopic Composition of Gases in the Martian Atmosphere from the Curiosity Rover. *Science,* 341**,** 263-266.

Mancinelli, R. L., Fahlen, T. F., Landheim, R. & Klovstad, M. R. 2004. Brines and evaporites: analogs for Martian life. *Advances in Space Research,* 33**,** 1244-1246.

Marion, G. M., Fritsen, C. H., Eicken, H. & Payne, M. 2003. The Search for Life on Europa: Limiting Environmental Factors, Potential Habitats and Earth Analogues. *Astrobiology,* 3**,** 785 - 811.

Marshall, C. P., Leuko, S., Coyle, C. M., Walter, M. R., Burns, B. P. & Neilan, B. A. 2007. Carotenoid Analysis of Halophilic Archaea by Resonance Raman Spectroscopy. *Astrobiology,* 7**,** 631-643.

Martin-Torres, F. J., Zorzano, M.-P., Valentin-Serrano, P., Harri, A.-M., Genzer, M., Kemppinen, O., Rivera-Valentin, E. G., Jun, I., Wray, J., Bo Madsen, M., Goetz, W., McEwen, A. S., Hardgrove, C., Renno, N., Chevrier, V. F., Mischna, M., Navarro-Gonzalez, R., Martinez-Frias, J., Conrad, P., McConnochie, T., Cockell, C., Berger, G., R. Vasavada, A., Sumner, D. & Vaniman, D. 2015. Transient liquid water and water activity at Gale crater on Mars. *Nature Geosci,* 8**,** 357-361.

Martín-Torres, F. J., Zorzano, M.-P., Valentín-Serrano, P., Harri, A.-M., Genzer, M., Kemppinen, O., Rivera-Valentin, E. G., Jun, I., Wray, J., Madsen, M. B., Goetz, W., McEwen, A. S., Hardgrove, C., Renno, N., Chevrier, V. F., Mischna, M.,

Navarro-González, R., Martínez-Frías, J., Conrad, P., McConnochie, T., Cockell, C., Berger, G., Vasavada, A. R., Sumner, D. & Vaniman, D. 2015. Transient liquid water and water activity at Gale crater on Mars. *Nature Geoscience,* 8, 357-361.

Martin, E. L., Reinhardt, R. L., Baum, L. L., Becker, M. R., Shaffer, J. J. & Kokjohn, T. A. 2000. The effects of ultraviolet radiation on the moderate halophile Halomonas elongata and the extreme halophile Halobacterium salinarum. *Canadian Journal of Microbiology,* 46**,** 180-187.

Martins, Z., Price, M. C., Goldman, N., Sephton, M. A. & Burchell, M. J. 2013. Shock synthesis of amino acids from impacting cometary and icy planet surface analogues. *Nature Geosci,* 6**,** 1045-1049.

Martins, Z., Sephton, M. A., Foing, B. H. & Ehrenfreund, P. 2011. Extraction of amino acids from soils close to the Mars Desert Research Station (MDRS), Utah. *International Journal of Astrobiology,* 10**,** 231-238.

Mateshvili, N., Fussen, D., Vanhellemont, F., Bingen, C., Dodion, J., Montmessin, F., Perrier, S., Dimarellis, E. & Bertaux, J.-L. 2007. Martian ice cloud distribution obtained from SPICAM nadir UV measurements. *Journal of Geophysical Research: Planets,* 112.

Matthews, M. J., Pimenta, M. A., Dresselhaus, G., Dresselhaus, M. S. & Endo, M. 1999. Origin of dispersive effects of the Raman D band in carbon materials. *Physical Review B,* 59**,** R6585-R6588.

Mazur, P. 1984. Freezing of living cells: mechanisms and implications. *American Journal of Physiology - Cell Physiology,* 247**,** C125-C142.

McCready, S. 1996. The repair of ultraviolet light-induced DNA damage in the halophilic archaebacteria, Halobacterium cutirubrum, Halobacterium halobium and Haloferax volcanii. *Mutat Res,* 364**,** 25 - 32.

McCready, S. & Marcello, L. 2003. Repair of UV damage in *Halobacterium salinarum*. *Biochemical Society Transactions,* 31**,** 694–698.

McEwen, A. S., Dundas, C. M., Mattson, S. S., Toigo, A. D., Ojha, L., Wray, J. J., Chojnacki, M., Byrne, S., Murchie, S. L. & Thomas, N. 2013. Recurring slope lineae in equatorial regions of Mars. *Nature Geosci,* 7**,** 53-58.

McEwen, A. S., Ojha, L., Dundas, C. M., Mattson, S. S., Byrne, S., Wray, J. J., Cull, S. C., Murchie, S. L., Thomas, N. & Gulick, V. C. 2011. Seasonal Flows on Warm Martian Slopes. *Science,* 333**,** 740-743.

McKay, C. P. 1997. The Search For Life On Mars. *Origins of Life and Evolution of Biospheres,* 27**,** 263-289.

McKay, C. P. 2004. What Is Life—and How Do We Search for It in Other Worlds? *PLoS Biol,* 2**,** e302.

McKay, D. S., Gibson Jr, E. K., Thomas-Keprta, K. L., Vali, H., Romanek, C. S., Simon, J. C., Chillier, X. D. F., Maechling, C. R. & Zare, R. N. 1996. Search for Past Life on Mars: Possible Relic Biogenic Activity in Martian Meteorite ALH84001. *Science,* 273**,** 924-930.

McLennan, S. M., Anderson, R. B., Bell, J. F., Iii, Bridges , J. C., Calef, F., Campbell, J. L., Clark, B. C., Clegg, S., Conrad, P., Cousin, A., Des Marais, D. J., Dromart, G., Dyar, M. D., Edgar, L. A., Ehlmann, B. L., Fabre, C., Forni, O., Gasnault, O., Gellert, R., Gordon, S., Grant, A., Grotzinger, J. P., Gupta, S., Herkenhoff, K. E., Hurowitz, J. A., King, P. L., Le Mouélic, S., Leshin, L. A., Léveillé, R., Lewis, K. W., Mangold, N., Maurice, S., Ming, D. W., Morris, R. V., Nachon, M., Newsom, H. E., Ollila, A., Perrett, G. M., Rice, M. S., Schmidt, M. E., Schwenzer, S. P., Stack, K., Stolper, E. M., Sumner, D. Y., Treiman, A. H., Vanbommel, S., Vaniman, D. T., Vasavada, A., Wiens, R. C. & Yingst, R. A. 2014. Elemental

Geochemistry of Sedimentary Rocks at Yellowknife Bay, Gale Crater, Mars. *Science,* 343.

Mehrens, S. M., Kale, U. J. & Qu, X. 2005. Statistical analysis of differences in the Raman spectra of polymorphs. *Journal of Pharmaceutical Sciences,* 94**,** 1354-1367.

Melosh, H. J. 1988. The rocky road to panspermia. *Nature,* 332**,** 687-688.

Miller, S. L. 1953. A Production of Amino Acids under Possible Primitive Earth Conditions. *Science,* 117**,** 528-529.

Minkov, V. S., Krylov, A. S., Boldyreva, E. V., Goryainov, S. V., Bizyaev, S. N. & Vtyurin, A. N. 2008. Pressure-Induced Phase Transitions in Crystalline l- and dl-Cysteine. *The Journal of Physical Chemistry B,* 112**,** 8851-8854.

Moeller, R., Reitz, G., Douki, T., Cadet, J., Horneck, G. & Stan-Lotter, H. 2010. UV photoreactions of the extremely haloalkaliphilic euryarchaeon Natronomonas pharaonis. *FEMS Microbiology Ecology,* 73**,** 271-277.

Moggach, S. A., Allan, D. R., Clark, S. J., Gutmann, M. J., Parsons, S., Pulham, C. R. & Sawyer, L. 2006. High-pressure polymorphism in l-cysteine: the crystal structures of l-cysteine-III and l-cysteine-IV. *Acta Crystallographica Section B,* 62**,** 296-309.

Möhlmann, D. T. F., Niemand, M., Formisano, V., Savijärvi, H. & Wolkenberg, P. 2009. Fog phenomena on Mars. *Planetary and Space Science,* 57**,** 1987-1992.

Molecular Probes Inc. 2004. *LIVE/DEAD ® BacLight™ Bacterial Viability and Counting Kit (L34856)* [Online]. Available: https://tools.lifetechnologies.com/content/sfs/manuals/mp34856.pdf [Accessed September 2013].

Monaghan, E. P. 2013. *The Habitability of the Martian Subsurface for Microbial Life.* PhD, The Open University.

Morozov, L. 1979. Mirror symmetry breaking in biochemical evolution. *Origins of life,* 9**,** 187-217.

Morrison, D. 2001. The NASA Astrobiology Program. *Astrobiology,* 1**,** 3-13.

Mumma, M. J., Villanueva, G. L., Novak, R. E., Hewagama, T., Bonev, B. P., Disanti, M. A., Mandell, A. M. & Smith, M. D. 2009. Strong Release of Methane on Mars in Northern Summer 2003. *Science,* 323**,** 1041-1045.

Munoz Caro, G. M., Meierhenrich, U. J., Schutte, W. A., Barbier, B., Arcones Segovia, A., Rosenbauer, H., Thiemann, W. H. P., Brack, A. & Greenberg, J. M. 2002. Amino acids from ultraviolet irradiation of interstellar ice analogues. *Nature,* 416**,** 403-406.

Murli, C., Thomas, S., Venkateswaran, S. & M Sharma, S. 2005. Raman spectroscopic investigation of α-glycine at different temperatures. *Physica B: Condensed Matter,* 364**,** 233-238.

Murray, A. E., Kenig, F., Fritsen, C. H., McKay, C. P., Cawley, K. M., Edwards, R., Kuhn, E., McKnight, D. M., Ostrom, N. E., Peng, V., Ponce, A., Priscu, J. C., Samarkin, V., Townsend, A. T., Wagh, P., Young, S. A., Yung, P. T. & Doran, P. T. 2012. Microbial life at −13 °C in the brine of an ice-sealed Antarctic lake. *Proceedings of the National Academy of Sciences,* 109**,** 20626-20631.

Mustard, J. F., Adler, M., Allwood, A., Bass, D. S., Beaty, D. W., Bell Iii, J. F., Brinckerhoff, W. B., Carr, M., Des Marais, D. J., Drake, B., Edgett, K. S., Eigenbrode, J., Elkins-Tanton, L. T., Grant, J. A., Milkovich, S. M., Ming, D., Moore, C., Murchie, S., Onstott, T. C., Ruff, S. W., Sephton, M. A., Steele, A. & Treiman, A. 2013. Report of the Mars 2020 Science Definition Team. 154 pp., posted July, 2013, by the Mars Exploration Program Analysis Group (MEPAG) at http://mepag.jpl.nasa.gov/reports/MEP/Mars_2020_SDT_Report_Final.pdf.

Mustard, J. F. & Bell, J. F. 1994. New composite reflectance spectra of Mars from 0.4 to 3.14 μm. *Geophysical Research Letters,* 21**,** 353-356.

Mutch, T. A., Arvidson, R. E., Binder, A. B., Guinness, E. A. & Morris, E. C. 1977. The Geology of the Viking Lander 2 Site. *J. Geophys. Res.,* 82**,** 4452-4467.

NASA. 2015. *2015 Astrobiology Strategy* [Online]. Available: https://astrobiology.nasa.gov/research/astrobiology-at-nasa/astrobiology-strategy/.

Navarrete, J. T. L., Hernández, V. & Ramírez, F. J. 1994. IR and Raman spectra of L-aspartic acid and isotopic derivatives. *Biopolymers,* 34**,** 1065-1077.

Navarro-González, R. & McKay, C. P. 2011. Reply to comment by Biemann and Bada on "Reanalysis of the Viking results suggests perchlorate and organics at midlatitudes on Mars". *Journal of Geophysical Research: Planets,* 116**,** E12002.

Navarro-González, R., Vargas, E., De La Rosa, J., Raga, A. C. & McKay, C. P. 2010. Reanalysis of the Viking results suggests perchlorate and organics at midlatitudes on Mars. *J. Geophys. Res.,* 115**,** E12010.

Newsom, H. E., Bishop, J. L., Cockell, C., Roush, T. L. & Johnson, J. R. 2001. Search for life on Mars in surface samples: Lessons from the 1999 Marsokhod rover field experiment. *J. Geophys. Res.,* 106**,** 7713-7720.

Ng, W. V., Kennedy, S. P., Mahairas, G. G., Berquist, B., Pan, M., Shukla, H. D., Lasky, S. R., Baliga, N. S., Thorsson, V., Sbrogna, J., Swartzell, S., Weir, D., Hall, J., Dahl, T. A., Welti, R., Goo, Y. A., Leithauser, B., Keller, K., Cruz, R., Danson, M. J., Hough, D. W., Maddocks, D. G., Jablonski, P. E., Krebs, M. P., Angevine, C. M., Dale, H., Isenbarger, T. A., Peck, R. F., Pohlschroder, M., Spudich, J. L., Jung, K.-H., Alam, M., Freitas, T., Hou, S., Daniels, C. J., Dennis, P. P., Omer, A. D., Ebhardt, H., Lowe, T. M., Liang, P., Riley, M., Hood, L. & DasSarma, S. 2000. Genome sequence of Halobacterium species NRC-1. *Proceedings of the National Academy of Sciences,* 97**,** 12176-12181.

Noblet, A., Stalport, F., Guan, Y. Y., Poch, O., Coll, P., Szopa, C., Cloix, M., Macari, F., Raulin, F., Chaput, D. & Cottin, H. 2012. The PROCESS Experiment: Amino and

Carboxylic Acids Under Mars-Like Surface UV Radiation Conditions in Low-Earth Orbit. *Astrobiology,* 12**,** 436-444.

Nørnberg, P., Schwertmann, U., Stanjek, H., Andersen, T. & Gunnlaugsson, H. P. 2004. Mineralogy of a burned soil compared with four anomalously red Quaternary deposits in Denmark. *Clay Minerals,* 39**,** 85-98.

Norton, C. F. & Grant, W. D. 1988. Survival of Halobacteria Within Fluid Inclusions in Salt Crystals. *Journal of General Microbiology,* 134**,** 1365-1373.

Obata, Y. & Tanaka, H. 1965. Studies on the Photolysis of l-Cysteine and l-Cystine. *Agricultural and Biological Chemistry,* 29**,** 191-195.

Ockert-Bell, M. E., Bell, J. F., Pollack, J. B., McKay, C. P. & Forget, F. 1997. Absorption and scattering properties of the Martian dust in the solar wavelengths. *Journal of Geophysical Research: Planets,* 102**,** 9039-9050.

Ojha, L., Wilhelm, M. B., Murchie, S. L., McEwen, A. S., Wray, J. J., Hanley, J., Masse, M. & Chojnacki, M. 2015. Spectral evidence for hydrated salts in recurring slope lineae on Mars. *Nature Geoscience,* 8, 829-832.

Olsson-Francis, K. & Cockell, C. S. 2010. Experimental methods for studying microbial survival in extraterrestrial environments. *Journal of Microbiological Methods,* 80**,** 1-13.

Olsson-Francis, K., Watson, J. S. & Cockell, C. S. 2013. Cyanobacteria isolated from the high-intertidal zone: a model for studying the physiological prerequisites for survival in low Earth orbit. *International Journal of Astrobiology,* 12**,** 292-303.

Oren, A. 2006. Life at High Salt Concentrations. *In:* Dworkin, M., Falkow, S., Rosenberg, E., Schleifer, K.-H. & Stackebrandt, E. (eds.) *The Prokaryotes.* New York, Springer.

Oren, A., Elevi Bardavid, R. & Mana, L. 2014. Perchlorate and halophilic prokaryotes: implications for possible halophilic life on Mars. *Extremophiles,* 18**,** 75-80.

Osterrothová, K. & Jehlička, J. 2011. Investigation of biomolecules trapped in fluid inclusions inside halite crystals by Raman spectroscopy. *Spectrochimica Acta Part A: Molecular and Biomolecular Spectroscopy,* 83**,** 288-296.

Otter, S. 2009. *Simulation of the radiative flux at the Martian surface between 180-1100 nanometres.* PhD, The Open University.

Owen, T., Biemann, K., Rushneck, D. R., Biller, J. E., Howarth, D. W. & Lafleur, A. L. 1977. The Composition of the Atmosphere at the Surface of Mars. *J. Geophys. Res.,* 82**,** 4635-4639.

Pappalardo, R. T., Vance, S., Bagenal, F., Bills, B. G., Blaney, D. L., Blankenship, D. D., Brinckerhoff, W. B., Connerney, J. E. P., Hand, K. P., Hoehler, T. M., Leisner, J. S., Kurth, W. S., McGrath, M. A., Mellon, M. T., Moore, J. M., Patterson, G. W., Prockter, L. M., Senske, D. A., Schmidt, B. E., Shock, E. L., Smith, D. E. & Soderlund, K. M. 2013. Science Potential from a Europa Lander. *Astrobiology,* 13**,** 740-773.

Parnell, J., Cullen, D., Sims, M. R., Bowden, S., Cockell, C. S., Court, R., Ehrenfreund, P., Gaubert, F., Grant, W., Parro, V., Rohmer, M., Sephton, M., Stan-Lotter, H., Steele, A., Toporski, J. & Vago, J. 2007. Searching for Life on Mars: Selection of Molecular Targets for ESA's Aurora ExoMars Mission. *Astrobiology,* 7**,** 578-604.

Pasteris, J. D., Freeman, J. J., Wopenka, B., Qi, K., Ma, Q. & Wooley, K. L. 2006. With a Grain of Salt: What Halite Has to Offer to Discussions on the Origin of Life. *Astrobiology,* 6**,** 625-643.

Patel, M. R., Bérces, A., Kolb, C., Lammer, H., Rettberg, P., Zarnecki, J. C. & Selsis, F. 2003. Seasonal and diurnal variations in Martian surface ultraviolet irradiation: biological and chemical implications for the Martian regolith. *International Journal of Astrobiology,* 2**,** 21-34.

Patel, M. R., Christou, A. A., Cockell, C. S., Ringrose, T. J. & Zarnecki, J. C. 2004. The UV environment of the Beagle 2 landing site: detailed investigations and detection of atmospheric state. *Icarus,* 168**,** 93-115.

Patel, M. R., Zarnecki, J. C. & Catling, D. C. 2002. Ultraviolet radiation on the surface of Mars and the Beagle 2 UV sensor. *Planetary and Space Science,* 50**,** 915-927.

Pawlukojć, A., Leciejewicz, J., Ramirez-Cuesta, A. J. & Nowicka-Scheibe, J. 2005. L-Cysteine: Neutron spectroscopy, Raman, IR and ab initio study. *Spectrochimica Acta Part A: Molecular and Biomolecular Spectroscopy,* 61**,** 2474-2481.

Payne, J. I., Sehgal, S. N. & Gibbons, N. E. 1960. Immersion Refractometry Of Some Halophilic Bacteria. *Canadian Journal of Microbiology,* 6**,** 9-15.

Pizzarello, S. & Cronin, J. R. 1998. Alanine enantiomers in the Murchison meteorite. *Nature,* 394**,** 236-236.

Power, L. F., Turner, K. E. & Moore, F. H. 1976. The crystal and molecular structure of α-glycine by neutron diffraction - a comparison. *Acta Crystallographica Section B,* 32**,** 11-16.

Preston, L. J. & Dartnell, L. R. 2014. Planetary habitability: lessons learned from terrestrial analogues. *International Journal of Astrobiology,* 13**,** 81-98.

Pullan, D., Sims, M. R., Wright, I. P. & Al., E. 2004. Beagle 2: the Exobiologucal Lander of Mars Express. *In:* Wilson, A. (ed.) *SP-1240 Mars Express: A European Mission to the Red Planet.* The Netherlands: ESA Publications Division.

Pullan, D., Westall, F., Hofmann, B. A., Parnell, J., Cockell, C. S., Edwards, H. G. M., Villar, S. E. J., Schröder, C., Cressey, G., Marinangeli, L., Richter, L. & Klingelhöfer, G. 2008. Identification of Morphological Biosignatures in Martian Analogue Field Specimens Using In Situ Planetary Instrumentation. *Astrobiology,* 8**,** 119-156.

Qiu, X., Sundin, G. W., Chai, B. & Tiedje, J. M. 2004. Survival of Shewanella oneidensis MR-1 after UV Radiation Exposure. *Applied and Environmental Microbiology,* 70**,** 6435-6443.

Raman, C. V. & Krishnan, K. S. 1928. A new type of secondary radiation. *Nature,* 121**,** 501 - 502.

Raulin, F. 2008. Astrobiology and habitability of Titan. *Space Sci Rev,* 135: 37.

Rieder, R., Gellert, R., Anderson, R. C., Brückner, J., Clark, B. C., Dreibus, G., Economou, T., Klingelhöfer, G., Lugmair, G. W., Ming, D. W., Squyres, S. W., D'uston, C., Wänke, H., Yen, A. & Zipfel, J. 2004. Chemistry of Rocks and Soils at Meridiani Planum from the Alpha Particle X-ray Spectrometer. *Science,* 306**,** 1746-1749.

Rolfe, M. D., Rice, C. J., Lucchini, S., Pin, C., Thompson, A., Cameron, A. D. S., Alston, M., Stringer, M. F., Betts, R. P., Baranyi, J., Peck, M. W. & Hinton, J. C. D. 2012. Lag Phase Is a Distinct Growth Phase That Prepares Bacteria for Exponential Growth and Involves Transient Metal Accumulation. *Journal of Bacteriology,* 194**,** 686-701.

Rosado, M. T. S., Duarte, M. L. R. S. & Fausto, R. 1997. Vibrational spectra (FT-IR, Raman and MI-IR) of α- and β-alanine. *Journal of Molecular Structure,* 410 - 411**,** 343-348.

Ross, H. N. M., Collins, M. D., Tindall, B. J. & Grant, W. D. 1981. A Rapid Procedure for the Detection of Archaebacterial Lipids in Halophilic Bacteria. *Journal of General Microbiology,* 123**,** 75-80.

Rothschild, L. J. & Mancinelli, R. L. 2001. Life in extreme environments. *Nature,* 409**,** 1092-1101.

Ryder, A. G. 2002. Classification of narcotics in solid mixtures using principal component analysis and Raman spectroscopy. *Journal of Forensic Sciences,* 47**,** 275-284.

Sagan, C., Reid Thompson, W., Carlson, R., Gurnett, D., & Hord, C. 1993. A search for life on Earth from the Galileo spacecraft. *Nature* 365, 715-721.

Saverwyns, S. 2010. Russian avant-garde… or not? A micro-Raman spectroscopy study of six paintings attributed to Liubov Popova. *Journal of Raman Spectroscopy,* 41**,** 1525-1532.

Schimel, J. P. & Clein, J. S. 1996. Microbial response to freeze-thaw cycles in tundra and taiga soils. *Soil Biology and Biochemistry,* 28**,** 1061-1066.

Schofield, J., Barnes, J., Crisp, D., Haberle, R., Larsen, S., Magalhães, J., Murphy, J., Seiff, A. & Wilson, G. 1997. The Mars Pathfinder atmospheric structure investigation/meteorology (ASI/MET) experiment. *Science (New York, N.Y.),* 278**,** 1752-1758.

Schuerger, A. C., Mancinelli, R. L., Kern, R. G., Rothschild, L. J. & McKay, C. P. 2003. Survival of endospores of Bacillus subtilis on spacecraft surfaces under simulated martian environments:: implications for the forward contamination of Mars. *Icarus,* 165**,** 253-276.

Schulze-Makuch, D., Irwin, L. N. & Guan, H. 2002. Search parameters for the remote detection of extraterrestrial life. *Planetary and Space Science,* 50**,** 675-683.

Schwenzer, S. P., Bridges, J. C., Wiens, R. C., Conrad, P. G., Kelley, S. P., Leveille, R., Mangold, N., Martín-Torres, J., McAdam, A., Newsom, H., Zorzano, M. P., Rapin, W., Spray, J., Treiman, A. H., Westall, F., Fairén, A. G. & Meslin, P. Y. 2016. Fluids during diagenesis and sulfate vein formation in sediments at Gale crater, Mars. *Meteoritics & Planetary Science,* 51, 2175–2202.

Seiferlin, K., Ehrenfreund, P., Garry, J., Gunderson, K., Hütter, E., Kargl, G., Maturilli, A. & Merrison, J. P. 2008. Simulating Martian regolith in the laboratory. *Planetary and Space Science,* 56**,** 2009-2025.

Shahmohammadi, H. R., Asgarani, E., Terato, H., Saito, T., Ohyama, Y., Gekko, K., Yamamoto, O. & Ide, H. 1998. Protective Roles of Bacterioruberin and Intracellular KCl in the Resistance of *Halobacterium salinarium* against DNA-damaging Agents. *Journal of Radiation Research,* 39**,** 251-262.

Shock, E. L. 2002. Astrobiology: Seeds of life? *Nature,* 416**,** 380-381.

Simoneit, B. R. T., Summons, R. E. & Jahnke, L. L. 1998. Biomarkers as Tracers for Life on Early Earth and Mars. *Origins of Life and Evolution of Biospheres,* 28**,** 475-483.

Sims, M. R., Pillinger, C. T., Wright, I. P., Dowson, J., Whitehead, S., Wells, A., Spragg, J. E., Fraser, G., Richter, L., Hamacher, H., Johnstone, A., Meredith, N. P., De La Nougerede, C., Hancock, B., Turner, R., Peskett, S., Brack, A., Hobbs, J., Newns, M., Senior, A., Humphries, M., Keller, H. U., Thomas, N., Lingard, J. S., Underwood, J. C., Sale, N. M., Neal, M. F., Klingelhofer, G. & Ng, T. C. 1999. Beagle 2: A proposed exobiology lander for ESA's 2003 Mars Express mission. *Advances in Space Research,* 23**,** 1925-1928.

Sjursen, H., Michelsen, A. & Holmstrup, M. 2005. Effects of freeze–thaw cycles on microarthropods and nutrient availability in a sub-Arctic soil. *Applied Soil Ecology,* 28**,** 79-93.

Smith, D. E., Zuber, M. T., Frey, H. V., Garvin, J. B., Head, J. W., Muhleman, D. O., Pettengill, G. H., Phillips, R. J., Solomon, S. C., Zwally, H. J., Banerdt, W. B., Duxbury, T. C., Golombek, M. P., Lemoine, F. G., Neumann, G. A., Rowlands, D. D., Aharonson, O., Ford, P. G., Ivanov, A. B., Johnson, C. L., McGovern, P. J., Abshire, J. B., Afzal, R. S. & Sun, X. 2001. Mars Orbiter Laser Altimeter: Experiment summary after the first year of global mapping of Mars. *J. Geophys. Res.,* 106**,** 23689-23722.

Spanovich, N., Smith, M. D., Smith, P. H., Wolff, M. J., Christensen, P. R. & Squyres, S. W. 2006. Surface and near-surface atmospheric temperatures for the Mars Exploration Rover landing sites. *Icarus,* 180**,** 314-320.

Squyres, S. W., Grotzinger, J. P., Arvidson, R. E., Bell, J. F., Calvin, W., Christensen, P. R., Clark, B. C., Crisp, J. A., Farrand, W. H., Herkenhoff, K. E., Johnson, J. R., Klingelhöfer, G., Knoll, A. H., McLennan, S. M., McSween, H. Y., Morris, R. V., Rice, J. W., Rieder, R. & Soderblom, L. A. 2004. In Situ Evidence for an Ancient Aqueous Environment at Meridiani Planum, Mars. *Science,* 306**,** 1709-1714.

Squyres, S. W., Knoll, A. H., Arvidson, R. E., Clark, B. C., Grotzinger, J. P., Jolliff, B. L., McLennan, S. M., Tosca, N., Bell, J. F., Calvin, W. M., Farrand, W. H., Glotch, T. D., Golombek, M. P., Herkenhoff, K. E., Johnson, J. R., Klingelhöfer, G., McSween, H. Y. & Yen, A. S. 2006. Two Years at Meridiani Planum: Results from the Opportunity Rover. *Science,* 313**,** 1403-1407.

Stan-Lotter, H., Fendrihan, S., Dornmayr-Pfaffenhuemer, M., Grösbacher, M., Musso, M., Holzinger, A., Weigl, A. & Legat, A. Detection methods for halite-embedded haloarchaea with potential relevance for extraterrestrial samples. European Planetary Science Congress 2010, 2010-259.

Starkey, N. A., Franchi, I. A. & Alexander, C. M. O. D. 2013. A Raman spectroscopic study of organic matter in interplanetary dust particles and meteorites using multiple wavelength laser excitation. *Meteoritics & Planetary Science,* 48**,** 1800-1822.

Stern, J. C., Navarro-Gonzalez, R., Freissinet, C., McKay, C. P., Archer Jr., P. D., Buch, A., Brunner, A. E., Coll, P., Eigenbrode, J. L., Franz, H. B., Glavin, D. P., McAdam, A. C., Ming, D. W., Steele, A., Sutter, B., Szopa, C., Wray, J. J., Conrad, P. G., Mahaffy, P. R., MSL Science Team. 2014. Detection and Quantification of Nitrogen Compounds in the First Drilled Martian Solid Samples by the Sample

Analysis at Mars (SAM) Instrument Suite on the Mars Science Laboratory (MSL). *45th Lunar and Planetary Science Conference*, 2743. Houston: Lunar and Planetary Institute.

Stern, J. C., Sutter, B., Freissinet, C., Navarro-González, R., McKay, C. P., Archer, P. D., Buch, A., Brunner, A. E., Coll, P., Eigenbrode, J. L., Fairen, A. G., Franz, H. B., Glavin, D. P., Kashyap, S., McAdam, A. C., Ming, D. W., Steele, A., Szopa, C., Wray, J. J., Martín-Torres, F. J., Zorzano, M.-P., Conrad, P. G., Mahaffy, P. R., Team, T. M. S. & Stern, J. 2015. Evidence for indigenous nitrogen in sedimentary and aeolian deposits from the Curiosity rover investigations at Gale crater, Mars. *Proceedings of the National Academy of Sciences,* 112**,** 4245-4250.

Stoker, C. R., Cabrol, N. A., Roush, T. R., Moersch, J., Aubele, J., Barlow, N., Bettis, E. A., Bishop, J., Chapman, M., Clifford, S., Cockell, C., Crumpler, L., Craddock, R., De Hon, R., Foster, T., Gulick, V., Grin, E., Horton, K., Hovde, G., Johnson, J. R., Lee, P. C., Lemmon, M. T., Marshall, J., Newsom, H. E., Ori, G. G., Reagan, M., Rice, J. W., Ruff, S. W., Schreiner, J., Sims, M., Smith, P. H., Tanaka, K., Thomas, H. J., Thomas, G. & Yingst, R. A. 2001. The 1999 Marsokhod rover mission simulation at Silver Lake, California: Mission overview, data sets, and summary of results. *Journal of Geophysical Research: Planets,* 106**,** 7639-7663.

Suo, Z., Avci, R., Schweitzer, M. H. & Deliorman, M. 2007. Porphyrin as an Ideal Biomarker in the Search for Extraterrestrial Life. *Astrobiology,* 7**,** 605-615.

Sutter, B., Ming, D. W., Boynton, W. V., Niles, P. B., Hoffman, J., Lauer, H. V. & Golden, D. C. 2009. Summary of Results from the Mars Phoenix Lander's Thermal Evolved Gas Analyzer. *The New Martian Chemistry Workshop.* Medford, MA; United States.

Taylor, G. A. 1971. Amino acids and proteins. *Organic Chemistry for students of biology and medicine.* London: Longman Group Limited.

Taylor, P. A., Kahanpää, H., Weng, W., Akingunola, A., Cook, C., Daly, M., Dickinson, C., Harri, A.-M., Hill, D., Hipkin, V., Polkko, J. & Whiteway, J. 2010. On pressure measurement and seasonal pressure variations during the Phoenix mission. *J. Geophys. Res.,* 115**,** E00E15.

Ten Kate, I. L., Garry, J. R. C., Peeters, Z., Foing, B. & Ehrenfreund, P. 2006. The effects of Martian near surface conditions on the photochemistry of amino acids. *Planetary and Space Science,* 54**,** 296-302.

Ten Kate, I. L., Garry, J. R. C., Peeters, Z., Quinn, R., Foing, B. & Ehrenfreund, P. 2005. Amino acid photostability on the Martian surface. *Meteoritics & Planetary Science,* 40**,** 1185-1193.

Tobin, M. C. 1971. *Laser Raman Spectroscopy,* John Wiley & Sons, Inc.

UNSCEAR. 2008. Sources And Effects Of Ionizing Radiation [Online]. Available: http://www.unscear.org/unscear/en/publications/2008_1.html [Accessed 28 April 2017].

Van Wart, H. E., Lewis, A., Scheraga, H. A. & Saeva, F. D. 1973. Disulfide Bond Dihedral Angles from Raman Spectroscopy. *Proceedings of the National Academy of Sciences,* 70**,** 2619-2623.

Vandenabeele, P., Jehlicka , J., Vítek, P. & Edwards, H. G. M. 2012. On the definition of Raman spectroscopic detection limits for the analysis of biomarkers in solid matrices. *Planetary and Space Science,* 62**,** 48-54.

Vidano, R. P., Fischbach, D. B., Willis, L. J. & Loehr, T. M. 1981. Observation of Raman band shifting with excitation wavelength for carbons and graphites. *Solid State Communications,* 39**,** 341-344.

Vítek, P., Edwards, H. G. M., Jehlička, J., Ascaso, C., De Los Ríos, A., Valea, S., Jorge-Villar, S. E., Davila, A. F. & Wierzchos, J. 2010. Microbial colonization of halite from the hyper-arid Atacama Desert studied by Raman spectroscopy. *Philosophical*

Transactions of the Royal Society A: Mathematical, Physical and Engineering Sciences, 368**,** 3205-3221.

Vítek, P., Osterrothová, K. & Jehlicka, J. 2009. Beta-carotene--A possible biomarker in the Martian evaporitic environment: Raman micro-spectroscopic study. *Planetary and Space Science,* 57**,** 454-459.

Wang, A., Lu, Y. L. & Bradley, A. The Detection of Biomarkers in Salt Mixtures by Laser Raman Spectroscopy. Geological Society of America, 125th Anniversary Annual Meeting and Expo, 2013 Denver, Colorado, USA.

Wang, H. & Ingersoll, A. P. 2002. Martian clouds observed by Mars Global Surveyor Mars Orbiter Camera. *Journal of Geophysical Research: Planets,* 107**,** 5078.

Webster, C. R., Mahaffy, P. R., Atreya, S. K., Flesch, G. J., Mischna, M. A., Meslin, P.-Y., Farley, K. A., Conrad, P. G., Christensen, L. E., Pavlov, A. A., Martín-Torres, J., Zorzano, M.-P., McConnochie, T. H., Owen, T., Eigenbrode, J. L., Glavin, D. P., Steele, A., Malespin, C. A., Archer, P. D., Sutter, B., Coll, P., Freissinet, C., McKay, C. P., Moores, J. E., Schwenzer, S. P., Bridges, J. C., Navarro-Gonzalez, R., Gellert, R., Lemmon, M. T. & Team, T. M. S. 2014. Mars methane detection and variability at Gale crater. *Science,* 347.

Wei, J., Wang, A., Lambert, J. L., Wettergreen, D., Cabrol, N. A. & Warren-Rhodes, K. Automated Core Sample Analysis by the Mars Microbeam Raman Spectrometer (MMRS) On-Board The Zoë Rover in Atacama: A Terrestrial Test for Mars Exploration. 45th Lunar and Planetary Science Conference, 2014 The Woodlands, Texas, USA. p. 2428.

Westall, F., Brack, A., Hofmann, B., Horneck, G., Kurat, G., Maxwell, J., Ori, G. G., Pillinger, C., Raulin, F., Thomas, N., Fitton, B., Clancy, P., Prieur, D. & Vassaux, D. 2000. An ESA study for the search for life on Mars. *Planetary and Space Science,* 48**,** 181-202.

Wharton, D. A. 2002. *Life at the limits: organisms in extreme environments,* Cambridge, United Kingdom, Unviersity Press.

Wierzchos, J., Ascaso, C. & McKay, C. P. 2006. Endolithic Cyanobacteria in Halite Rocks from the Hyperarid Core of the Atacama Desert. *Astrobiology,* 6**,** 415-422.

Williams, R. M. E., Grotzinger, J. P., Dietrich, W. E., Gupta, S., Sumner, D. Y., Wiens, R. C., Mangold, N., Malin, M. C., Edgett, K. S., Maurice, S., Forni, O., Gasnault, O., Ollila, A., Newsom, H. E., Dromart, G., Palucis, M. C., Yingst, R. A., Anderson, R. B., Herkenhoff, K. E., Le Mouélic, S., Goetz, W., Madsen, M. B., Koefoed, A., Jensen, J. K., Bridges, J. C., Schwenzer, S. P., Lewis, K. W., Stack, K. M., Rubin, D., Kah, L. C., Bell, J. F., Farmer, J. D., Sullivan, R., Van Beek, T., Blaney, D. L., Pariser, O., Deen, R. G. & Team, M. S. 2013. Martian Fluvial Conglomerates at Gale Crater. *Science,* 340**,** 1068-1072.

Wipf, S., Sommerkorn, M., Stutter, M. I., Wubs, E. R. J. & Van Der Wal, R. 2015. Snow cover, freeze-thaw, and the retention of nutrients in an oceanic mountain ecosystem. *Ecosphere,* 6**,** 1-16.

Woese, C. R. & Fox, G. E. 1977. Phylogenetic structure of the prokaryotic domain: the primary kingdoms. *Proceedings of National Academy of Science USA*, 74**,** 5088 - 5090.

Woese, C. R., Kandler, O., and Wheelis, M. L. 1990. Towards a natural system of organisms: proposal for the domains Archaea, Bacteria, and Eucarya. *PNAS*, 87 (12), 4576-4579.

Woese, C. R., Magrum, L. J. & Fox, G. E. 1978. Archaebacteria. *Journal of Molecular Evolution*, 11**,** 245-252.

Wolff, M. J., Smith, M. D., Clancy, R. T., Arvidson, R., Kahre, M., Seelos, F., Murchie, S. & Savijärvi, H. 2009. Wavelength dependence of dust aerosol single scattering

albedo as observed by the Compact Reconnaissance Imaging Spectrometer. *Journal of Geophysical Research: Planets,* 114.

Wolff, M. J., Todd Clancy, R., Goguen, J. D., Malin, M. C. & Cantor, B. A. 2010. Ultraviolet dust aerosol properties as observed by MARCI. *Icarus,* 208**,** 143-155.

Wright, I. P., Sims, M. R. & Pillinger, C. T. 2003. Scientific objectives of the Beagle 2 lander. *Acta Astronautica,* 52**,** 219-225.

Yang, Y., Yatsunami, R., Ando, A., Miyoko, N., Fukui, T., Takaichi, S. & Nakamura, S. 2015. Complete Biosynthetic Pathway of the C50 Carotenoid Bacterioruberin from Lycopene in the Extremely Halophilic Archaeon Haloarcula japonica. *Journal of Bacteriology,* 197**,** 1614-1623.

Yen, A. S., Kim, S. S., Hecht, M. H., Frant, M. S. & Murray, B. 2000. Evidence That the Reactivity of the Martian Soil Is Due to Superoxide Ions. *Science,* 289**,** 1909-1912.

Zahnle, K., Freedman, R. S. & Catling, D. C. 2011. Is there methane on Mars? *Icarus,* 212**,** 493-503.

Zhu, G., Zhu, X., Fan, Q. & Wan, X. 2011. Raman spectra of amino acids and their aqueous solutions. *Spectrochimica Acta Part A: Molecular and Biomolecular Spectroscopy,* 78**,** 1187-1195.

Zhukova, A. I. & Kondratyev, I. I. 1965. On Artificial Martian Conditions Reproduced For Microbiological Research. *Life Sci. Space Res.,* 3**,** 120-126.

Zurek, R. W., Chicarro, A., Allen, M. A., Bertaux, J.-L., Clancy, R. T., Daerden, F., Formisano, V., Garvin, J. B., Neukum, G. & Smith, M. D. 2011. Assessment of a 2016 mission concept: The search for trace gases in the atmosphere of Mars. *Planetary and Space Science,* 59**,** 284-291.